**Distribution Agreement**

In presenting this thesis or dissertation as a partial fulfillment of the requirements for an advanced degree from Emory University, I hereby grant to Emory University and its agents the non-exclusive license to archive, make accessible, and display my thesis or dissertation in whole or in part in all forms of media, now or hereafter known, including display on the world wide web. I understand that I may select some access restrictions as part of the online submission of this thesis or dissertation. I retain all ownership rights to the copyright of the thesis or dissertation. I also retain the right to use in future works (such as articles or books) all or part of this thesis or dissertation.

Signature:

_____ _____

Katie M. Vance Date

Mechanisms of GluN2D subunit-specific control of synaptic signaling

By

Katie M. Vance
Doctor of Philosophy

Graduate Division of Biological and Biomedical Science
Molecular Systems Pharmacology

_____
Dr. Stephen F. Traynelis
Advisor

_____
Dr. Criss Hartzell
Committee Member

_____
Dr. Ellen Hess
Committee Member

_____
Dr. Andrew Jenkins
Committee Member

_____
Dr. D. James Surmeier
Committee Member

Accepted:

_____
Lisa A. Tedesco, Ph.D. Dean of the James T. Laney School of Graduate Studies

_____ Date

Mechanisms of GluN2D subunit-specific control of synaptic signaling

By

Katie M. Vance
B.S.

Advisor: Dr. Stephen F. Traynelis, Ph.D.

An abstract of
A dissertation submitted to the Faculty of the
James T. Laney School of Graduate Studies of Emory University
in partial fulfillment of the requirements for the degree of
Doctor of Philosophy
in 2012

**Abstract**

Mechanisms of GluN2D subunit-specific control of synaptic signaling

By Katie M. Vance

NMDA receptors are members of a class of ionotropic glutamate receptors that also includes AMPA, kainate, and delta receptors. NMDA receptors mediate the slow component of excitatory synaptic transmission in the central nervous system and have a role in learning, memory, and neuronal development. Two glycine-binding GluN1 subunits assemble with two glutamate-binding GluN2 subunits to form a functional NMDA receptor, while the four GluN2 subunits (GluN2A-D) control a majority of the properties of the receptor. GluN2D-containing NMDA receptors have an unusually slow deactivation time course following the removal of L-glutamate and low channel open probability compared to the other GluN2 subunits. This dissertation focuses on the molecular mechanisms that control the key properties of GluN1/GluN2D NMDA receptors and how these properties contribute to the synaptic activity of the subthalamic nucleus. The data presented here show that the deactivation time course of GluN1/GluN2D NMDA receptors is ligand-dependent, with L-glutamate causing a slower deactivation time course than any other linear ligand evaluated. RNA splicing of the GluN1 amino-terminal domain also controls the deactivation time course, agonist $EC_{50}$, and channel open probability of GluN1/GluN2D receptors. A gating scheme of NMDA receptor activation is presented that describes the key characteristics of GluN1/GluN2D NMDA receptor gating as well as identifies specific rate constants controlled by the GluN1 amino-terminal domain. Finally, the data presented here suggest

that GluN2D-containing NMDA receptors contribute to the excitatory postsynaptic currents of the subthalamic nucleus.

# Mechanisms of GluN2D subunit-specific control of synaptic signaling

By

Katie Vance
B.S.

Advisor: Dr. Stephen F. Traynelis, Ph.D.

A dissertation submitted to the Faculty of the
James T. Laney School of Graduate Studies of Emory University
in partial fulfillment of the requirements for the degree of
Doctor of Philosophy
in 2012

**Acknowledgements**

I am very fortunate to have a number of people who have helped me throughout my graduate school training. I would like to thank the Emory Molecular and Systems Pharmacology program and the Emory Department of Pharmacology for their assistance and support. I also would like to thank my thesis committee, including Drs. Criss Hartzell, Ellen Hess, Andrew Jenkins, and D. James Surmeier for their invaluable advice and input on my research project. I am especially grateful for the tremendous support and guidance from my advisor, Dr. Stephen F. Traynelis, who has been a truly wonderful mentor both personally and professionally. I am thankful to have had the opportunity to work with the current and previous members of the Traynelis lab. I would like to thank my parents, Geary and Estrid Vance, and my sister, Laura Vance, who have been a constant source of love and motivation for me. Finally, I would like to thank my husband, Brian Giandelone, who has love, supported, encouraged, and inspired me.

**Table of Contents**

## Figures and Tables

## List of Abbreviations

| | |
|---|---|
| 7-CKA | 7-chlorokynurenic acid |
| ACPC | 1-aminocyclopropane-1-carboxylic acid. |
| aCSF | artificial cerebrospinal fluid |
| APV (or AP5) | 2-amino-5-phosphonopentanoate |
| AP7 | 2-amino-7-phosphonopentanoate |
| ATD | Amino-terminal domain |
| CGS-19755 | (2R, 4S)-4-(phosphonomethyl)piperidine-2-carboxylic acid |
| *cis*-ACPD | (1R,3R)-aminocyclopentane-cis-dicarboxylate |
| CP 101,606 | (S,S)-1-(4-hydroxyphenyl)-2-[4-hydroxy-4-phenylpiperidin-1-yl)-1-propanol methanesulfonate trihydrate |
| R-CPP | (R)-4-(3-phosphonopropyl) piperazine-2-carboxylic acid |
| CTD | Carboxyl-terminal domain |
| CIQ | 3-chlorophenyl)(6,7-dimethoxy-1-((4-methoxyphenoxy)methyl)-3,4-dihydroisoquinolin-2(1H)-yl)methanone |
| DMEM | Dulbecco's Modified Eagle Medium |
| DQP-1105 | 4-(5-(4-bromophenyl)-3-(6-methyl-2-oxo-4-phenyl-1,2-dihydroquinolin-3-yl)-4,5-dihydro-1*H*-pyrazol-1-yl)-4-oxobutanoic acid |
| $EC_{50}$ | Half-maximal effective concentration |
| EPSC | Excitatory postsynaptic current |
| GFP | Green fluorescent protein |
| GPe | External globus pallidus |
| GPi | Internal globus pallidus |
| HEK 293 | Human embryonic kidney-293 cell line |
| KA | Kainate |
| L-CCG-IV | (2S,3R,4S)-2-(carboxycyclopropyl)glycine |
| LBD | Ligand-binding domain |
| MK-801 | (5R,10S)-5-methyl-10,11-dihydro-5H-dibenzo[a,d]cyclohepten-5,10-imine |
| NMDA | N-methyl-D-aspartate |
| NVP-AAM077 | (R)-[(S)-1-(4-bromo-phenyl)-ethylamino]-(2,3-dioxo-1,2,3,4-tetrahydroquinoxalin-5-yl)-methyl]-phosphonic acid |
| PBPD | (2S,3R)-1-(biphenyl-4-carbonyl)piperazine-2,3-dicarboxylic acid |
| PMPA | (RS)-4-(phosphonomethyl)-piperazine-2-carboxylic acid |
| $P_{OPEN}$ | Open probability |
| PPDA | (2S,3R)-1-(phenanthren-2-carbonyl)piperazine-2,3-dicarboxylic acid |
| Ro 25-6981 | [R-(R*,S*)]-α-(4-hydroxyphenyl)-β-methyl-4-(phenylmethyl)-1-piperidinepropanol hydrochloride |
| QNZ46 | (E)-4-(6-methoxy-2-(3-nitrostyryl)-4-oxoquinazolin-3(4H)-yl)-benzoic acid |
| QX-314 | *N*-(2,6-Dimethylphenylcarbamoylmethyl)triethylammonium chloride |
| SNc | Substantia nigra pars compacta |
| SNr | Substantia nigra pars reticula |
| STN | Subthalamic nucleus |
| SYM-2081 | (2*S*,4*R*)-4-methylglutamate |

| | |
|---|---|
| TCN-201 | 3-Chloro-4-fluoro-*N*-[4-[[2-(phenylcarbonyl)hydrazino]carbonyl]benzyl]benzenesulfonamide |
| TMD | Transmembrane domain |
| *trans*-ACBD | Trans-1-aminocyclobutane-1,3-dicarboxylate |
| UBP141 | (2R,3S)-1-(phenanthrenyl-3-carbonyl)piperazine-2,3-dicarboxylic Acid |

# Chapter 1: Background

## 1.1. Abstract

NMDA receptors mediate the slow component of excitatory synaptic transmission in the central nervous system and typically are composed of two glycine-binding GluN1 subunits and two glutamate-binding GluN2 subunits. Four GluN2 subunits (GluN2A-D) have been identified and are thought to control a majority of the functional properties of the receptor. GluN2D-containing NMDA receptors are the subject of this dissertation. This thesis describes the mechanisms controlling the pharmacology and kinetic features of activation of GluN1/GluN2D receptors, as well as how the GluN2D subunit contributes to the synaptic activity of the subthalamic nucleus. This introductory chapter presents information on the general structure of NMDA receptors, including a description of the GluN2D ligand-binding domain. I also summarize the pharmacology of NMDA receptor agonists, antagonists, and allosteric modulators and their subunit selectivity. The macroscopic and single channel properties of NMDA receptors are described, as are previously published models of NMDA receptor gating. Finally, I summarize the expression of the GluN2D subunit in the brain as well as what is known about its role in neuronal function.

## 1.2. Introduction to NMDA receptors

NMDA receptors are members of a class of ionotropic glutamate receptors subdivided by pharmacology and sequence homology that also includes the α-amino-3-hydroxy-5-methyl-4-propionic acid (AMPA), kainate, and delta receptors (Mayer, 2005; Traynelis et al., 2010). NMDA receptors mediate the slow, $Ca^{2+}$-permeable component of excitatory postsynaptic currents (EPSCs) in the central nervous system and have roles in synaptic plasticity, learning, memory, and neuronal development (Lisman, 2003; Cull-Candy and Leszkiewicz, 2004; Pérez-Otaño and Ehlers, 2005; Traynelis et al., 2010). NMDA receptors are diheteromeric assemblies typically composed of two GluN1 subunits and two GluN2 subunits and are unique from other glutamate receptors in that receptor activation requires concurrent binding of glycine to the GluN1 subunits and glutamate to the GluN2 subunits (Johnson and Ascher, 1987; Kleckner and Dingledine, 1988).

Eight GluN1 isoforms have been identified and are formed by mRNA splicing from the same gene, while four separate genes encode the four GluN2 subunits (GluN2A-D), and two genes encode the GluN3 subunits (GluN3A-B) (Durand et al., 1992; Ikeda et al., 1992; Monyer et al., 1992; Hollmann et al., 1993; Chatterton et al., 2002; reviewed in Traynelis et al., 2010). The GluN1 subunit influences the pharmacological properties, deactivation time course, and intracellular binding partners of NMDA receptors (Hollmann et al., 1993; Ehlers et al., 1995; Zukin and Bennett, 1995; Johnson et al., 1996; Ehlers et al., 1998; Bassand et al., 1999; Logan et al., 1999). A majority of the functional differences between NMDA receptors are determined by the identity of the GluN2 subunit assembled within the receptor, including deactivation time course,

channel open probability, agonist potencies, and pharmacological modulation (Monyer et al., 1994; Vicini et al., 1998; Erreger et al., 2004).

The single channel and macroscopic current properties as well as the neuronal expression of GluN2D-containing NMDA receptors differ substantially from other NMDA receptor subunits. GluN2D-containing receptors have an exceptionally prolonged deactivation time course upon removal of agonist, which is more than 50 times slower than the deactivation time course of GluN2A-containing NMDA receptors (Monyer et al., 1994; Vicini et al., 1998; Wyllie et al., 1998; Yuan et al., 2009; Vance et al., 2011). GluN2D-containing receptors have a low channel open probability of less than 0.02 (Wyllie et al., 1998; Yuan et al., 2009; Vance et al., 2012). Agonist affinities are higher for GluN1/GluN2D than any other NMDA receptor (Kutsuwada et al., 1992; Matsui et al., 1995; Erreger et al., 2007; Chen et al., 2009; reviewed in Traynelis et al., 2010). The expression of the GluN2D subunit peaks early in development, and later only can be found in specific regions of the adult brain (Monyer et al., 1994; Standaert et al., 1994; Dunah et al., 1996; Wenzel et al., 1996), including the subthalamic nucleus, substantia nigra, spinal cord, cerebellar Golgi and Purkinje cells, interneurons, and the dentate gyrus (Standaert et al., 1993; Laurie and Seeburg, 1994; Monyer et al., 1994; Standaert et al., 1994; Dunah et al., 1996; Standaert et al., 1996; Wenzel et al., 1996; Goebel and Poosch, 1999; Standaert et al., 1999).

Although the GluN2D subunit has many unique properties and is expressed in areas of the brain affected in diseases such as Parkinson's disease and schizophrenia, little is known about the mechanisms controlling the properties of GluN2D-containing receptors or how these receptors influence neuronal function. Of approximately 30,000 peer-

reviewed publications that discuss NMDA receptors, fewer than 300, or less than 1%, discuss any aspect of the GluN2D subunit (PubMed.gov search). In this thesis, I will describe my work on the characterization of the mechanisms controlling a number of the key features of GluN2D-containing receptors as well as how they contribute to the synaptic activity in the subthalamic nucleus. I will describe how the prolonged deactivation time course of GluN1/GluN2D receptors, long thought to be the defining characteristic of these receptors, is controlled by the structure and potency of the activating ligand. I also describe how the deactivation time course, agonist affinities, and open probability of GluN1/GluN2D receptors are controlled by the GluN1 splice variant assembled within the receptor. Understanding the mechanisms that determine these important characteristics in recombinant GluN2D-containing receptors may give us a better idea of how these receptors function in neurons. Finally, I will use what I learned in my studies of recombinant GluN2D-containing receptors to evaluate their function in the subthalamic nucleus.

The following sections within this introductory chapter will summarize findings on the structure, pharmacological modulation, channel activation, and neuronal role of NMDA receptors.

## 1.3. NMDA receptor structure

### *1.3.a. Subunit organization and stoichiometry*

NMDA receptors are members of a class of ionotropic glutamate receptors that includes AMPA, kainate, and delta receptors. The ionotropic glutamate receptors are structurally similar, formed by four subunits, each with four semiautonomous domains

(Fig. 1.1-1.2; Table 1.1), including the extracellular amino-terminal (ATD) and ligand-binding (LBD) domains (S1 and S2), a pore-forming transmembrane domain (TMD; composed of 4 segments designated M1-M4), and a carboxyl-terminal domain (CTD) (Mayer, 2005; Mayer, 2006; Sobolevsky et al., 2009; reviewed in Traynelis et al., 2010). The residues forming the ATD and CTDs are the most divergent between the classes, while the transmembrane domains share the most homology (Table 1.1; Traynelis et al., 2010).

While the crystal structure of a full-length NMDA receptor has not yet been solved, the Gouaux lab recently published the structure of the nearly full-length rat GluA2 AMPA receptor (Fig. 1.2; Sobolevsky et al., 2009). The GluA2 extracellular ATDs and LTDs are arranged as dimers of dimers, with 2-fold symmetry perpendicular to the plasma membrane (Fig. 1.2; Sobolevsky et al., 2009). The subunit arrangement of the extracellular domains causes a symmetry mismatch between the ATDs and LBDs of the GluA2 structure. When the four subunits within the GluA2 structure are named as subunits A, B, C, and D, the ATDs dimerize as A/B and C/D, while the LBDs dimerize as B/C and A/D (Fig. 1.2; Sobolevsky et al., 2009). The A/B and C/D dimers have intersubunit contacts similar to those observed in the isolated dimeric ATD crystal structures for the GluA2 AMPA and GluK2 kainate receptors (Clayton et al., 2009; Jin et al., 2009; Kumar et al., 2009). Like the ATD dimers, the LBD dimers also form inter-dimer contacts within the assembled receptor, with interactions between the A subunit of the A/D dimer and C subunit of the B/C dimer (Fig. 1.2; Sobolevsky et al., 2009). The transmembrane domain, formed by three transmembrane helices (M1, M3, and M4) and a re-entrant loop (M2) from each of the four subunits, forms the pore of the GluA2 AMPA

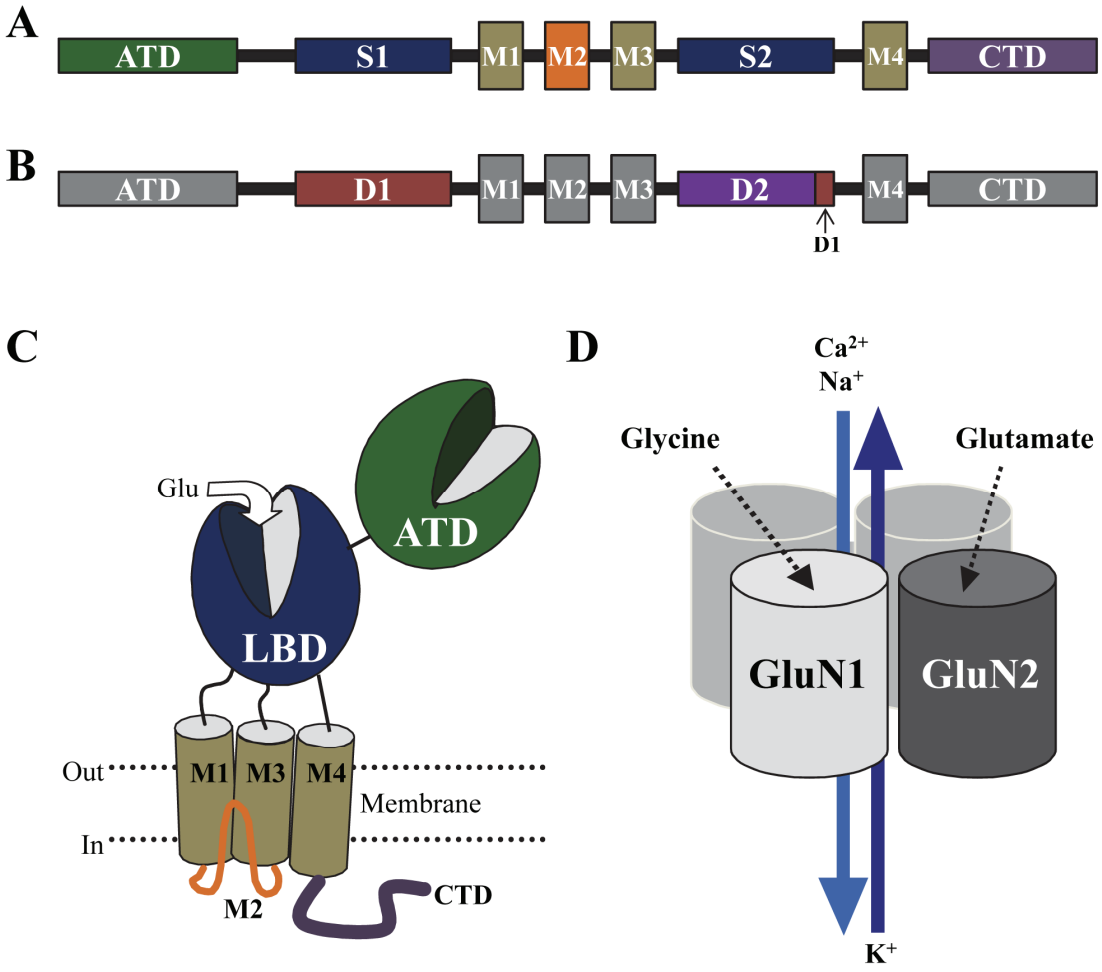


**Figure 1.1.** NMDA receptors are formed by four semiautonomous domains. A diagram of the linear sequence of a glutamate receptor subunit is given in ***A***. **B,** The upper half of the NMDA receptor ligand-binding domain, the D1 region (pink), is composed of the full S1 domain and the final 32 residues of the S2 domain. The lower half of the LBD, the D2 region (purple), is composed of most of the S2 domain. ***C***, Each subunit is formed by an extracellular amino-terminal domain (ATD) and ligand-binding domain (LBD), three transmembrane domains (M1, M3, M4) and a re-entrant loop (M2) that form the pore of the channel, and an intracellular carboxyl-terminal domain (CTD). ***D***, NMDA receptors typically are formed of two glycine-binding GluN1 subunits and two glutamate-binding GluN2 subunits. Adapted with permission from Vance et al. (2011).

**Table 1.1.** Sequence homology in percentage between glutamate receptor subunits

| Receptor | ATD | S1 | S2 | LBD | TMD | CTD | Full Receptor |
|---|---|---|---|---|---|---|---|
| **GluA1-4 (AMPA)** | 35 | 74 | 84 | 80 | 87 | 9 | 54 |
| **GluK1-5 (Kainate)** | 16 | 54 | 53 | 53 | 56 | 0 | 29 |
| **GluN1 GluN2A-D GluN3A-B (NMDA)** | 1 | 19 | 18 | 19 | 14 | 0.0 | 5 |
| **GluN2A-D (NMDA)** | 19 | 60 | 66 | 63 | 73 | 2 | 25 |
| **GluD1-2 (Delta)** | 60 | 67 | 57 | 62 | 54 | 34 | 54 |
| **All subunits** | 0.2 | 7 | 6 | 6 | 10 | 0.0 | 2 |

The numbers represent the percentage of residues within the identified glutamate receptor subunit class that are identical between all subunits within the class. The amino-terminal domain (ATD) includes the signal peptide, the ligand-binding domain (LBD) is composed of S1 and S2, and the transmembrane domain (TMD) is M1, M2, M3, and M4. The full receptor is composed of the ATD, LBD, TMD, and carboxyl-terminal domain (CTD) (Traynelis et al., 2010).

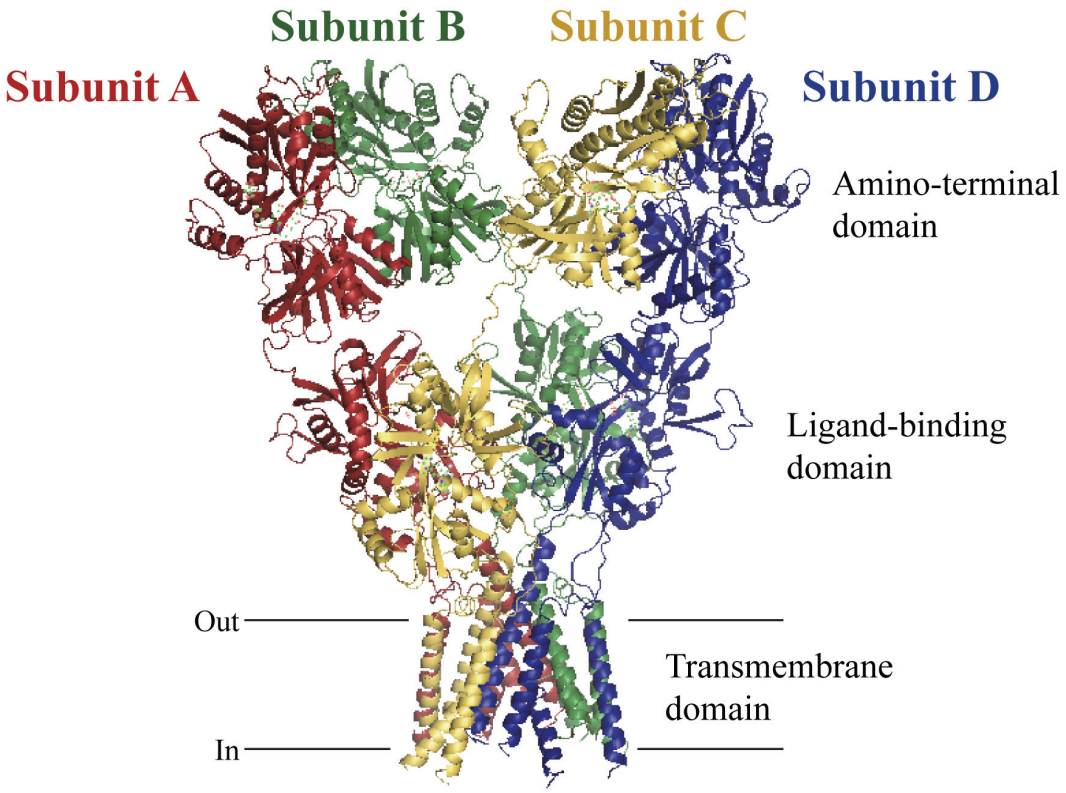


**Figure 1.2.** The GluA2 AMPA receptor high resolution crystal structure. The nearly full-length high resolution structure of the GluA2 AMPA receptor was published recently by Sobolevsky et al. (2009). The homomeric receptor is composed of subunits A (red), B (green), C (yellow), and D (blue). The amino-terminal domains assemble as A/B and C/D dimers, while the ligand-binding domains assemble as A/D and B/C dimers.

receptor, similar to the structure of an inverted tetrameric $K^+$ channel (Wo and Oswald, 1995; Wood et al., 1995; Kuner et al., 2003; Sobolevsky et al., 2009). In addition, the pre-M1 helix, a short helical element identified in the GluA2 receptor structure, resting at a 90º angle from the top of the M1 transmembrane helix and parallel to the cell membrane, makes contacts with helices M3 and M4 (Sobolevsky et al., 2009).

GluN1/GluN2A, GluN1/GluN2C, and GluN1/GluN2D homology models based on the GluA2 structure have been developed to evaluate the subunit arrangement within the receptor (Sobolevsky et al., 2009; Acker et al., 2011; Salussolia et al., 2011). Unlike AMPA receptors, NMDA receptors are always heteromeric, composed typically of two GluN1 subunits and two GluN2 subunits (Monyer et al., 1992; Schorge and Colquhoun, 2003; Ulbrich and Isacoff, 2008), giving rise to several potential subunit arrangements within an assembled NMDA receptor (Figs. 1.1-1.2; Sobolevsky et al., 2009). Using redox-dependent crosslinking of cysteine substitutions on the GluN1 and GluN2A LBDs, Sobolevsky et al. (2009) proposed that the NMDA receptor LBD dimers are arranged in diagonal pairs of GluN1/GluN2A LBD dimers, with the GluN1 subunits adopting the A and C subunit arrangements of the GluA2 structure, and the GluN2A subunits adopting the B and D subunit arrangements of the GluA2 structure (Fig. 1.2; Sobolevsky et al., 2009). The structure of the GluN1/GluN2C NMDA receptor appears similar, as cysteine crosslinking of the linkers between the LBD and the TMD suggest that the GluN1 subunits adopt the A and C subunit arrangement, and the GluN2C subunits adopt the B and D arrangement of the GluA2 structure (Fig. 1.2; Salussolia et al., 2011). Like the GluA2 structure, the GluN1/GluN2C NMDA receptor has been proposed to have a pre-M1 region parallel to the plasma membrane at the top of the TMD of the receptor

(Talukder et al., 2010; Mony et al., 2011; Paoletti, 2011; Salussolia et al., 2011; Stroebel et al., 2011).

In addition to forming diheteromeric GluN1/GluN2 NMDA receptors, NMDA receptors may assemble as triheteromeric receptors in which two different GluN2 subtypes are assembled with two GluN1 subunits. A number of studies have identified GluN1/GluN2A/GluN2B, GluN1/GluN2A/GluN2C, GluN1/GluN2A/GluN2D, and GluN1/GluN2B/GluN2D as functional NMDA receptors expressed within a recombinant system or native tissues (Chazot and Stephenson, 1997; Luo et al., 1997; Cheffings and Colquhoun, 2000; Pina-Crespo and Gibb, 2002; Brickley et al., 2003; Dunah and Standaert, 2003; Fu et al., 2005; Hatton and Paoletti, 2005; Jones and Gibb, 2005; Brothwell et al., 2008; Mullasseril et al., 2010). While single channel studies on triheteromeric NMDA receptors show the inclusion of a lower conductance sublevel when GluN2C or GluN2D is included in the receptor (Cheffings and Colquhoun, 2000; Pina-Crespo and Gibb, 2002; Brickley et al., 2003; Jones and Gibb, 2005), it is not yet known how triheteromeric receptors differ in agonist pharmacology or deactivation time course from diheteromeric NMDA receptors. The roles of the GluN3 subunits remain unclear, as GluN1/GluN3 receptors are functional in *Xenopus* oocytes, but only are functional when expressed in GluN1/GluN3A/GluN3B triheteromeric form in HEK 293 cells (Chatterton et al., 2002; Smothers and Woodward, 2007). Previous studies have suggested that the GluN3 subunit can form triheteromeric NMDA receptors composed of two GluN1 subunits, a GluN2 subunit, and a GluN3 subunit, as GluN1/GluN2/GluN3 receptors are active in *Xenopus* oocytes (Das et al., 1998; Perez-Otano et al., 2001; Ulbrich and Isacoff, 2008) and cortical neurons (Sasaki et al., 2002).

### *1.3.b. Amino-terminal domain*

Glutamate receptor amino-terminal domains are large (~450 residues), semiautonomous extracellular domains (Fig. 1.1-1.2). The ionotropic glutamate receptor ATDs and the metabotropic GPCR glutamate receptor mGluR1 LBD have sequence and structural homology and are similar in their clamshell-like structure to the soluble bacterial periplasmic amino acid binding proteins, including the leucine/isoleucine/valine binding protein (LIVBP; Masuko et al., 1999; Paoletti et al., 2000; Jin et al., 2009; Karakas et al., 2009; Kumar et al., 2009; Karakas et al., 2011). Structural information exists only for the isolated ATD of the GluN2B subunit, as crystal structures have been solved for the homomeric GluN2B/GluN2B ATD dimer and heteromeric GluN1-1b/GluN2B ATD dimer (Karakas et al., 2009; Karakas et al., 2011). The GluN1-1b and GluN2B ATDs both are bi-lobed clamshell-like structures formed by an upper R1 and a lower R2 domain (Karakas et al., 2009; Karakas et al., 2011) and are arranged roughly back-to-back in the ATD dimer.

Although the GluN1-1b/GluN2B ATD structures are similar to the ATDs of other ionotropic glutamate receptors (Clayton et al., 2009; Jin et al., 2009; Kumar et al., 2009; Sobolevsky et al., 2009), the GluN1-1b/GluN2B ATD dimer is unique in its asymmetry through the R1-R1 and GluN1-1b R1 and GluN2B R2 interactions (Karakas et al., 2011). The R1 domain of the GluN2B ATD is rotated about 50º relative to the R2 domain when compared to the ATDs of other ionotropic glutamate receptors (Karakas et al., 2009; Hansen et al., 2010). The “twisted” arrangement of the R1 and R2 domains of the GluN2B ATD is due to a lack of a helix-loop motif found on the backside of AMPA and kainate receptor ATDs that tethers the R1 and R2 domains into a non-twisted alignment

(Karakas et al., 2009; Hansen et al., 2010). Interestingly, no residue from the GluN1-1b R2 domain interacts with the other GluN1-1b and GluN2B subunits.

Recent work crosslinking the GluN2A ATD cleft with disulphide bonds suggests that the GluN2A ATD undergoes a similar, twisted conformation, indicating that the twisted conformation may be a general feature of NMDA receptors (Stroebel et al., 2011). Because of their twisted R1-R2 orientation, it is possible the NMDA receptor ATDs may have a unique arrangement within a fully assembled NMDA receptor compared to what was observed in the GluA2 structure (Sobolevsky et al., 2009). Indeed, the GluN2B ATD R2 domain clashes with the GluA2 R2 domain when the two structures are superimposed at the R1 domain (Karakas et al., 2009; Hansen et al., 2010).

### *1.3.c. Ligand-binding domain*

The ligand-binding domains of all ionotropic glutamate receptors are formed by the S1 and S2 domains, two segments of amino acids separated by three transmembrane domains that join to form a clamshell-like conformation (Fig. 1.1; Armstrong and Gouaux, 2000; Furukawa and Gouaux, 2003; Furukawa et al., 2005; Sobolevsky et al., 2009; Vance et al., 2011). The S1 segment forms the top half of the clamshell (D1), while most of the S2 segment forms the bottom half of the clamshell (D2; Furukawa et al., 2005; Mayer, 2006). While a majority of the studies on glutamate receptor LBDs have been conducted on the two isolated S1 and S2 segments separated by an artificial linker, the recently published full-length GluA2 structure shows similar LBD conformations as the isolated structures (Sobolevsky et al., 2009).

In an assembled receptor, the LBDs are arranged back-to-back, and upon agonist

binding, the lower D2 lobes move toward the D1 lobes (Fig. 1.2; Armstrong and Gouaux, 2000; Furukawa and Gouaux, 2003; Jin et al., 2003; Furukawa et al., 2005; Inanobe et al., 2005; Sobolevsky et al., 2009). This movement likely causes channel opening when the linkers that connect the D2 region to the M3 domain of the transmembrane region are rearranged (Erreger et al., 2004; Mayer, 2006; Traynelis et al., 2010). Receptor desensitization occurs when the D1 domains separate, rearranging and destabilizing the dimer interface and closing the ion channel pore (Sun et al., 2002; Jin et al., 2003; Jin et al., 2005; Armstrong et al., 2006; Weston et al., 2006).

The agonist binding pocket for glycine in the GluN1 subunit and glutamate in the GluN2 subunit lies within the cleft between the D1 and D2 domains (Furukawa et al., 2005). Crystal structures of the GluN1 ligand binding domain have been solved with full agonists, partial agonists, and antagonists bound (Furukawa and Gouaux, 2003; Furukawa et al., 2005; Inanobe et al., 2005). Glycine binds within the crevice between the D1 and D2 domains and is surrounded by the N-termini of helices D, F, and H, as well as β-strand 14. The residue Trp731 within the binding pocket of the GluN1 subunit acts as a barrier to the binding of glutamate because the indole of Trp731 is too large to allow the γ-carboxyl group of glutamate to bind (Furukawa and Gouaux, 2003). Crystal structures of the GluN1 subunit indicate the degree of closure of the ligand-binding domain is not correlated to agonist efficacy as has been demonstrated with the GluA2 AMPA receptor (Armstrong and Gouaux, 2000; Jin et al., 2003; Inanobe et al., 2005). For example, partial agonists 1-aminocyclobutane-1-carboxylic acid and 1-aminocyclopentane-1-carboxylic acid induced the same degree of GluN1 domain closure as glycine (Inanobe et al., 2005).

The crystal structure of the GluN1-GluN2A heterodimer has been solved and suggests the mechanism of selectivity for the binding of glutamate and NMDA to the NMDA receptor compared to the AMPA GluA2 receptor (Furukawa et al., 2005). The GluN2A subunit has a negatively charged Asp731 within the binding pocket, while the GluA2, GluK1, and GluK2 receptor subunits have a negatively charged glutamate residue at the corresponding position that interacts with the amino group of the L-glutamate ligand (Armstrong and Gouaux, 2000; Jin et al., 2003; Mayer et al., 2006). Because the aspartate residue within the GluN2A subunit is a methylene group shorter than the glutamate residue found in other ionotropic glutamate receptors, the salt bridge between the aspartate residue and the amino group of the glutamate ligand is eliminated (Furukawa et al., 2005). Instead, the amino group of the L-glutamate ligand forms water-mediated hydrogen bonds with residues Glu413 and Tyr761 (Furukawa et al., 2005). The specific agonist NMDA is able to fit within the GluN2A binding pocket because the subunit does not have the steric barrier formed by the analogous glutamate residue of the AMPA and kainate receptor ligand-binding domains. The strong affinity for glutamate by the NMDA receptor subunits may be influenced by the Tyr730 within the ligand-binding domain of GluN2A and the corresponding conserved residues within the other GluN2 subunits, which form van der Waals interactions with the γ-carboxylate group of the glutamate ligand as well as hydrogen bonds with another residue, Glu413, within the ligand-binding domain (Furukawa et al., 2005; Vance et al., 2011).

High resolutions structures of the homomeric GluN2D ligand-binding domain in complex with L-glutamate, D-glutamate, NMDA, and L-aspartate also have been solved recently by our collaborator Hiro Furukawa of Cold Spring Harbor Laboratories, with

crystals showing x-ray diffractions higher than 1.9 Å. The structures included the electron densities of the proteins, ligands, and water molecules. The GluN2D LBD had a similar structure to that of the ligand-binding domain in AMPA (Figure 1.3; Armstrong and Gouaux, 2000; Jin et al., 2005; Mayer, 2006; Gill et al., 2008; Sobolevsky et al., 2009), kainate (Mayer et al., 2006; Plested and Mayer, 2007), and GluN1 and GluN1/GluN2A NMDA receptors (Furukawa and Gouaux, 2003; Furukawa et al., 2005; Inanobe et al., 2005), with a bi-lobed clamshell-shaped structure composed of two domains, designated D1 and D2 (Fig. 1.3A; Vance et al., 2011). The L-glutamate-bound GluN2A and GluN2D structures could be superimposed, with a root-mean-square deviation of 0.88 Å over 240 out of 285 possible Cα positions (Fig. 1.3B; Vance et al., 2011). Two regions in the clamshell structures, Loop 1 of domain 1 and the "hinge loop" at the rear of the LBD in domain 2, varied significantly between the two structures (Fig. 1.3B; Vance et al., 2011). Interestingly, the position of the hinge loop in the GluN2D structures in complex with D-glutamate, L-aspartate, and NMDA was similar to the position of the hinge loop in the GluN2A structure when in complex with L-glutamate (Fig. 1.3C; Furukawa et al., 2005; Vance et al., 2011).

The differences in the GluN2D LBD high resolution structures caused by the four ligands and solved by Dr. Furukawa are shown in Figure 1.4. The hinge loop region, which spans eight residues from Ile775 to Ala782, exhibits variability in the Cα positions ranging from approximately 1.4 Å to 9.8 Å between the L-glutamate-bound structures and the other three structures (Fig. 1.4; Vance et al., 2011). The hinge loops of the structures in complex with L-aspartate-, D-glutamate-, and NMDA have similar conformations and interact with Helix E and F of the LBD mainly through hydrophobic

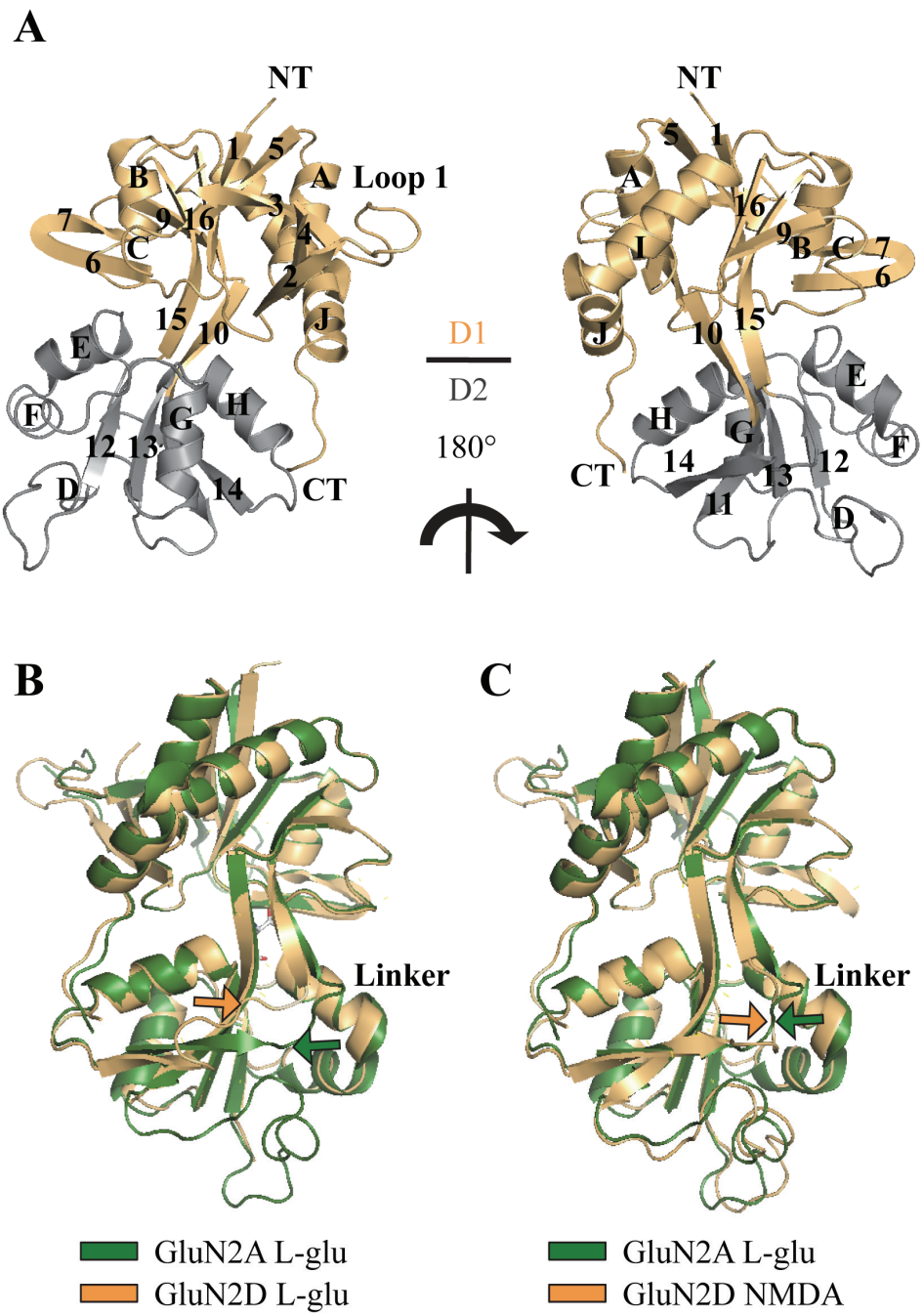


**Figure 1.3.** The GluN2D ligand-binding domain has a clamshell structure with D1 and D2 domains (***A***), similar to the structures for GluN1 and GluN2A (Furukawa and Gouaux, 2003; Furukawa et al., 2005; Inanobe et al., 2005; Vance et al., 2011). ***B***, While the GluN2A (*green*) and GluN2D (*tan*) LBD structures are similar, the position of the hinge region within the GluN2D D2 region is shifted compared to GluN2A. ***C***, When rapidly deactivating NMDA is bound to the GluN2D LBD, the hinge region is in a similar conformation to GluN2A when bound to L-glutamate.

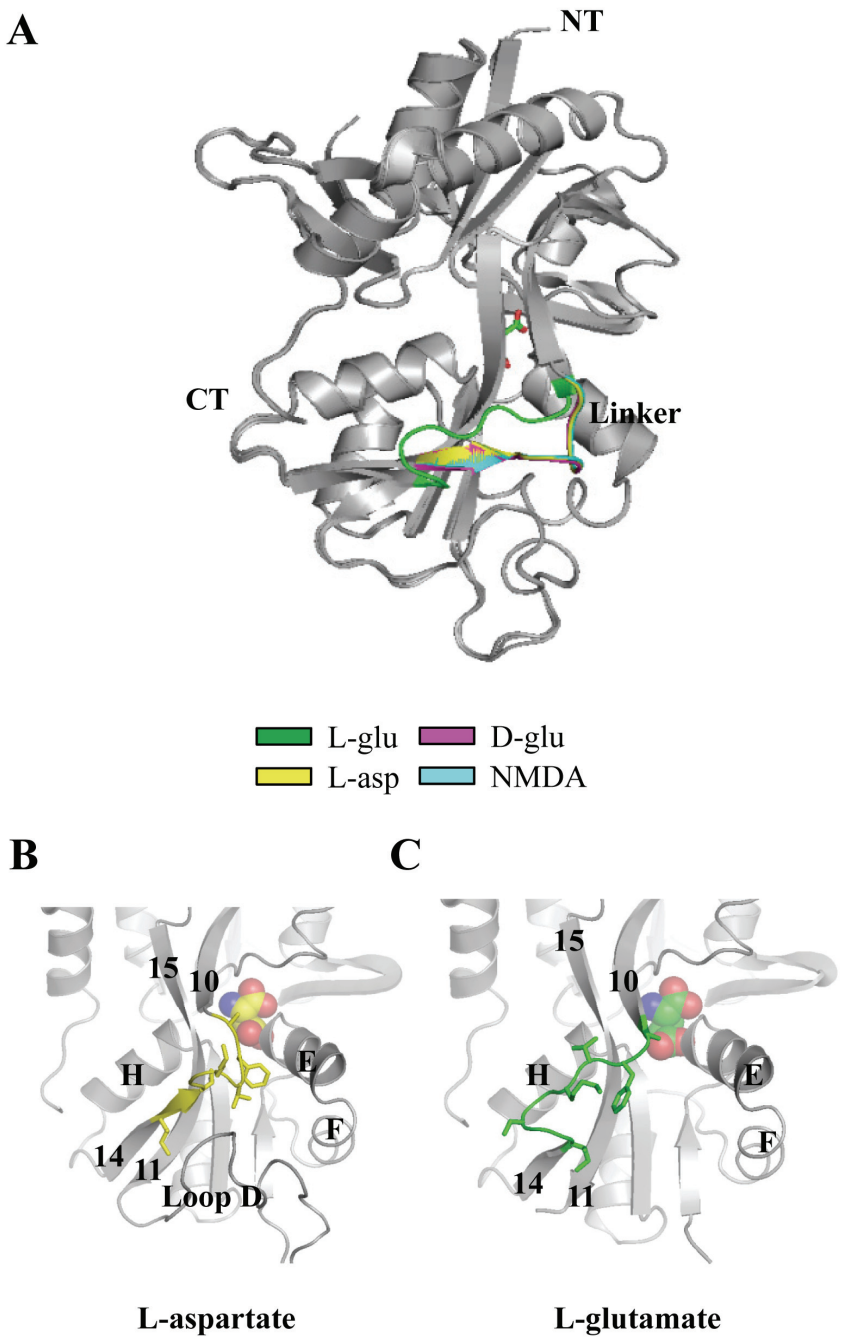


**Figure 1.4.** The hinge region of the GluN2D ligand-binding domain is sensitive to activating ligand. ***A***, L-glutamate (green) forces the hinge loop of the GluN2D LBD into a unique conformation compared to D-glutamate (magenta), L-aspartate (yellow), or NMDA (blue) (Vance et al., 2011). The hinge loop interacts with Helix E, F, and D and loop D through hydrophobic interactions when bound to the the rapidly deactivating L-aspartate (***B***). When bound to L-glutamate, these interactions with the hinge region are lost, and the Helix D and loop D are highly disordered (***C***).

interactions involving Tyr723, Val780, and Phe781 (Fig. 1.4B; Vance et al., 2011). This conformation of the hinge loop enables interactions with Helix D and Loop D through hydrophobic interactions (Fig. 1.4C; Appendix A; Vance et al., 2011). However, the hinge loop of the L-glutamate bound structure interacts with Helix H rather than Helix E and F through the non-polar interactions of Val780 and Ala757 (Appendix A; Vance et al., 2011). This prevents the hinge region from interacting with Loop D, perhaps causing Helix D and Loop D to be disordered. The differences in hinge loop conformation between the evaluated agonists could have profound effects on the kinetic properties of GluN2D NMDA receptors.

## 1.4. NMDA receptor pharmacology

### *1.4.a. NMDA receptor agonists*

A series of endogenous and synthetic ligands act as full or partial agonists for the GluN1 and GluN2 NMDA receptor subunits. In addition to glycine (Johnson and Ascher, 1987; Kleckner and Dingledine, 1988), other endogenous ligands for the GluN1 subunit include the D- and L- isomers of alanine and serine (Pullan et al., 1987; McBain et al., 1989). Indeed, D-serine may act as the primary ligand for GluN1 in regions of the brain such as the supraoptic nucleus (Panatier et al., 2006; Basu et al., 2009). Synthetic partial agonists of the GluN1 subunit include cyclic and halogenated glycine analogues (Hood et al., 1989; Priestley and Kemp, 1994; Sheinin et al., 2001; Dravid et al., 2010).

Although the GluN2 subunit does not directly contact residues within the ligand-binding cleft of the GluN1 subunit, the identity of the GluN2 subunit strongly influences the potency of the glycine-site agonist (Table 1.2). When GluN1 is assembled with the

**Table 1.2.** $EC_{50}$ values (in μM) of GluN1 subunit agonists

| Glycine-site agonist | GluN2A μM (%) | GluN2B μM (%) | GluN2C μM (%) | GluN2D μM (%) | 2A/2D Fold Selectivity |
|---|---|---|---|---|---|
| **Glycine** | 1.1 (100) | 0.72 (100) | 0.34 (100) | 0.13 (100) | 8.5 |
| **L-serine** | 212 (95) | 77 (98) | 27 (110) | 15 (98) | 14 |
| **D-serine** | 1.3 (98) | 0.65 (96) | 0.32 (110) | 0.16 (93) | 8.1 |
| **L-alanine** | 96 (79) | 36 (65) | 28 (92) | 13 (97) | 7.4 |
| **D-alanine** | 3.1 (96) | 0.89 (84) | 0.56 (96) | 0.22 (99) | 14 |
| **D-cycloserine** | 19 (90) | 8.2 (65) | 3.3 (190) | 2.9 (94) | 6.6 |
| **ACPC** | 1.3 (79) | 0.65 (89) | 0.35 (88) | 0.083 (89) | 16 |

Data are $EC_{50}$ in μM with relative efficacy compared to glycine given in parentheses (%). Efficacy is given as the current response to a maximally effective concentration of agonist relative to the response to maximally effective concentration of glycine. All values are from recombinant rat NMDA receptors expressed in *Xenopus laevis* oocytes and co-activated by glutamate (Chen et al., 2008) except D-cycloserine experiments, in which rat NMDA receptors were expressed in *Xenopus* oocytes and were co-activated by NMDA (Sheinin et al., 2001). ACPC, 1-aminocyclopropane-1-carboxylic acid.

GluN2D subunit, glycine and other glycine-site agonists have the highest affinity for the GluN1 subunits (Matsui et al., 1995; Chen et al., 2008). The $EC_{50}$ of glycine for a GluN1/GluN2D receptor is around 0.1 μM, significantly more potent than in GluN1/GluN2A receptors, which have a glycine $EC_{50}$ around 1.1 μM (Chen et al., 2008; Vance et al., 2012; Table 1.2). Because glycine must be bound to the GluN1 subunit in order for the channel to open, the high affinity of glycine to GluN2D-containing receptors could have a profound impact on the function of the receptor in neurons. While glycine concentration is high enough in certain synapses, including the cerebellar mossy fiber – granule cell synapse (Billups and Attwell, 2003), to saturate NMDA receptors, in other regions of the brain, including the thalamus, neocortex, brainstem, and hippocampus, synaptic currents are increased by 50 to 100% by bath-applied glycine-site agonists (Salt, 1989; Berger et al., 1998; Bergeron et al., 1998; Thompson et al., 2002; Chen et al., 2003). Given the higher potency (lower $EC_{50}$) of GluN2D-containing receptors, these receptors may be saturated at the glycine site and thus could be activated preferentially under conditions in which GluN2A-containing NMDA receptors may not be activated.

Like the GluN1 subunit, both endogenous and synthetic ligands have been identified that act as partial or full agonists for the GluN2 subunits. Endogenous agonists of the GluN2 subunit include L-glutamate, D- and L-aspartate (Benveniste, 1989; Nicholls, 1989; Fleck et al., 1993; Schell et al., 1997; Wang and Nadler, 2007; Errico et al., 2008), homocysteate, and cysteinesulfinate (Do et al., 1986; Olney et al., 1987; Do et al., 1988; Yuzaki and Connor, 1999). Other agonists of the GluN2 subunit include cyclic glutamate analogues with conformationally constrained rings, some of which are more potent than L-glutamate (Table 1.3; Shinozaki et al., 1989; Schoepp et al., 1991; Erreger et al., 2007).

**Table 1.3.** $EC_{50}$ values (in μM) for GluN2 subunit agonists

| Glutamate-site agonist | GluN2A μM (%) | GluN2B μM (%) | GluN2C μM (%) | GluN2D μM (%) | 2A/2D Fold Selectivity |
|---|---|---|---|---|---|
| **L-glutamate** | 3.3 (100) | 2.9 (100) | 1.7 (100) | 0.51 (100) | 6.5 |
| **D-glutamate** | 250 (99) | 160 (120) | 110 (100) | 42 (110) | 6.0 |
| **L-aspartate** | 48 (99) | 14 (78) | 41 (110) | 12 (91) | 4.0 |
| **D-aspartate** | 30 (103) | 10 (91) | 9.3 (99) | 2.1 (90) | 14 |
| ***N*-methyl-L-aspartate** | 580 (99) | 130 (69) | 150 (66) | 40 (75) | 15 |
| ***N*-methyl-D-aspartate** | 94 (93) | 30 (78) | 22 (86) | 7.3 (92) | 13 |
| **(2*S*,4*R*)-4-methylglutamate (SYM 2081)** | 140 (72) | 25 (89) | 18 (71) | 3.2 (75) | 44 |
| **(2*S*,4*S*)-4-methylglutamate** | 404 (78) | 76.2 (75) | 87.4 (80) | 31.4 (83) | 13 |
| **L-homocysteate** | 34 (86) | 8.1 (90) | 12 (53) | 3.4 (69) | 10 |
| **D-homocysteate** | 180 (92) | 86 (94) | 110 (74) | 22 (87) | 8.2 |
| **(*RS*)-(tetrazol-5-yl)glycine** | 1.7 (98) | 0.52 (97) | 0.49 (89) | 0.099 (78) | 17 |
| **L-CCG-IV** | 0.26 (99) | 0.083 (120) | 0.11 (90) | 0.036 (110) | 7.2 |
| ***trans*-ACBD** | 3.1 (91) | 0.99 (81) | 1.2 (67) | 0.51 (81) | 6.1 |
| ***cis*-ACPD** | 61 (76) | 21 (75) | 22 (49) | 11 (77) | 5.5 |

Data are $EC_{50}$ in μM with relative efficacy given in parentheses (%). Efficacy is given as the current response to a maximally effective concentration of agonist relative to the response to maximally effective concentration of glutamate. All values are from recombinant rat NMDA receptors co-expressed with the GluN1 subunit in *Xenopus laevis* oocytes and activated by agonist plus maximally effective concentration of glycine. All values from Erreger et al. (2007) and are given to 2 significant digits. Abbreviations: L-CCG-IV, (2S,3R,4S)-2-(carboxycyclopropyl)glycine; *trans*-ACBD, trans-1-aminocyclobutane-1,3-dicarboxylate; *cis*-ACPD, (1R,3R)-aminocyclopentane-cis-dicarboxylate.

As with the GluN1 subunit, the identity of the GluN2 subunit determines agonist potencies and relative agonist effectiveness. In general, agonists are least potent at GluN1/GluN2A receptors and most potent at GluN1/GluN2D receptors; GluN2B/C agonists have intermediate potencies (Table 1.3; Kutsuwada et al., 1992; Monyer et al., 1992; Erreger et al., 2007). While glutamate concentrations are thought to reach millimolar concentrations within the synaptic cleft during excitatory transmission, lower concentrations of L-glutamate that remain in the cleft or spill over into extrasynaptic areas may be high enough to activate GluN2D-containing receptors but not GluN2A-containing receptors (Clements et al., 1992; Edmonds et al., 1995; Timmerman and Westerink, 1997; Rusakov and Kullmann, 1998; Mainen et al., 1999; Lozovaya et al., 2004; Harney et al., 2008).

### *1.4.b. NMDA receptor competitive antagonists*

Numerous competitive antagonists for the NMDA receptor GluN2 subunits have been developed. (R)-2-amino-5-phosphonopentanoate (R-AP5 or D-APV) and its analogues commonly are used to isolate NMDA receptor-mediated activity from AMPA and kainate receptor activity in neuronal preparations but show little subunit-selectivity (Davies et al., 1981; Evans et al., 1981; Lester et al., 1990). While some selectivity has been reported for (R)-4-(3-phosphonopropyl) piperazine-2-carboxylic acid (R-CPP), which has ~50-fold higher affinity for GluN2A over GluN2D, intermediate affinities for GluN2B and GluN2C have been observed (Table 1.4; Ikeda et al., 1992; Kutsuwada et al., 1992; Feng et al., 2005). Other competitive antagonists have been developed that have somewhat higher affinity for GluN2C- and GluN2D-containing NMDA receptors, including the

**Table 1.4.** Equilibrium dissociation constants (in μM) for NMDA receptor competitive antagonists

| Competitive Antagonist | GluN2A (μM) | GluN2B (μM) | GluN2C (μM) | GluN2D (μM) | 2A/2D Fold Selectivity |
|---|---|---|---|---|---|
| **(R)-AP5** | 0.28 | 0.46 | 1.6 | 3.7 | 0.076 |
| **(R)-AP7** | 0.49 | 4.1 | 6.4 | 17 | 0.029 |
| **(R)-CPP** | 0.041 | 0.27 | 0.63 | 1.99 | 0.020 |
| **PMPA** | 0.84 | 2.7 | 3.5 | 4.2 | 0.20 |
| **NVP-AAM077** | 0.015 | 0.078 | -- | -- | -- |
| **PPDA** | 0.55 | 0.31 | 0.096 | 0.13 | 4.2 |
| **PBPD** | 16 | 5.0 | 8.9 | 4.3 | 3.7 |
| **UBP141** | 14 | 19 | 4.2 | 2.8 | 5.0 |
| **CGS-19755** | 0.15 | 0.58 | 0.58 | 1.1 | 0.14 |

Data presented as $K_i$ in μM, except NVP-AAM077, which is the $K_b$ and is given in μM. Abbreviations: (R)-AP5, (R)-2-amino-5-phosphonopentanoate; (R)-AP7, (R)-2-amino-7-phosphonopentanoate; PMPA, (RS)-4-(phosphonomethyl)-piperazine-2-carboxylic acid; (R)-CPP, (R)-4-(3-phosphonopropyl) pizerazine-2-carboxylic acid; NVP-AAM077, (R)-[(S)-1-(4-bromo-phenyl)-ethylamino]-(2,3-dioxo-1,2,3,4-tetrahydroquinoxalin-5-yl)-methyl]-phosphonic acid; PPDA, (2S,3R)-1-(phenanthren-2-carbonyl)piperazine-2,3-dicarboxylic acid; PBPD, (2S,3R)-1-(biphenyl-4-carbonyl)piperazine-2,3-dicarboxylic acid; UBP141, (2R,3S)-1-(phenanthrenyl-3-carbonyl)piperazine-2,3-dicarboxylic Acid; CGS-19755, (2R, 4S)-4-(phosphonomethyl)piperidine-2-carboxylic acid. (R)-AP5, (R)-AP7, PMPA, (R)-CPP, and CGS-19755 are from Feng et al., (2005). NVP-AAM077 is from Frizelle et al. (2006). PPDA and PBPD are from Feng et al. (2004). UPB141 is from Morley et al. (2005).

phenanthrene-piperazine dicarboxylic acid analogues PPDA and UBP141, which have 10-fold higher affinity for GluN2C- and GluN2D-containing receptors over GluN2A and GluN2B (Table 1.4; Feng et al., 2004; Feng et al., 2005; Morley et al., 2005; Costa et al., 2010).

While subunit-selective competitive antagonists may be useful to elucidate the roles of individual GluN2 subunits in the brain, homology between the ligand-binding domains of the GluN2 subunits have limited the subunit specificity, which in turn has limited the utility of this class of antagonists as tools (Table 1.1). Thirty-nine residues line the glutamate binding pocket of the GluN2 LBDs, and of these residues, only 8 are divergent between GluN2A and GluN2D (Furukawa et al., 2005; Paoletti and Neyton, 2007; Vance et al., 2011). Indeed, the 10 residues that directly contact glutamate within the binding pocket are conserved across all GluN2 subunits (Furukawa et al., 2005; Kinarsky et al., 2005).

### *1.4.c. NMDA receptor noncompetitive antagonists*

A significant breakthrough in NMDA receptor pharmacology occurred when the phenylethanolamine ifenprodil was found to be a subunit-selective NMDA receptor antagonist (Williams et al., 1993). Ifenprodil is a noncompetitive, voltage-independent antagonist of GluN2B-containing receptors, with maximal inhibition around 90%, and is ~200-fold more potent for GluN2B receptors than GluN2A-, GluN2C-, and GluN2D-containing receptors (Table 1.5; Williams, 1993; Hess et al., 1998). However, ifenprodil appears to be both less potent as well as less efficacious in triheteromeric GluN1/GluN2A/GluN2B (Hatton and Paoletti, 2005) and GluN1/GluN2B/GluN2D

**Table 1.5.** $IC_{50}$ values (in μM) for noncompetitive NMDA receptor antagonists

| Noncompetitive antagonist | GluN2A (μM) | GluN2B (μM) | GluN2C (μM) | GluN2D (μM) | 2A/2D Fold Selectivity |
|---|---|---|---|---|---|
| **Ifenprodil** | 39 | 0.15 | 29 | 76 | 0.51 |
| **Ro 25-6981** | 52 | 0.0090 | -- | -- | -- |
| **CP 101,606** | >100 | 0.039 | >100 | >100 | -- |
| **Eliprodil** | >100 | 3.02 | -- | -- | -- |
| **QNZ46** | 180 | 190 | 7.1 | 3.9 | 46 |
| **DQP-1105** | NE | 113 | 7.0 | 2.7 | -- |

Data are $IC_{50}$ in μM for rat recombinant receptors. NE, <10% inhibition at 300 μM. Data for ifenprodil are from Hess et al. (1998), Ro 25-6981 are from Fischer et al. (1997), CP 101,606 from Mott et al. (1998), eliprodil from Avenet et al. (1997), QNZ46 from Hansen et al. (2011), and DQP-1105 from Acker et al. (2011). Abbreviations: Ro 25-6981, [R-(R*,S*)]-α-(4-hydroxyphenyl)-β-methyl-4-(phenylmethyl)-1-piperidinepropanol hydrochloride; CP 101,606, (S,S)-1-(4-hydroxyphenyl)-2-[4-hydroxy-4-phenylpiperidin-1-yl)-1-propanol methanesulfonate trihydrate, QNZ46, (E)-4-(6-methoxy-2-(3-nitrostyryl)-4-oxoquinazolin-3(4H)-yl)-benzoic acid; DQP-1105, 4-(5-(4-bromophenyl)-3-(6-methyl-2-oxo-4-phenyl-1,2-dihydroquinolin-3-yl)-4,5-dihydro-1*H*-pyrazol-1-yl)-4-oxobutanoic acid.

(Brothwell et al., 2008) NMDA receptors, which may limit its ability to selectively inhibit native GluN2B receptors when in complex with other GluN2 subunits.

Since the identification of ifenprodil as a GluN2B-selective antagonist, more potent ifenprodil derivatives have been identified, including Ro 25-6981 and CP 101,606 (Table 1.5; Gotti et al., 1988; Williams, 1993; Chenard et al., 1995; Fischer et al., 1997; Bardoni et al., 1998; Gill et al., 2002; Barton and White, 2004). Unlike competitive antagonists that bind in a cleft of the ligand-binding domain, ifenprodil and its analogues are thought to bind at the interface of the GluN1 and GluN2B ATDs and may act by stabilizing a state with low open probability (Kew et al., 1996; Fischer et al., 1997; Hansen et al., 2010; Karkaras et al., 2011; Furukawa, 2012). The availability of GluN2B-specific ligands has allowed for a number of studies on the role of this subunit in synaptic activity as well as toxicity. These studies have collectively moved our understanding of the GluN2B subunit far above that of other subunits, especially GluN2C and GluN2D (Dogan et al., 1997; Hoffmann et al., 2000; Nikam and Meltzer, 2002; Neyton and Paoletti, 2006; Zhou and Baudry, 2006; Mony et al., 2009; reviewed in Traynelis et al., 2010).

Although far less progress has been made in the development of subunit-specific antagonists for the GluN2C and GluN2D subunits, a number of new modulators have been described recently that are capable of selectively inhibiting these subunits over GluN2A/B. The allosteric inhibitor QNZ46 is a member of a new class of noncompetitive NMDA receptor antagonists and shows moderate selectivity for GluN2C- and GluN2D-containing NMDA receptors (Mosley et al., 2009; Hansen and Traynelis, 2011). This class, developed on an (E)-3-phenyl-2-styrylquinazolin-4(3H)-one

backbone, exhibits nearly 50-fold selectivity for GluN2C/D-containing NMDA receptors over GluN2A/B (Table 1.5; Mosley et al., 2009; Hansen and Traynelis, 2011). QNZ46 is a voltage-independent, noncompetitive GluN2C/D antagonist that is also use-dependent, as glutamate must be bound to the GluN2 subunit before QNZ46 can act (Hansen and Traynelis, 2011). QNZ46 has unique structural determinants of action, which have been shown to reside in the S2 domain of the GluN2C/D ligand-binding domains, near the transmembrane domain (Hansen and Traynelis, 2011).

The DQP class, represented by DQP-1105, is another recently published novel class of GluN2C/D-containing NMDA receptor inhibitors. This class, although developed on a dihydroquinilone-pyrazoline backbone, is structurally similar to QNZ46 and has a similar mechanism of action and structural determinants (Acker et al., 2011). Like QNZ46, DQP-1105 is a noncompetitive, voltage-independent antagonist, with approximately 50-fold selectivity for GluN2C/D-containing NMDA receptors over GluN2A/B (Table 1.5; Acker et al., 2011). Inhibition by DQP-1105 also is use-dependent, as glutamate must first be bound to the GluN2C/D subunits before the receptor can be inhibited (Acker et al., 2011). DQP-1105 shares similar structural determinants of action with QNZ46, as residues in the S2 domain of the GluN2D ligand-binding domain are required for inhibition (Acker et al, 2011).

QNZ46 and DQP-1105 represent the first published antagonists with nearly 50-fold selectivity for GluN2C/D-containing NMDA receptors over GluN2A/B and may provide an excellent opportunity to evaluate how these subunits contribute to neuronal function. Their use-dependent mechanisms may confer unique therapeutic properties for neurological diseases, such as Parkinson's disease, in which the affected neurons express

GluN2D-containing receptors (Monyer et al., 1994; Standaert et al., 1994; Wenzel et al., 1996), as only overactive receptors would be inhibited (Parsons et al., 1999; Chen and Lipton, 2006; Kotermanski and Johnson, 2009; Kotermanski et al., 2009). In fact, Inhibiting hyperglutamatergic activity has been shown to be beneficial in the treatment of moderate to severe Alzheimer's disease with the use-dependent NMDA receptor antagonist memantine (Reisberg et al., 2003; Chen and Lipton, 2006; Tariot et al., 2006).

### *1.4.d. NMDA receptor uncompetitive antagonists*

Several classes of uncompetitive NMDA receptor channel blockers have been developed and include polyamines, phencyclidine, ketamine, MK-801, and adamantane derivatives. NMDA receptor channel blockers exhibit a range of subunit-selectivities. Aryl-polyamines show some selectivity for GluN2A-containing receptors over GluN2D, with $N^1$-dansyl-spermine showing a 40-fold lower $IC_{50}$ on GluN2A (Chao et al., 1997; Igarashi et al., 1997; Jin et al., 2007). Recent studies on ketamine and memantine suggest selectivity is influenced by physiological concentrations of $Mg^{2+}$, with GluN2C- and GluN2D-containing receptors having 5- to 10-fold selectivity over GluN2A- and GluN2B at 1 mM $Mg^{2+}$ (Table 1.6; Kotermanski and Johnson, 2009). Channel blockers act at distinct but overlapping sites within the NMDA receptor pore, acting on residues within the M1, M3, and M4 transmembrane domains, the M2 reentrant loop, and the pre-M1 region (Yamakura et al., 1993; Yamakura and Shimoji, 1999; Kashiwagi et al., 2002; LePage et al., 2005; Jin et al., 2007). Because these channel blockers have some selectivity for GluN2C/D-containing NMDA receptors at physiological concentrations of magnesium, it is possible that their therapeutic actions may be due to the inhibition of

**Table 1.6.** $IC_{50}$ value (in μM) for uncompetitive NMDA receptor antagonists

| Uncompetitive Antagonist | GluN2A (μM) | GluN2B (μM) | GluN2C (μM) | GluN2D (μM) | 2A/2D Fold Selectivity |
|---|---|---|---|---|---|
| **(+)-MK-801** | 0.015 | 0.009 | 0.024 | 0.038 | 0.39 |
| **(-)-MK-801** | 0.35 | 0.32 | 0.038 | 0.17 | 2.1 |
| **Dextromethorphan** | 11 | 3.7 | 1.1 | 5.4 | 2.0 |
| **Dextrorphan** | 1.3 | 0.33 | 0.15 | 0.74 | 1.8 |
| **Phencyclidine** | 0.82 | 0.16 | 0.16 | 0.22 | 3.7 |
| **Amantadine** | 130 | 70 | 35 | 38 | 3.4 |
| **Memantine** | 0.80 | 0.57 | 0.52 | 0.54 | 1.5 |
| **Memantine –1 mM $Mg^{2+}$** | 13 | 10 | 1.6 | 1.8 | 7.2 |
| **(±)-ketamine** | 0.33 | 0.31 | 0.51 | 0.83 | 0.40 |
| **(±)-ketamine–1 mM $Mg^{2+}$** | 5.4 | 5.08 | 1.2 | 2.9 | 1.9 |

Data are $IC_{50}$ in μM. All values were measured in 0 $Mg^{2+}$, unless otherwise indicated. Values for memantine and (±)-ketamine are from Kotermanski and Johnson (2009). All remaining values are from (Dravid et al. (2007). Abbreviation: MK-801, (5R,10S)-5-methyl-10,11-dihydro-5H-dibenzo[a,d]cyclohepten-5,10-imine.

GluN2C/D-containing NMDA receptors (Kotermanski and Johnson, 2009; Retchless et al., 2012).

### *1.4.e. NMDA receptor allosteric potentiators*

NMDA receptor allosteric modulators have gained interest due to the possibility of having both subunit-selectivity as well as therapeutic potential. A recent study by Mullasseril et al. (2010) evaluated a new class of NMDA receptor positive allosteric modulators that increases the activity of GluN2C- and GluN2D-containing NMDA receptors about 2-fold. The potentiator CIQ (3-chlorophenyl)(6,7-dimethoxy-1-((4-methoxyphenoxy)methyl)-3,4-dihydroisoquinolin-2(1H)-yl)methanone), a substituted tetrahydroisoquinoline, has little to no effect on GluN2A- or GluN2B-containing NMDA receptors, AMPA receptors, or kainate receptors. The molecular determinants of activity for CIQ have been identified as a single residue within the M1 region as well as the linker between the GluN2C/D ATD and S1 region. This modulator acts by approximately doubling the channel open time, independent of glutamate and glycine concentration, voltage, pH, $Mg^{2+}$ concentration, or GluN1 splice variant (Mullasseril et al., 2010).

## 1.5. NMDA receptor channel activation and gating

### *1.5.a. Functional features of NMDA receptor activation*

The four GluN2 subunits control many of the macroscopic and single channel characteristics of the NMDA receptor in which they are expressed. One key feature of the macroscopic current response of NMDA receptors that is controlled by the GluN2 suunit is the deactivation time course following removal of the agonist (Fig. 1.5A).

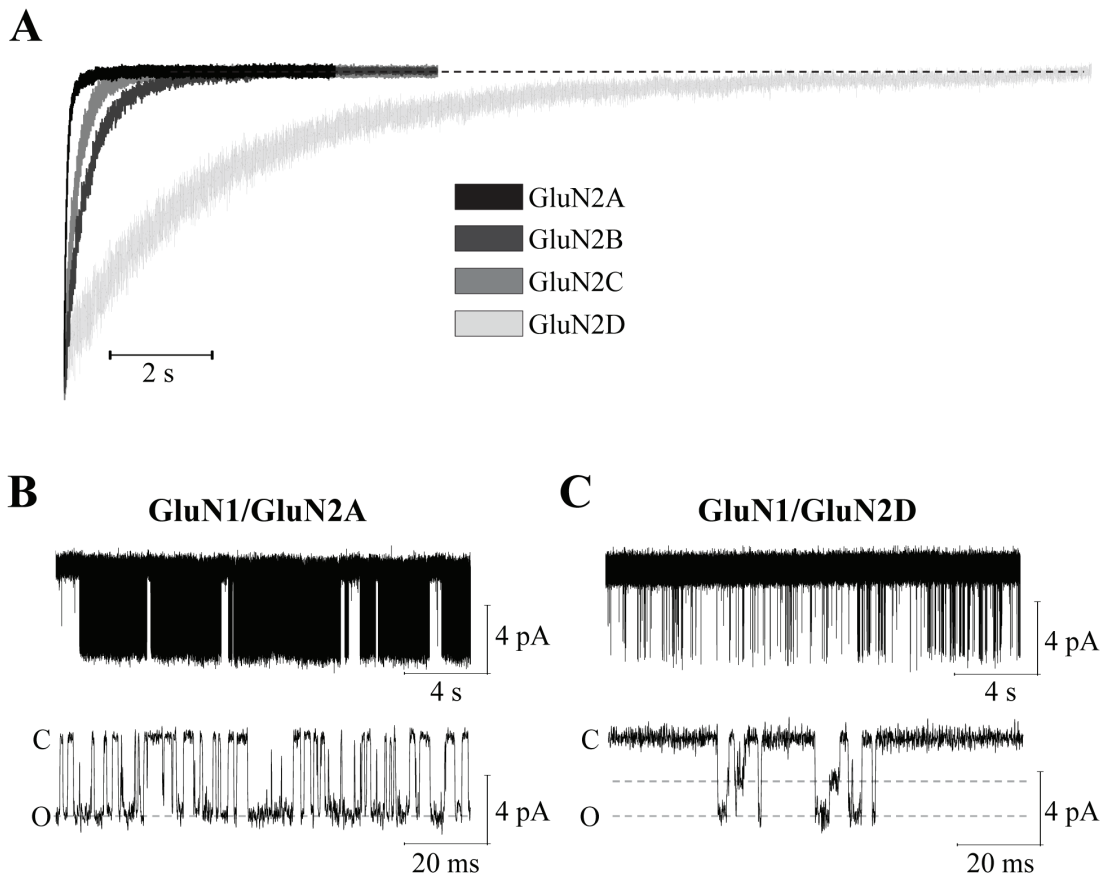


**Figure 1.5.** The GluN2 subunit controls the deactivation time course and single channel open probability of NMDA receptors. ***A***, Normalized currents for GluN1/GluN2A, GluN1/GluN2B, GluN1/GluN2C, and GluN1/GluN2D are given and show the dramatic difference in deactivation time course caused by the four GluN2 subunits. ***B***, A GluN1/GluN2A single channel recording shows high open probability and only one conductance level at pH 8.0 and 0.5 mM $Ca^{2+}$ when activated by 1 mM L-glutamate and 0.05 mM glycine. ***C***, A GluN1/GluN2D single channel recorded at pH 8.0 with 0.5 mM $Ca^{2+}$ and activated by 1 mM glutamate and 0.05 mM glycine shows very low open probability and two conductance levels (Vance and Traynelis, unpublished data).

GluN2A-containing receptors deactivate more rapidly than any other GluN2 subunit, with dual exponential deactivation time constants around 40 and 400 ms (Table 1.7; Figure 1.5; Monyer et al., 1994; Vicini et al., 1998; Erreger et al., 2005a; Zhang et al., 2008; Vance et al., 2011). GluN2D-containing NMDA receptors have the slowest deactivation time course, with dual exponential deactivation time constants of approximately 1000 and 4400 ms (Table 1.7; Figure 1.5; Vicini et al., 1998; Wyllie et al., 1998; Vance et al., 2011; Vance et al., 2012). GluN2B- and GluN2C-containing NMDA receptors have intermediate deactivation time constants (Table 1.7; Figure 1.5; Monyer et al., 1994; Vicini et al., 1998; Rumbaugh et al., 2000; Erreger et al., 2005a; Dravid et al., 2008). As AMPA receptors deactivate and desensitize more rapidly than NMDA receptors (Mosbacher et al., 1994; Edmonds et al., 1995; Erreger et al, 2004; Traynelis et al., 2010), it is the deactivation time course of NMDA receptors that determines the time course of excitatory postsynaptic currents (EPSCs; Lester et al., 1990; Clements et al., 1992; Edmonds et al., 1995). Therefore, the deactivation time course of EPSCs may vary greatly according to which GluN2 subunits are expressed at the synapse, giving rise to the possibility that synapses in which the GluN2D subunit is expressed have a slower deactivation time course than synapses in which the GluN2A subunit is predominant (Lozovaya et al., 2004; Brothwell et al., 2008; Harney et al., 2008).

Desensitization, another important characteristic of the NMDA receptor macroscopic current, also is dependent upon the GluN2 subunit assembled within the receptor. While AMPA receptors desensitize by more than 90% in fewer than 20 ms after activation (Mosbacher et al., 1994; Edmonds et al., 1995; Traynelis et al., 2010), NMDA receptors

**Table 1.7.** Activation characteristics of NMDA receptors

| GluN2 Subunit | $\tau_{Deactivation}$ (ms) | $\tau$ Desensitization (ms) | $P_{OPEN}$ |
|---|---|---|---|
| **GluN2A** | 22-38; 330-400[a-d] | 390-750[a] | 0.36 - 0.50[c,h,i] |
| **GluN2B** | 71-95; 540-620[a,e] | 100-450[e] | 0.07 - 0.17[e,i] |
| **GluN2C** | 260-380[a,f] | 59-720[f] | 0.01[f] |
| **GluN2D** | 930-1700; 3400-4400[a,b,d,g] | N/A | 0.01-0.04[c,g,j] |

The $\tau_{Deactivation}$ is dual exponential for all GluN2 subunits except GluN2C. N/A denotes not applicable.
[a]Vicini et al. (1998); [b]Monyer et al. (1994); [c]Yuan et al. (2009); [d]Vance et al. (2011); [e]Banke and Traynelis (2003); [f]Dravid et al. (2008); [g]Wyllie et al. (1998); [h]Popescu and Auerbach (2003); [i]Erreger et al. (2005a); [j]Vance et al. (2012)

have slower and less pronounced desensitization. NMDA receptor desensitization has several causes, including $Ca^{2+}$-dependent inactivation (Legendre et al., 1993; Vyklický, 1993), glycine-dependent desensitization (Mayer et al., 1989; Benveniste et al., 1990; Lester et al., 1993), and $Ca^{2+}$/glycine-independent desensitization (Hu and Zheng, 2005; Sessoms-Sikes et al., 2005), although the mechanisms controlling these forms of desensitization are not yet known. GluN2A- and GluN2B-containing NMDA receptors show the most desensitization, while GluN2C- and GluN2D-containing NMDA receptors have little to no desensitization (Table 1.7; Vicini et al., 1998; Nahum-Levy et al., 2001; Krupp et al., 2002; Banke and Traynelis, 2003; Dravid et al., 2008; Vance et al., 2011; Vance et al., 2012).

The single channel properties of NMDA receptors also vary greatly according to the GluN2 subunit expressed within the receptor. Channel open probability is highly dependent upon GluN2 subunit, as GluN2A-containing NMDA receptors have an open probability that can approach 0.5, while GluN2D-containing receptors have open probabilities near 0.02 (Table 1.7; Figure 1.5; Stern et al., 1992; Wyllie et al., 1998; Popescu and Auerbach, 2003; Erreger et al., 2005a; Schorge et al., 2005; Yuan et al., 2009; Vance et al., 2012). Another important single channel characteristic is the presence of subconductance levels in GluN2C- and GluN2D-containing NMDA receptors that are not observed at low calcium concentrations in GluN2A- and GluN2B-containing NMDA receptors (Fig. 1.5; Stern et al., 1992; Wyllie et al., 1998; Banke and Traynelis, 2003; Erreger et al., 2005a; Dravid et al., 2008; Vance et al., 2012). Recently, a single residue within the M3 transmembrane domain, GluN2D Leu657, was found to control the GluN2D subconductance level (Retchless et al., 2012).

The activation properties of GluN2D-containing NMDA receptors often are used to identify the subunit in a neuron. Because subunit-selective ligands or modulators for GluN2D have only recently become available, the low open probability and lower conductance level of GluN2D receptors have been used to determine if the GluN2D subunit is expressed in neurons of the substantia nigra (Jones and Gibb; 2005), cerebellar Golgi cells (Brickley et al., 2003), and cerebellar Purkinje cells (Momiyama et al., 1996). Additionally, the slow deactivation time course following removal of L-glutamate has also been used to identify the GluN2D subunit in the brain (Misra et al., 2000b; Lozovaya et al., 2004; Brothwell et al., 2008; Harney et al., 2008).

### *1.5.b. Conceptual models of NMDA receptor gating*

In the last twenty years, multiple conceptual gating models have been proposed to describe NMDA receptor gating. The first gating scheme, published by Lester and Jahr (1992), was a simple model containing two binding steps, a desensitized state, and a single open state (Fig. 1.6; Lester and Jahr, 1992). This straightforward model, while not used to predict single channel behavior, was the first gating scheme able to describe macroscopic NMDA receptor data in patches pulled from hippocampal cultures and activated by L-glutamate or other ligands of lower affinity (Lester and Jahr, 1992). This model was groundbreaking for two important reasons. First, it was the first to describe how NMDA receptor deactivation is controlled by both ligand unbinding as well as return from the desensitized state. Second, and more importantly, the model suggested that NMDA receptor deactivation following removal of L-glutamate controlled the time course of synaptic currents (Lester et al., 1990; Clements et al.,1992; Lester and Jahr,

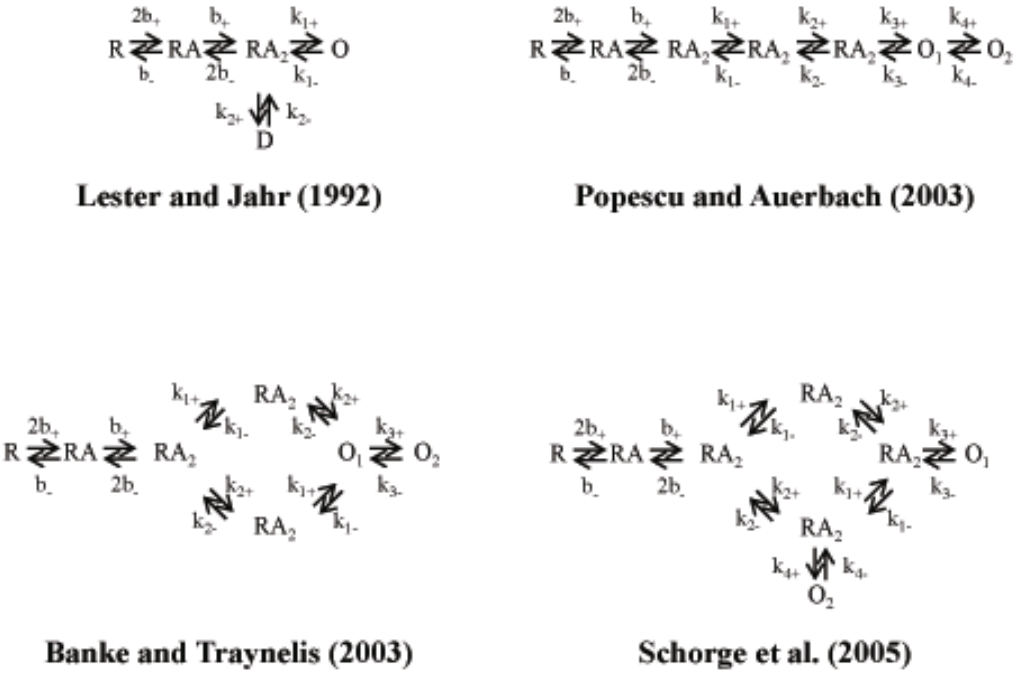


**Figure 1.6.** Conceptual models of NMDA receptor gating. The Lester and Jahr model was the first to describe the deactivation time course of glutamate-activated NMDA receptors in patches pulled from hippocampal cultures (Lester and Jahr, 1992). The Popescu and Auerbach (2003) model was an expansion of the Lester and Jahr model and included two additional closed gating steps. The Banke and Traynelis (2003) gating scheme was a cyclic model used to evaluate the individual contributions of the GluN1 and GluN2B subunits to channel gating. The Schorge gating scheme had nonadjacent open states that could predict the correlation between open times and adjacent shut durations (Schorge et al., 2005).

1992; Edmonds et al., 1995).

While the Lester and Jahr model was a major advance in the NMDA receptor gating field, the model has a number of limitations. First, the model only incorporates binding steps for the GluN2 subunit agonist, while NMDA receptors must bind agonist to both the GluN1 and the GluN2 subunits to activate (Johnson and Ascher, 1987; Kleckner and Dingledine, 1988). Second, the model only contains one desensitized state and another closed state in which the ligand is bound to both GluN2 subunits but the channel is not open. While this is adequate to describe NMDA receptor macroscopic currents, this model does not predict enough shut or open states to describe the multiple time components observed in histograms of open and shut times derived from single channel recordings (Popescu and Auerbach, 2003; Banke and Traynelis, 2003; Erreger et al., 2005a; Schorge et al., 2005; Dravid et al., 2008; Kussius and Popescu, 2009; Vance et al., 2012).

Since Lester and Jahr proposed the first gating model of NMDA receptor activation, other models of increasing complexity have been developed. An expansion of the Lester and Jahr model, containing three shut states, an additional desensitized state, and an additional open state has been used to describe GluN1/GluN2A and GluN1/GluN2B receptor macroscopic and single channel recordings (Fig. 1.6; Popescu and Auerbach, 2003; Erreger et al., 2005a; Kussius and Popescu, 2009; Amico-Ruvio and Popescu, 2010). While this model still only includes binding steps for the GluN2 agonist, the additional shut components improve the model's ability to predict NMDA receptor single channel records. In addition, the linear arrangement of the model is adequate in predicting the macroscopic current rise times of GluN2A and GluN2B, NMDA receptors

with relatively high channel open probability (Popescu and Auerbach, 2003; Erreger et al., 2005a; Kussius and Popescu, 2009; Amico-Ruvio and Popescu, 2010). This linear model does have limitations, as it does not predict the correlations that are present between the open time and adjacent shut periods in GluN1/GluN2A receptors (Schorge et al., 2005). The model also cannot predict the rapid rise times of the low open probability GluN2C and GluN2D receptors, as the forward rates must be too slow to drive down open probability (Dravid et al., 2008; Vance et al., 2012).

Banke and Traynelis (2003) developed a cyclic gating model for GluN1/GluN2B receptors with a two-step activation process that attempted to describe structurally what occurs during NMDA receptor activation (Fig. 1.6). Using GluN1 and GluN2 subunit partial agonists, the authors identified the specific gating steps controlled by each subunit (Banke and Traynelis, 2003). The authors hypothesized that each subunit undergoes a conformational change that leads to pore dilation and channel opening, with the "fast" gating step controlled by the GluN1 subunit, and the "slow" step controlled by the GluN2 subunit (Banke and Traynelis, 2003). A similar model later was published by Auerbach and Zhou (2005) in which the NMDA receptor also activates through a dual pathway mechanism, although the authors did not attempt to define which subunits mediate the gating steps (Auerbach and Zhou, 2005).

A cyclic model developed in David Colquhoun's lab attempted to improve upon models previously published to describe NMDA receptor gating using single channel and macroscopic GluN1/GluN2A recordings (Fig. 1.6). Rather than have two connected open states, the model has two open states separated by two shut states (Schorge et al., 2005). This separation of the open states allows the model to predict the correlations between

open times and adjacent shut times, which could not be predicted using other published models. The model also incorporated binding steps for both GluN1 and GluN2 agonists, which would allow it to better predict the time course of EPSCs in which the NMDA receptors are not already saturated by glycine (Berger et al., 1998; Martina et al., 2004). While this model was developed on the assumption that NMDA receptors are assembled as a dimer of two GluN1 subunits and a dimer of two GluN2 subunits, the scheme would be the same if the receptor was comprised of two GluN1-GluN2 dimers (Schorge et al., 2005).

Although a number of models have been developed for NMDA receptor gating, the models were developed for specific GluN2 subunits. As of yet, no model has been described that can predict the single channel and macroscopic behavior of every GluN2 subunit. However, due to the pronounced differences conferred upon the NMDA receptor by the individual GluN2 subunits, it is possible that a single model may not be able to describe gating by each GluN2 subunit.

### 1.6. Neuronal GluN2D-containing NMDA receptors

GluN2D subunit expression is regulated both temporally and according to brain region. The GluN1, GluN2B, and GluN2D subunits are the only detectable NMDA receptor subunits in embryonic brains and predominate over the GluN2A and GluN2C subunits early in postnatal development (Monyer et al., 1994; Standaert et al., 1994; Wenzel et al., 1996). Later, the GluN2A and GluN2C subunits become the more abundant GluN2 subunits in most regions of the adult brain (Monyer et al., 1994; Standaert et al., 1994; Wenzel et al., 1996; Goebel and Poosch, 1999). GluN2D subunit

expression reaches its peak in the developing rat brain around postnatal day 7, after which expression drops in most regions of the brain to adult levels (Monyer et al., 1994). Although GluN2D subunit expression is limited in adult brains, the subunit still can be found at relatively high levels within the basal ganglia in the subthalamic nucleus (STN), substantia nigra, the globus pallidus, thalamus, nucleus accumbens, and striatum (Monyer et al., 1994; Standaert et al., 1994; Wenzel et al., 1996). The GluN2D subunit also is expressed in the dentate gyrus, hippocampal basket cells, and is commonly found in interneurons, including hippocampal interneurons of the hilar region, stratum oriens, and stratum radiatum (Monyer et al., 1994; Standaert et al., 1996), as well as in striatal and neocortex interneurons (Standaert et al., 1996).

The characteristics of native NMDA receptors containing the GluN2D subunit and the role the GluN2D subunit in the brain have not been evaluated as thoroughly as for other GluN2 subunits. Single channel recordings in patches pulled from the soma of neurons expressing native GluN2D-containing receptors show the two conductance levels observed in recombinantly expressed GluN1/GluN2D receptors (39-44 pS and 18-20 pS), suggesting that native GluN2D receptors retain this distinguishing characteristic (Misra et al., 2000a; Momiyama, 2000; Brickley et al., 2003; Jones and Gibb, 2005; Renzi et al., 2007; Brothwell et al., 2008). Likewise, a slow deactivation time course of approximately 3000 ms has been observed in cerebellar Purkinje cells (Misra et al., 2000b), similar to the slow deactivation time course observed for recombinant GluN1/GluN2D receptors (Vicini et al., 1998; Wyllie et al., 1998; Vance et al., 2011; Vance et al., 2012).

Due to a lack of subunit-selective pharmacological tools for the GluN2D subunit,

evidence of synaptic GluN2D is lacking. However, Brothwell and colleagues found that EPSCs in the rat substantia nigra pars compacta are not fully inhibited by ifenprodil and can be partially inhibited by UBP141, a 5-fold selective antagonist for GluN2D-containing receptors (see Section 1.4.b and Table 1.4; Brothwell et al., 2008). Because of the relatively rapid deactivation time course of the EPSC, the authors proposed that GluN2D was assembled in triheteromeric receptors containing GluN1 and GluN2B subunits (Brothwell et al., 2008). Additionally, Harney et al. (2008) suggest that the GluN2D subunit is located extrasynaptically in the dentate gyrus but moves into the synapse during LTP (Harney et al., 2008). These studies suggest that the GluN2D subunit has a role in the synaptic activity of certain neurons in the brain, but more work remains on the role of the GluN2D subunit in other regions of the brain in which it is expressed. A GluN2D knockout mouse has been developed and evaluated for several behavioral phenotypes (Ikeda et al, 1995). In an open field test, the GluN2D knockout mice show significantly reduced spontaneous activity but no difference in exploratory behavior or novelty preference compared to wild-type mice (Ikeda et al., 1995).

The GluN2D subunit has properties and localizations to imply that it plays critical roles in the brain. If structural concepts can be used to understand profound functional differences, there is an opportunity to make significant headway in understanding how this class of receptor works. In addition, if subunit-selective modulators can be developed, these could be used to understand the role of GluN2D in circuit function, normal brain processes, and neurological diseases. The goal of this study was first to evaluate the mechanisms that control GluN1/GluN2D NMDA receptor function, and second to evaluate how GluN2D-containing NMDA receptors contribute to the synaptic

currents of the subthalamic nucleus. In this thesis, I will evaluate the mechanisms by which the GluN2D ligand-binding domain and GluN1 amino-terminal domain control the properties of GluN2D-containing NMDA receptors using two-electrode voltage clamp recordings from *Xenopus* oocytes as well as whole cell and single channel voltage-clamp recordings of recombinant NMDA receptors. I will determine how GluN1/GluN2D receptors are modulated by inhibitors and a novel potentiator developed in the Traynelis and Liotta labs. Finally, I will study the role the GluN2D receptor has in the synaptic activity of the STN by evaluating how inhibitors or potentiators influence agonist-evoked currents as well as evoked excitatory postsynaptic currents of the subthalamic nucleus.

# Chapter 2: Methods

## 2.1. Molecular biology

cDNAs for the recombinant rat wild type NMDA receptor subunits GluN2A (GenBank D13211), GluN2B (GenBank U11419), GluN2C (GenBank Q00961), and GluN2D (GenBank L31611) were used for electrophysiological recordings. Constructs encoding rat GluN2A and GluN2D chimeras and point mutants were developed as previously described (Chen et al., 2008; Yuan et al., 2009). GluN1 splice variants used were GluN1-1a (GenBank U11418, U08261), GluN1-1b (GenBank U08263), GluN1-2a (GenBank U08262), GluN1-2b (GenBank U08264), GluN1-3a (GenBank U08265), GluN1-3b (GenBank U08266), GluN1-4a (GenBank U08267), and GluN1-4b (GenBank U08268). All wild type, chimeric, and point mutant receptors were verified by DNA sequencing.

## 2.2. Two-electrode voltage-clamp recordings

Preparation and injection of cRNAs encoding the NMDA receptor subunits into *Xenopus laevis* oocytes as well as all two-electrode voltage-clamp recordings were performed as previously described (Traynelis et al., 1998). Briefly, oocytes were stored at 15ºC in Barth's culture bath containing (in mM) 88 NaCl, 5 Tris-HCl, 2.4 $NaHCO_3$, 1 KCl, 0.82 $MgSO_4$, 0.41 $CaCl_2$, and 0.33 $Ca(NO_3)_2$ at pH 7.4. Oocytes were injected with 5-10 ng cRNAs synthesized *in vitro* from linearized template cDNA at a ratio of 1 GluN1 subunit to 2 GluN2 subunits. Recordings were performed 2-4 days post-injection at 23ºC (room temperature). The external bath solution contained (in mM) 90 NaCl, 10 HEPES, 1 KCl, 0.5 $BaCl_2$, and 0.01 EDTA at pH 7.4. Voltage electrodes were filled with 0.3 M

KCl, and current electrodes contained 3 M KCl. Current responses were recorded at a holding potential of -30 to -60 mV. Voltage control and data acquisition were controlled with a two-electrode voltage-clamp amplifier (OC725, Warner Instruments), and an 8-modular valve positioner (Digital MVP Valve) controlled solution exchange. Recording solutions were prepared in external bath solution.

### 2.3. Cell culture

Human embryonic kidney-293 cell line (CRL 1573; ATCC, Rockville, MD, USA; hereafter HEK 293) were plated on 5 mm diameter glass coverslips (Warner Instruments, Hamden, CT) coated in 100 μg/mL poly-D-lysine and were maintained in 5% humidified $CO_2$ at 37ºC in DMEM with Glutamax (Dulbecco's Modified Eagle Medium Cat. No. 11960; Invitrogen) supplemented with 10% fetal bovine serum, 10 units/ml penicillin, and 10 μg/ml streptomycin. HEK 293 cells were transiently transfected using the Fugene6 transfection reagent (Roche Diagnostics) with cDNA encoding green fluorescent protein (GFP), GluN1, and GluN2 subunit at a ratio of 1:1:1 for 0.5 μg/well total cDNA, as previously described (Yuan et al., 2009). Following transfection, cells were incubated in media supplemented with NMDA receptor antagonists D,L-2-amino-5-phosphonovalerate (200 μM) and 7-chlorokynurenic acid (200 μM).

### 2.4. Electrophysiology

Voltage-clamp recordings were made from outside-out patches excised from transfected HEK 293 cells ($V_{HOLD}$ = -80 mV), cell-attached patches ($V_{HOLD}$ = +80 mV), or whole cells lifted from the bottom of a coverslip ($V_{HOLD}$ = -60 mV). Current

recordings were made using an Axopatch 200B amplifier (Molecular Devices, Union City, CA) and digitized using Axon pClamp10 software. Single channel and macroscopic recordings were filtered at 8 kHz using an eight-pole Bessel filter (-3 dB; Frequency Devices) and digitized at 40 kHz. Thick-walled (World Precision Instruments) or thin-walled (Warner Instruments) borosilicate glass was used to form recording electrodes for single channel or whole cell patch recordings, respectively. Electrodes for whole cell and outside-out patch recordings were filled with an internal solution containing (in mM) 110 Cs-gluconate, 30 CsCl, 5 HEPES, 4 NaCl, 0.5 $CaCl_2$, 2 $MgCl_2$, 5 BAPTA, 2 $Na_2ATP$, and 0.3 NaGTP (pH 7.35). For cell-attached single channel recordings, the internal solution was comprised of (in mM) 150 NaCl, 10 HEPES, 30 D-mannitol, 3 KCl, 0.5 $CaCl_2$, 0.01 EDTA, 1 L-glutamate, and 0.05 glycine at pH 8.0. Cells were bathed at 23ºC in external solution that contained (in mM) 150 NaCl, 10 HEPES, 30 D-mannitol, 3 KCl, 0.5 $CaCl_2$, and 0.01 EDTA at pH 8.0. For whole cell macroscopic and outside-out single channel recordings, the recording solution was comprised of external solution with 0.05 mM glycine and 1 mM L-glutamate at pH 8.0. Rapid solution exchange for macroscopic recordings was performed using a two-barrel theta glass pipette controlled by a piezoelectric translator (Burleigh Instruments). The open tip 10 to 90% rise time of the solution exchange time course was under 0.6 ms; tips were not used if the rise time was slower than 1 ms. Solution exchange time (10 to 90%) around a whole cell was 3.30 $\pm$ 0.48 ms (n=7 ms) and was determined as previously described (Vance et al., 2011).

**2.5. Single channel analysis**

Single channel recordings were analyzed as previously described (Vance et al., 2012) and were determined to have one functional NMDA receptor when no double openings were observed through the duration of the recording. I used the following approximation of Colquhoun and Hawkes (1990) to determine whether a patch contains a single active channel when no double openings were observed:

$$E_r = (2/P_{o2})(100.5P_{o2} - 0.75P_{o2}^2), \quad (1)$$

where $E_r$ is the mean number of consecutive openings in a run, and $P_{o2}$ is the probability that a channel is open during an observed run of single openings that originate from two individual channels. This method previously has been confirmed to apply to NMDA receptor channels with a very low open probability (Dravid *et al.*, 2008), and only patches with a probability of $p > 0.001$ for containing only one active channel (i.e. probability of <0.001 that a patch had 2 or more channels) were used for data analysis.

Idealization of single channel records was performed using the time course fitting method (SCAN), for which each transition between open and closed states is fitted with a filtered step response function. Dwell time and amplitude histograms were analyzed using maximum likelihood fitting (EKDIST; www.ucl.ac.uk/Pharmacology/dcpr95.html). Adjacent open periods with different amplitudes were combined. A 53 μs open resolution and 31 μs shut resolution were imposed on the data record (Colquhoun and Hawkes, 1990). Both resolution values were calculated based on the filter rise time ($\tau_F$), with the open resolution equal to $0.54*\tau_F$, and the shut resolution equal to $0.31*\tau_F$. Fitted single channel unitary current amplitudes ranging from 0.0 to 8.0 pA were used to construct open-point amplitude histograms, which could be fitted best by the sum of two Gaussians components; addition of a third component did not improve the maximum log

likelihood by more than 10 units, my threshold for an improvement on the quality of a fit. To determine the transitions between amplitudes, amplitudes were assigned to the higher or lower amplitude level when they were within one standard deviation of the mean value for each level.

I evaluated my single channel data for correlations between successive open durations using the runs test (Colquhoun and Sakmann, 1985). Briefly, the runs test is used to determine randomness of data in a sequence. Open periods were separated into brief and long openings using a $T_{crit}$ determined as previously described (Jackson et al., 1983). In the runs test, the openings shorter than the $T_{crit}$ were assigned a value of 0, while the longer openings were assigned a value of 1. A run is defined as a series consisting entirely of one or more brief or long openings, with a total of $n_0$ values designated as 0 and $n_1$ values designated as 1 in the full data record, while the total number of openings in the data record is $n_0 + n_1 = n$. If the openings occur at random, the mean and variance of the number of runs ($T$) will be:

$$\text{Mean}\ (T) = [(2n_0n_1) / n] + 1 \tag{2}$$

$$\text{Var}\ (T) = [(2n_0n_1)(2n_0n_1 - n)] / [n^2\ (n - 1)] \tag{3}$$

The test statistic, z, has a zero mean and unit standard deviation if the open durations lengths are occurring at random and can be defined as

$$z = [T - \text{Mean}(T)] / [\text{var}(T)]^{1/2} \tag{4}$$

and would have an absolute value greater than 2 if not random (Colquhoun and Sakmann, 1985).

Single channel records idealized by time course fitting were converted to a QUB-compatible format (www.qub.buffalo.edu) to allow fitting of gating models to the data

using maximum interval likelihood fitting (MIL), in which a hypothetical gating scheme was fit to the sequence of open and closed durations (Qin et al., 1997). Conversion to the QUB-compatible format eliminated information on the amplitude levels of the openings, so the amplitudes of the openings were assumed to be equal (see Appendix B). Because QUB only allows a single resolution value, a 50 μs resolution was imposed during maximum likelihood fitting on the data records, and gating schemes were constrained to obey microscopic reversibility. The random model generating feature of the QUB software was used to produce potential kinetic schemes for my data. The search allowed for three to four closed states with one or two open states. The software was allowed to generate linear or cyclic schemes while maintaining microscopic reversibility. The gating schemes then were evaluated using their log likelihood values and predicted macroscopic current characteristics.

### 2.6. Analysis of macroscopic recordings and concentration-response curves

Macroscopic current recordings were analyzed as described in Vance et al. (2011) and Vance et al. (2012). For each experimental condition, the individual sweeps of current recordings conducted under voltage-clamp were averaged and pre-application baseline subtracted. Current amplitude, the 10 to 90% rise time of peak amplitude, and deactivation time constant were determined using ChanneLab. The deactivation time constant was calculated by fitting the following equation to the data:

$$Response = Amp_{FAST} \exp(-time / \tau_{FAST}) + Amp_{SLOW} \exp(-time / \tau_{SLOW}) \quad (5)$$

where $\tau_{FAST}$ is the fast deactivation time constant, $\tau_{SLOW}$ is the slow deactivation time constant, $Amp_{FAST}$ is the current amplitude of the fast deactivation component, and

$Amp_{SLOW}$ is the current amplitude of the slow deactivation component. Weighted deactivation time constants ($\tau_W$) were calculated using the following equation:

$$\tau_W = \{ [Amp_{FAST} / (Amp_{FAST} + Amp_{SLOW}) ] \tau_{FAST} \} + \{ [Amp_{SLOW} / (Amp_{FAST} + Amp_{SLOW}) ] \tau_{SLOW} \} \quad (6)$$

Concentration-response curves for were fitted with the Hill equation:

$$Percent\ current\ response = 100 / (1 + ( EC_{50} / [ Agonist ] )^n ), \quad (7)$$

where $EC_{50}$ is the agonist concentration that produces a half-maximal effect, and *n* is the Hill coefficient.

The concentration-response curve for CIQ was fit with the following equation:

$$Percent\ response\ (\%\ Control) = (\text{Maximal potentiation - 100 / } (1 + ( EC_{50} / [ CIQ ] )^n ) + 100, \quad (8)$$

where $EC_{50}$ is the CIQ concentration that produces a half-maximal effect, and *n* is the Hill coefficient.

Macroscopic response waveforms obtained from excised outside-out patches and whole cell recordings were used to determine the binding and unbinding rate constants for the NMDA receptor gating schemes. No differences were observed in rise times or deactivation time courses between macroscopic patches and whole cell recordings of the same receptor, so both were used in the determination of the binding and unbinding rate constants. Macroscopic responses to high and low glutamate concentrations for both long and short durations of agonist applications were normalized, aligned, and averaged for each condition and then normalized again to the average maximum open probability of the receptor determined from the excised single channel recordings. A nonlinear least squares fitting algorithm was used to simultaneously fit models to waveforms from each

recording condition. A Runge-Kutta numerical integrator was used to simulate each response waveform for the macroscopic fits using the same rate constants. During the fitting of models to the macroscopic response time course, rate constants obtained from the single channel MIL fits were held constant, and only the binding and unbinding rate constants were allowed to vary. Following the fitting of *Scheme 5* (see Chapter 5; Fig. 5.3) to the macroscopic response time course, I repeated the maximum interval likelihood fitting of the model to my single channel data, holding the binding rate constant and allowing the remaining rate constants (including the unbinding rate) to vary. The rate constants obtained from the original MIL fit did not significantly change even though a new exit rate was present in the model.

Relative $P_{OPEN}$ was estimated for chimeric receptors and point mutants by analyzing the time course for the onset of MK-801 inhibition, as previously described (Blanke and VanDongen, 2008). Briefly, the rate of onset of MK-801 inhibition was calculated using the following equation:

$$\text{Block rate}_{\text{MK-801}} = 1 / \tau_{\text{MK-801}} \quad (9)$$

where $\tau_{\text{MK-801}}$ is the time constant describing the onset of MK-801 block. $\tau_{\text{MK-801 block}}$ was calculated using the single-exponential equation

$$\textit{Response} = \textit{Amp} \exp(-\text{time} / \tau_{\text{MK-801}}) + \textit{steady-state} \quad (10)$$

where *Amp* is the amplitude of the current response and *steady-state* describes the steady-state current observed in the presence of incomplete MK801 block. Open probability ($P_{OPEN}$) for the chimeric receptors and point mutants were calculated from wild type receptor open probability (determined by dividing the total open time by the total recording time of GluN1/GluN2A or GluN1/GluN2D single channel recordings) and the

block rate of MK-801 using the following equation:

$$P_{OPEN\ (MUT)} = P_{OPEN\ (WT)} \left( \tau_{MK\text{-}801\ (WT)} / \tau_{MK\text{-}801\ (MUT)} \right) \quad (11)$$

where GluN2A $P_{OPEN}$ was 0.48, and GluN2D $P_{OPEN}$ was 0.012, determined from single channel data (Yuan et al., 2009).

The time course of inhibition of a drug during co-application with glycine and L-glutamate could be described by $\tau_{ONSET}$, a single exponential function determined using equation 5. The dissociation constant, $K_D$, of DQP-1105 and 997-33 was calculated by plotting $1 / \tau_{ONSET}$ versus drug concentration. Linear regression analysis was calculated using the following formula:

$$1 / \tau_{ONSET} = k_{on} [\text{drug}] + k_{off}, \quad (12)$$

where $k_{on}$ is the slope of the line and represents the association rate of the compound, $k_{off}$ is the y-intercept of the line and represents the dissociation rate, and [drug] is the concentration of the compound.

The dissociation constant can be calculated using the following forumula:

$$K_d = k_{off} / k_{on}. \quad (13)$$

**2.7. Patch clamp recording from neurons in thin slices**

Rats (Sprague-Dawley, age P11 to P18) were anaesthetized using isoflurane, decapitated, and the brain was hemisected and glued to the stage of a vibrating microtome (Leica VT1000S). Sagittal brain slices (250 μm; Fig. 2.1) were cut in cold artificial cerebrospinal fluid (ACSF) composed of (in mM) 130 NaCl, 24 $NaHCO_3$, 10 glucose, 3 KCl, 3 $MgSO_4$, 1.25 $NaH_2PO_4$, and 1 $CaCl_2$ and incubated at room temperature in the same solution for at least one hour before use. Slices containing the

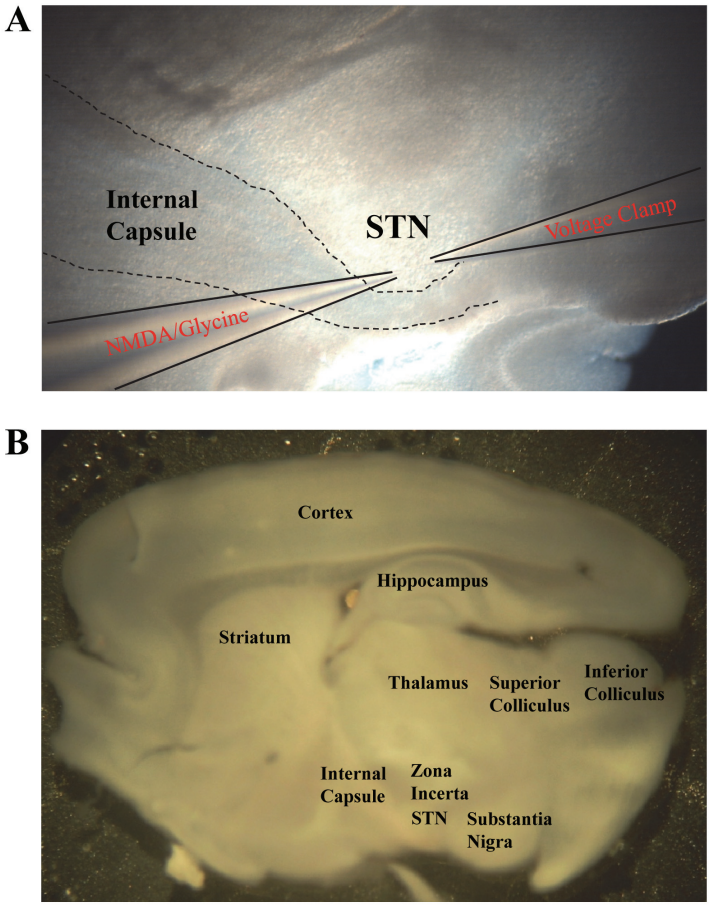


**Figure 2.1.** An example of a slice containing the subthalamic nucleus (***A***). Currents were evoked by pressure application of NMDA and glycine onto the rat brain slice near the STN neuron being held under voltage-clamp. A bipolar stimulating electrode was placed in the STN near the internal capsule to evoke excitatory postsynaptic currents from afferents projecting from the cortex, thalamus, and pedunculopontine nuclues. ***B***, A rat brain slice containing the subthalamic nucleus also contains the cortex, hippocampus, substantia nigra, striatum, and zona incerta, among other brain regions (Paxinos and Watson, 1998).

subthalamic nucleus were placed in the recording chamber of an upright microscope for whole cell voltage-clamp recordings (Fig. 2.1). Slices were perfused with aCSF comprised of (in mM) 130 NaCl, 24 $NaHCO_3$, 10 glucose, 3 KCl, 0.2-1.5 $MgSO_4$, 1.5-3 $CaCl_2$, and 1.25 $NaH_2PO_4$ saturated with 95%$O_2$ / 5% $CO_2$ (23$^oC$). During the picospritzer recordings, the external solution also contained 0.5 μM TTX, 10 μM bicuculline, and 5 μM nimodipine (Lee et al., 2007). Evoked EPSCs were conducted using the external solution described above supplemented with 10 μM bicuculline and 10 μM glycine. Voltage-clamp recordings were performed at -60 mV or +40 mV, filtered at 5 kHz, and digitized at 20 kHz. Patch recording electrodes were filled with (in mM) 120 Cs-methanesulfonate, 15 CsCl, 10 tetraethylammonim chloride, 10 HEPES, 8 NaCl, 3 Mg-ATP, 1.5 $MgCl_2$, 0.3 Na-GTP, and 0.2 EGTA at pH 7.3 (Guzman et al., 2009). The internal solution also contained 1 mM QX-314 for all of the picospritzer recordings.

Currents were evoked by the picospritzer when NMDA (1-2 mM) and glycine (0.003-0.5 mM) were pressure-applied through a borosilicate capillary tube (3.5 MOhm) in brief pulses (4-12 psi; 3-100 ms) using a Picospritzer II (Parker Hannifin Corp). After 3-10 stable measurements were obtained in the presence of the control solution at 90 second intervals, the NMDA receptor modulator (3-100 μM, prepared in recording solution) or vehicle was bath applied for 10-15 min. Current responses evoked by pressure application of NMDA and glycine were compared to currents obtained during application of control aCSF. Following bath application of the modulator, the slice was washed with the control recording solution and NMDA and glycine continued to be pressure applied at 90 second intervals to determine the degree of modulating drug washout. The NMDA receptor competitive antagonist D,L-APV (200-400 μM) was

subsequently bath applied during NMDA and glycine applications (Lee et al., 2007). The $I_h$ current was recorded under current-clamp using the same intracellular solution by injecting 0.1 nA of hyperpolarizing current into the cell. Synaptic responses were evoked by injecting 50 – 500 μA of current for 0.1 ms using a bipolar tungsten stimulating electrode (FHC) of the internal capsule fibers rostral to the subthalamic nucleus (Baufreton et al., 2009). Slice experiments were approved by the Institutional Animal Care and Use Committee of Emory University.

### 2.8. Cerebellar granule cell culture

Cerebellar granule cell cultures were performed as previously described (Traynelis and Cull-Candy, 1991). Briefly, the cerebellum was removed from P3 to P7 Sprague-Dawley rats killed by decapitation. Cerebella then were chopped in Dulbecco's Modified Eagle Medium supplemented with 10% fetal bovine serum, and 100 units/ml each of penicillin and streptomycin. The chopped cerebella were passed through a sterile 200 μm mesh filter, and the media containing cerebellar tissue was plated on coverslips coated in 0.01 mg/mL poly-D-lysine. Cells were maintained in 5% humidified $CO_2$ at 37ºC for 7 days. One day after plating, the culture media was changed to the media with the components listed above supplemented with 25 mM KCl. Culture experiments were approved by the Institutional Animal Care and Use Committee of Emory University.

### 2.9. Statistical analysis

Data are reported as mean $\pm$ s.e.m. and were evaluated statistically using one-way ANOVA and Tukey's *post hoc* test or a paired or unpaired t-test. Significance for all

tests was set at $p < 0.05$. $EC_{50}$ values are reported as mean $\pm$ s.e.m., but statistical analyses were performed on the $\log(EC_{50})$, as $EC_{50}$ demonstrates a lognormal distribution (Christopoulos, 1998). Tukey's *post hoc* test was used to make multiple comparisons across the data, and $p < 0.05$ was chosen as the significance level because I believed there was an acceptable degree of risk that I incorrectly rejected the null hypothesis at that level.

## Chapter 3: NMDA receptor agonist pharmacology

### 3.1. Abstract

The deactivation time course of NMDA receptors following the removal of L-glutamate is thought to determine the time course of excitatory synaptic currents. One important characteristic of GluN1/GluN2D NMDA receptors is an unusually long deactivation time course upon the removal of L-glutamate. I have assessed the role that the activating agonist has in the prolonged deactivation time course of GluN2D-containing NMDA receptors. GluN1/GluN2D receptors were activated by a range of structurally diverse linear and cyclic ligands, and the deactivation time course for each agonist was evaluated. The deactivation time course of GluN1/GluN2D receptors is ligand-dependent, as the endogenous ligand L-glutamate evokes a slower deactivation time course than any other linear ligand evaluated. Cyclic ligands with more potent $EC_{50}$ values than L-glutamate evoked similar or more rapid deactivation time courses compared to L-glutamate, suggesting that the deactivation time course of GluN1/GluN2D receptors is not fully dependent upon agonist potency. Chimeric receptors in which all or segments of the GluN2D ligand-binding domain were inserted into the GluN2A subunit have slower deactivation time courses for L-glutamate than wild type GluN1/GluN2A. However, the chimeric receptors did not have slower deactivation time courses when activated by the enantiomer D-glutamate when compared to wild type GluN1/GluN2A receptors. These data suggest that the deactivation time course of GluN2D receptors is complex and is controlled distinctly by the GluN2D ligand-binding domain for the endogenous neurotransmitter L-glutamate.

### 3.2. Introduction

One unique property of GluN1/GluN2D NMDA receptors is an unusually long deactivation time course that lasts for several seconds following the removal of L-glutamate, and is more than 50 times longer than the deactivation time course of GluN2A-containing receptors (Vicini et al., 1998; Wyllie et al., 1998; Yuan et al., 2009; Vance et al., 2011). The GluN2D subunit also confers higher agonist potencies (i.e. lower $EC_{50}$ values) for both glycine and glutamate than observed for NMDA receptors containing GluN2A-C subunits (Kutsuwada et al., 1992; Matsui et al., 1995; Erreger et al., 2007; Chen et al., 2008). These two unique properties of GluN2D-containing NMDA receptors may be important determinants of the synaptic activity in neurons in which they are expressed.

Both the GluN1 and GluN2 subunits are composed of an amino-terminal domain (ATD), a ligand-binding domain, a transmembrane domain that forms the channel pore, and an intracellular carboxyl-terminal domain (Mayer, 2006; Sobolevsky et al., 2009). Recently, the high resolution structures of the homomeric GluN2D ligand-binding domain bound to L-glutamate, D-glutamate, L-aspartate, and NMDA were published (Vance et al., 2011). The structures revealed that one region of the LBD, the hinge loop region, changed in conformation depending upon which ligand was bound (see Figs. 1.3 and 1.4; Vance et al., 2011). While the hinge loop region had a similar conformation when bound to D-glutamate, L-aspartate, or NMDA, the hinge loop shifted when the LBD was bound to L-glutamate, forming a number of unique intraprotein interactions (Vance et al., 2011).

The mechanism of the unusually slow deactivation time course of GluN2D-

containing NMDA receptors remains enigmatic. Numerous studies have suggested that the ligand association and dissociation rates control the deactivation time course of GluN2A-containing NMDA receptors and AMPA and kainate receptors (Lester and Jahr, 1992; Furukawa et al., 2005; Jin et al., 2005; Weston et al., 2006). Interestingly, recent data suggest that the ATD region of the GluN2 subunit also can influence deactivation time course (Gielen et al., 2009; Yuan et al., 2009), indicating that both the GluN2D ligand-binding domain and the amino-terminal domain exert significant control over GluN2D deactivation time course.

In this study, I use a range of linear and cyclic aspartate and glutamate analogues to evaluate the role of the GluN2D ligand-binding domain in the unusually slow deactivation time course of recombinant GluN1/GluN2D receptors. I use crystallographic data from our collaboration with Dr. Hiro Furukawa of Cold Spring Harbor Laboratories (see Fig. 1.3-1.4) to produce GluN2D-GluN2A chimeras and point mutations and show that GluN1/GluN2D deactivation time course, in addition to being influenced by amino-terminal domain (Gielen et al., 2009; Yuan et al., 2009), is controlled by structural features within the GluN2D ligand-binding domain, particularly the hinge loop region within the D2 domain. I further show that L-glutamate appears unique among evaluated ligands, as no other ligand can induce a longer deactivation time course.

## 3.3. Results

### *3.3.a. GluN1/GluN2D deactivation time course is ligand-dependent*

To determine if the uniquely long deactivation time course of GluN1/GluN2D

NMDA receptors is dependent on the structure of the activating ligand, I recorded whole cell responses under voltage-clamp from HEK 293 cells expressing recombinant GluN1/GluN2D and compared the response time course of a series of glutamate and aspartate analogues. The co-agonist glycine was present in all solutions (0.05 mM; $EC_{50}$ 0.13 μM; Chen et al., 2008), and current responses were evoked with a 1 s pulse of 0.1 to 1 mM agonist. Following a 1 s pulse of 1 mM L-glutamate, the GluN1/GluN2D receptors deactivated slowly with a dual exponential time course with time constants of $\tau_{FAST}$=930 $\pm$ 100 ms and $\tau_{SLOW}$=3200 $\pm$ 240 ms (n=30; Fig. 3.1A*;* Table 3.1), as previously described (Vicini et al., 1998; Wyllie et al., 1998; Yuan et al., 2009). Interestingly, the stereoisomer D-glutamate caused the receptor to deactivate much more rapidly, with deactivation time constants of $\tau_{FAST}$=27 $\pm$ 2.4 ms and $\tau_{SLOW}$=440 $\pm$ 120 ms (n=12), significantly faster than the deactivation time constants evoked by L-glutamate (Fig. 3.1B*;* Table 3.1; $p < 0.05$; one-way ANOVA). These data indicate that the prolonged deactivation time course of GluN1/GluN2D receptors is dependent on the activating ligand.

I subsequently assessed deactivation time course for other linear agonists. The glutamate analogues L-homocysteate ($\tau_{FAST}$=160 $\pm$ 27 ms and $\tau_{SLOW}$=540 $\pm$ 59 ms; n=5) and D-homocysteate ($\tau_{FAST}$=35 $\pm$ 2.9 ms and $\tau_{SLOW}$=300 $\pm$ 97 ms; n=10), which have been detected in the brain and may act as endogenous neurotransmitters (Do et al., 1986; Olney et al., 1987; Do et al., 1988; Yuzaki and Connor, 1999), also cause the GluN1/GluN2D receptor to deactivate more rapidly than when activated by L-glutamate (Table 3.1). Whereas the GluN1/GluN2D receptor is sensitive to the stereochemistry of the glutamate analogues with longer side chains, aspartate, which has a shorter side

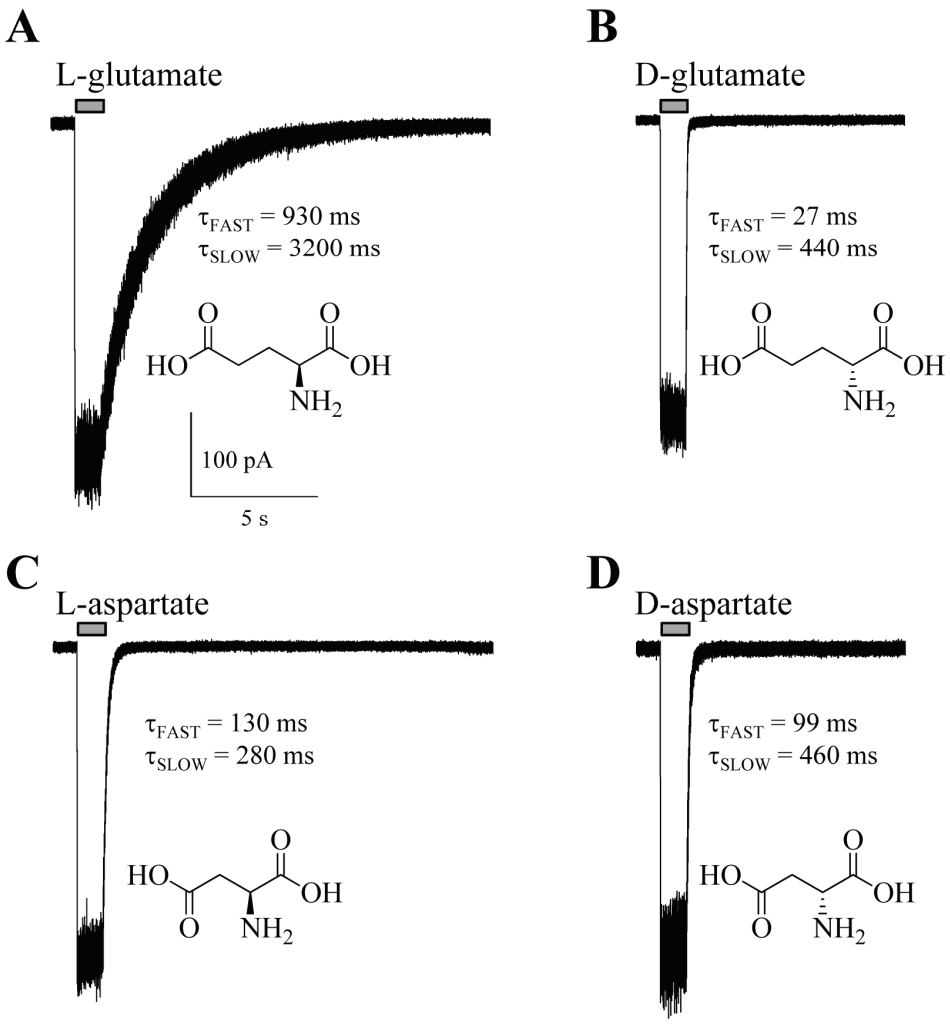


**Figure 3.1.** Deactivation time course is dependent on ligand structure for GluN1/GluN2D NMDA receptors. HEK cells were activated under voltage-clamp by 1 s rapid application of maximally effective concentrations of various linear agonists (all solutions contained 0.05 mM glycine). ***A***, L-glutamate evoked the slowest deactivation time course of all linear ligands examined. ***B***, The enantiomer D-glutamate evoked a deactivation time course more than 50-fold more rapid than L-glutamate. Ligands with shorter side chains, such as L-aspartate (***C***) and D-aspartate (***D***), showed deactivation time courses somewhat less sensitive to ligand potency. The deactivation time constants are given as the mean of 7-30 cells. Adapted with permission from Vance et al. (2011).

**Table 3.1.** Summary of the deactivation time course of GluN1/GluN2D receptors activated by linear glutamate and aspartate analogues

| Ligand | $\tau_{FAST}$ (ms) | $\tau_{SLOW}$ (ms) | $\tau_W$ (ms) | % fast | $EC_{50}$ (μM) | Rise Time (ms) | Relative Maximum Response (%) | n |
|---|---|---|---|---|---|---|---|---|
| **L-glutamate** | 930 ± 100 | 3200 ± 240 | 2300 ± 96 | 37 ± 4.3 | 0.48 | 6.7 ± 0.42 | 100 ± 0.0 | 30 |
| **D-glutamate** | 27 ± 2.4* | 440 ± 120* | 42 ± 4.8* | 93 ± 2.4* | 42 | 9.6 ± 0.99 | 89 ± 4.5 | 12 |
| **L-aspartate** | 130 ± 10* | 280 ± 25* | 160 ± 4.5* | 74 ± 7.9* | 5.0 | 7.0 ± 0.91 | 98 ± 7.2 | 8 |
| **D-aspartate** | 99 ± 8.3* | 460 ± 100* | 130 ± 13* | 90 ± 1.5* | 2.1 | 7.1 ± 1.1 | 95 ± 6.1 | 7 |
| **N-methyl-L-aspartate** | 17 ± 4.5* | 91 ± 18* | 38 ± 2.5* | 62 ± 11 | 40 | 7.6 ± 0.57 | 86 ± 8.4 | 6 |
| **N-methyl-D-aspartate** | 60 ± 2.2* | 280 ± 36* | 75 ± 3.4* | 93 ± 1.9* | 7.3 | 7.1 ± 0.69 | 80 ± 5.4 | 5 |
| **L-homocysteate** | 160 ± 27* | 540 ± 59* | 370 ± 23* | 43 ± 9.7 | 3.4 | 8.4 ± 0.98 | 60 ± 4.8* | 5 |
| **D-homocysteate** | 35 ± 2.9* | 300 ± 97* | 45 ± 3.2* | 91 ± 4.0* | 22 | 9.4 ± 1.3 | 71 ± 2.9* | 10 |
| **(2*S*,4R)-4-methylglutamate (SYM 2081)** | 130 ± 32* | 520 ± 76* | 330 ± 47* | 48 ± 9.5 | 3.2 | 6.7 ± 0.61 | 57 ± 6.7* | 5 |
| **(2*S*,4*S*)-4-methylglutamate** | 25 ± 5.0* | 190 ± 59* | 56 ± 10* | 66 ± 15 | 31 | 8.1 ± 0.75 | 93 ± 3.9 | 5 |

$\tau_{FAST}$, $\tau_{SLOW}$, $\tau_W$, % fast, rise time, and relative maximum response values are shown as mean ± s.e.m., and n is the number of cells. Values are given to two significant figures. Relative maximum response is the ratio (in percent) of the response to a maximally effective concentration of a test agonist compared to the response to a maximally effective concentration of L-glutamate recorded in the same cell. All steady-state $EC_{50}$ values except L-glutamate and L-aspartate, which are from Vance et al. (2011), are from Erreger et al. (2007). *$p < 0.05$ compared to L-glutamate; one-way ANOVA with Tukey's *post hoc* test.

chain, does not cause stereo-specific differences in deactivation time course. L-aspartate ($\tau_{FAST}$=130 $\pm$ 10 ms and $\tau_{SLOW}$=280 $\pm$ 25 ms; n=8) and D-aspartate ($\tau_{FAST}$=99 $\pm$ 8.3 ms and $\tau_{SLOW}$=460 $\pm$ 100 ms; n=7) have similar deactivation time constants, both of which are significantly faster than L-glutamate (Fig. 3.1C,D*;* Table 3.1; $p < 0.05$; one-way ANOVA). This suggests that any GluN2D-containing NMDA receptor at synapses at which L-aspartate participates as a primary neurotransmitter may deactivate more rapidly than synapses at which only L-glutamate is released (Benveniste, 1989; Nicholls, 1989; Fleck et al., 1993; Wang and Nadler, 2007; Zhang and Nadler, 2009).

In addition to deactivation time course, I also examined how ligand structure influences the response rise time following rapid agonist application. The measured 10 to 90% open tip solution exchange times were typically under 0.5 ms; 10% to 90% solution exchange around a whole cell was determined to be 3.3 $\pm$ 0.48 ms (n=7). No linear ligand evoked a significant difference in the measured rise time compared to L-glutamate (one-way ANOVA and Tukey's *post hoc* test, $p < 0.05$; Table 3.1). The relative agonist effectiveness when compared to the maximal current response of L-glutamate ranged from 57% for SYM 2081 to 98% for L-aspartate (Table 3.1).

Compounds with conformationally constrained rings have been identified as partial agonists of NMDA receptors, and several have higher potency (i.e. lower $EC_{50}$) or similar potency to L-glutamate (Schinozaki et al., 1989; Schoepp et al., 1991; Erreger et al., 2007). Previous studies have suggested that the deactivation time course of AMPA receptors is correlated with agonist potency, as ligands with lower $EC_{50}$s caused slower time courses than L-glutamate (Zhang et al., 2006). I therefore evaluated whether compounds with higher potencies could evoke longer deactivation time courses than L-

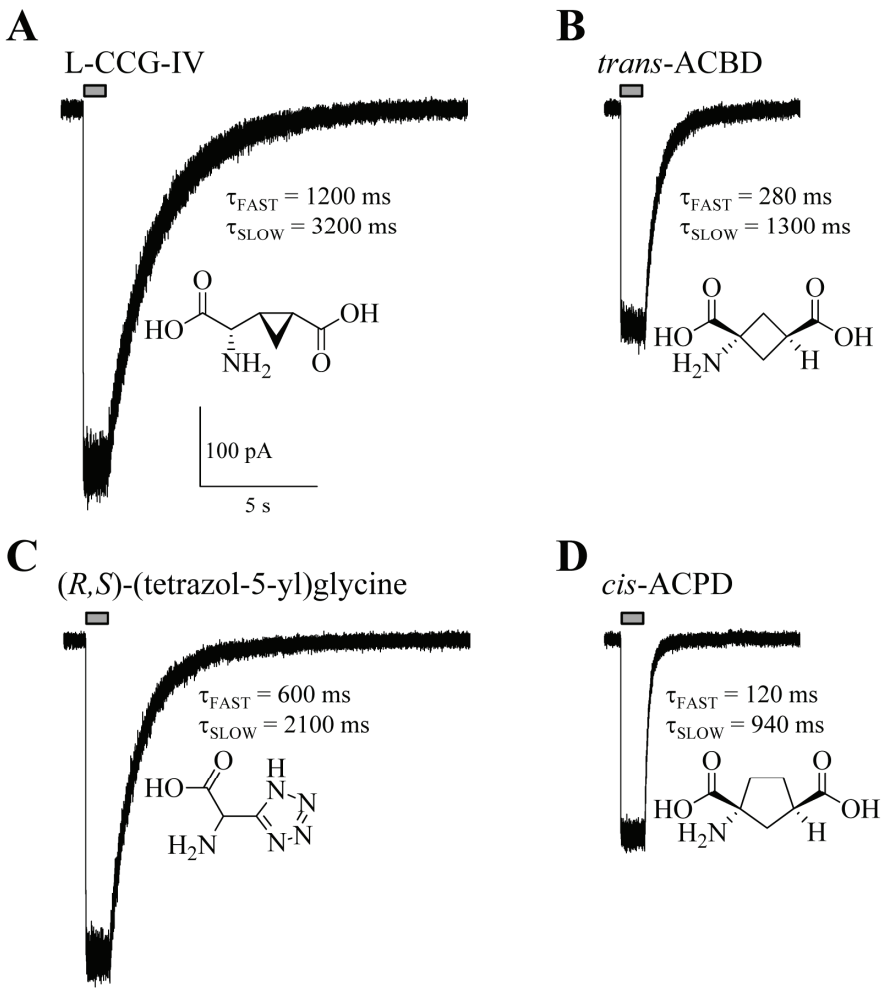


**Figure 3.2.** More potent cyclic ligands do not evoke slower deactivation time courses than L-glutamate on GluN1/GluN2D NMDA receptors. ***A***, L-CCG-IV, a ligand more than 10-fold more potent than L-glutamate, does not further slow deactivation time course compared to L-glutamate. Trans-ACBD (***B***), which has the same GluN1/GluN2D potency, and (R,S)-(tetrazol-5-yl)glycine (***C***), which is more potent than L-glutamate, have significantly faster deactivation time courses ($p<0.05$; one-way ANOVA with Tukey's *post hoc* test). Adapted with permission from Vance et al. (2011).

**Table 3.2.** Summary of the deactivation time course of GluN1/GluN2D receptors activated by cyclic glutamate analogues

| Ligand | $\tau_{FAST}$ (ms) | $\tau_{SLOW}$ (ms) | $\tau_W$ (ms) | % fast | $EC_{50}$ (μM) | Rise Time (ms) | Relative Maximum Response (%) | n |
|---|---|---|---|---|---|---|---|---|
| **L-glutamate** | 930 ± 100 | 3200 ± 240 | 2300 ± 96 | 37 ± 4.3 | 0.48 | 6.7 ± 0.42 | 100 ± 0.0 | 30 |
| **L-CCG-IV** | 1200 ± 290 | 3200 ± 600 | 2500 ± 370 | 32 ± 4.5 | 0.036 | 8.3 ± 0.86 | 88 ± 5.0 | 5 |
| **(*RS*)-(tetrazol-5-yl)glycine** | 600 ± 140 | 2100 ± 340 | 1400 ± 190*,# | 42 ± 12 | 0.099 | 9.3 ± 1.5 | 76 ± 5.2 | 5 |
| ***trans*-ACBD** | 280 ± 69*,# | 1300 ± 320* | 620 ± 77*,# | 59 ± 10 | 0.51 | 5.5 ± 0.78* | 61 ± 6.6* | 5 |
| ***cis*-ACPD** | 120 ± 23*,# | 940 ± 190*,# | 350 ± 88*,# | 72 ± 11 | 11 | 9.1 ± 0.96 | 54 ± 7.9* | 5 |

$\tau_{FAST}$, $\tau_{SLOW}$, $\tau_W$, % fast, rise time, and relative maximum response values are shown as mean ± s.e.m., and n is the number of cells. Values are given to two significant figures. All $EC_{50}$ values except L-glutamate are from Erreger et al. (2007). *$p < 0.05$ when compared to the deactivation time course of L-glutamate (one-way ANOVA with Tukey's *post hoc* test). #$p < 0.05$ when compared to the deactivation time course of L-CCG-IV (one-way ANOVA with Tukey's *post hoc* test). Data for L-glutamate from Table 3.1 are shown here for comparison.

glutamate in GluN1/GluN2D NMDA receptors (Fig. 3.2; Table 3.2). Agonists were applied in 1 s pulses at 0.1 to 1 mM concentrations (in 0.05 mM glycine) to HEK 293 cells expressing GluN1/GluN2D. L-CCG-IV, the most potent of the cyclic ligands ($EC_{50}$ 0.036 μM) and the compound with the smallest ring, deactivated with a time course that was not significantly different to L-glutamate ($\tau_{FAST}$=1200 $\pm$ 290 ms; $\tau_{SLOW}$=3200 $\pm$ 600 ms; n=5; Fig. 3.2A, Table 3.2; $p > 0.05$) even though its $EC_{50}$ was more than 10-fold more potent. The remaining constrained ligands had significantly more rapid deactivation time courses even though they were more potent than or as potent as L-glutamate on GluN1/GluN2D. The ligand (*RS*)-(tetrazol-5-yl)glycine, although more potent than L-glutamate ($EC_{50}$ 0.099 μM), deactivated more rapidly than L-glutamate with time constants of $\tau_{FAST}$=600 $\pm$ 120 ms and $\tau_{SLOW}$=2100 $\pm$ 340 ms (n=5; Fig. 3.2C, Table 3.2). *Trans*-ACBD, with a four-member ring and an $EC_{50}$ similar to L-glutamate (0.51 μM), also deactivated rapidly with time constants of $\tau_{FAST}$=280 $\pm$ 69 ms and $\tau_{SLOW}$=1300 $\pm$ 320 ms (n=5; Fig. 3.2B, Table 3.2).

I evaluated the constrained ligands to determine if they had a more rapid rise time on GluN1/GluN2D than L-glutamate. Only *trans*-ACBD had a significantly more rapid 10% to 90% rise time than L-glutamate (Table 3.2; $p < 0.05$). Maximum relative effectiveness for the cyclic ligands ranged from 54% for *cis*-ACPD to 88% for L-CCG-IV (Table 3.2).

### *3.3.b. The relationship between GluN1/GluN2D deactivation rate and agonist potency*

Previous studies have suggested that deactivation time course is correlated with the ligand $EC_{50}$ for AMPA receptors (Zhang et al., 2006) and NMDA receptors (Lester and

Jahr, 1992). However, my data suggest that the relationship between deactivation time course and ligand $EC_{50}$ is more complex in GluN1/GluN2D receptors, as ligands with more potent $EC_{50}$ values than L-glutamate do not cause the receptor to deactivate more slowly. I fit previously published gating models for GluN1/GluN2A (Schorge et al., 2005), GluN1/GluN2B (Amico-Ruvio and Popescu, 2010), and GluN1/GluN2C (Dravid et al., 2008) to six GluN1/GluN2D single channel recordings from excised outside-out patches activated by 1 mM L-glutamate and 0.05 mM glycine to explore the relationship between deactivation and $EC_{50}$ values (Fig. 3.3A). I used models to determine how changing the association or dissociation rate constants influence $EC_{50}$ and deactivation time course. I simplified these analyses by assuming that channel gating rates do not change between activating agonists. However, previous studies have shown that NMDA receptor partial agonists influence channel gating rates, so my simulations may be compromised by differences in the channel gating rate constants (Banke and Traynelis, 2003; Erreger et al., 2005b; Kussius and Popescu, 2009). I compared the relationship between the theoretical $EC_{50}$ values and deactivation time constants determined using modeling to evaluate the relationship between experimentally determined $EC_{50}$ and $\tau_{SLOW}$ for GluN1/GluN2D receptors activated by ligands for which $\tau_{SLOW}$ accounted for >10% of the deactivation time course.

Figure 3.3B shows that the theoretical relationships predicted by the gating models provide a reasonable approximation of the experimentally determined $\tau_{SLOW}$ and $EC_{50}$ for all linear agonists that have a sufficiently large slow component (>10%) of deactivation to allow reliable determinations of $\tau_{SLOW}$. However, the deactivation time courses of the cyclic ligands were not predicted by the same gating rate constants as the linear ligands.

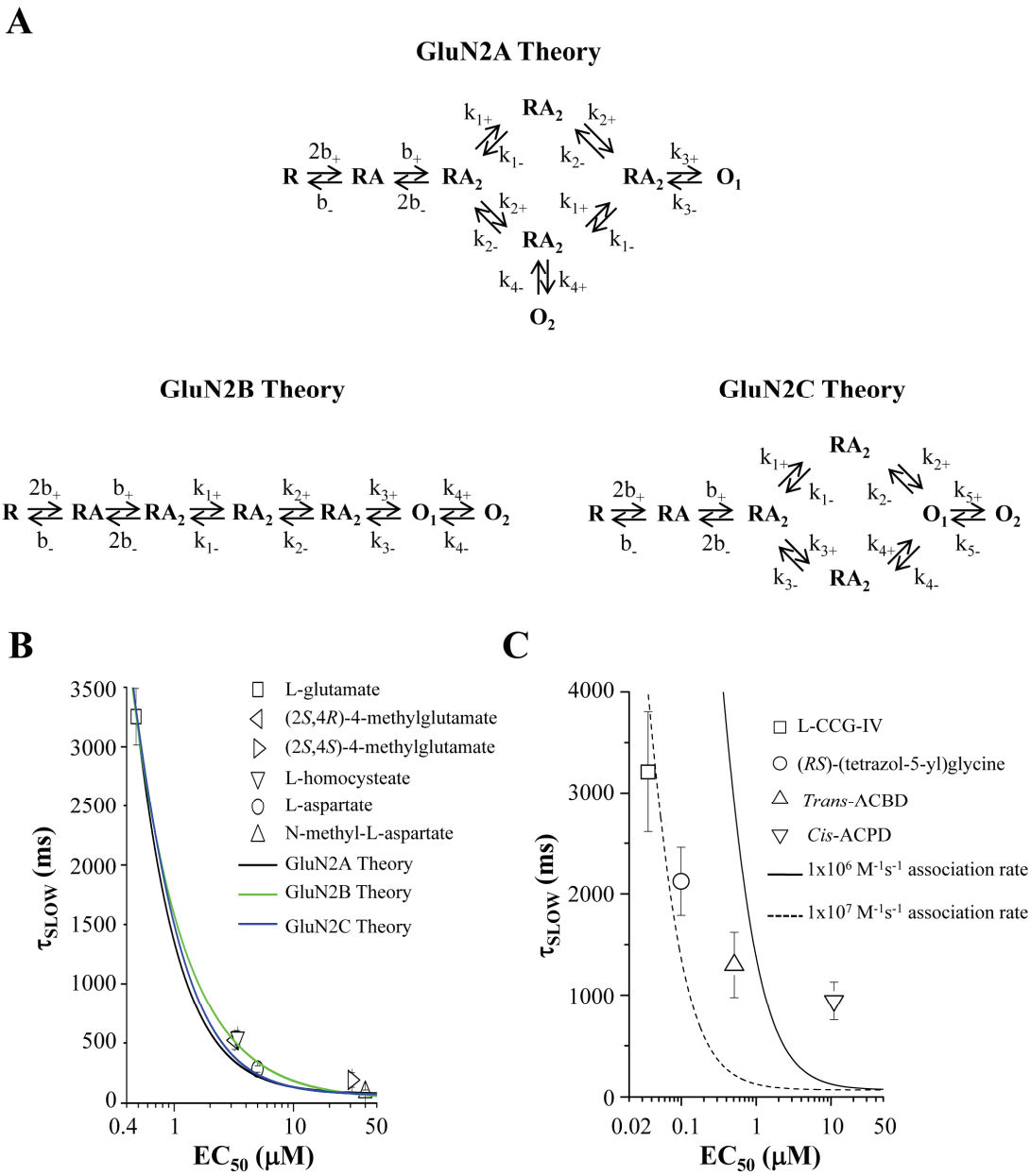


**Figure 3.3.** Deactivation time course cannot be fully predicted by ligand potency. ***A***, Previously published models of NMDA receptor gating for GluN2A (Schorge et al., 2005), GluN2B (Erreger et al., 2005a), and GluN2C (Dravid et al., 2008) were fitted to six single channel recordings of GluN1/GluN2D activated by L-glutamate. The rate constants derived from fitting my GluN1/GluN2D single channel data then were used to simulate the relationship between ligand potency and deactivation time course. ***B***, The deactivation time course of linear agonists for GluN2D are moderately predicted by simulations from NMDA receptor

gating models, although these models do not adequately predict the deactivation time course of the ligands with shorter side chains such as L-aspartate. ***C***, Cyclic ligands, which are as potent or more potent than L-glutamate, cannot be predicted with the same rate constants as the linear ligands. Using a faster association rate improves the prediction of deactivation time course based on ligand potency, but cannot predict the slower deactivation time courses observed for *trans*-ACBD or *cis*-ACPD. Adapted with permission from Vance et al. (2011).

Cyclic ligands have fewer conformational degrees of freedom than linear agonists and may also have association and gating rates that differ substantially from L-glutamate (Fig. 3.3C). Indeed, simulations with a 10-fold faster association rate were better able to approximate the slow deactivation time constants of L-CCG-IV and (RS)-(tetrazol-5-yl)glycine but still could not predict $\tau_{SLOW}$ for *trans*-ACBD or *cis*-ACPD. These data suggest that cyclic ligands may have different gating rate constants than linear ligands.

While the models were able to approximate a single exponential deactivation time course for the GluN1/GluN2D receptor activated by each ligand, no model was able to produce the dual exponential component I observed in my recordings. The nature of the dual exponential time course seen in all NMDA receptors is unclear, although modal gating has been suggested as a cause of the biphasic deactivation of GluN1/GluN2A receptors (Zhang et al., 2008). Although the relationship between deactivation time course and ligand $EC_{50}$ is not as well predicted for the cyclic ligands as for the linear ligands, it is clear that a relationship between deactivation time course and agonist potency is present for a majority of GluN2D ligands.

### *3.3.c. Molecular correlates of the LBD control of GluN1/GluN2D deactivation time course*

Our collaborator Dr. Hiro Furukawa of Cold Spring Harbor Laboratories produced and solved using x-ray crystallography the crystal structures of the monomeric GluN2D ligand-binding domain in complex with L-glutamate, D-glutamate, L-aspartate, and NMDA and evaluated if the GluN2D ligand-binding domain undergoes ligand-dependent conformational changes (See Section 1.3c; Figs. 1.3-1.4; Vance et al., 2011). The high

resolution structures had x-ray diffractions higher than 1.9 Å. While the structures of the GluN2D ligand-binding domain in general could be superimposed, one region, the hinge loop region in the D2 domain, showed a unique conformation when the slowly deactivating L-glutamate was bound compared to when the rapidly deactivating D-glutamate, L-aspartate, or NMDA was bound (see Figs. 1.3-1.4; Vance et al., 2011). GluN1/GluN2A receptors do not exhibit a striking ligand-dependence in deactivation time course (Fig. 3.4; Table 3.3), suggesting that the GluN2D LBD and the GluN2A LBD may not undergo similar ligand-specific conformation changes. I evaluated this hypothesis by producing GluN2A and GluN2D chimeric subunits engineered based on the GluN2D and GluN2A LBD crystal structures (Furukawa et al., 2005; Vance et al., 2011). I measured the deactivation time courses evoked by both D- and L-glutamate and compared the deactivation of the chimeric receptors to wild type GluN1/GluN2A and GluN1/GluN2D. I used the GluN2A subunit to make chimeric receptors due to the availability of L-glutamate-bound GluN2A crystal structures (Table 3.4; Furukawa et al., 2005). The GluN2A subunit also has a faster deactivation time course than any other GluN2 subunit, thus providing the greatest difference in deactivation time course from GluN2D (see Tables 3.1 and 3.3; Fig. 3.4; Vicini et al., 1998; Wyllie et al., 1998; Yuan et al., 2009; Vance et al., 2011).

GluN2A-(GluN2D D1D2) chimeric receptors, in which the full GluN2D ligand-binding domain has been inserted into the GluN2A subunit, first were evaluated. These receptors had a significantly slower deactivation time course for L-glutamate ($\tau_{FAST}$=170 $\pm$ 35 ms; $\tau_{SLOW}$=740 $\pm$ 230 ms; n=5) than wild-type GluN1/GluN2A (Fig. 3.5; Table 3.5). However, I found no significant difference between GluN1/GluN2A and GluN2A-

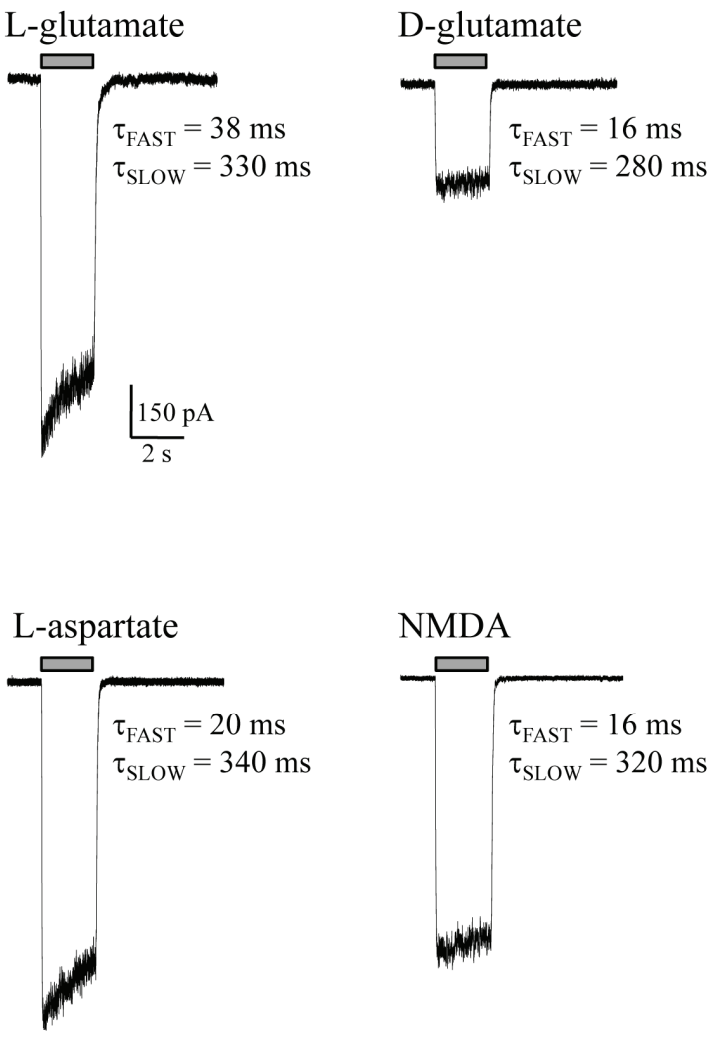


**Figure 3.4.** GluN1/GluN2A receptors deactivate rapidly compared to GluN1/GluN2D. The deactivation time course of GluN1/GluN2A receptors does not differ as much as GluN1/GluN2D (see Fig. 3.1) when different ligands are applied. L-glutamate, D-glutamate, L-aspartate, and NMDA have similar deactivation time courses. This suggests the ligand-dependence of GluN1/GluN2D receptors may be unique.

**Table 3.3.** Summary of the deactivation time course of GluN1/GluN2A receptors activated by glutamate and aspartate analogues

| Ligand | $\tau_{FAST}$ (ms) | $\tau_{SLOW}$ (ms) | $\tau_W$(ms) | % fast | n | $EC_{50}$ (μM) |
|---|---|---|---|---|---|---|
| **L-glutamate** | 38 ± 1.7 | 330 ± 50 | 54 ± 3.2 | 88 ± 4.0 | 21 | 4.5 |
| **D-glutamate** | 16 ± 1.3* | 280 ± 130 | 22 ± 3.0* | 95 ± 1.9 | 7 | 250 |
| **L-aspartate** | 20 ± 2.5* | 340 ± 72 | 32 ± 6.1* | 96 ± 1.4 | 7 | 48 |
| **D-aspartate** | 26 ± 3.3 | 810 ± 540 | 35 ± 6.5 | 83 ± 9.2 | 6 | 30 |
| **N-methyl-L-aspartate** | 9.5 ± 1.4* | 170 ± 130 | 11 ± 1.3* | 96 ± 3.0 | 6 | 580 |
| **N-methyl-D-aspartate** | 16 ± 1.8* | 320 ± 58 | 20 ± 2.1* | 98 ± 1.4 | 4 | 94 |
| **L-homocysteate** | 15 ± 3.5* | 430 ± 190 | 31 ± 6.9 | 80 ± 17 | 5 | 34 |
| **D-homocysteate** | 15 ± 3.0* | 290 ± 16 | 22 ± 3.1* | 98 ± 0.22 | 4 | 180 |
| **(2*S*,4*R*)-4-methylglutamate (SYM 2081)** | 39 ± 4.2 | 350 ± 49 | 52 ± 5.6 | 95 ± 18 | 5 | 144 |
| **(2*S*,4*S*)-4-methylglutamate** | 11 ± 1.0* | 47 ± 15 | 13 ± 1.2* | 93 ± 3.9 | 5 | 404 |
| **L-CCG-IV** | 54 ± 7.2* | 240 ± 43 | 70 ± 8.4 | 89 ± 5.8 | 5 | 0.26 |
| **(*R*,*S*)-(tetrazol-5-yl)glycine** | 60± 8.2* | 300 ± 58 | 89 ± 9.0* | 84 ± 6.8 | 5 | 1.7 |
| ***Trans*-ACBD** | 40 ± 5.4 | 420 ± 77 | 59 ± 6.0 | 96 ± 0.98 | 5 | 3.1 |
| ***Cis*-ACPD** | 39 ± 4.2 | 350 ± 49 | 52 ± 5.6 | 95 ± 1.9 | 5 | 61 |

$\tau_{FAST}$, $\tau_{SLOW}$, $\tau_W$, and % fast values are shown as mean ± s.e.m., and n is the number of cells. Values are given to two significant figures. All $EC_{50}$ values except L-glutamate are from Erreger et al. (2007). * $p$ <0.05 when compared to the deactivation time course of GluN1/GluN2A activated by L-glutamate and analyzed by one-way ANOVA with Tukey's *post hoc* test.

**Table 3.4.** Amino acid composition for GluN2A-GluN2D chimeras shown in Figure 3.5

| | GluN2A | GluN2D |
|---|---|---|
| **GluN2A** | 1-1464 | -- |
| **GluN2D** | -- | 1-1323 |
| **GluN2A-(GluN2D D1D2)** | 1-403; 539-660; 798-1464 | 427-563; 686-822 |
| **GluN2A-(GluN2D D1)** | 1-403; 539-765; 798-1464 | 427-563; 791-822 |
| **GluN2A-(GluN2D D2)** | 1-660; 766-1464 | 686-790 |

Amino acid composition of the chimeras is listed as the residues included from GluN2A and GluN2D. Amino acid numbering is according to the respective full-length GluN2 subunits, including the signal peptide (initiating methionine is 1).

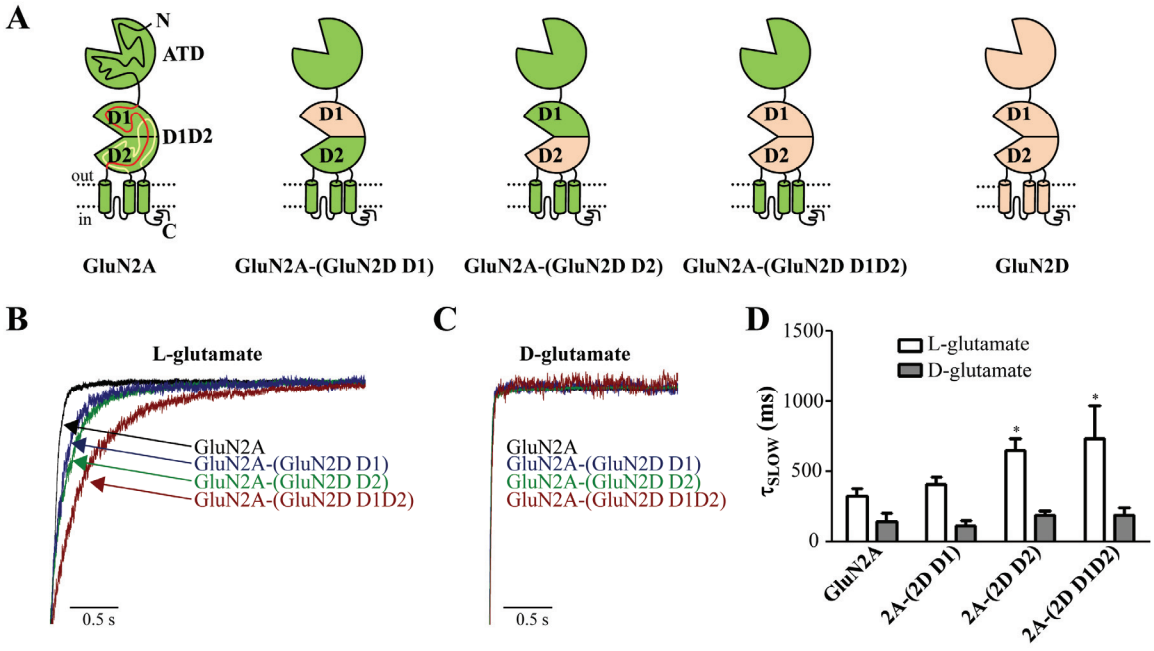


**Figure 3.5.** Chimeric GluN2A-GluN2D receptors are used to examine the molecular determinants of ligand binding domain control of GluN2D deactivation time course. ***A,*** Chimeric receptors were produced that contain the full GluN2D ligand binding domain (D1 + D2) in the GluN2A subunit or only the GluN2D D1 or D2 domain in the GluN2A subunit. ***B,*** L-glutamate-evoked currents are significantly slower for the GluN2A-GluN2D chimeric receptors than the wild-type GluN2A receptor, although no mutant fully restores the prolonged deactivation time course of GluN2D-containing receptors. The GluN2A-(GluN2D D1) and GluN2A-(GluN2D D2) chimeric receptors have similar deactivation time courses, while the receptor in which the full LBD was inserted into GluN2A, GluN2A-(GluN2D D1D2), has the slowest deactivation time course. ***C***, While differences in L-glutamate deactivation time course was observed for the chimeric receptors, none of the receptors had a significantly different D-glutamate deactivation time course compared to wild-type GluN2A. ***D***, The summary of the chimeric receptor deactivation time courses for L-glutamate and D-glutamate are give. *$p < 0.05$, one-way ANOVA with Tukey's *post hoc* test. Adapted with permission from Vance et al. (2011).

**Table 3.5.** GluN2A-GluN2D chimeric receptors activated by L-glutamate

| Receptor | $\tau_{FAST}$ (ms) | $\tau_{SLOW}$ (ms) | $\tau_W$ (ms) | % fast | n | $EC_{50}$ (μM) |
|---|---|---|---|---|---|---|
| **GluN2A WT** | 39 ± 1.8 | 360 ± 53 | 54 ± 3.5 | 89 ± 4.4 | 21 | 4.5 ± 0.42 |
| **GluN2A-(GluN2D D1)** | 98 ± 4.7* | 410 ± 56 | 150 ± 11 | 80 ± 7.1 | 5 | 0.68 ± 0.20** |
| **GluN2A-(GluN2D D2)** | 110 ± 5.6* | 660 ± 83* | 160 ± 4.5* | 88 ± 2.7 | 7 | 1.2 ± 0.2** |
| **GluN2A-(GluN2D D1D2)** | 170 ± 35* | 740 ± 230* | 280 ± 42* | 72 ± 8.0 | 5 | 0.44 ± 0.082** |
| **GluN2D WT** | 930 ± 100* | 3200 ± 240* | 2300 ± 96* | 37 ± 4.3* | 30 | 0.48 |

$\tau_{FAST}$, $\tau_{SLOW}$, $\tau_W$, % fast, and $EC_{50}$ values are shown as mean ± s.e.m., and n is the number of cells for deactivation measurements; $EC_{50}$ values were determined in 4-6 oocytes for each receptor. All data are given to two significant figures. *$p < 0.05$ when compared to the deactivation time course of GluN1/GluN2A activated by L-glutamate and analyzed by one-way ANOVA with Tukey's *post hoc* test. **$p< 0.05$ when $\log(EC_{50})$ is compared to the $\log(EC_{50})$ of L-glutamate for GluN1/GluN2A and analyzed by one-way ANOVA with Tukey's *post hoc* test. Data for L-glutamate on wild-type GluN1/GluN2A and GluN1/GluN2D from Tables 3.1 and 3.3 are shown here for comparison.

**Table 3.6.** GluN2A-GluN2D chimeric receptors activated by D-glutamate

| Receptor | $\tau_{FAST}$ (ms) | $\tau_{SLOW}$ (ms) | $\tau_W$ (ms) | % fast | n |
|---|---|---|---|---|---|
| **GluN2A WT** | 16 ± 1.3 | 280 ± 130 | 22 ± 3.0 | 95 ± 1.9 | 7 |
| **GluN2A-(GluN2D D1)** | 13 ± 1.0 | 120 ± 36 | 22 ± 5.3 | 92 ± 1.2 | 5 |
| **GluN2A-(GluN2D D2)** | 15 ± 0.91 | 200 ± 30 | 23 ± 1.3 | 95 ± 1.2 | 5 |
| **GluN2A-(GluN2D D1D2)** | 12 ± 1.9 | 200 ± 49 | 26 ± 5.4 | 93 ± 1.7 | 5 |
| **GluN2D WT** | 27 ± 2.4 | 440 ± 120 | 42 ± 4.8 | 93 ± 2.4 | 12 |

$\tau_{FAST}$, $\tau_{SLOW}$, $\tau_W$, and % fast values are shown as mean ± s.e.m., and n is the number of cells. All data are given to two significant figures. Data was evaluated for statistical significance by comparison to the deactivation time course of GluN1/GluN2A activated by D-glutamate and analyzed by one-way ANOVA with Tukey's *post hoc* test. No significant differences between experimental conditions or control were detected ($p > 0.05$). Data for D-glutamate on wild-type GluN1/GluN2A and GluN1/GluN2D from Tables 3.1 and 3.3 are shown here for comparison.

(GluN2D D1D2) receptors when they were activated by D-glutamate ($\tau_{FAST}$=12 $\pm$ 1.9 ms; $\tau_{SLOW}$=200 $\pm$ 49 ms; n=5; Table 3.6; Fig. 3.5). These observations suggest that the deactivation time course of L-glutamate may be uniquely influenced by the conformation of the GluN2D ligand-binding domain. While the deactivation time course of GluN2A-(GluN2D D1D2) activated by L-glutamate is slower than wild-type GluN2A, insertion of the GluN2D LBD alone does not fully interconvert the deactivation time course of GluN2A to GluN2D, consistent with the recently suggested role of the ATD in the control of deactivation (Gielen et al., 2009; Yuan et al., 2009).

In order to determine the contributions of the individual D1 and D2 domains to the deactivation time course of GluN2D-containing receptors, I conducted voltage-clamp recordings of chimeric receptors containing either the D1 or the D2 domain. Insertion of the GluN2D D1 domain into GluN2A in GluN1/GluN2A-(GluN2D-D1) receptors resulted in a slower deactivation time course when activated by L-glutamate compared to the wild type GluN1/GluN2A receptors ($\tau_{FAST}$=98 $\pm$ 4.7 ms; $\tau_{SLOW}$=410 $\pm$ 56 ms; n=5; Fig. 3.5; Table 3.5). The GluN2A-(GluN2D D2) chimeric receptor, which contains the GluN2D D2 domain and the GluN2D hinge loop region, also deactivated more slowly than wild type GluN1/GluN2A following the removal of L-glutamate ($\tau_{FAST}$=110 $\pm$ 5.6 ms; $\tau_{SLOW}$=660 $\pm$ 83 ms; n=7; Fig. 3.5; Table 3.5). These data suggest that both lobes of the ligand-binding domain similarly influence the deactivation time course of the GluN1/GluN2D NMDA receptors and appear to have an additive effect on deactivation time course.

I used site-directed mutagenesis to evaluate residues within the GluN2A and GluN2D hinge loops to determine whether the two residues within the region that varied between

GluN2A and GluN2D might mediate ligand-specific deactivation time course. To determine if I could slow the deactivation time course of GluN2A, I exchanged individual residues within the structurally divergent hinge. Like the chimeric receptors, GluN2A-Y754K had a slower deactivation time course for L-glutamate ($\tau_{FAST}$=110 $\pm$ 7.5 ms; $\tau_{SLOW}$=950 $\pm$ 150 ms; n=20; Table 3.7) and D-glutamate ($\tau_{FAST}$=27 $\pm$ 1.4 ms; $\tau_{SLOW}$=400 $\pm$ 130 ms; n=8; Table 3.7) compared to wild type GluN2A. This result suggests that bringing some elements of the GluN2D hinge region into GluN2A can slow deactivation. However, exchanging both divergent residues in the GluN2A region did not significantly alter deactivation time course (Table 3.7).

While I was able to slow the deactivation of GluN2A using mutagenesis, the deactivation time course of GluN2D was not significantly slowed when the divergent regions of GluN2A were inserted into the hinge loop. Indeed, GluN2D-V780I and GluN2D-K779Y,V780I had slower deactivation time constants than wild-type GluN2D (Table 3.7). As observed with the chimeric receptors, the deactivation time course following the removal of D-glutamate was not significantly different than the deactivation time course of the respective wild-type receptor, with the exception of GluN2A-Y735K (Table 3.8; one-way ANOVA). These data show that the structurally divergent hinge region, while capable of influencing deactivation, by itself cannot fully account for differences in deactivation rates observed in the GluN2A-(GluN2D D2) chimeric receptors. Rather, elements up or downstream of the hinge loop must influence its orientation and stability. This is consistent with the idea that the structural determinants of deactivation within these multimeric receptors are complex, and may involve parts of the ligand-binding domain outside the hinge region and perhaps in parts

**Table 3.7.** GluN2A and GluN2D point mutant receptors activated by L-glutamate

| Receptor | $\tau_{FAST}$ (ms) | $\tau_{SLOW}$ (ms) | $\tau_W$(ms) | % fast | n |
|---|---|---|---|---|---|
| **GluN2A WT** | 38 ± 1.7 | 330 ± 50 | 54 ± 3.2 | 88 ± 4.0 | 21 |
| **GluN2A-Y754K** | 110 ± 7.5* | 950 ± 150* | 170 ± 18* | 91 ± 1.3 | 20 |
| **GluN2A-Y754K, I755V** | 32 ± 1.5 | 370 ± 60 | 55 ± 4.6 | 90 ± 2.6 | 12 |
| **GluN2D WT** | 930 ± 100 | 3200 ± 240 | 2300 ± 96 | 37 ± 4.3 | 30 |
| **GluN2D-K779Y** | 670 ± 150 | 2900 ± 260 | 2200 ± 94 | 32 ± 6.5 | 9 |
| **GluN2D-V780I** | 440 ± 170 | 4800 ± 630 | 4100 ± 630^ | 17 ± 4.1 | 5 |
| **GluN2D-K779Y, V780I** | 1100 ± 170 | 4400 ± 400 | 3300 ± 190^ | 34 ± 6.6 | 5 |

$\tau_{FAST}$, $\tau_{SLOW}$, $\tau_W$, and % fast values are shown as mean ± s.e.m., and n is the number of cells. All data are given to two significant figures. *$p < 0.05$ when compared to the deactivation time course of GluN1/GluN2A activated by L-glutamate and analyzed by one-way ANOVA with Tukey's *post hoc* test. ^$p < 0.05$ when compared to the deactivation time course of GluN1/GluN2D activated by L-glutamate and analyzed by one-way ANOVA with Tukey's *post hoc* test.

**Table 3.8.** GluN2A and GluN2D point mutant receptors activated by D-glutamate

| Receptor | $\tau_{FAST}$ (ms) | $\tau_{SLOW}$ (ms) | $\tau_W$(ms) | % fast | n |
|---|---|---|---|---|---|
| **GluN2A WT** | 16 ± 1.2 | 110 ± 33 | 20 ± 2.9 | 95 ± 2.3 | 7 |
| **GluN2A-Y754K** | 27 ± 1.4* | 400 ± 130 | 41 ± 5.6* | 96 ± 0.94 | 8 |
| **GluN2A-Y754K, I755V** | 11 ± 1.0* | 180 ± 46 | 14 ± 2.4 | 98 ± 1.1 | 8 |
| **GluN2D WT** | 27 ± 2.4 | 440 ± 120 | 42 ± 4.8 | 93 ± 2.4 | 12 |
| **GluN2D-K779Y** | 26 ± 1.3 | 500 ± 190 | 44 ± 7.2 | 94 ± 2.8 | 3 |
| **GluN2D-V780I** | 17 ± 4.4 | 82 ± 14 | 43 ± 0.48 | 53 ± 13^ | 5 |
| **GluN2D-K779Y, V780I** | 34 ± 3.5 | 550 ± 270 | 49 ± 6.0 | 92 ± 3.4 | 6 |

$\tau_{FAST}$, $\tau_{SLOW}$, $\tau_W$, and % fast values are shown as mean ± s.e.m., and n is the number of cells. All data are given to two significant figures. *$p < 0.05$ when compared to the deactivation time course of GluN1/GluN2A activated by D-glutamate and analyzed by one-way ANOVA with Tukey's *post hoc* test. ^$p < 0.05$ when compared to the deactivation time course of GluN1/GluN2D activated by L-glutamate and analyzed by one-way ANOVA with Tukey's *post hoc* test.

of the receptor not represented in the crystal structures studied in Vance et al. (2011).

I also measured the L-glutamate $EC_{50}$ (Table 3.5) and estimated the open probability ($P_{OPEN}$; Table 3.9) using the rate of onset of MK-801 block following activation by L-glutamate and glycine (Blanke and VanDongen, 2008) for the chimeric NMDA receptors expressed in *Xenopus* oocytes to determine if the differences in deactivation time course in the chimeric receptors were caused by agonist unbinding or channel gating. The estimated $P_{OPEN}$ values of the chimeric receptors did not significantly differ from GluN2A (Table 3.9). Only one point mutant (GluN2D-K779Y,V780I) had a significantly different estimated $P_{OPEN}$ compared to GluN2D, consistent with previous studies showing that the ATD is the primary determinant of the $P_{OPEN}$ of both GluN2A and GluN2D (Yuan et al., 2009). While the estimated $P_{OPEN}$ remained largely unaffected, the L-glutamate potency of GluN2A-(GluN2D D1D2) receptors ($EC_{50}$ = 0.44 $\pm$ 0.082; n=6) was similar to that of the wild type GluN2D NMDA receptors ($EC_{50}$ = 0.48 $\pm$ 0.078; n=4), in contrast to deactivation time course, which is shifted only partially toward the value for wild type GluN2A (Table 3.9). The $EC_{50}$ values for L-glutamate for GluN2A-(GluN2D D1) and GluN2A-(GluN2D D2) ($EC_{50}$ = 0.68 $\pm$ 0.20; n=4 and $EC_{50}$ = 1.2 + 0.20; n=4, respectively) were intermediate between GluN2A and GluN2D (Table 3.9).

### 3.4. Discussion

While NMDA receptors in general deactivate more slowly than the other members of the ionotropic glutamate receptor class, an exceptionally prolonged deactivation time course is a hallmark of GluN1/GluN2D receptors and distinguishes them from GluN2A-,

**Table 3.9.** Estimated open probability of GluN2A-GluN2D chimeric receptors and point mutants.

| Receptor | $\tau_{MK\text{-}801\ block}$ (ms) | Relative $P_{OPEN}$ | n |
|---|---|---|---|
| **GluN2A WT** | 2200 ± 200 | 0.48** | 13 |
| **GluN2A-(GluN2D D1D2)** | 4200 ± 490* | 0.27 ± 0.044 | 11 |
| **GluN2A-(GluN2D D1)** | 3200 ± 630 | 0.45 ± 0.097 | 10 |
| **GluN2A-(GluN2D D2)** | 3200 ± 630 | 0.33 ± 0.043 | 11 |
| **GluN2A-Y754K** | 2700 ± 490 | 0.45 ± 0.086 | 6 |
| **GluN2A-Y754K, I755V** | 2400 ± 490 | 0.47 ± 0.072 | 7 |
| | | | |
| **GluN2D WT** | 15000 ± 820 | 0.012** | 7 |
| **GluN2D-K779Y** | 14000 ± 1400 | 0.013 ± 0.0015 | 5 |
| **GluN2D-V780I** | 15000 ± 2400 | 0.012 ± 0.0018 | 4 |
| **GluN2D-K779Y, V780I** | 4700 ± 620 * | 0.037 ± 0.0028 * | 7 |

τ describing onset of MK-801 block and relative $P_{OPEN}$ are shown as mean ± s.e.m., and n is the number of cells. Relative $P_{OPEN}$ was calculated using the ratio of the block rate of MK-801 to the previously reported values for GluN2A and GluN2D $P_{OPEN}$. All data are given to two significant figures. **$P_{OPEN}$ values from Yuan et al. (2009). * $p < 0.05$ when analyzed by one-way ANOVA with Tukey's *post hoc* test.

GluN2B, and GluN2C-containing NMDA receptors. Every other NMDA receptor deactivates at least 5-fold more rapidly than GluN2D-containing receptors, with the most prominent difference occurring with the GluN2A-containing receptors, which deactivate at least 50-fold more rapidly (Vicini et al., 1998; Wyllie et al., 1998; Yuan et al., 2009; Vance et al., 2011). The underlying cause of the unusually prolonged deactivation time course of NMDA receptors remains elusive, although both ligand unbinding as well as the GluN2 subunit amino-terminal domain have been identified as potential mediators of deactivation. Here, I show that the GluN2D ligand-binding domain also contributes to the unusually long deactivation time course of GluN1/GluN2D receptors.

My data suggest that the GluN2D ligand-binding domain has a role in deactivation time course beyond ligand potency. L-glutamate, the endogenous NMDA receptor ligand in a majority of neuronal synapses, causes the receptor to deactivate slowly following the rapid removal of L-glutamate. GluN1/GluN2D deactivates rapidly when activated by other linear ligands, including L-aspartate, which may act as an endogenous ligand in several regions of the brain (Nicholls, 1989; Curras and Dingledine, 1992; Fleck et al., 1993; Zhang and Nadler, 2009). When activated by D-glutamate, the GluN1/GluN2D receptor deactivation time course is indistinguishable from its much more rapidly deactivating NMDA receptor family member GluN1/GluN2A. Although the deactivation time course of GluN1/GluN2D receptors appears to be related to agonist $EC_{50}$, ligands with shorter side chains, such as L-aspartate and D-aspartate, have deactivation time courses than cannot fully be predicted by ligand potency. Moreover, the stereoselective actions on deactivation are absent with aspartate analogues.

The relationship between deactivation time course and ligand potency previously has

been observed in both recombinant AMPA receptors and native NMDA receptors. AMPA receptors deactivate more rapidly when AMPA is the activating ligand than when 2-Me-Tet-AMPA, a much more potent ligand, is used to activate AMPA receptors (Zhang et al., 2006). Likewise, Lester and Jahr (1992) demonstrated that native NMDA receptors in hippocampal cultures are sensitive to ligand potency, deactivating more rapidly when activated by the less potent ligands NMDA, L-aspartate, or L-homocysteate than when activated by L-glutamate (Lester and Jahr, 1992). However, my data suggest that the deactivation time course of GluN1/GluN2D receptors cannot fully be predicted by ligand potency and must also be controlled by the structure of the receptor. While chimeras in which the GluN2D D1, D2, and D1D2 regions were inserted into GluN2A had slower deactivation time courses than wild type GluN2A when L-glutamate was the activating ligand, they did not significantly differ in D-glutamate deactivation time course compared to GluN2A. These data suggest that the GluN2D LBD may uniquely sense L-glutamate compared to D-glutamate or other linear ligands.

# Chapter 4: GluN1 splice variant control of GluN2D-containing NMDA receptors

## 4.1 Abstract

There are 8 GluN1 splice variants, which have been shown to influence NMDA receptor pharmacology, deactivation time course, and intracellular binding partners. Four GluN1 splice variants contain exon 5, which encodes a 21-amino acid insert in the amino-terminal domain. I investigated how the GluN1 subunit controls agonist potency, deactivation time course, and the single channel properties of GluN2D-containing receptors. I show GluN2D receptors containing the GluN1 splice variants that include exon 5 in the amino-terminal domain have less potent glutamate $EC_{50}$ values and have 3-fold more rapid deactivation time courses than the GluN1 subunits lacking exon 5. Lys211, a residue within GluN1 exon 5, mediates this shift in glutamate $EC_{50}$ and deactivation time course. Excised outside-out and cell-attached single channel patches show that GluN1-1b/GluN2D receptors, which include exon 5 in the GluN1 subunit, have a two-fold higher open probability than GluN1-1a/GluN2D, which does not have exon 5 within the GluN1 amino-terminal domain. This exon 5-mediated increase in the open probability of GluN1-1b/GluN2D NMDA receptors is due to a shortened mean shut time resulting from more rapid shut duration components. Cell-attached single channel recordings of GluN1-1a/GluN2D and GluN1-1b/GluN2D are similar to the excised patch single channel recordings and show that the key characteristics of GluN2D-containing single channel recordings are not dependent upon recording condition. These data indicate that the GluN1 subunit's amino-terminal domain is a key determinant of the single channel and macroscopic current properties of GluN2D-containing NMDA receptors.

## 4.2. Introduction

A single gene encodes the GluN1 subunit, but alternative splicing of three exons, exons 5, 21, and 22, leads to eight separate GluN1 isoforms (Fig. 4.1). The inclusion of exon five (in GluN1-b subunits), which encodes a 21-amino acid segment in the GluN1 amino-terminal domain, controls the deactivation time course, proton and zinc inhibition, and spermine potentiation of GluN2B-containing NMDA receptors (Durand et al., 1992; Hollmann et al., 1993; Williams, 1994; Zhang et al., 1994; Traynelis et al., 1995; Traynelis et al., 1998; Rumbaugh et al., 2000). Exon 21 encodes a 37-amino acid segment of the carboxyl-terminal, exon 22 encodes a separate 38-amino acid segment of the carboxyl-terminal, and deletion of exon 22 also eliminates a stop codon, leading to the inclusion of an alternate 22-amino acid C22' cassette in the C-terminal (Zukin and Bennett, 1995; reviewed in Traynelis et al., 2010). The GluN1 C-terminal mediates interactions with a number of intracellular proteins, including PSD-95 (Kornau et al., 1995; Rutter et al., 2002; Lin et al., 2004), calmodulin (Ehlers et al., 1996), and neurofilament-F (Ehlers et al., 1998), and may dictate the subcellular distribution of the GluN1 subunit (Ehlers et al., 1995; Horak and Wenthold, 2009).

The neuronal expression of both the GluN2D subunit and the individual GluN1 splice variants is region-specific. GluN1 splice variants containing residues encoded by exon 5 have significant expression within the subthalamic nucleus, thalamus, hippocampal neurons, the dentate, cortex, and the cerebellar granule layer, although it is not known what controls splice variant expression (Standaert et al., 1993; Laurie and Seeburg, 1994; Monyer et al., 1994; Standaert et al., 1994). The GluN2D subunit is expressed in abundance in all of these regions except the CA1 and the cortex, suggesting that native

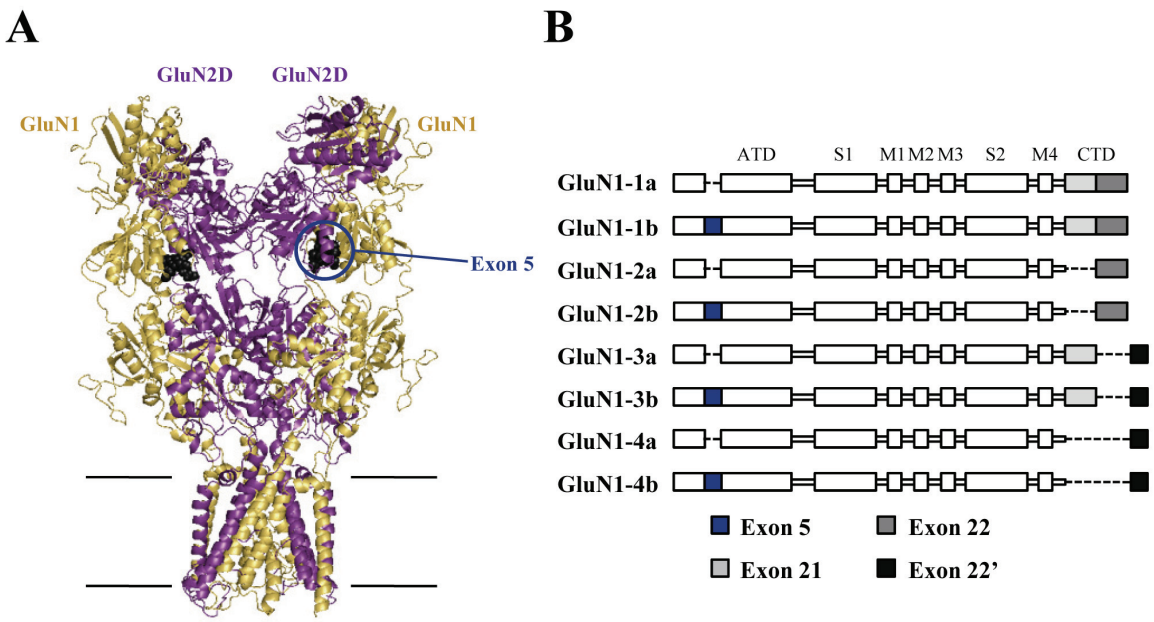


**Figure 4.1.** Eight GluN1 subunit splice variants have been identified. ***A***, A model of GluN1/GluN2D based on the GluA2 crystal structure (Sobolevsky et al., 2009) is shown (Acker et al., 2011). The GluN1 subunits are in yellow, and the GluN2D subunits are in purple. The region within the GluN1-1b amino-terminal domain where exon 5-encoded residues would be present is shown as dark gray. The intracellular carboxyl-terminal domain is omitted from the model. ***B***, A linear representation of the GluN1 polypeptide chain is shown for the 8 splice variants. The GluN1 splice variants are comprised of the amino-terminal domain (ATD), S1 and S2 domains which form the ligand binding domain, three transmembrane helices (M1, M3, and M4) and one reentrant loop (M2) that comprise the ion channel pore, and an intracellular carboxyl-terminal domain (CTD). Exon 5 (*blue*) encodes a 21-amino acid region within the ATD. Exon 21 (*gray*) encodes a 37-amino acid segment of the carboxyl-terminal tail, while exon 22 encodes a 38-amino acid segment of the CTD (*dark gray*). Deletion of exon 22 creates a shift in the open reading frame that results in the production of an alternate exon 22' (*black*), encoding a 22-amino acid region of the CTD. Adapted with permission from Vance et al. (2012).

GluN2D receptors may have unique gating properties compared to recombinant GluN1-1a/GluN2D.

I evaluated the role of the GluN1 subunit in GluN2D receptor pharmacology, deactivation time course, and channel open probability. I show that exon 5 of the GluN1 ATD controls deactivation time course and L-glutamate potency in GluN2D-containing NMDA receptors. Lys211, a residue in the GluN1-1b ATD encoded by exon 5, contributes to exon 5's control of L-glutamate deactivation time course and potency. The GluN1 subunit also has a role in the open probability of GluN2D-containing receptors, as GluN1-1b/GluN2D has a two-fold higher open probability compared to GluN1-1a/GluN2D in single channel recordings from excised outside-out and cell-attached patches of GluN1-1a/GluN2D and GluN1-1b/GluN2D. These data suggest that the GluN1 amino-terminal domain is a key determinant of GluN1/GluN2D NMDA receptor function.

## 4.3. Results

### *4.3.a. Exon 5 of the GluN1 ATD decreases agonist potencies*

GluN1 subunits containing exon 5-encoded residues are expressed in neurons that express GluN2D (Standaert et al., 1993; Laurie and Seeburg, 1994; Monyer et al., 1994; Standaert et al., 1994). Therefore, I evaluated whether inclusion of exon 5 into the GluN1 subunit influenced the pharmacology, deactivation time course, and single channel properties of GluN2D-containing NMDA receptors. I used two-electrode voltage-clamp recordings of GluN2D expressed with each of the GluN1 subunits to determine how the GluN1 splice variant influences L-glutamate and glycine potencies.

The inclusion of exon 5 in the GluN1 subunit appears to somewhat decrease glycine potency (i.e. raise $EC_{50}$) when expressed with GluN2D, but no significant difference was detected between the GluN1-1a splice variant and splice variants containing exon 5-encoded residues (one-way ANOVA; Table 4.1; Fig. 4.2A).

By contrast, the GluN1 exon 5 significantly influenced L-glutamate $EC_{50}$. L-glutamate has high potency (i.e. low $EC_{50}$) for GluN1-1a/GluN2D, with an $EC_{50}$ of 0.51 $\pm$ 0.039 μM (n=8; Table 4.1; Fig. 4.2B). Every GluN1 subunit containing the exon 5 insert in the ATD had at least 2-fold less potent L-glutamate $EC_{50}$ values than GluN1-1a/GluN2D (Table 4.1; Fig. 4.2B). The GluN1 C-terminal splice variants did not alter glutamate $EC_{50}$ values (Table 4.1; Fig. 4.2B). These data provide evidence that the amino-terminal domain of GluN1 controls agonist potency for GluN2D-containing receptors.

### *4.3.b. GluN1 splice variant control of GluN2D deactivation time course*

GluN1-1a/GluN2D receptors have been shown to have a slow deactivation time course following glutamate removal, a characteristic that is often considered a hallmark of GluN2D-containing receptors (Monyer et al., 1994; Vicini et al., 1998; Wyllie et al., 1998; Yuan et al., 2009; Vance et al., 2011). Previous studies suggest the GluN1 exon 5 splice variant controls the deactivation time course of other GluN2 subunits, as GluN1-1b/GluN2B receptors deactivate significantly more rapidly than GluN1-1a/GluN2B receptors (Rumbaugh et al., 2000). Therefore, I hypothesized that GluN2D subunits assembled with exon 5-containing GluN1 subunits likely would have significantly more rapid deactivation time courses upon the removal of L-glutamate than GluN2D-

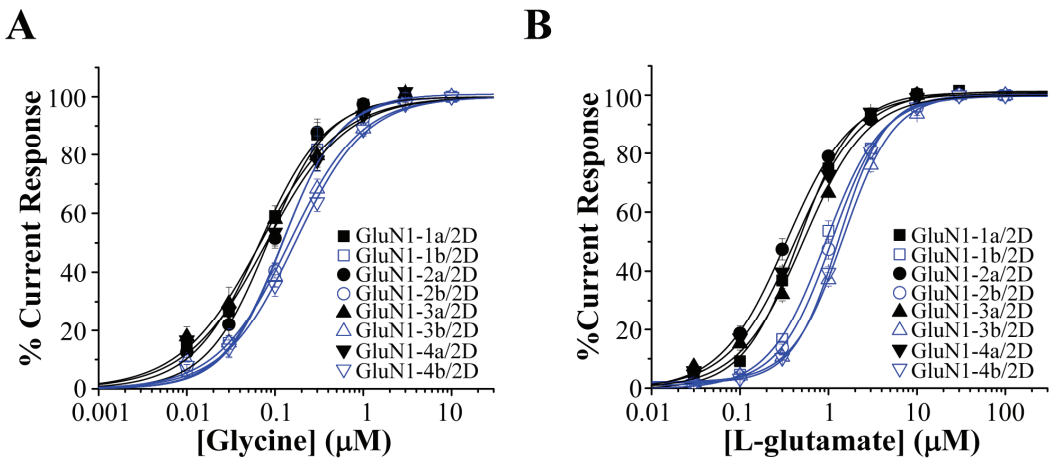


**Figure 4.2.** The inclusion of exon 5 in the GluN1 subunit decreases the potency of L-glutamate. ***A***, Two-electrode voltage-clamp recordings from *Xenopus* oocytes were used to determine the $EC_{50}$ values of glycine and L-glutamate for each GluN1 subunit. GluN1 splice variants that contain exon 5 are in blue, and exon 5-lacking GluN1 splice variants are in black. The $EC_{50}$ value for glycine was determined for each of the GluN1 splice variants (in the presence of 100 μM L-glutamate at pH 7.4). No GluN1 splice variant had a significantly different glycine $EC_{50}$ when compared to GluN1-1a/GluN2D ($p > 0.05$, one-way ANOVA). ***B***, The $EC_{50}$ value for L-glutamate was determined for each of the GluN1 splice variants in the presence of 30 μM glycine at pH 7.4. Exon 5 influenced L-glutamate $EC_{50}$, as every GluN1 splice variant containing exon 5 had an $EC_{50}$ significantly higher (i.e. less potent) than GluN1-1a/GluN2D ($p < 0.05$, one-way ANOVA with Tukey's *post hoc* test). Adapted with permission from Vance et al. (2012).

**Table 4.1.** GluN1 splice variant influences glutamate $EC_{50}$ values.

| Receptor | Glycine $EC_{50}$ (μM) | Slope | n | Glutamate $EC_{50}$ (μM) | Slope | n |
|---|---|---|---|---|---|---|
| **GluN1-1a/GluN2D** | 0.092 ± 0.0057 | 0.99 | 6 | 0.51 ± 0.039 | 1.3 | 8 |
| **GluN1-2a/GluN2D** | 0.087 ± 0.0070 | 1.4 | 7 | 0.36 ± 0.045 | 1.3 | 8 |
| **GluN1-3a/GluN2D** | 0.080 ± 0.015 | 0.90 | 4 | 0.58 ± 0.039 | 1.2 | 5 |
| **GluN1-4a/GluN2D** | 0.095 ± 0.21 | 0.90 | 4 | 0.47 ± 0.040 | 1.2 | 8 |
| **GluN1-1b/GluN2D** | 0.15 ± 0.027 | 1.8 | 7 | 0.93 ± 0.056* | 1.7 | 8 |
| **GluN1-2b/GluN2D** | 0.14 ± 0.017 | 1.5 | 7 | 1.1 ± 0.097* | 1.5 | 10 |
| **GluN1-3b/GluN2D** | 0.16 ± 0.023 | 1.0 | 4 | 1.5 ± 0.12* | 1.5 | 8 |
| **GluN1-4b/GluN2D** | 0.18 ± 0.024 | 1.0 | 4 | 1.3 ± 0.065* | 1.6 | 9 |

$EC_{50}$ values are reported as mean + s.e.m., and n is the number of cells. All data are given to two significant figures. Data were evaluated for statistical significance by comparison to the glycine or glutamate $EC_{50}$ value of GluN1-1a/GluN2D and analyzed by one-way ANOVA with Tukey's *post hoc* test. *$p<0.05$ when compared to the $EC_{50}$ value of glutamate on GluN1-1a/GluN2D. Statistical analyses were performed on the log($EC_{50}$), as $EC_{50}$ demonstrates a lognormal distribution (Christopoulos, 1998).

containing receptors assembled with GluN1 subunits lacking exon 5. I conducted whole cell voltage-clamp recordings of recombinant rat GluN2D expressed with each GluN1 subunit in HEK cells and evaluated how alternative splicing of the GluN1 subunit influences the deactivation time course of GluN2D-containing NMDA receptors.

GluN1/GluN2D receptors were activated by rapid application of 1 mM L-glutamate for 2 s (the co-agonist glycine (0.05 mM) was in all solutions), and the deactivation time course was measured following the removal of L-glutamate. GluN1-1a/GluN2D receptors deactivated slowly following removal of L-glutamate, with a deactivation time course that could best be described by a dual exponential function with time constants $\tau_{FAST}$ = 1100 $\pm$ 200 ms and $\tau_{SLOW}$ = 3400 $\pm$ 370 ms (n=5; Fig. 4.3A; Table 4.2). GluN1-1b/GluN2D, in which exon 5 of the GluN1 ATD and exons 21, and 22 of the GluN1 CTD are present (Fig. 4.1B), deactivates over 3-fold more rapidly than GluN1-1a/GluN2D receptors, with deactivation time constants $\tau_{FAST}$ = 420 $\pm$ 29 ms and $\tau_{SLOW}$ = 1100 $\pm$ 84 ms (n=9; Fig. 4.3B; Table 4.2; $p < 0.05$, one-way ANOVA). GluN1-2a ($\tau_{FAST}$ = 870 $\pm$ 150 ms and $\tau_{SLOW}$ = 2800 $\pm$ 190 ms; n=5) and GluN1-3a ($\tau_{FAST}$ = 1100 $\pm$ 200 ms and $\tau_{SLOW}$ = 3600 $\pm$ 350 ms; n=8) assembled with GluN2D did not deactivate significantly slower than GluN1-1a (Table 4.2), although GluN1-4a did cause a slight slowing in deactivation time course ($\tau_{FAST}$ = 910 $\pm$ 310 ms and $\tau_{SLOW}$ = 4000 $\pm$ 360 ms; n=6; $p<0.05$, one-way ANOVA with Tukey's *post hoc* test). This suggests that the carboxyl-terminal tail may have a modest role in deactivation time course in addition to the extracellular ATD (Fig. 4.3A; Table 4.2). Like GluN1-1b, GluN1-2b ($\tau_{FAST}$ = 370 $\pm$ 47 ms and $\tau_{SLOW}$ = 930 $\pm$ 110 ms, n = 6), GluN1-3b ($\tau_{FAST}$ = 410 $\pm$ 45 ms and $\tau_{SLOW}$ = 1500 $\pm$ 400 ms, n = 4), and GluN1-4b ($\tau_{FAST}$ = 630 $\pm$ 16 ms and $\tau_{SLOW}$ =

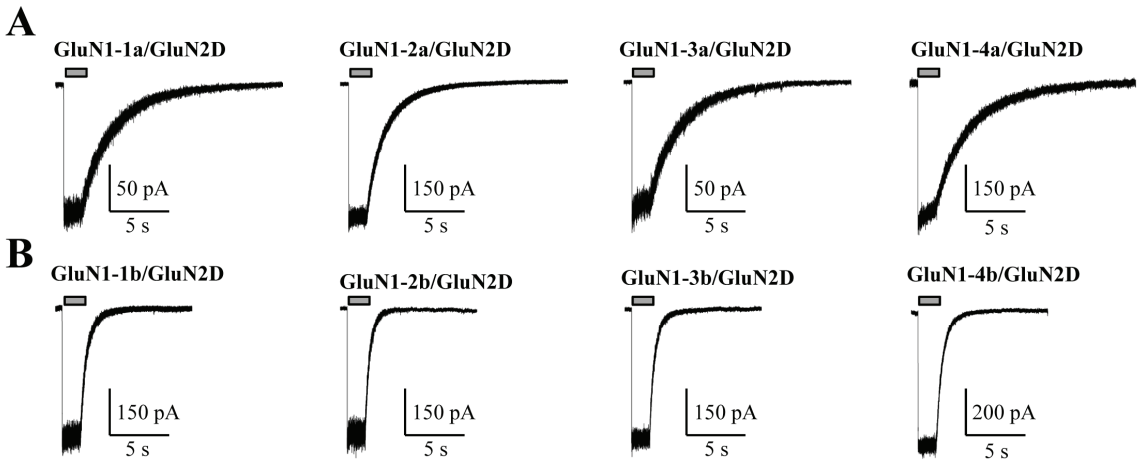


**Figure 4.3.** Exon 5 decreases the deactivation time course of GluN1/GluN2D NMDA receptors. ***A***, The deactivation time course of GluN1/GluN2D receptors was determined by applying L-glutamate (1 mM) to transfected HEK 293 cells for 2 s (gray bars), while 0.05 mM glycine was present in all solutions. GluN1-1a/GluN2D receptors deactivate slowly upon removal of glutamate, with $\tau_{FAST}$ = 1100 $\pm$ 200 ms and $\tau_{SLOW}$ = 3400 $\pm$ 370 ms (n=5). ***B***, GluN1-1b/GluN2D receptors deactivate more rapidly, with $\tau_{FAST}$ = 420 $\pm$ 29 ms and $\tau_{SLOW}$ = 1100 $\pm$ 84 ms (n=9). Every GluN1 splice variant containing exon 5 (GluN1-b) deactivated significantly more rapidly than GluN1-1a/GluN2D, but did not have deactivation time courses significantly different than each other ($p < 0.05$, one-way ANOVA with Tukey's *post hoc* test). Adapted with permission from Vance et al. (2012).

**Table 4.2.** GluN1 splice variants containing exon 5 have more rapid deactivation time courses.

| GluN1 Subunit | $\tau_{FAST}$ (ms) | $\tau_{SLOW}$ (ms) | $\tau_{W}$ (ms) | % fast | Rise Time (ms) | n |
|---|---|---|---|---|---|---|
| **GluN1-1a** | 1100 ± 200 | 3400 ± 370 | 2500 ± 300 | 41 ± 6.1 | 4.4 ± 0.59 | 5 |
| **GluN1-2a** | 870 ± 150 | 2800 ± 190 | 2300 ± 100 | 28 ± 8.9 | 3.3 ± 0.30 | 5 |
| **GluN1-3a** | 1100 ± 200 | 3600 ± 350 | 3300 ± 280 | 29 ± 4.0 | 4.7 ± 0.77 | 8 |
| **GluN1-4a** | 910 ± 310 | 4000 ± 360 | 3500 ± 210* | 16 ± 6.1 | 6.9 ± 0.76 | 6 |
| **GluN1-1b** | 420 ± 29 | 1100 ± 84* | 680 ± 32* | 52 ± 7.6 | 5.4 ± 0.51 | 9 |
| **GluN1-2b** | 370 ± 47 | 930 ± 110* | 680 ± 59* | 42 ± 5.3 | 4.5 ± 0.53 | 6 |
| **GluN1-3b** | 410 ± 45 | 1500 ± 400* | 600 ± 50* | 73 ± 8.7 | 4.1 ± 0.36 | 4 |
| **GluN1-4b** | 630 ± 16 | 1900 ± 170* | 1100 ± 230* | 91 ± 6.4 | 5.9 ± 1.0 | 6 |

$\tau_{FAST}$, $\tau_{SLOW}$, $\tau_{W}$, % fast values, and rise time are shown as mean ± s.e.m., and n is the number of cells. All data are given to two significant figures. *$p$<0.05 when compared to the deactivation time course of GluN1-1a/GluN2D and analyzed by one-way ANOVA with Tukey's *post hoc* test.

1900 ± 170 ms, n = 6) assembled with GluN2D had significantly more rapid deactivation time courses than GluN1-1a/GluN2D (Fig. 4.3B; Table 4.2; $p<0.05$, one-way ANOVA with Tukey's *post hoc* test). GluN1 splice variant did not influence 10-90% response rise time for any subunit combinations (Table 4.2). Desensitization did not appear to be a major characteristic of GluN2D receptors, as only 10 of the 49 total cells evaluated showed more than 10% desensitization of the agonist-evoked current, and no cell had more than 15% desensitization of the current.

### *4.3.c. Lys211 in the GluN1-1b ATD is necessary for exon 5 control of potency and deactivation time course*

The residues encoded by GluN1 exon 5 contain a number of charged or electronegative residues that may form intra- or inter-subunit contacts that influence NMDA receptor function, including agonist $EC_{50}$, deactivation time course, and sensitivity to pH, $Zn^{2+}$, and polyamines (Fig. 4.4A; Hollmann et al., 1993; Williams, 1994; Traynelis et al., 1995; Traynelis et al., 1998; Rumbaugh et al., 2000). To identify the structural determinants of exon 5's control of potency and deactivation time course on GluN1/GluN2D receptors, we mutated individually or in groups of three each charged residue within exon 5 to neutral residues. Of the evaluated mutants, GluN1-1b-K207G R208G K211G, GluN1-1b-K211G, GluN1-1b-K211A, and GluN1-1b-K211L significantly decreased glutamate $EC_{50}$ (Fig. 4.4B). GluN1-1b-E197A D200A D205A also significantly decreased glutamate $EC_{50}$, but the individual point mutants GluN1-1b-E197A, GluN1-1b-D200A, and GluN1-1b-D205A had no effect (Fig. 4.4B). GluN1-1b-K207G R208G K211G, GluN1-1b-K211A, GluN1-1b-K211L, and GluN1-1b-K211G

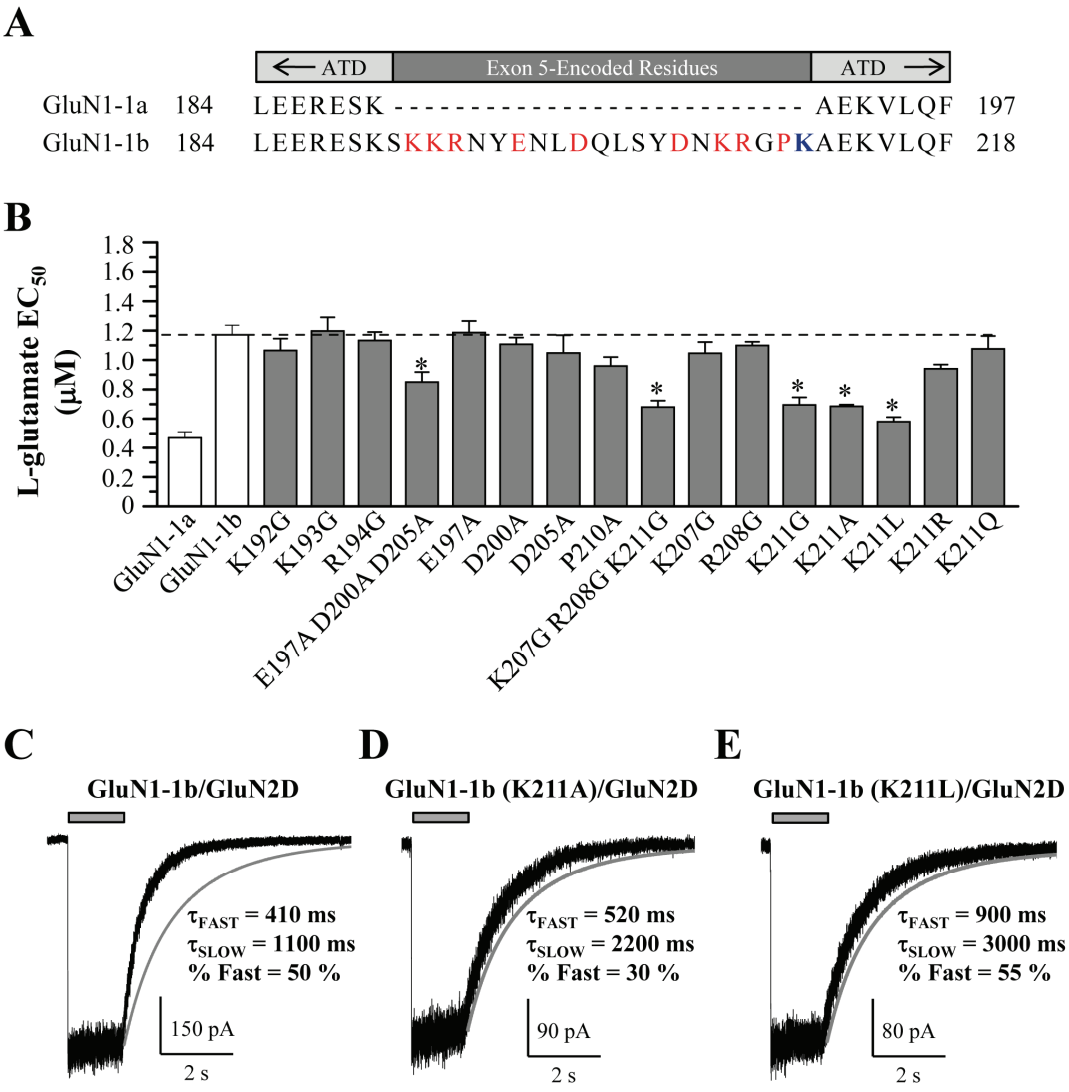


**Figure 4.4.** Lys211 of the GluN1 subunit ATD controls GluN2D L-glutamate potency and deactivation time course. Exon 5 encodes a highly charged 21-amino acid insert in the GluN1 ATD (***A***). Screening GluN1-1b exon 5 point mutants in which one or more of the charged residues has been converted to an uncharged residue (*red*) using two-electrode voltage-clamp recordings of *Xenopus* oocytes shows that removing the size and charge of Lys211 (*blue*) significantly increases L-glutamate potency (***B***). Whole cell voltage-clamp recordings of transfected HEK 293 cells were conducted by rapidly applying 1 mM L-glutamate to cells for 2 s; 0.05 mM glycine was present in all solutions. ***C***, GluN1-1b-K211A and GluN1-1b-K211L slow the deactivation time course compared to GluN1-1b/GluN2D, suggesting that Lys211 has a role in exon 5-mediated control of the deactivation time course. Adapted with permission from Vance et al. (2012).

significantly decreased glutamate $EC_{50}$ (i.e. increased potency) compared to wild-type GluN1-1b (Fig. 4.4B; one-way ANOVA with Tukey's *post hoc* test). Lys211, a residue encoded by exon 5, previously has been identified as the key determinant of exon 5-mediated control of spermine potentiation, proton inhibition, and $Zn^{2+}$ inhibition of GluN2B-containing NMDA receptors (Traynelis et al., 1995; Traynelis et al., 1998).

Because ligand $EC_{50}$ is related to NMDA receptor deactivation time course (e.g. Vance et al., 2011), I hypothesized that mutations at the GluN1-1b Lys211 that show lower (i.e. more potent) L-glutamate $EC_{50}$ values also would have a slower deactivation time course than wild-type GluN1-1b. I conducted whole cell voltage-clamp recordings of transfected HEK cells, and currents were evoked by rapid 2 s application of 1 mM L-glutamate (0.05 mM glycine was in all solutions). GluN1-1b-K211G/GluN2D, GluN1-1b-K211A/GluN2D, and GluN1-1b-K211L/GluN2D had significantly slower deactivation time courses compared to wild type GluN1-1b/GluN2D ($p < 0.05$, one-way ANOVA with Tukey's *post hoc* test; Fig. 4.4C-E; Table 4.3). GluN1-1b-K211R and GluN1-1b-K211Q, which replaced the lysine side chain with a similarly charged group (R) or hydrogen bonding group (Q), did not significantly influence L-glutamate potency or deactivation time course compared to wild-type GluN1-1b (Table 4.3). These data suggest that among the various charged residues encoded by exon 5, Lys211 is an important determinant of deactivation time course.

### *4.3.d. Exon 5 increases the open probability of GluN2D-containing NMDA receptors*

To determine how the GluN1 splice variant influences the single channel properties of GluN2D-containing NMDA receptors, I recorded excised outside-out patches of

**Table 4.3.** Point mutations within exon 5 influence the deactivation time course of GluN1-1b/GluN2D receptors.

| Receptor | $\tau_{FAST}$ (ms) | $\tau_{SLOW}$ (ms) | $\tau_W$ (ms) | % fast | n |
|---|---|---|---|---|---|
| **GluN1-1b / GluN2D** | 420 ± 29 | 1100 ± 84 | 680 ± 32 | 52 ± 7.6 | 9 |
| **GluN1-1b-K207G R208G K211G / GluN2D** | 490 ± 100 | 1500 ± 130 | 1100 ± 48* | 31 ± 8.8 | 6 |
| **GluN1-1b-K211G / GluN2D** | 470 ± 130 | 1400 ± 100 | 1200 ± 43* | 29 ± 7.8 | 5 |
| **GluN1-1b-K211R / GluN2D** | 210 ± 79 | 890 ± 110 | 700 ± 39 | 26 ± 8.0 | 6 |
| **GluN1-1b-K211Q / GluN2D** | 280 ± 70 | 890 ± 140 | 660 ± 53 | 33 ± 11 | 5 |

$\tau_{FAST}$, $\tau_{SLOW}$, $\tau_W$, and % fast values are shown as mean ± s.e.m., and n is the number of cells. All data are given to two significant figures. *$p<0.05$ when compared to the deactivation time course of GluN1-a/GluN2D and analyzed by one-way ANOVA with Tukey's *post hoc* test. Data for GluN1-1b/GluN2D is reproduced here for comparison.

GluN1-1a/GluN2D and GluN1-1b/GluN2D that contained a single active channel GluN1/GluN2D receptors were activated by steady-state applications of maximally effective concentrations of L-glutamate (1 mM) and glycine (0.05 mM) in 0.5 mM extracellular $Ca^{2+}$, with a holding potential of -80 mV. Even while in saturating ligand, GluN1-1a/GluN2D receptors open rarely, showing brief openings and prolonged periods of inactivation, as demonstrated by the representative trace in Fig. 4.5A. GluN1-1a/GluN2D receptors have an exceptionally low open probability ($P_{OPEN}$) of 0.017 $\pm$ 0.003 (Table 4.4; n=10), which is more than 20-fold lower than GluN1-1a/GluN2A receptors (~0.48; Yuan et al., 2009). The apparent mean open time of GluN1-1a/GluN2D receptors is brief, at 0.44 $\pm$ 0.039 ms, and the open duration histograms could be fit with the sum of two exponential components for each of the ten single channel recordings (representative histogram given in Fig 4.5B). The fitted time constants from the GluN1-1a/GluN2D receptor open duration histogram are $\tau_1$ of 0.039 $\pm$ 0.0058 ms (29%) and a slower time constant $\tau_2$ of 0.60 $\pm$ 0.039 ms (71%) (Table 4.4).

Open probability increases more than 2-fold in GluN1-1b/GluN2D receptors, with a $P_{OPEN}$ of 0.037 $\pm$ 0.0087 (n=5; Fig. 4.6A). While the open probability is increased, the open periods remain brief (Fig. 4.6B). The mean open time of GluN1-1b/GluN2D receptors is not significantly different than GluN1-1a/GluN2D receptors, at 0.58 $\pm$ 0.057 ms ($p > 0.05$; unpaired t-test). The GluN1-1b/GluN2D open time duration histograms could be fit with the sum of two exponential equations, with a short open time constant of $\tau_1$ of 0.011 $\pm$ 0.021 ms (20%) and a longer time constant $\tau_2$ of 0.70 $\pm$ 0.043 ms (80%) (Fig. 4.6B; Table 4.4). Although the GluN2D-containing receptor is sensitive to protons,

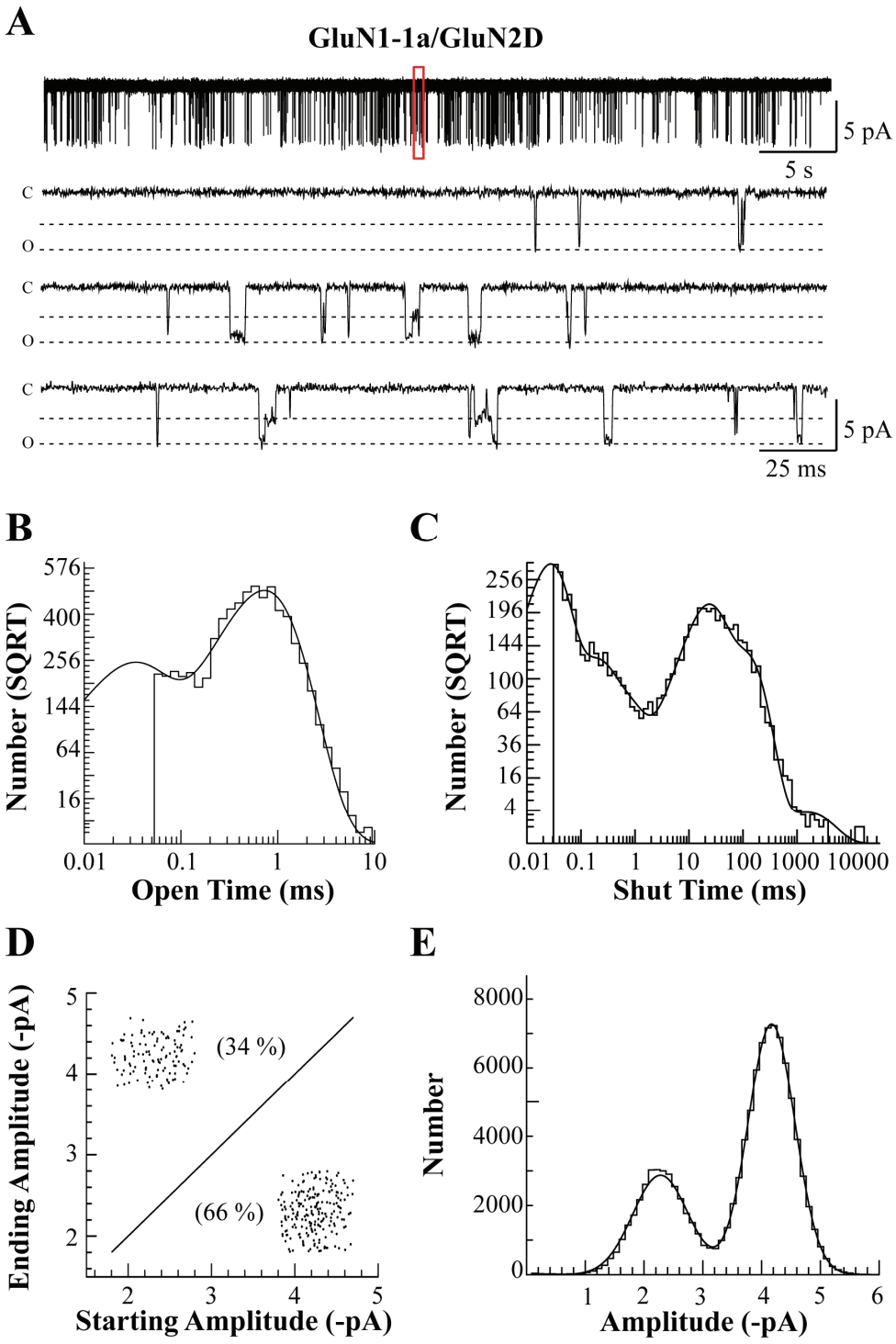


**Figure 4.5.** GluN1-1a/GluN2D channels have low open probability. Single channel voltage-clamp recordings of 10 excised outside-out patches with 1 active channel were recorded in 1 mM L-glutamate, 0.05 mM glycine, and 0.5 mM $CaCl_2$ ($V_{HOLD}$ = -80 mV). ***A***, A representative steady-state GluN1-

1a/GluN2D single channel recording is shown. ***B***, Open duration histogram for this representative patch for GluN1-1a/GluN2D channels can be fitted by two brief exponential components, whereas the shut time histogram (***C***) was best fit with seven exponential components. ***D***, GluN1-1a channels opened to two conductance levels (***E***) that had asymmetrical transitions between sublevels, with transitions from the higher to the lower conductance level being more frequent. For all figures, "SQRT" indicates that the ordinate of the histograms is plotted on a square root scale. Adapted with permission from Vance et al. (2012).

**Table 4.4.** Single channel properties of GluN1-1a/GluN2D and GluN1-1b/GluN2D in excised outside-out patches

| Parameters | GluN1-1a/GluN2D | GluN1-1b/GluN2D |
|---|---|---|
| **n** | 10 | 5 |
| **$P_{OPEN}$** | 0.017 ± 0.0033 | 0.037 ± 0.0087* |
| **Mean open duration (ms)** | 0.44 ± 0.039 | 0.58 ± 0.057 |
| **τ1, ms (%)** | 0.039 ± 0.0058 (29%) | 0.11 ± 0.029* (20%) |
| **τ2, ms (%)** | 0.60 ± 0.039 (71%) | 0.70 ± 0.043 (80%) |
| **Mean shut duration (ms)** | 47 ± 9.1 | 22 ± 4.7 |
| **τ0, ms (%)** | 0.030 ± 0.0028 (31%) | 0.030 ± 0.0021 (40%) |
| **τ1, ms (%)** | 0.28 ± 0.076 (12%) | 0.25 ± 0.038 (17%) |
| **τ2, ms (%)** | 4.5 ± 0.90 (6%) | 3.3 ± 0.35 (8%) |
| **τ3, ms (%)** | 25 ± 4.0 (20%) | 16 ± 2.3 (24%) |
| **τ4, ms (%)** | 66 ± 5.6 (19%) | 73 ± 11 (10%) |
| **τ5, ms (%)** | 220 ± 57 (11%) | - |
| **τ6, ms (%)** | 3700 ± 910 (1%) | 1200 ± 180 (<1%) |

Data are reported as mean + s.e.m., are given to two significant figures, and n is the number of patches. Each patch was recorded from a different cell. Patches contained a single active channel and were recorded at pH 8.0. Contiguous open periods with different unitary currents were combined. Data analyzed for statistical significance by unpaired two-tailed t-test. *$p$<0.05 when compared to the corresponding value for GluN1-1a/GluN2D.

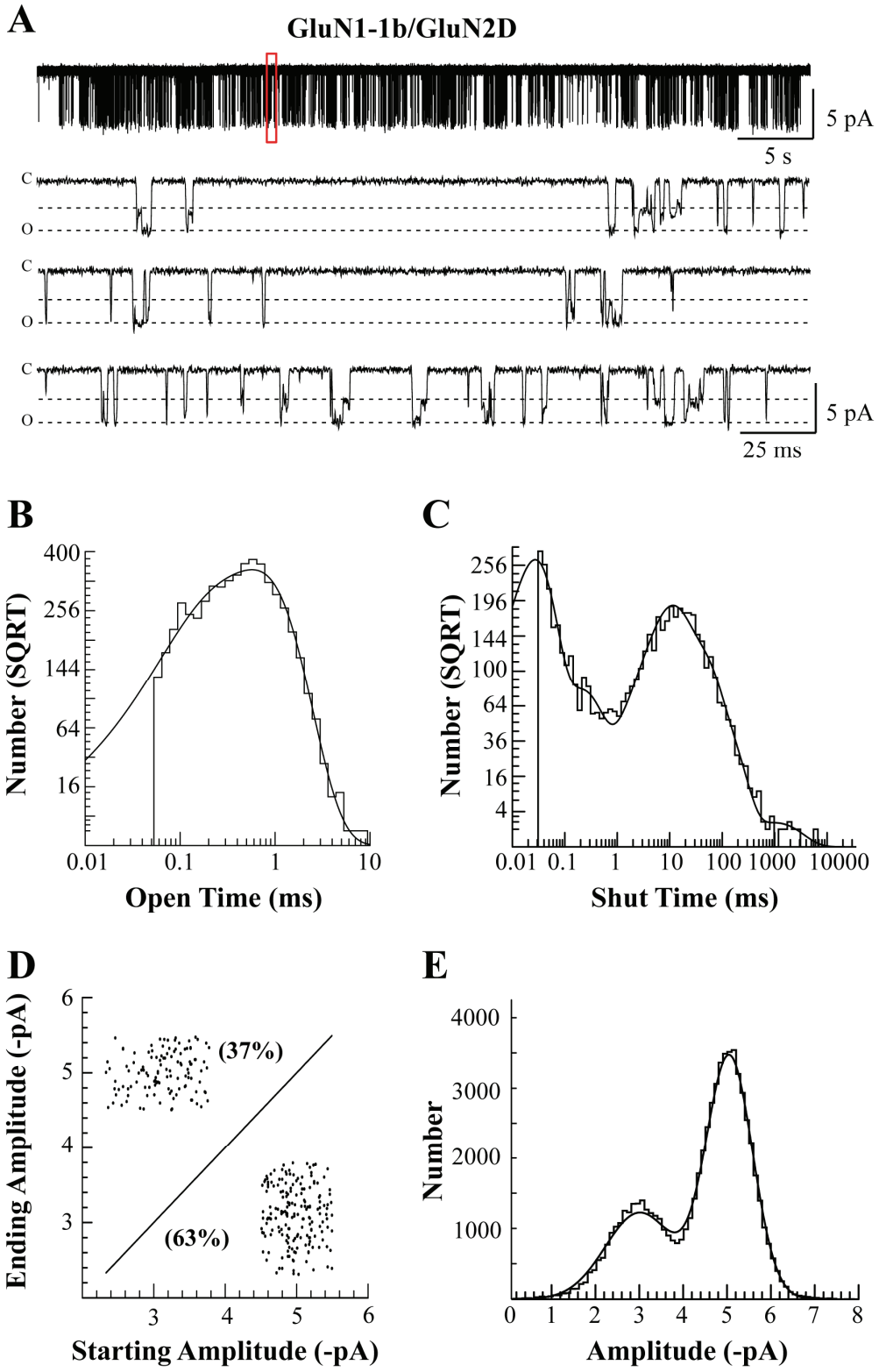


**Figure 4.6.** GluN1-1b/GluN2D channels have a higher open probability than GluN1-1a/GluN2D channels. I evaluated 5 excised outside-out patches each with 1 active channel. ***A***, A representative single channel

recording of channels recorded in 1 mM L-glutamate, 0.05 mM glycine, and 0.5 mM $CaCl_2$ ($V_{HOLD}$ = -80 mV). ***B***, Two exponential components were required to describe the open duration histogram for GluN1-1b/GluN2D channels. ***C***, The shut duration histogram was best fit with six components, of which three were more rapid than GluN1-1a/GluN2D. ***D***, GluN1-1b/GluN2D channels have two conductance levels (***E***), with direct transitions between these levels being asymmetric. The majority of direct transitions originated in the higher conductance state. Adapted with permission from Vance et al. (2012).

recording at pH 8.0 eliminated tonic proton inhibition for GluN1 containing exon 5-encoded residues and reduced tonic inhibition for GluN1 lacking exon 5-enocded residues to 17%. Using the fitted $IC_{50}$ values for proton inhibition (Traynelis et al., 1995), I calculated that at most only 20% of the increase in open probability observed for exon 5-containing receptors reflects reduced proton inhibition compared to exon 5-lacking receptors.

While no significant changes were observed in the mean open times and open duration histograms, the shut time histograms differed between GluN1-1a/GluN2D and GluN1-1b/GluN2D. GluN1-1a/GluN2D single channel records had a mean shut time of 47 $\pm$ 9.1 ms (Table 4.4). The shut duration histogram of GluN1-1a/GluN2D (Fig. 4.5C) could be fitted with seven exponential functions with time constants and areas of 0.030 $\pm$ 0.0028 ms (31%), 0.28 $\pm$ 0.076 ms (12%), 4.5 $\pm$ 0.90 ms (6%), 25 $\pm$ 4.0 ms (20%), 66 $\pm$ 5.6 ms (19%), 220 $\pm$ 57 ms (11%), and 3700 $\pm$ 910 ms (1%). The mean shut time of GluN1-1b/GluN2D was decreased to 22 $\pm$ 4.7 ms, and the number of shut time constants describing the shut time distribution was reduced to six (Table 4.4). The shut duration histograms for GluN1-1b/GluN2D receptors (Fig. 4.6C) were fitted with six exponential functions to give time constants and areas of 0.030 $\pm$ 0.0021 ms (40%), 0.25 $\pm$ 0.038 ms (17%), 3.3 $\pm$ 0.35 ms (8%), 16 $\pm$ 2.3 ms (24%), 73 $\pm$ 11 ms (10%), and 1200 $\pm$ 180 ms (<1%). This analysis shows that the open probability of GluN1-1b/GluN2D is increased due to the loss of the second longest closed state observed in GluN1-1a/GluN2D receptors (see Table 4.4).

Because one goal was to later evaluate a number of kinetic models in order to further assess the effects of exon 5-encoded residues on NMDA receptor function, I tested

whether correlations between successive open periods were present in GluN1-1a/GluN2D and GluN1-1b/GluN2D single channel records. The presence of correlations in the single channel data record could suggest certain patterns of connectivity between closed and open states (Colquhoun and Hawkes, 1987). I found no significant correlation between different open periods for GluN1-1a/GluN2D (n=10) when using a critical open time of 0.075 ms in the runs test or GluN1-1b/GluN2D (n=5) when using a critical open time of 0.14 ms in the runs test (Jackson et al., 1983; Colquhoun and Sakmann, 1985).

Although I did not observe strong detectable correlations between successive open periods, I explored the potential relationship between adjacent open and closed periods by calculating the mean duration of conditional open periods preceding shut periods of a specific duration (Fig. 4.7). Shut periods were determined from the critical times calculated to optimally separate shut time components (Jackson et al., 1983). Figure 4.7B shows the conditional open durations for GluN1-1a/GluN2D, and suggests a 50% decrease in the conditional mean open times adjacent to the slowest shut times compared to those adjacent to the briefest shut times ($p < 0.05$; one-way ANOVA with Tukey's *post hoc* test). Similar results were obtained by looking at the relationship of open times adjacent to shut times of a specified duration for GluN1-1b/GluN2D ($p < 0.05$; one-way ANOVA with Tukey's *post hoc* test).

### *4.3.e. Exon 5 does not influence GluN1/GluN2D conductance levels*

GluN1-1a/GluN2D channels exhibited two main conductance levels in the presence of 0.5 mM extracellular $Ca^{2+}$ in all ten outside-out patches, with a higher conductance level of 51 $\pm$ 1.7 pS (69 $\pm$ 1.1%) and a lower sublevel of 30 $\pm$ 0.92 pS (31 $\pm$ 1.1%;

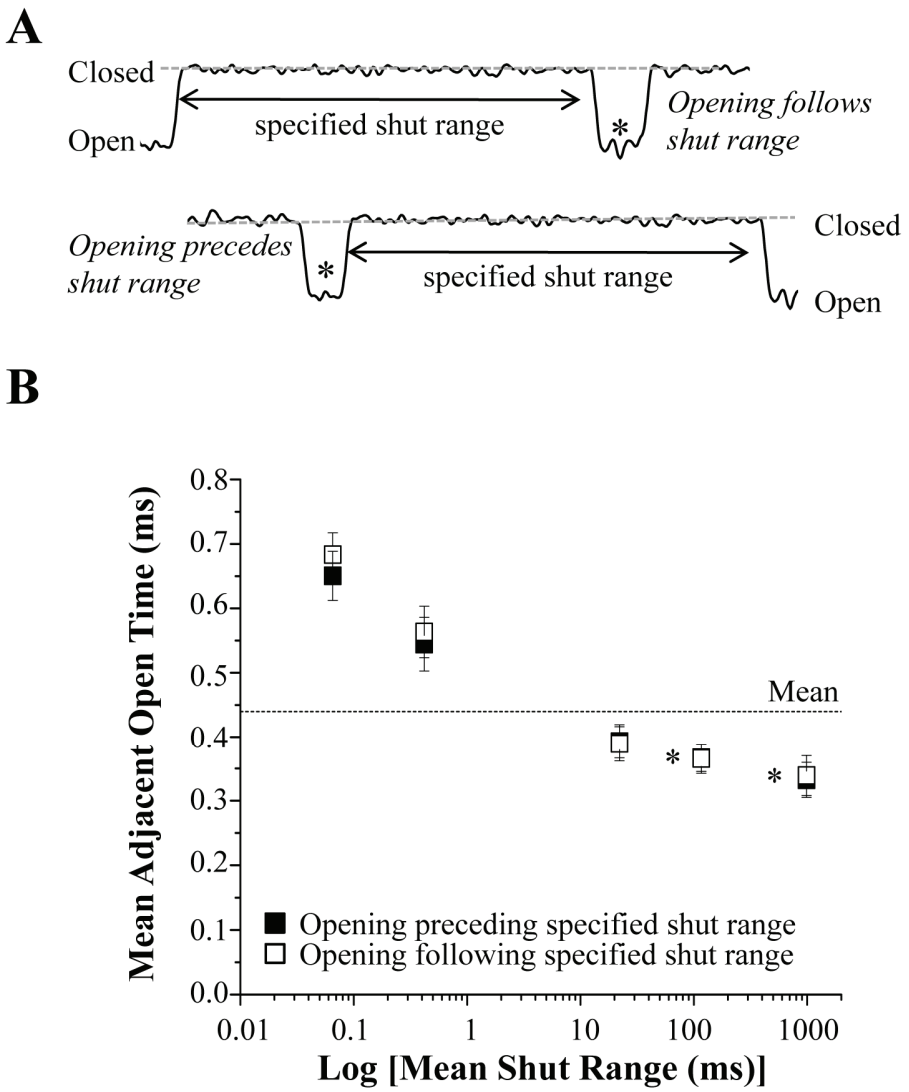


**Figure 4.7.** Evaluation of potential correlations between adjacent open and shut durations in GluN2D-containing receptors. ***A***, Single channel recordings can be evaluated to determine the mean open time when an opening follows or precedes a shut range. ***B***, I used time constants describing the closed duration histogram to determine critical closed times, as described in Jackson et al. (1983). The critical closed times for GluN1-1a/GluN2D receptors were 0.10, 0.74, 43, 190, and 1800 ms. Conditional apparent open duration distributions for 10 single channel recordings in 1 mM L-glutamate and 0.05 mM glycine at pH

8.0 were constructed for openings preceding (■) or following (□) the specified shut duration ranges. The mean adjacent open time is plotted against the center of the mean shut range. The specified shut ranges were 0.031-0.1, 0.1-0.74, 0.74-43, 43-190, and 190-1800 ms. The conditional mean open times of openings adjacent to the longest shut durations were significantly shorter than the openings adjacent to the shortest shut duration ($p < 0.05$; one-way ANOVA with Tukey's *post hoc* test). The dashed line represents the mean open time from 10 GluN1-1a/GluN2D patches (0.44 ms). Adapted with permission from Vance et al. (2012).

Fig. 4.5A,D,E). The transitions between the two conductance levels are asymmetric, with more transitions occurring from the higher to lower conductance level, as has been previously reported in recordings from GluN1/GluN2D receptors expressed in oocytes (Wyllie et al., 1996; Chen et al., 2004) and HEK cells (Yuan et al., 2009). I detected 2035 direct transitions between the two conductance states (Fig. 4.5D), with 1310 transitions from the higher to lower conductance level (66 $\pm$ 2.0%) and 725 transitions from the lower to higher conductance level (34 $\pm$ 2.0%).

GluN1-1b/GluN2D receptors also have two main conductance levels, with a higher conductance level of 54 $\pm$ 2.5 pS (63 $\pm$ 4.5%) and a lower conductance level of 39 $\pm$ 0.66 pS (Fig. 4.6A,D,E; 37 $\pm$ 4.5%; n=5). The transitions between conductance levels are asymmetric, and in a total of 1733 direct transitions between the two conductance states, 1066 transitions were from the high conductance level to the subconductance level (63 $\pm$ 2.2%), while 667 transitions (37 $\pm$ 2.2%) were observed for transitions from the lower to higher conductance level (Fig. 4.6D). These data suggest that residues encoded by exon 5 do not influence channel conductance or the ability of the channel to transition between conductance levels. These results are consistent with recently published work suggesting that conductance levels, $Mg^{2+}$ block, and $Ca^{2+}$ permeability are controlled by a single residue within the GluN2D pore (Retchless et al., 2012).

### *4.3.f. The properties of GluN2D-containing NMDA receptors are conserved in cell-attached patches*

In addition to recording from excised patches, I evaluated the single channel properties for GluN2D-containing receptors in cell-attached patches (Fig. 4.8), as it is possible that

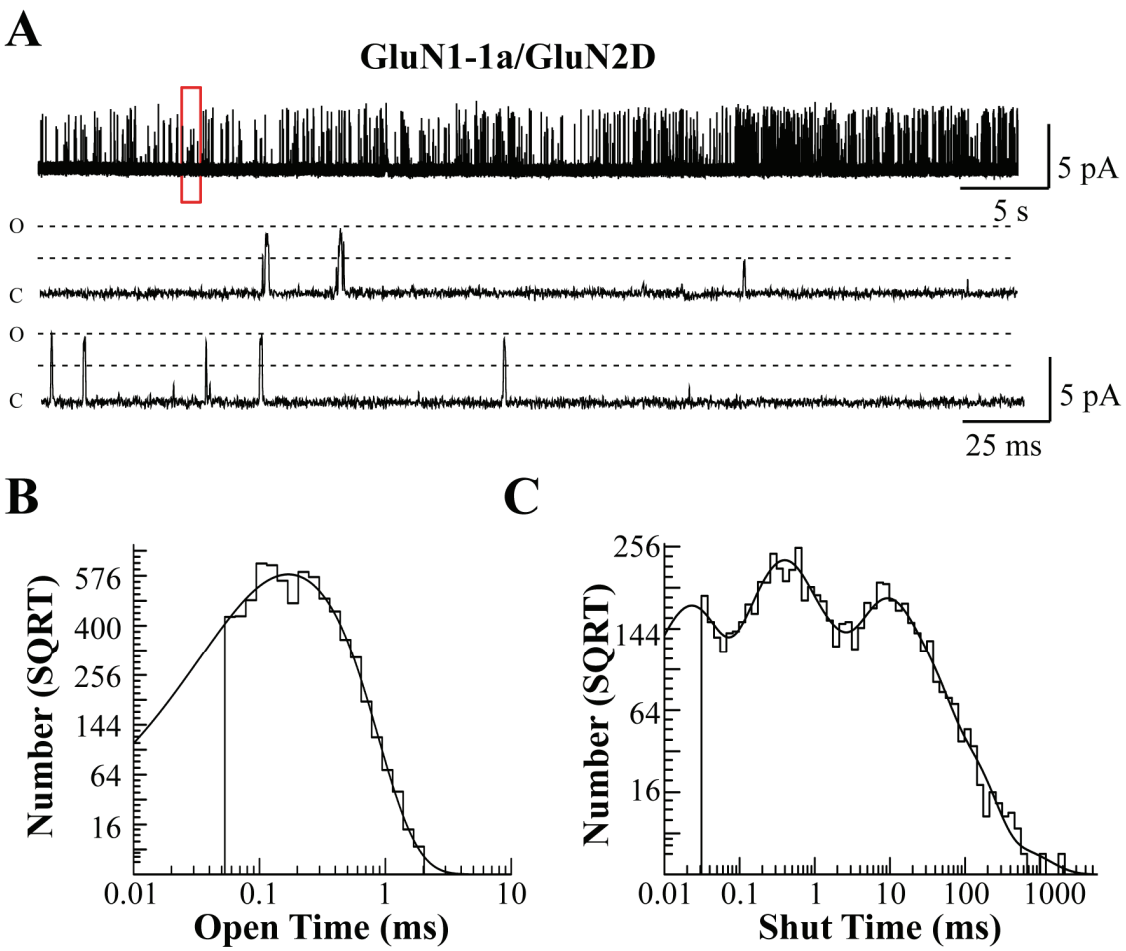


**Figure 4.8.** GluN1-1a/GluN2D receptors in cell-attached patches have low open probabilities. ***A***, I evaluated the single channel characteristics of GluN1-1a/GluN2D receptors in cell-attached patches in transfected HEK 293 cells. Channels were activated by a solution containing 1 mM L-glutamate, 0.05 mM glycine, and 0.5 mM $CaCl_2$ at pH 8.0 ($V_{HOLD}$ = +80 mV); patches contained a single active channel. ***B***, Two exponential components were fitted to the open duration histogram for GluN1-1a/GluN2D channels and were similar to the open components of GluN1-1a/GluN2D in excised outside-out patches. ***C***, The shut duration histogram was best fitted with seven exponential components.

important intracellular binding partners and other factors may be lost when a patch is excised from the plasma membrane. I found that the open probability of GluN1-1a/GluN2D remained low in cell-attached patches with one active channel (0.0091 ± 0.0032; n=5; Table 4.5). The open periods in 5 recordings with a total of 23,802 open periods were brief, with a mean open duration of 0.21 ± 0.014 ms and mean time constants describing the open time distribution of 0.047 ± 0.012 ms (26%) and 0.26 ± 0.015 ms (74%) (Table 4.5; Fig. 4.8B). The mean shut time was 51 ± 15 ms, and the shut time histogram was again best fit by 7 exponential components, which were similar to the components of GluN1-1a/GluN2D in excised patches, with time constants 0.028 ± 0.0056 ms (17%), 0.31 ± 0.041 ms (25%), 5.1 ± 2.2 ms (14%), 28 ± 5.4 ms (16%), 81 ± 15 ms (17%), 200 ± 30 ms (11%), and 3200 ± 810 ms (<1%) (Table 4.5; Fig. 4.8C).

As in excised patches, the open probability of GluN1-1b/GluN2D was significantly higher than GluN1-1a/GluN2D, with an open probability of 0.037 ± 0.011 (n=5) (Fig. 4.9A). The mean open time was 0.35 ± 0.12 ms in 5 recordings with a total of 36,136 open periods, with open duration time components of 0.080 ± 0.038 ms (24%) and 0.43 ± 0.14 ms (76%) (Table 4.5; Fig. 4.9B). GluN1-1b/GluN2D receptors closed for significantly shorter durations than GluN1-1a/GluN2D receptors, with a mean shut time of 13 ± 2.7 ms ($p < 0.05$, unpaired t-test). The shut time histogram was similar to GluN1-1b/GluN2D in excised patches and could best be fit by 6 exponential components, with time constants 0.022 ± 0.0038 ms (25%), 0.32 ± 0.034 ms (26%), 2.1 ± 1.5 ms (17%), 15 ± 3.4 ms (16%), 42 ± 2.2 ms (15%), and 890 ± 300 ms (<1%) (Table 4.5; Fig. 4.9C). I interpret these data to suggest that the key gating characteristics of GluN2D-

**Table 4.5.** Single channel properties of GluN1-1a/GluN2D and GluN1-1b/GluN2D in cell-attached patches

| Parameters | GluN1-1a/GluN2D | GluN1-1b/GluN2D |
|---|---|---|
| ***n*** | 5 | 5 |
| **$P_{OPEN}$** | 0.0091 ± 0.0032 | 0.037 ± 0.011* |
| **Mean open duration (ms)** | 0.21 ± 0.016 | 0.35 ± 0.12 |
| **τ1, ms (%)** | 0.047 ± 0.012 (26%) | 0.080 ± 0.038* (24%) |
| **τ2, ms (%)** | 0.26 ± 0.015 (74%) | 0.43 ± 0.14 (76%) |
| **Mean shut duration (ms)** | 51 ± 15 | 13 ± 2.7* |
| **τ0, ms (%)** | 0.028 ± 0.0056 (17%) | 0.022 ± 0.0038 (25%) |
| **τ1, ms (%)** | 0.31 ± 0.041 (25%) | 0.32 ± 0.034 (26%) |
| **τ2, ms (%)** | 5.1 ± 2.2 (14%) | 2.1 ± 1.5 (17%) |
| **τ3, ms (%)** | 28 ± 5.4 (16%) | 15 ± 3.4 (16%) |
| **τ4, ms (%)** | 81 ± 15 (17%) | 42 ± 2.2* (15%) |
| **τ5, ms (%)** | 200 ± 30 (11%) | - |
| **τ6, ms (%)** | 3200 ± 810 (<1%) | 890 ± 300* (<1%) |

Data are reported as mean + s.e.m. and are given to two significant figures. Patches contained a single active channel and were recorded at pH 8.0. Data analyzed for statistical significance by unpaired two-tailed t-test. *$p$<0.05 when compared to the corresponding value for GluN1-1a/GluN2D.

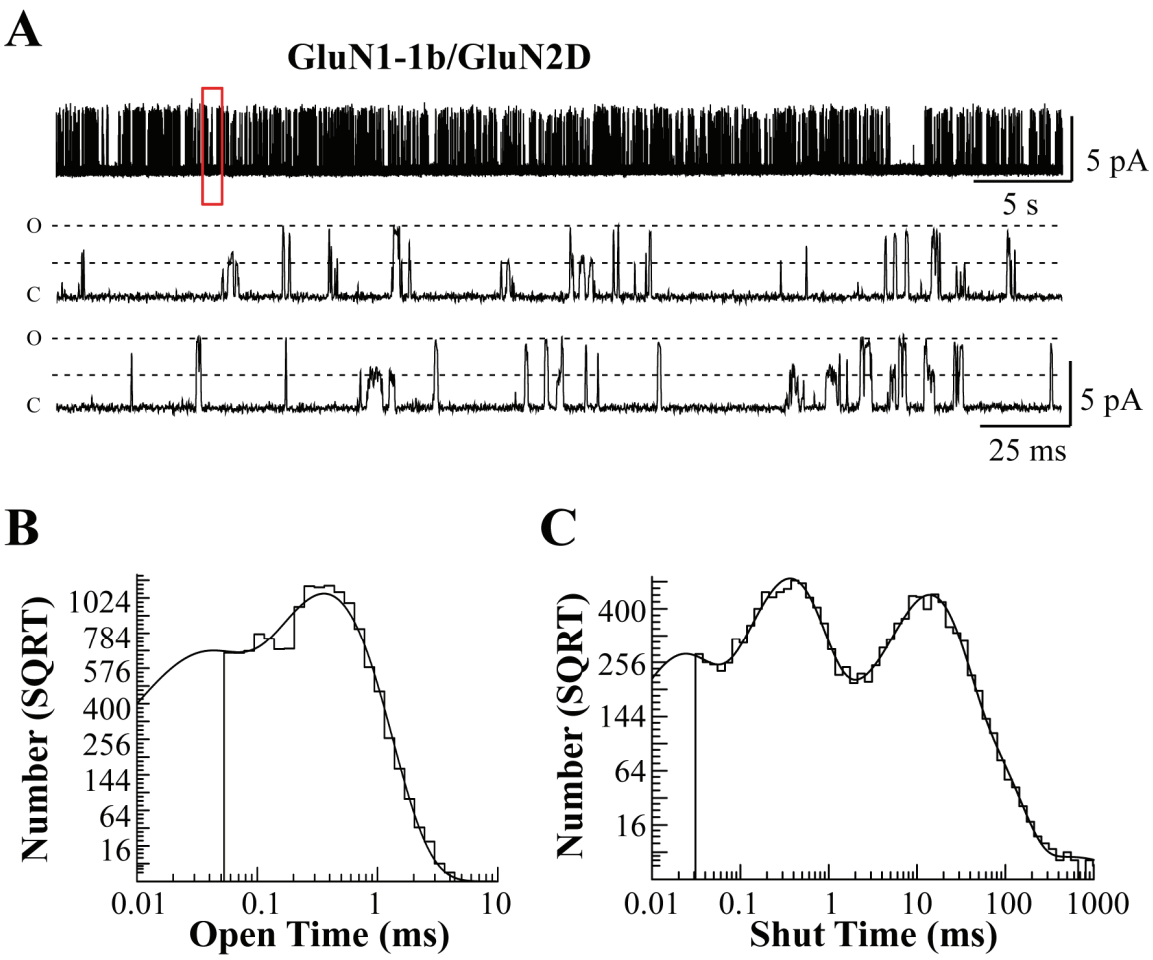


**Figure 4.9.** GluN1-1b/GluN2D receptors in cell-attached patches have a higher open probability than GluN1-1a/GluN2D receptors. ***A***, GluN1-1b/GluN2D channels in cell-attached patches were activated by 1 mM L-glutamate, 0.05 mM glycine, and 0.5 mM $CaCl_2$ at pH 8.0 ($V_{HOLD}$ = +80 mV). The open duration histogram (***B***) could best be fit by two exponential components, whereas the closed duration histogram (***C***) was best fit by 6 exponential components.

containing receptors are similar in cell-attached and excised outside-out patches.

### *4.3.g. GluN1/GluN2D receptors exhibit brief periods of high open probability*

One prominent feature of GluN2A and GluN2B-containing NMDA receptor function is modal gating, in which the characteristics of channel behavior change over a time scale of seconds (Popescu and Auerbach, 2003; Zhang et al., 2008; Kussius and Popescu, 2009; Amico-Ruvio and Popescu, 2010). For GluN2A, modal gating is described by a prolonged 3- to 30-fold shift in mean open time that corresponds to a change in open probability (Popescu and Auerbach, 2003). I noted that five of the 25 outside-out and cell-attached recordings that contained one active channel exhibited periods of extraordinarily high open probability, which endured at least 100 ms. Figure 4.10A-C shows one such event in an outside-out patch, which we refer to as a "supercluster" of openings. These periods of high open probability were brief, with a mean duration of 320 $\pm$ 60 ms. The mean percentage of time in which the receptors had supercluster characteristics across all five patches in which they were evident was 0.05%.

In excised, outside-out patches, GluN1-1a/GluN2D $P_{OPEN}$ increased over 40-fold from 0.017 to 0.79 in one 540 ms supercluster (Fig. 4.10D), while the mean shut time decreased to 0.28 ms, and mean open time was 1.03 ms. GluN1-1b/GluN2D $P_{OPEN}$ also increased to 0.40-0.53 in two superclusters of approximately 350 ms in duration with mean shut times of 0.66 and 1.10 ms and mean open times of 0.75 ms and 0.72 ms. Cell-attached patches also exhibited the superclusters of openings, with GluN1-1a/GluN2D $P_{OPEN}$ increasing to 0.29 in one 240 ms burst with a mean shut time of 1.30 ms and a mean open time of 0.52. GluN1-1b/GluN2D $P_{OPEN}$ increasing to 0.33-0.49 in two 100 to

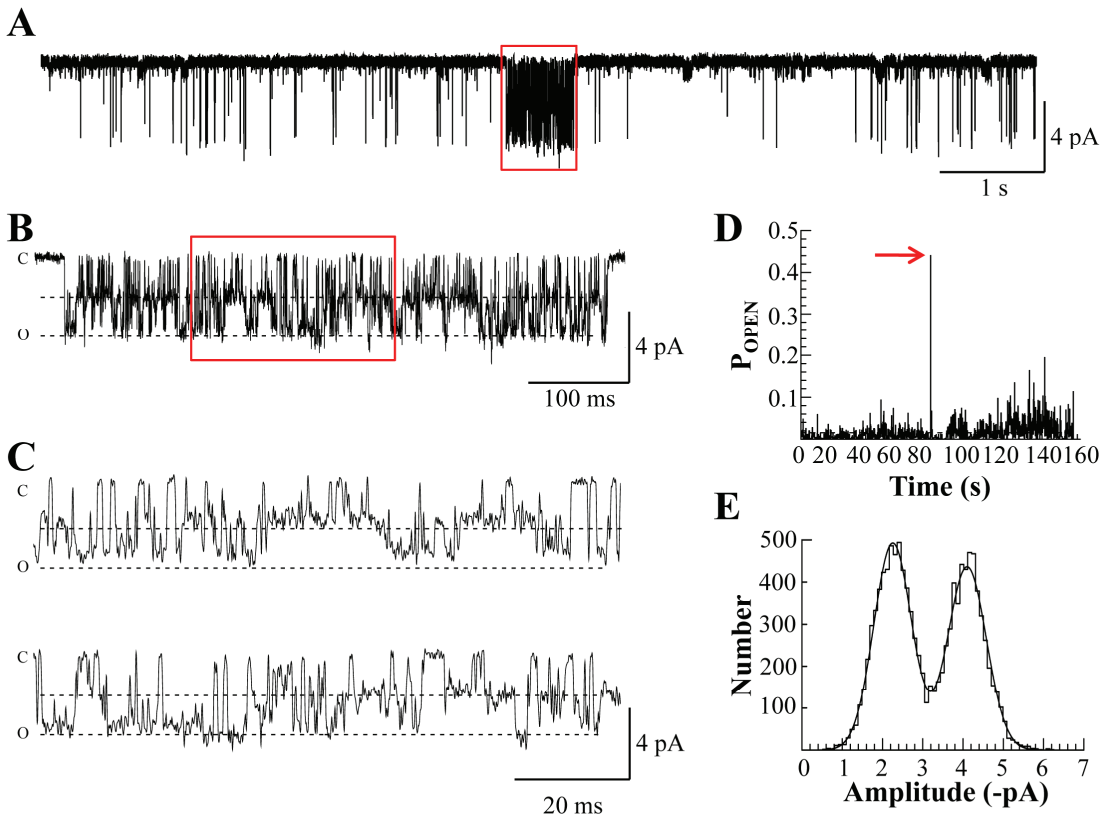


**Figure 4.10.** GluN1/GluN2D receptors exhibit superclusters of high open probability in excised and cell attached patches. ***A***, A representative trace of an outside-out GluN1-1a/GluN2D single channel recording exhibiting a "supercluster" of high open probability than is sustained for over 100 ms. The full supercluster is shown in (***B***), while the supercluster is expanded in (***C***). An open probability histogram is given in (***D***), where the $P_{OPEN}$ of the recording has been analyzed over 100 ms increments. Note the sharp increase in $P_{OPEN}$ at about 90 s into the recording when the channel displays a burst of high open probability. ***E***, A representative amplitude histogram of a supercluster from the GluN1-1a/GluN2D single channel recording shown in ***A***. The GluN1-1a/GluN2D supercluster had two conductance levels similar to the remainder of the single channel recording, with conductances of 29 pS and 51 pS.

determine if the shift in mean open time was significant. Therefore, I cannot at this time describe the superclusters as modal gating as defined for GluN2A and GluN2B. 310 ms bursts, with mean shut times of 0.54 and 0.66 ms and mean open times of 0.53 ms and 0.33 ms, respectively, in cell-attached patches. The superclusters exhibited the two conductance levels characteristic of GluN2D-containing NMDA receptors (Fig. 4.10E). Because the superclusters only occurred in 5 patches, I did not have enough data to

However, this behavior suggests that the receptor protein is capable of adopting a conformation in which pore opening occurs with high probability for agonist bound receptors.

### 4.4. Discussion

There are four primary findings of this study of GluN1/GluN2D NMDA receptor activation. First, glutamate potencies are decreased (i.e. $EC_{50}$ values are increased) for GluN1/GluN2D receptors that contain residues encoded by exon 5 in the GluN1 subunit, even though exon 5 encodes a region within the amino-terminal domain of GluN1 that does not make atomic contacts with L-glutamate. Second, the deactivation time course of GluN2D-containing NMDA receptors accelerates when GluN2D is assembled with GluN1 containing exon 5-encoded residues (e.g. GluN1-1b). Third, Lys211 appears to mediate most of the effects of exon 5 on both $EC_{50}$ and deactivation time course, consistent with previous reports that this residue is a key determinant of $Zn^{2+}$, proton, and polyamine sensitivity (Hollmann et al., 1993; Williams, 1994; Traynelis et al., 1995; Traynelis et al., 1998; Rumbaugh et al., 2000). Given the wide range of properties that this single residue impacts, I suggest that it alters a key conformation or inter-domain

interaction within the receptor. This change in conformation could impact the ability of the amino-terminal domain to influence receptor function (Stroebel et al., 2011). Finally, the open probability of GluN2D-containing receptors is doubled in excised outside-out and cell-attached single channel recordings when the subunit is assembled with the GluN1 subunit containing exon 5. This increase in channel open probability is mirrored by a significant decrease in channel mean shut time, while mean open time is unaffected by the insertion of exon 5-encoded residues into the GluN1 ATD. The GluN1 splice variant does not appear to influence channel conductance or transitions between channel conductance levels.

Previous studies have shown that the amino-terminal domain of the GluN2 subunit is important to NMDA receptor deactivation time course, open probability, and pharmacology (Gielen et al., 2009; Yuan et al., 2009). My data suggest that in addition to the GluN2 amino-terminal domain, the GluN1 amino-terminal domain also is a key determinant in the deactivation time course, channel open probability, and pharmacology of NMDA receptors. When the GluN1 amino-terminal domain includes exon 5-encoded residues, a more rapid deactivation time course is accompanied by an increase in channel open probability. The mechanism by which exon 5-encoded residues can control both channel gating as well as deactivation and agonist pharmacology in GluN2D-containing NMDA receptors is unclear. The crystallographic data describing the GluN1-1b/GluN2B ATD heterodimer suggest that Lys211 may reside in a flexible loop in the GluN1 R2, the lower domain of the GluN1-GluN2 ATD heterodimer (Karakas et al., 2011) (Fig. 4.1A). Lys211 does not appear to form direct intramolecular interactions with the GluN1 or GluN2B ATD in the crystal structure of the GluN1-1b/GluN2B ATDs. However, only a

few of the residues encoded by exon 5 were included in the crystal structure, so the structure of the full 21-amino acid insert encoded by exon 5 remains uncertain (Karakas et al., 2011). Evaluation of Lys211's potential position in GluN1/GluN2D models built from the nearly full length AMPA receptors (Sobolevsky et al., 2009) raise the possibility that if Lys211 is included in a flexible loop, it is possible that it could interact with the D1 domain of the GluN1 ligand-binding domain (Fig. 4.1A). The potential interaction between Lys211 and the GluN1 D1 domain could result in a higher open probability when GluN1 contains exon 5-encoded residues.

The slow deactivation time course, higher glycine and glutamate potencies, and low open probability observed in recordings of recombinant GluN1-1a/GluN2D receptors have been thought to be characteristics of native GluN2D-containing receptors. Native NMDA receptors containing the GluN2D subunit have been observed in EPSCs, single channel, or whole cell patch-clamp recordings from neurons in several regions of the brain, including the dorsal horn neurons of the adult rat spinal cord (Momiyama, 2000), cerebellar Golgi cells (Misra et al., 2000a; Brickley et al., 2003), the substantia nigra (Jones and Gibb, 2005; Brothwell et al., 2008), Purkinje cells (Momiyama et al., 1996; Misra et al., 2000b; Renzi et al., 2007), the dentate gyrus (Harney et al., 2008), and the subthalamic nucleus (Mullasseril et al., 2010). In cerebellar Purkinje cells, the deactivation time constant was approximately 3000 ms, similar to previously published recordings of recombinant GluN1-1a/GluN2D as well as that described here (Vicini et al., 1998; Wyllie et al., 1998; Misra et al., 2000b; Yuan et al., 2009; Vance et al., 2011). However, in recordings from other neuronal cell types and brain regions, the deactivation time courses were much more rapid, suggesting the possibility that the GluN2D subunit

was not abundant in these synapses or was co-assembled with another GluN2 subunit in a triheteromeric receptor (Misra et al., 2000a; Momiyama, 2000).

My data suggest that native GluN2D-containing receptors that contain GluN1 exon 5 may not deactivate as slowly as predicted based on recombinant data with GluN1-1a. Indeed, previous studies have suggested that the localization of the GluN1 splice variants containing exon 5 is region-specific, with significant expression within the subthalamic nucleus, thalamus, CA1/CA3 hippocampal neurons, dentate, cortex, and the cerebellar granule layer (Standaert et al., 1993; Laurie and Seeburg, 1994; Standaert et al., 1994). The more rapid deactivation time course, higher open probability, and lower agonist potencies of exon 5-containing GluN1-b may hold important implications for the function of the GluN2D subunit in regions that express GluN1 splice variants containing exon 5-encoded residues. In particular, the shorter duration of individual activations may decrease temporal summation of excitatory postsynaptic potentials and thus decrease the sensitivity to extrasynaptic glutamate and thereby alter neuronal excitability (Forsythe and Westbrook, 1988; Carmignoto and Vicini, 1992; Edmonds et al., 1995).

# Chapter 5: GluN1/GluN2D gating and channel activation

## 5.1. Abstract

NMDA receptor gating models have been developed that can describe the single channel and macroscopic characteristics of GluN2A-, GluN2B-, and GluN2C-containing NMDA receptors. However, the ability of these models to predict the single channel and macroscopic recordings of GluN2D-containing receptors, which have very low open probability, rapid macroscopic current rise times, little desensitization, and slow deactivation time course, has not been evaluated. I fit previously published NMDA receptor gating models to my excised outside-out patch single channel recordings of GluN1-1a/GluN2D and GluN1-1b/GluN2D NMDA receptors. These models are not capable of simultaneously describing both the rapid rise time and the minimal desensitization of the macroscopic current and the low open probability and multiple shut components of the single channel recordings of GluN2D-containing NMDA receptors. Therefore, I developed a model of GluN1/GluN2D receptor gating with two parallel interconnecting arms that is capable of adequately describing many of the characteristics of GluN1/GluN2D receptors. One arm activates rapidly with higher open probability and allows for a rapid macroscopic current rise time. The second arm opens rarely and slowly, allowing for the low open probability of the receptor. Finally, I use my GluN1/GluN2D gating model to identify specific gating rate constants controlled by exon 5-encoded residues.

## 5.2. Introduction

Conceptual models of activation have been developed that can predict the single channel and macroscopic properties of GluN1-1a/GluN2A (Popescu and Auerbach, 2003; Auerbach and Zhou, 2005; Erreger et al., 2005a; Schorge et al., 2005), GluN1-1a/GluN2B (Banke and Traynelis, 2003; Banke et al., 2005; Amico-Ruvio and Popescu, 2010), and GluN1-1a/GluN2C (Dravid et al., 2008). Models of GluN1/GluN2A and GluN1/GluN2B are capable of describing the desensitization, rapid deactivation, and high open probability of these receptors, and the same model is capable of describing data to a first approximation from both of these receptors when a single rate constant is varied (Erreger et al., 2005a). However, the single channel and macroscopic properties of the GluN1/GluN2D receptor differ greatly from the NMDA receptors for which these models were developed. GluN1/GluN2D has a slow deactivation time course, minimal desensitization, and a rapid rise time, while the receptor's single channels have low open probability and multiple shut components (Vicini et al., 1998; Wyllie et al., 1998; Yuan et al., 2009; Vance et al., 2011; Vance et al., 2012).

In order to study the gating kinetics of GluN1/GluN2D NMDA receptors and to determine if specific gating steps are controlled by GluN1 exon 5, I first evaluated the ability of previously published NMDA receptor gating models to describe both the single channel and macroscopic properties of GluN1/GluN2D NMDA receptors. Because the same model could not describe both the rapid rise time and little desensitization of the macroscopic current and the low open probability and multiple shut components of the single channel recordings of GluN1/GluN2D receptors, we developed a model with interconnected parallel arms that allows for the receptor to have rapid macroscopic

current rise while maintaining a low channel open probability. Finally, I use this GluN1/GluN2D model to identify specific rate limiting gating steps controlled by exon 5 within the GluN1 subunit.

## 5.3. Results

### *5.3.a. Previously published NMDA receptor gating models cannot predict the single channel and macroscopic characteristics of GluN2D-containing NMDA receptors*

I first sought to determine whether previously published NMDA receptor gating models could describe my single channel and macroscopic data by fitting to my excised GluN1-1a/GluN2D single channel records to a series of models described for GluN1-1a/GluN2A (Popescu and Auerbach, 2003; Auerbach and Zhou, 2005; Erreger et al., 2005a; Schorge et al., 2005), GluN1-1a/GluN2B (Banke and Traynelis, 2003; Banke et al., 2005; Amico-Ruvio and Popescu, 2010), and GluN1-1a/GluN2C (Dravid et al., 2008) using the maximum interval likelihood (MIL) method (Fig. 5.1; Table 5.1). To determine if the previously published models also were capable of describing the macroscopic current characteristics of GluN1-1a/GluN2D receptors, I recorded excised macroscopic patches and whole cell responses at saturating (1 mM) and low (2.5 μM) L-glutamate concentrations. I determined the GluN1-1a/GluN2D L-glutamate $EC_{50}$ in HEK cells to be $2.0 \pm 0.27$ μM (n=5), so 2.5 μM L-glutamate produced a response that was approximately half maximal. I obtained response waveforms for the following conditions (0.05 mM glycine present in all solutions): 10 s duration of application of 1 mM L-glutamate; 5-10 ms duration of application of 1 mM L-glutamate; and a 10 s duration of application

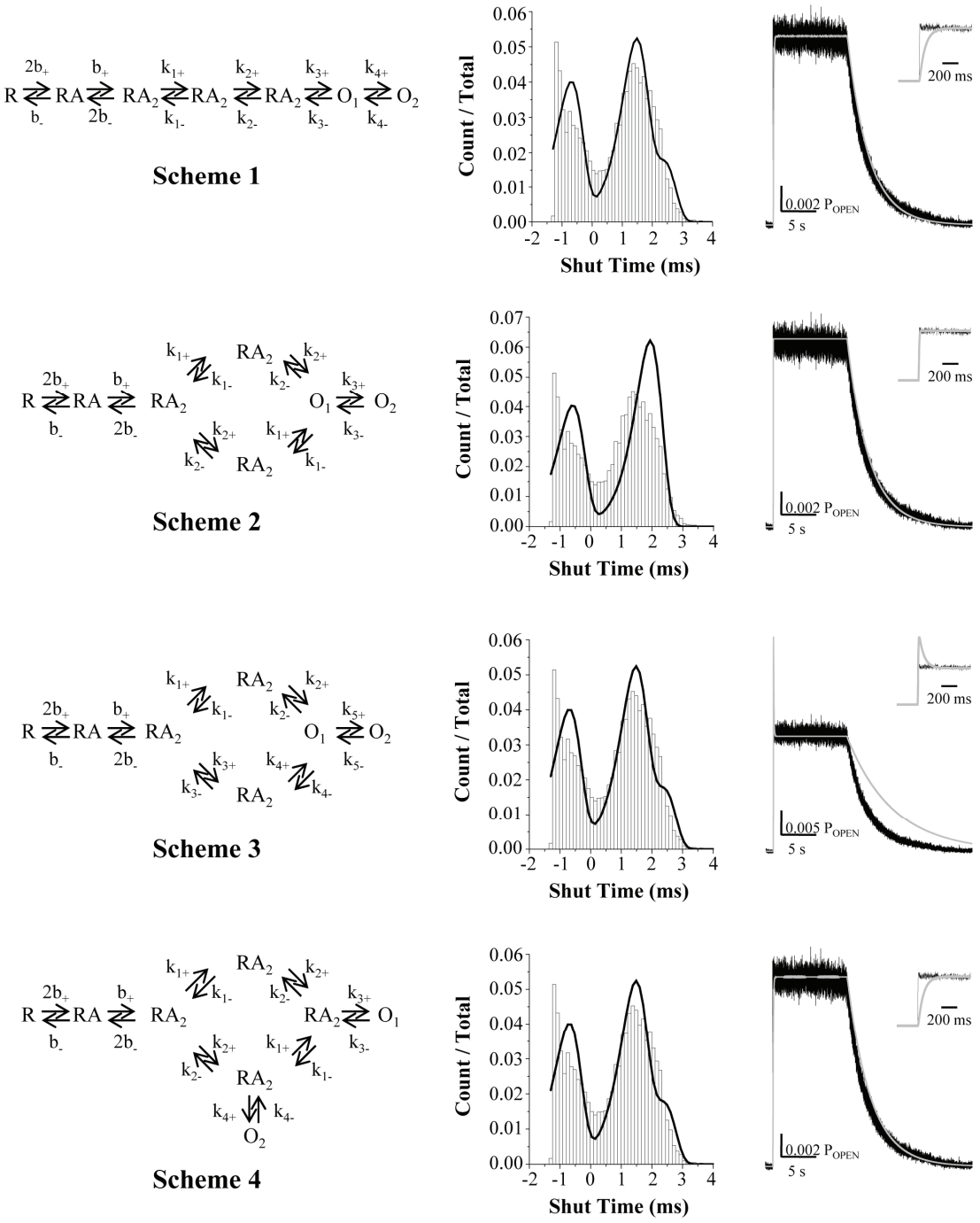


**Figure 5.1.** Conceptual models of NMDA receptor gating. Four previously published NMDA receptor gating schemes were fitted without the ligand association and dissociation steps to single channel data from excised outside-out patches with only a single active channel to examine the properties of GluN1-1a/GluN2D and GluN1-1b/GluN2D receptors (*left*). For each NMDA receptor gating scheme, the MIL fit

for a representative GluN1-1a/GluN2D single channel recording from an excised outside-out patch is given (*center*). The gating schemes with more shut components more accurately predict the recorded single channel data. Macroscopic recordings were fit with the models in which agonist binding and unbinding steps have been added. The results of least squares fitting of each scheme to averaged macroscopic GluN1-1a/GluN2D macroscopic recordings are given in gray superimposed on a representative current trace for GluN1-1a/GluN2D (*right*). Expansions of the rise times predicted by the models are given in the insets. No scheme was able to approximate all of the features of the macroscopic and single channel data. For example, *Scheme 2* can predict a rapid rise time without significant desensitization, but does not produce GluN1-1a/GluN2D single channel properties that are consistent with the data. *Scheme 1* was published in Popescu and Auerbach (2003); *Scheme 2* was published in Banke and Traynelis (2003); *Scheme 3* was published in Auerbach and Zhou (2005); *Scheme 4* was published in Schorge et al. (2005). Adapted with permission from Vance et al. (2012).

**Table 5.1.** Fitted rate constants from previously published NMDA receptor gating models to GluN1-1a/GluN2D excised outside-out data

| Rates ($s^{-1}$) | *Scheme 1* | *Scheme 2* | *Scheme 3* | *Scheme 4* |
|---|---|---|---|---|
| $k_{1+}$ | 8.3 ± 1.6 | 26 ± 3.4 | 7.1 ± 2.9 | 80 ± 6.0 |
| $k_{1-}$ | 9.8 ± 3.5 | 2100 ± 350 | 4.5 ± 1.0 | 4600 ± 450 |
| $k_{2+}$ | 130 ± 10 | 2700 ± 340 | 4.2 ± 2.6 | 9.3 ± 1.7 |
| $k_{2-}$ | 4800 ± 470 | 3700 ± 930 | 550 ± 270 | 10 ± 3.2 |
| $k_{3+}$ | 2300 ± 300 | 7800 ± 2300 | 110 ± 16 | 2200 ± 270 |
| $k_{3-}$ | 6700 ± 1300 | 3200 ± 740 | 4300 ± 600 | 1600 ± 110 |
| $k_{4+}$ | 8900 ± 2300 | | 2500 ± 330 | 14 ± 1.7 |
| $k_{4-}$ | 3600 ± 700 | | 5700 ± 1200 | 17000 ± 3300 |
| $k_{5+}$ | | | 8400 ± 2200 | |
| $k_{5-}$ | | | 3700 ± 730 | |
| **LL** | 36180 ± 5517 | 35384 ± 5399 | 36087 ± 5502 | 36034 ± 5541 |

Idealized data records were fit with four gating schemes shown in Fig. 5.1. All rates are in $s^{-1}$, and data are reported as mean ± s.e.m to two significant digits.

of 2.5 μM L-glutamate. The averaged waveforms for each condition were normalized to the maximum open probability of the receptor in saturating agonist as determined in the excised patch single channel recordings. The waveforms then were simultaneously fitted by the models including glutamate binding and unbinding steps (Fig. 5.1) using a nonlinear least squares fitting algorithm that simultaneously evaluated the fit to all three waveforms at each iteration. During the fit, the rate constants derived from the MIL fit of the single channel data (Table 5.1) were held constant, and only the binding and unbinding rates were allowed to vary. Including desensitization steps in the gating schemes decreased the quality of the macroscopic fits, so desensitization steps were omitted.

While each model was capable of describing several of the characteristics of my GluN1-1a/GluN2D data, no previously published model could predict a single channel record with a low open probability and more than 4 shut components within the shut duration histogram or a macroscopic current with fast 10 to 90% rise time, slow deactivation, and minimal desensitization characteristic of GluN1-1a/GluN2D (Tables 5.1-5.2). For example, the linear model (*Scheme 1*; Fig. 5.1) composed of three shut states followed by two adjacent open states, which can describe GluN2A and GluN2B channel recordings (Popescu and Auerbach, 2003; Erreger et al., 2005a; Kussius and Popescu, 2009; Amico-Ruvio and Popescu, 2010), predicted the low open probability and multiple shut components of GluN1-1a/GluN2D single channels. However, this model predicted a rise time for GluN1-1a/GluN2D that was more than 10-fold too slow (Table 5.2; Fig. 5.1). This result is similar to that observed for the GluN1-1a/GluN2C receptor (Dravid et al., 2008).

T**able 5.2.** Fitting of the macroscopic GluN1-1a/GluN2D current response time course

| **Rates** | ***Experiment*** | ***Scheme 1*** | ***Scheme 2*** | ***Scheme 3*** | ***Scheme 4*** | ***Scheme 5*** |
|---|---|---|---|---|---|---|
| $\mathbf{k_{ON}}$ | -- | 0.27 | 0.26 | 0.28 | 0.27 | 0.25 |
| $\mathbf{k_{OFF}}$ | -- | 0.33 | 0.30 | 0.21 | 0.32 | 0.21 |
| $\mathbf{P_{OPEN}}$ | 0.017 | 0.013 | 0.017 | 0.026 (Pk)<br>0.013 (SS) | 0.012 | 0.014 |
| $\mathbf{EC_{50}}$ **(μM)** | 2.0 | 2.0 | 2.0 | 1.4 | 2.1 | 2.0 |
| $\mathbf{\tau_{DEACTIVATION}}$ **(ms)** | 2500 | 3000 | 3000 | 6200 | 2900 | 3000 |
| **Rise Time (ms)** | 5.3 | 130 | 10.5 | 8.5 | 120 | 5.4 |

The five NMDA receptor gating models were fit to the GluN1-1a/GluN2D macroscopic data, and rise time and $\tau_{DEACTIVATION}$ were derived from the fits. All gating rates were fixed to the values obtained from the MIL fits of the single channel data, while the agonist binding and unbinding rates were set as free parameters. L-glutamate $EC_{50}$ values are given in μM, agonist binding rates are in $\mu M^{-1}$ $s^{-1}$, agonist unbinding rates are in $s^{-1}$, and rise time and $\tau_{DEACTIVATION}$ are in ms.

I also evaluated cyclic models derived from previously published papers in which the open states were adjacent (*Schemes 2* and *3*; Fig. 5.1) or separated by two closed states (*Scheme 4*; Fig. 5.1). *Scheme 2*, previously shown to describe GluN2A and GluN2C channels (Auerbach and Zhou, 2005; Schorge et al., 2005; Dravid et al., 2008), has a cycle with two independent pregating steps preceding two open states. Unlike the linear *Scheme 1*, *Scheme 2* predicts a rapid rise time similar to the rise time observed experimentally (Table 5.2). However, this gating scheme does not accurately predict the single channel behavior of GluN1-1a/GluN2D as it predicts too few shut components (Fig. 5.1).

*Scheme 3*, which has been used to describe GluN2A channels by Auerbach and Zhou (2005) and GluN2C channels by Dravid et al. (2008), is composed of a cycle that is constrained to microscopic reversibility but does not have rate constants that are symmetrically constrained as in *Scheme 2*. This allows for an extra degree of freedom when fit to the single channel records, and therefore could more closely predict the GluN1-1a/GluN2D single channel data. Some characteristics of the macroscopic data also were better predicted by this model, such as the rapid rise time. However, this scheme predicted rapid, pronounced desensitization in the macroscopic data, which does not occur in experimental records of GluN1-1a/GluN2D responses (Table 5.2; Fig. 5.1).

Finally, I evaluated *Scheme 4*, previously used by Schorge et al. (2005) to describe GluN2A channels. Unlike *Schemes 2* and *3*, *Scheme 4* is comprised of a cycle with non-adjacent open states that can account for the significant correlation observed between open and shut durations in GluN2A single channel recordings (Schorge et al., 2005). The model does predict multiple shut and open duration components similar to my single

channel data, but rate constants providing the best fit to the single channel data yielded macroscopic simulated currents that were more than 10-fold slower than experimental data (Table 5.2; Fig. 5.1).

While each model was able to predict a subset of the characteristics of GluN1-1a/GluN2D single channel and macroscopic data, none of the schemes could describe all of the key features of GluN1-1a/GluN2D activation. Moreover, no model predicted a two-exponential component deactivation time course, which we have observed experimentally. The 4 previously published schemes were used to evaluate GluN1-1b/GluN2D macroscopic and single channel records, but the same limitations as observed in the fits of GluN-1a/GluN2D data were apparent (Tables 5.3-5.4).

### *5.3.b. A model with two parallel interconnected arms best describes the single channel and macroscopic characteristics of GluN1/GluN2D NMDA receptors*

Because the previously published models could not predict both the single channel and macroscopic GluN1-1a/GluN2D properties, I modified the schemes to increase their number of closed states, degrees of freedom, and complexity. Additional closed states to the gating schemes, while increasing the number of shut duration components predicted for a single channel recording, also increased the predicted rise time of the macroscopic current. Adding states to represent receptor desensitization again improved the complexity of the single channel histograms by increasing the number of free parameters, but also predicted significant, rapid desensitization that I did not observe in my GluN1-1a/GluN2D macroscopic current recordings. We subsequently sought to develop a new model that could accurately predict both the single channel and macroscopic properties

**Table 5.3.** Fitted rate constants from previously published NMDA receptor gating models to GluN1-1b/GluN2D excised outside-out data

| **Rates ($s^{-1}$)** | ***Scheme 1*** | ***Scheme 2*** | ***Scheme 3*** | ***Scheme 4*** |
|---|---|---|---|---|
| $\mathbf{k_{1+}}$ | 15 ± 7.2 | 36 ± 4.4 | 1.6 ± 0.51 | 100 ± 17 |
| $\mathbf{k_{1-}}$ | 18 ± 6.9 | 1200 ± 140 | 0.52 ± 0.070 | 4000 ± 890 |
| $\mathbf{k_{2+}}$ | 180 ± 11 | 5100 ± 2000 | 10 ± 4.0 | 17 ± 9.7 |
| $\mathbf{k_{2-}}$ | 4900 ± 1100 | 2500 ± 1100 | 380 ± 95 | 23 ± 13 |
| $\mathbf{k_{3+}}$ | 4300 ± 1500 | 4700 ± 2000 | 200 ± 14 | 5200 ± 2100 |
| $\mathbf{k_{3-}}$ | 3900 ± 1200 | 3900 ± 920 | 4200 ± 820 | 1500 ± 66 |
| $\mathbf{k_{4+}}$ | 4500 ± 2000 | | 5000 ± 2000 | 35 ± 6.9 |
| $\mathbf{k_{4-}}$ | 4000 ± 920 | | 3500 ± 1100 | 6400 ± 3200 |
| $\mathbf{k_{5+}}$ | | | 4500 ± 2000 | |
| $\mathbf{k_{5-}}$ | | | 4000 ± 940 | |
| **LL** | 53582 ± 8612 | 52434 ± 8290 | 53583 ± 8612 | 53653 ± 8622 |

Idealized data records were fit to four gating schemes shown in Fig. 5.1. All rates are in $s^{-1}$, and data are reported as mean ± s.e.m to two significant digits.

**Table 5.4.** Fitting of the macroscopic GluN1-1b/GluN2D current response time course

| Rates | Experiment | *Scheme 1* | *Scheme 2* | *Scheme 3* | *Scheme 4* | *Scheme 5* |
|---|---|---|---|---|---|---|
| $k_{ON}$ | -- | 0.36 | 0.40 | 2.5 | 0.35 | 0.28 |
| $k_{OFF}$ | -- | 1.5 | 2.3 | 6.7 | 1.4 | 0.92 |
| $P_{OPEN}$ | 0.037 | 0.036 | 0.042 | 0.096 (Pk)<br>0.036 (SS) | 0.038 | 0.04 |
| $EC_{50}$ (μM) | 5.0 | 5.87 | 5.72 | 1.69 | 5.88 | 6.6 |
| $\tau_{DEACTIVATION}$ (ms) | 680 | 690 | 730 | 310 | 720 | 700 |
| Rise Time (ms) | 5.4 | 73 | 8.9 | 2.7 | 58 | 7.7 |

The five NMDA receptor gating models were fit to the GluN1-1a/GluN2D macroscopic data. All gating rates were fixed to the values obtained from the MIL fits of the single channel data, while the agonist binding and unbinding rates were set as free parameters. L-glutamate $EC_{50}$ values are given in μM, agonist binding rates are in $\mu M^{-1}\ s^{-1}$, agonist unbinding rates are in $s^{-1}$, and rise time and $\tau_{DEACTIVATION}$ are in ms.

of GluN1-1a/GluN2D receptor activation. I evaluated more than 50 potential kinetic schemes containing unique state connectivity using random model generating software to look for unconventional relationships between open and closed states that might account for my data. None of these schemes were able to reproduce GluN1-1a/GluN2D properties; a subset of the gating schemes fit to one representative GluN1-1a/GluN2D single channel recording is given in Figure 5.2 and Appendix C.

Our ability to develop a gating model of GluN1/GluN2D receptor gating was hindered by two paradoxical properties of the receptor, the low open probability of the single channel recordings and the rapid response rise time of the macroscopic currents. In order to predict a channel with low open probability given the closing rate set by the open times, the fitting algorithms reduced the forward rate constants, which in turn slowed the predicted macroscopic rise time. Because of this, we considered the possibility that GluN1/GluN2D may oscillate between two different configurations that undergo the same activation pathway at different rates. We created a gating scheme with two linear, parallel pathways. I evaluated which connectivity between the two pathways best described my single channel data, and found that my data was best described when all closed states were connected (*Scheme 5*; Fig. 5.3-5.4; Table 5.5). A parallel arm model in which only the upper arm had open states predicted a 10-fold too slow 10 to 90% rise time of the macroscopic current, so open states in both arms were required to predict the rapid rise time I observed in my macroscopic current recordings. Likewise, connecting the open states between the two arms resulted in a maximum log likelihood that was 200 units lower than when the open states were not connected, reflecting a worse fit of the data. The three closed states in both the upper and lower arms were required

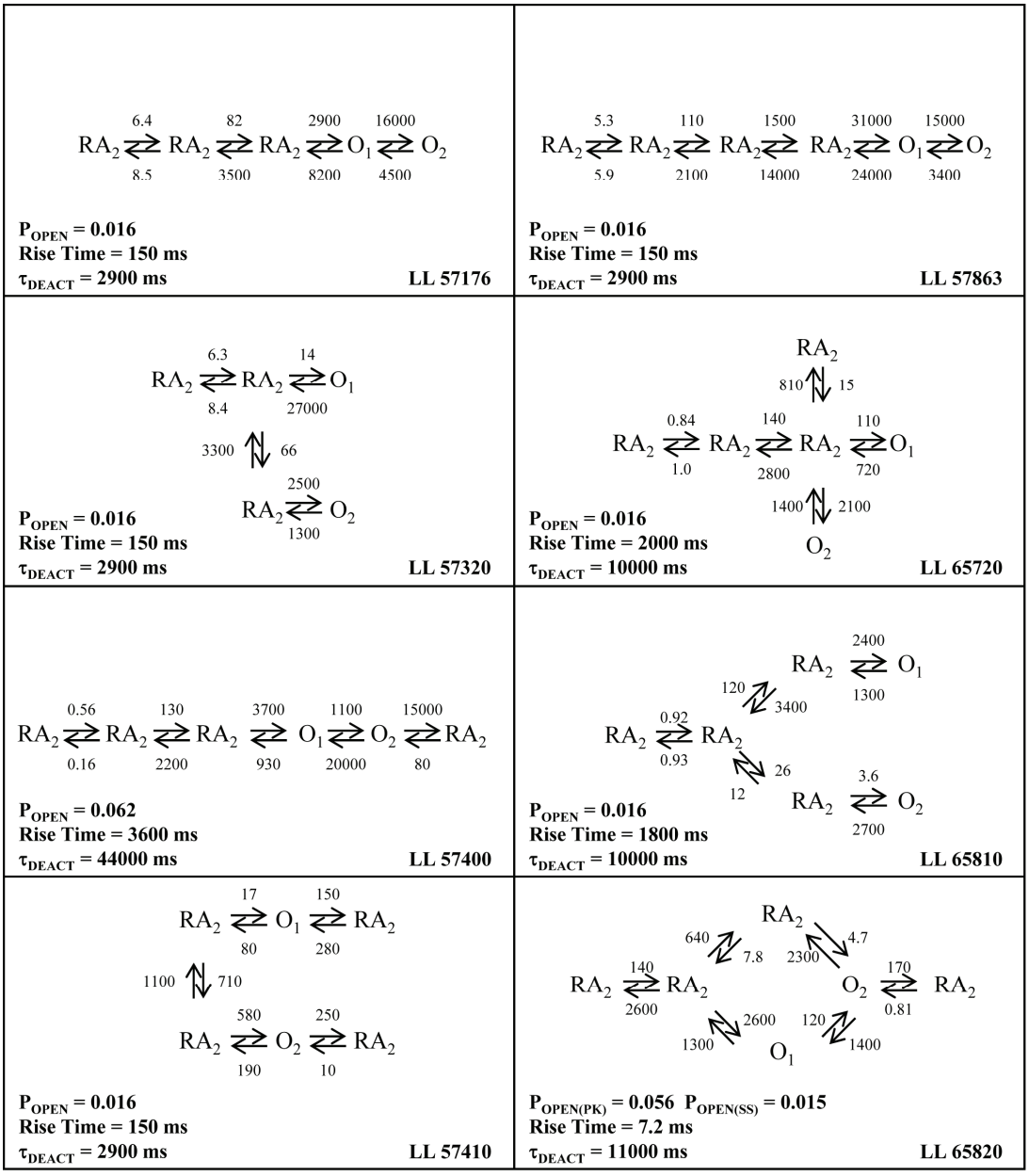


**Figure 5.2.** The model search feature in QuB software was utilized to evaluate potential novel models for GluN1/GluN2D gating. I varied the number of closed and open states and allowed for both linear and cyclic models. The search was performed using data from one representative excised outside-out GluN1-1a/GluN2D single channel recording. The model search algorithm generated many potential gating schemes. The 8 best schemes as judged by log likelihood values are shown. Macroscopic currents were simulated using the on and off rates determined for *Scheme 5*, and the predicted tau deactivation ($\tau_{DEACT}$), rise time, and open probability are given.

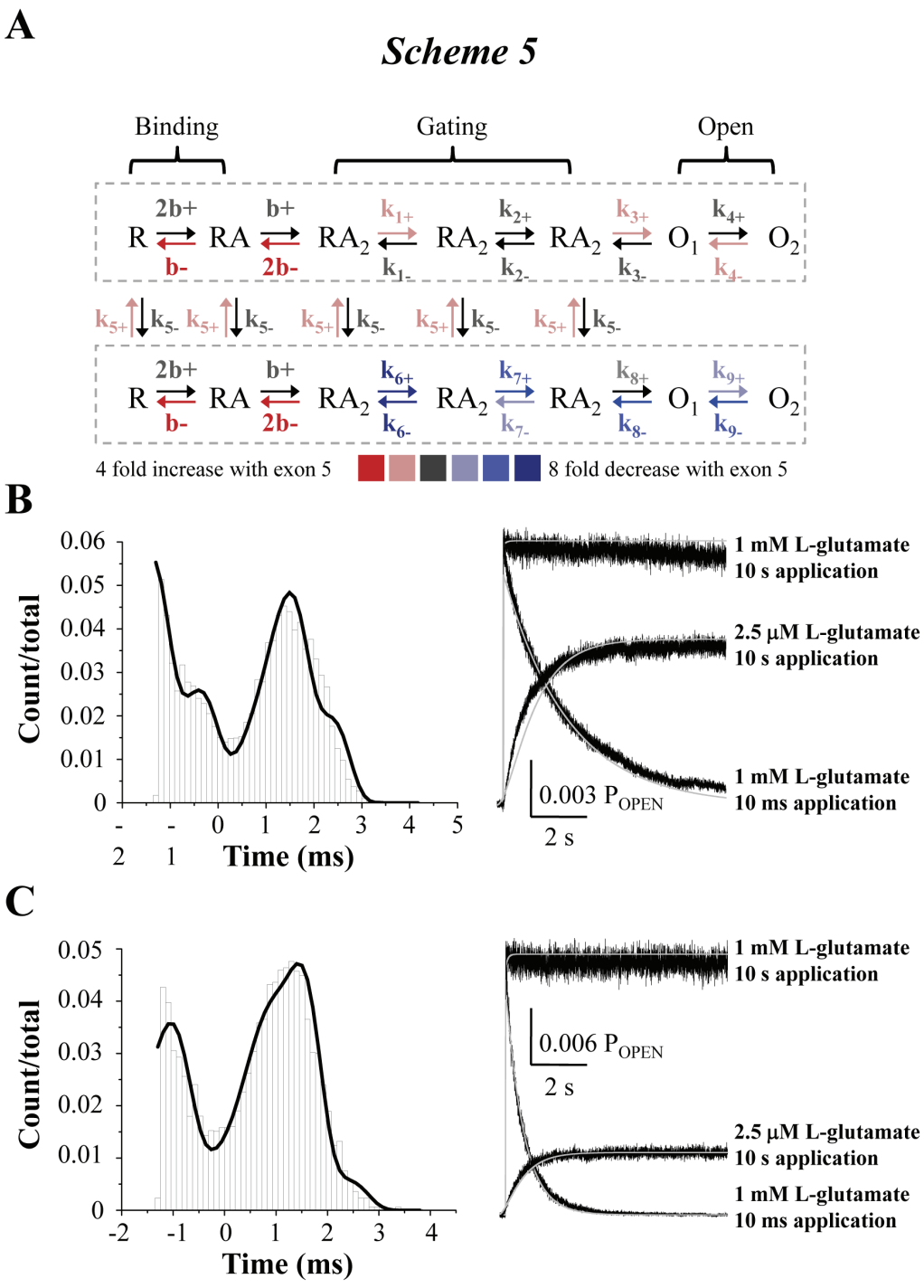


**Figure 5.3.** A model of GluN1/GluN2D function can predict macroscopic and single channel properties. ***A***, A model in which 2 arms, each with 3 shut states and 2 open states, that are in equilibrium is shown as *Scheme 5*. Rates are color-coded based on the change between *Scheme 5* fit to GluN1-1b compared to GluN1-1a. Dark red indicates a 4-fold increase, pink indicates 1.5-fold increase, gray indicates no change,

light blue indicates a 1.5-fold decrease, medium blue indicates a 2-5-fold decrease, and dark blue indicates 8-fold decrease for exon 5. ***B***, A MIL fit of *Scheme 5* to data from one representative GluN1-1a/GluN2D excised outside-out single channel recording without the ligand association and dissociation steps (*left*), which were fixed to those determined from macroscopic fitting (see *Methods*). The result of least squares fitting of *Scheme 5* to macroscopic recordings of GluN1-1a/GluN2D activated by 1 mM L-glutamate for 10 sec, 1 mM L-glutamate for 10 ms, and 0.0025 mM L-glutamate for 10 sec is given (*right*). The agonist binding and unbinding rates were allowed to vary while all remaining gating rates were fixed to the rates obtained with the maximum interval likelihood fitting of the single channel data. Re-running the maximum likelihood fitting with the fitted agonist unbinding rate added did not change any rate constants. ***C***, The MIL fit of a representative GluN-1b/GluN2D excised outside-out single channel recording with *Scheme 5* is given (*left*). The result of least squares fitting of *Scheme 5* (*right*) to macroscopic recordings of GluN1-1b/GluN2D activated by 1 mM L-glutamate for 10 sec, 1 mM L-glutamate for 10 ms, and 0.0025 mM L-glutamate for 10 sec is given. For both (***B***) and (***C***), waveforms predicted from the fitted rate constants are superimposed as white lines. Adapted with permission from Vance et al. (2012).

**Table 5.5.** Fitted rate constants from *Scheme 5* to GluN1-1a/GluN2D and GluN1-1b/GluN2D excised outside-out data

| Rates ($s^{-1}$) | GluN1-1a/GluN2D | GluN1-1b/GluN2D | Fold Difference (1a/1b) |
|---|---|---|---|
| $\mathbf{k_{1+}}$ | 130 ± 31 | 230 ± 37 | 0.57 |
| $\mathbf{k_{1-}}$ | 990 ± 330 | 900 ± 230 | 1.1 |
| $\mathbf{k_{2+}}$ | 880 ± 280 | 1200 ± 470 | 0.73 |
| $\mathbf{k_{2-}}$ | 11000 ± 1800 | 12000 ± 2200 | 0.92 |
| $\mathbf{k_{3+}}$ | 6800 ± 1900 | 12000 ± 1600 | 0.57 |
| $\mathbf{k_{3-}}$ | 6200 ± 1200 | 4400 ± 1800 | 1.4 |
| $\mathbf{k_{4+}}$ | 7400 ± 2300 | 5900 ± 1900 | 1.3 |
| $\mathbf{k_{4-}}$ | 3600 ± 740 | 6000 ± 1200 | 0.60 |
| $\mathbf{k_{5+}}$ | 4.6 ± 2.8 | 7.4 ± 1.8 | 0.62 |
| $\mathbf{k_{5-}}$ | 3.4 ± 1.9 | 4.7 ± 2.1 | 0.72 |
| $\mathbf{k_{6+}}$ | 140 ± 110 | 10 ± 5.7 | 14 |
| $\mathbf{k_{6-}}$ | 480 ± 270 | 56 ± 42 | 8.6 |
| $\mathbf{k_{7+}}$ | 410 ± 120 | 200 ± 59 | 2.1 |
| $\mathbf{k_{7-}}$ | 9100 ± 3300 | 4700 ± 1600 | 1.9 |
| $\mathbf{k_{8+}}$ | 820 ± 230 | 950 ± 280 | 0.86 |
| $\mathbf{k_{8-}}$ | 12000 ± 3100 | 5300 ± 2000 | 2.3 |
| $\mathbf{k_{9+}}$ | 5600 ± 1500 | 3100 ± 1800 | 1.8 |
| $\mathbf{k_{9-}}$ | 4500 ± 1100 | 2200 ± 1000 | 2 |
| **LL** | 36303 ± 5532 | 53889 ± 8679 | -- |

Idealized data records were fit to our new NMDA receptor gating scheme. All rates are in $s^{-1}$, and data are reported as mean ± s.e.m to two significant digits.

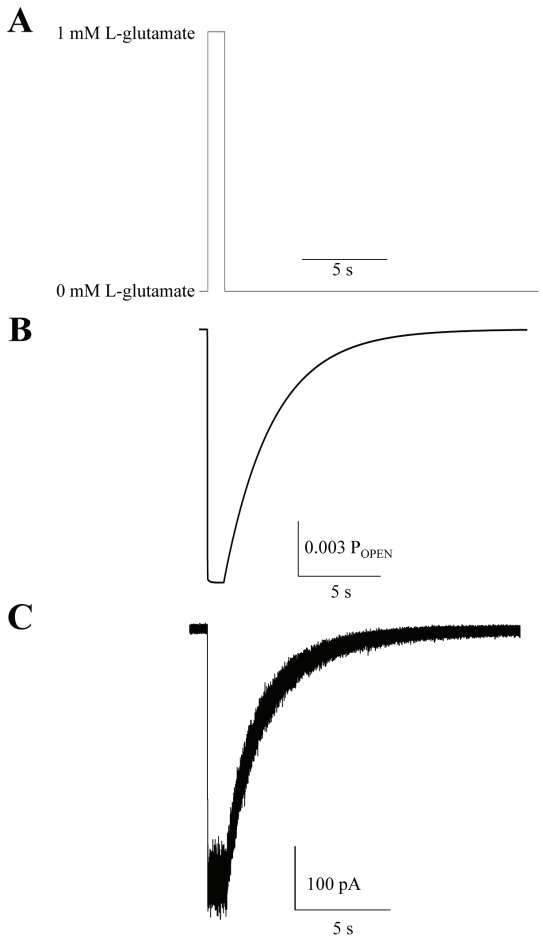


**Figure 5.4.** *Scheme 5* predicts the rapid rise and slow deactivation time course of GluN1-1a/GluN2D NMDA receptors. ***A***, A stimulus file with a 1 s application of 1 mM L-glutamate was used to simulate *Scheme 5's* prediction of GluN1-1a/GluN2D macroscopic recordings. *Scheme 5's* prediction of GluN1-1a/GluN2D activation by 1 s application of L-glutamate is given in ***B***. A macroscopic recording of GluN1-1a/GluN2D NMDA receptors transiently expressed in HEK 293 cells and activated by L-glutamate (0.05 mM glycine was present in all solutions) is given in ***C***.

to predict a single channel record with multiple shut components, while the two open states per arm were required to predict the two open components observed in my single channel records.

*Scheme 5*, with two parallel arms, suggests the existence of two GluN1/GluN2D receptor configurations, one that activates rapidly at a higher open probability, and another that opens slowly and less frequently. The two parallel arms could represent a number of structural possibilities. The GluN1/GluN2D receptor may exist in two states due the arrangement of its intra-domain or intra-subunit interfaces. This would allow the receptor to transition through the two arms before, during, and after agonist binding.

Fitting *Scheme 5* to the GluN1-1a/GluN2D single channel records yielded a good fit, as judged both by the maximum likelihood and similarity in the predicted and experimental open and closed time histograms (Fig. 5.3B). The higher occupancy of the lower, slow gating arm of *Scheme 5* allows for a low open probability without slowing the rise time of the macroscopic current (Fig. 5.5A,B; Table 5.2). The two arms have different mean open times, as the mean open time of the upper arm is longer ($0.49 \pm 0.00058$ ms) than the lower arm ($0.19 \pm 0.0014$ ms). *Scheme 5* also was able to predict at least 5 detectable shut components and 2 detectable open time components, similar to what I observe in single channel recordings (Fig. 5.3B). In addition, *Scheme 5* predicted the response time course, $EC_{50}$, deactivation time course, and open probability (Table 5.5; Fig. 5.3B). Therefore, *Scheme 5* was the only model of more than 50 evaluated that was able to predict the low open probability and multiple shut components of GluN1-1a/GluN2D while maintaining the ability to open rapidly enough to yield a rise time similar to the rise time observed in my experimental data.

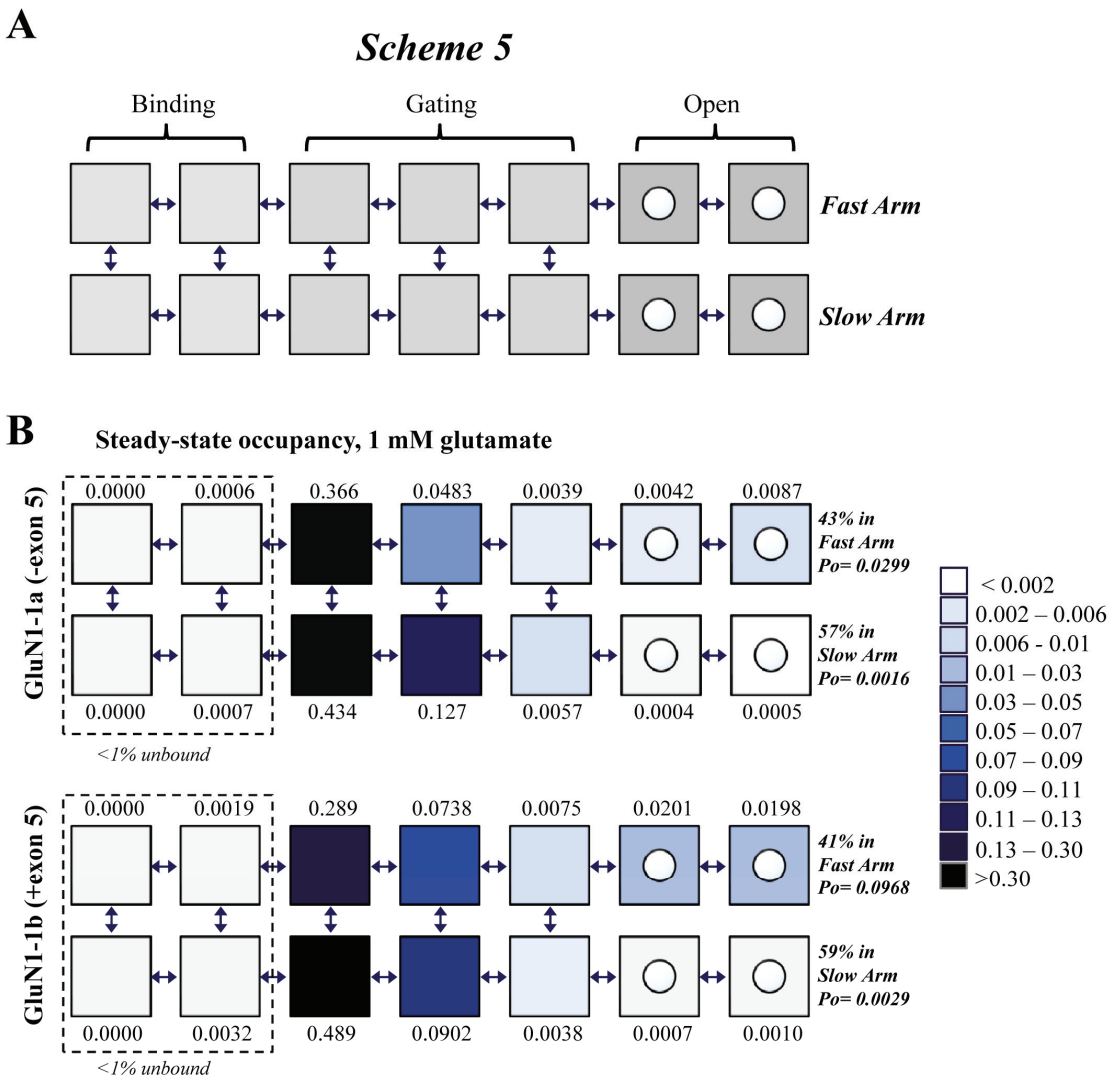


**Figure 5.5.** Exon 5 preferentially increases occupancy of the open state in the fast-gating arm. ***A***, The block representation of *Scheme 5* illustrates the fast- and slow-gating arms of the model, including the binding, gating, and open states. ***B***, The occupancy of each state is given at steady state in response to a maximally active concentration of glutamate; occupancy is given to two significant figures in increments of 0.0001 for GluN1-1a/GluN2D and GluN1-1b/GluN2D. The open probabilities of the fast- and slow-gating arms are calculated. Occupancy is color-coded as indicated on the right to visually illustrate how exon 5 is predicted by *Scheme 5* to alter receptor function. Adapted with permission from Vance et al. (2012).

Monte Carlo simulations of a GluN1-1a/GluN2D single channel activated by 1 mM L-glutamate using *Scheme 5* predict a single channel record similar to what I observed in my single channel recordings. Figure 5.6 shows a representative GluN1-1a/GluN2D single channel activated by 0.05 mM glycine and 1 mM L-glutamate. The mean open time and open probability, when assessed in 500 ms increments, are stable without significant fluctuation (Fig. 5.6A,B). Although the two arms of *Scheme 5* have considerable differences in open probability and mean open time, *Scheme 5* does not predict that the receptor oscillates slowly and infrequently between high open probability bursts and prolonged periods of inactivation (Fig 5.6C,D). Rather, *Scheme 5* predicts that the receptor transitions between the two arms multiple times within a second (Fig. 5.6D). Moreover, channel openings for each arm are not clearly clustered together for the fast-gating upper arm of *Scheme 5*, making it impossible to detect in a single channel record whether the openings occur in the upper or lower arm of the model (Fig. 5.6D). S*cheme 5* also could predict a similar correlation between the conditional open times and the shut durations as what I observed in my GluN1-1a/GluN2D single channel recordings, consistent with the idea that this dual arm model can reproduce a number of complex features of GluN1/GluN2D gating. However, although the predicted deactivation time course was slow, *Scheme 5* could not predict a detectable dual exponential time course. Scheme 5 also could not predict the multiple conductance levels that I observed in my single channel recordings. A single residue, GluN2D Leu657, controls the GluN2D subconductance level, and mutating this residue to the corresponding residue in GluN2A eliminates the subconductance level without altering channel shut times (Retchless et al., 2012). In addition, the open state distributions of the higher and lower amplitude levels

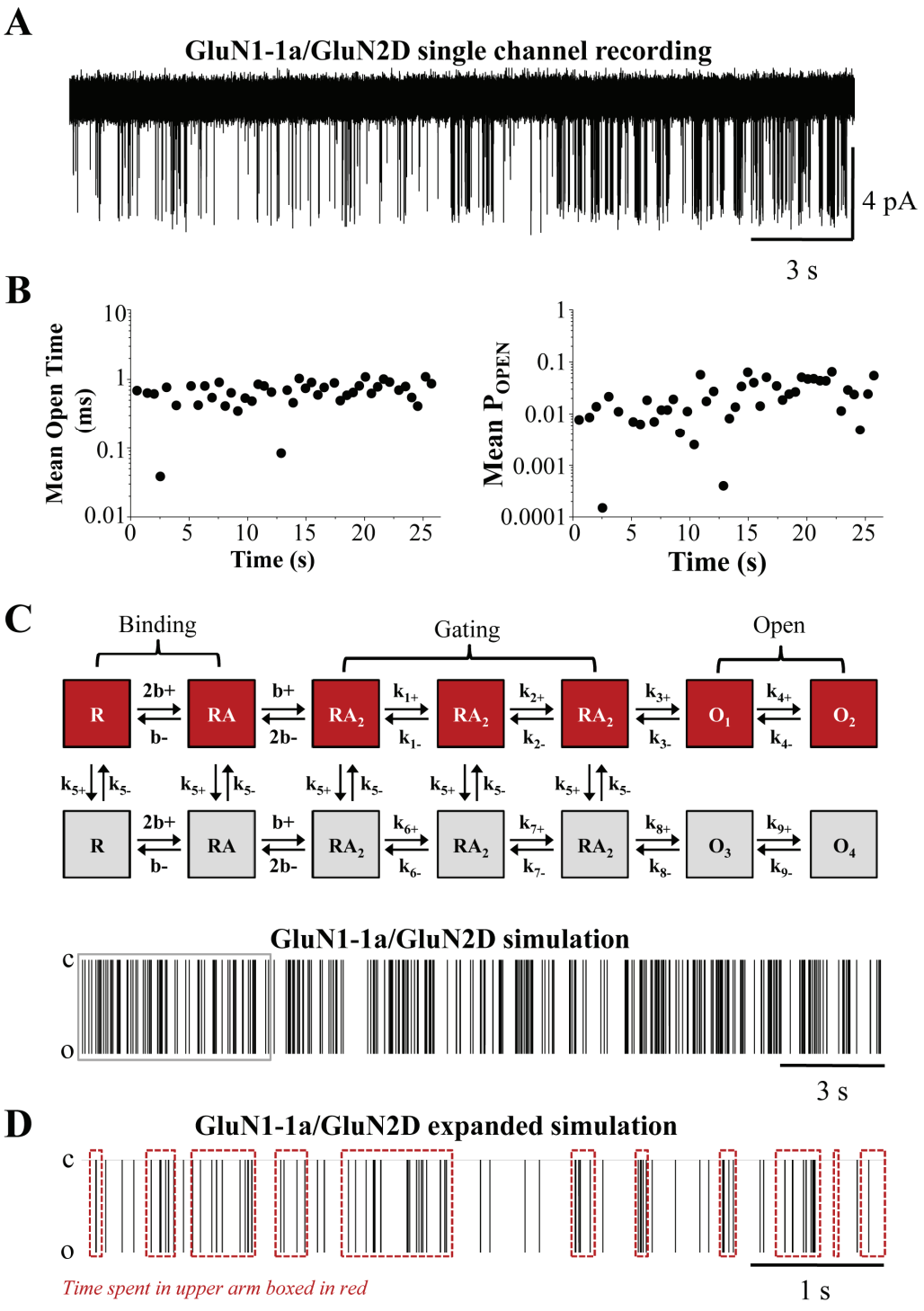


**Figure 5.6.** GluN1/GluN2D receptors transition between two arms of *Scheme 5*. A 25 s segment of a representative GluN1-1a/GluN2D single channel recording, activated by 1 mM L-glutamate and 50 μM glycine at pH 8.0, is shown in ***A***. ***B***, Stability plots of the mean open time (*left*) and mean open probability

(*right*), which were averaged in 500 ms increments, suggest both are reasonably stable. These plots demonstrate that the GluN1-1a/GluN2D NMDA receptor does not enter into prolonged periods of markedly high mean open time or open probability, as has been described in detail for other NMDA receptors (Popescu and Auerbach, 2003; Zhang et al., 2008; Amico-Ruvio and Popescu, 2010). ***C***, Using the rate constants derived from fitting *Scheme 5* to GluN1-1a/GluN2D data (given in Table 5.5), I simulated the response of a single GluN1-1a/GluN2D channel activated by steady application of 1 mM L-glutamate. "C" indicates closed, and "o" indicates open. The occupancy of all open states is plotted over a 25 s time period. Simulations of *Scheme 5* predict openings similar to those observed in the experimental data (***A***). The segment of the simulated response boxed in gray is expanded in ***D***. The red boxes indicate when the receptor is occupying any of the states of the upper arm, including the binding, gating, and open states. The receptor is able to transition freely between the upper and lower arms of *Scheme 5* and does not remain in either of the arms for prolonged periods of time. Adapted with permission from Vance et al. (2012).

in my GluN1-1a/GluN2D recordings are similar (Fig. 5.7). The more rapid open component is absent in the lower conductance state, although this could be due to my recording or idealization conditions.

### *5.3.c. Scheme 5 identifies specific gating steps controlled by GluN1 exon 5*

Because *Scheme 5* was able to predict many of the single channel and macroscopic current properties of GluN1-1a/GluN2D receptors, I subsequently evaluated whether *Scheme 5* could describe GluN1-1b/GluN2D receptors. The maximum likelihood fit of *Scheme 5* to the excised GluN1-1b/GluN2D single channel data again yielded a good fit Table 5.5). *Scheme 5* also identified specific gating steps controlled by the inclusion of exon 5 into the GluN1 subunit. The fitted rate constants predicted that the upper arm of the gating scheme has an opening rate constant nearly twice as fast in GluN1-1b/GluN2D as GluN1-1a/GluN2D (Fig. 5.3A; Table 5.5). In addition, in the lower arm of *Scheme 5*, the rate constants between the first shut state in which both ligands are bound and the second are more than 8 times slower in GluN1-1b/GluN2D than GluN1-1a/GluN2D. The remaining rate constants within the lower arm of *Scheme 5* are in general at least 1.5 times slower (Fig. 5.3A; Table 5.5). *Scheme 5* also was able to approximate the rapid rise time and more rapid deactivation time course of GluN1-1b/GluN2D (Table 5.4; Fig. 5.3C). These data suggest that *Scheme 5* is able to describe the single channel and macroscopic properties of GluN2D-containing receptors when expressed with or without GluN1 exon 5-encoded residues.

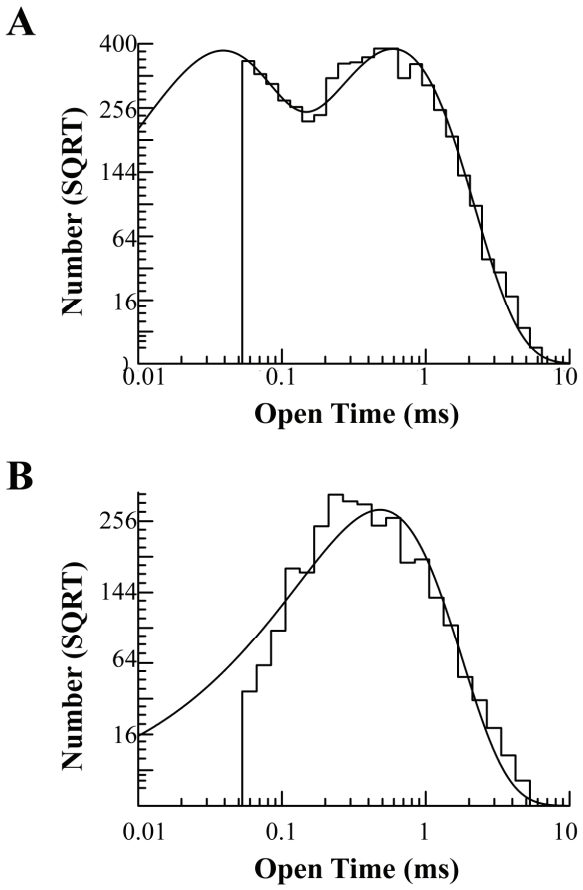


**Figure 5.7.** GluN1/GluN2D open states by conductance level. The open components of both GluN-1a/GluN2D conductance levels can be identified by isolating the open states of amplitudes within 1.5 standard deviations of the mean amplitude of each conductance level. ***A***, The open duration histogram of openings occurring in the higher conductance level of a representative GluN1-1a/GluN2D single channel recording can be fit by the sum of two exponential components, with $\tau_1$ = 0.033 ms (45%) and $\tau_2$ = 0.59 (55%). ***B***, The open duration histogram of the openings occurring in the subconductance level of the same recording can be fit by one exponential component with $\tau_1$ = 0.48 ms (100%). The loss of the brief open component in the subconductance level could be due to my experimental or idealization conditions.

**5.4. Discussion**

There are three main findings in this study of GluN1/GluN2D NMDA receptor gating. First, the key features of GluN1/GluN2D NMDA receptor single channel and macroscopic currents cannot be reproduced by models previously published for GluN2A, GluN2B, or GluN2C. Second, kinetic analysis of GluN1/GluN2D single channel data suggest that macroscopic and single channel responses can be described by a model composed of two interconnected arms, each with 3 closed states and 2 open states. This model predicts the low open probability, rapid response rise time, and channel mean open time, while approximating the shut duration histograms and the slow deactivation time course of the macroscopic response. Finally, *Scheme 5* also is able to distinguish between the two GluN1 splice variants. Specific rate constants are altered by exon 5, resulting in a 3-fold increase in open probability within the fast-gating arm of the model. The glutamate dissociation rate also is increased in GluN1-1b/GluN2D receptors, which is consistent with the accelerated deactivation time course, decreased $EC_{50}$ value, and decreased $K_D$.

While *Scheme 5* can adequately predict many of the key features of GluN1/GluN2D receptor responses, there remain several shortcomings. This model did not produce a dual exponential deactivation time course and predicted 1 or 2 fewer shut time components than observed in the data record. Moreover, *Scheme 5* did not incorporate features that would allow it to predict the two conductance states characteristic of GluN2D-containing NMDA receptor single channels. Recent work suggests that a single residue within the M3 pore forming helix (GluN2D Leu657) controls NMDA receptor subconductance levels, $Ca^{2+}$ permeability, and $Mg^{2+}$ block (Retchless et al., 2012).

Mutating this residue in GluN2D to the corresponding residue from GluN2A converts the sublevel to the conductance pattern observed in GluN2A without affecting channel shut times. This suggests that the subconductance level is a feature of the GluN2D pore rather than ligand-driven channel opening (Retchless et al., 2012). The lower subconductance level in my GluN1-1a/GluN2D single channel recordings did lack the brief open component (Fig. 5.7). It is possible that the receptor only opens for prolonged periods when in the subconductance state, but I also might not be able to observe the brief openings in the subconductance state due to my recording or idealization conditions.

Although *Scheme 5* was derived from a linear model and included a low open probability "arm," it is possible that cyclic models that include similar "arms" may be able to better fit GluN2D single channel and macroscopic data and describe subunit-specific gating. However, due to the complexities in fitting schemes with multiple fused cycles, we focused on the two-arm linear model. Nevertheless, Scheme 5 represents the best model described to date that can adequately predict the characteristics of GluN1/GluN2D NMDA receptors.

Modal gating is an unusual feature of NMDA receptor function and is clearly evident in cell-attached single channel recordings of GluN1/GluN2A receptors and in recordings of GluN1/GluN2B receptors to a lesser extent (Popescu and Auerbach, 2003; Zhang et al., 2008; Amico-Ruvio and Popescu, 2010). *Scheme 5* is similar to a model previously used to describe modal gating of GluN1/GluN2A receptors (Zhang et al., 2008); however, my single channel recordings of GluN1/GluN2D receptors show a stable open time throughout the data record, unlike the clear transitions between the gating modes that are observed in GluN1/GluN2A (Popescu and Auerbach, 2003; Zhang et al., 2008).

*Scheme 5* predicts the stable open times and open probabilities I observed in my experimental recordings. Therefore, if *Scheme 5* is describing a form modal gating of GluN1/GluN2D NMDA receptors, it occurs on a much more rapid timescale in a manner unlike GluN1/GluN2A and GluN1/GluN2B receptors.

# Chapter 6. GluN2D subunit control of the synaptic activity of the subthalamic nucleus

## 6.1. Abstract

The GluN2D subunit is expressed in a number of regions of the brain, including the subthalamic nucleus, substantia nigra, dentate gyrus, thalamus, and interneurons. However, due to the lack of pharmacological tools selective for the GluN2D subunit, little data exist addressing the role the subunit has in synaptic activity. I evaluated novel antagonists DQP-1105 and 997-33 and the potentiator CIQ for potency and selectivity for the GluN2D subunit over GluN2A/B-containing subunits. I show that CIQ selectively potentiates GluN2C/D-containing receptors over GluN2A/B receptors expressed in HEK 293 cells. I show that of the two antagonists, 997-33 has the best selectivity for GluN2D over GluN2B. I then used these modulators to evaluate the role of the GluN2D subunit in the subthalamic nucleus and found that NMDA and glycine-evoked currents could be potentiated by CIQ and inhibited by 997-33, suggesting that the GluN2D subunit is functionally expressed in the STN. The GluN2B subunit inhibitor ifenprodil also inhibited agonist-evoked currents, while the GluN2A modulator TCN and the GluN2C modulator 1616 had no effect. I also determined that the GluN2D subunit contributes to the synaptic activity of the STN, as evoked EPSCs were inhibited by 997-33 and potentiated by CIQ; evoked EPSCs also were inhibited by ifenprodil. These data suggest that the GluN2D subunit, along with the GluN2B subunit, plays an important role in the synaptic activity of the subthalamic nucleus.

## 6.2. Introduction

The subthalamic nucleus (STN) is the lone region in the basal ganglia with glutamatergic projections. The STN receives excitatory glutamatergic input primarily from the thalamus, cortex and pedunculopontine nucleus, inhibitory input from the globus pallidus external, and dopaminergic input from the midbrain (Fig. 6.1A) (Bevan et al., 2002; Wilson and Bevan, 2011). In turn, the STN provides excitatory output to the substantia nigra pars reticula and the globus pallidus internal and external (Fig. 6.1A) (Bolam et al., 2000; Bevan et al., 2002; Wilson and Bevan, 2011). Regular activity in the STN results in voluntary movement; however, the death of the dopaminergic neurons of the substantia nigra pars compacta leads to overactivation and excessive burst firing of the STN, resulting in increased output to the SNr and the GPi, lead to the inhibition of the basal ganglia and contribute to the symptoms of Parkinson's disease, such as akinesia, bradykinesia, and tremor (Fig. 6.1B; Bergman et al., 1990; DeLong, 1990; Rodriguez et al., 1998; Levy et al., 2000; Obeso et al., 2000).

Neurons in the STN express several subunits from the AMPA, kainate, and NMDA receptor classes of ionotropic glutamate receptors. The GluN1 subunit containing the exon 5 splice variant (GluN1-b) is expressed in abundance in the STN when evaluated by *in situ* hybridization (Standaert et al., 1993; Laurie and Seeburg, 1994; Standaert et al., 1994). Likewise, the GluN2D subunit has been shown to be the predominant GluN2 NMDA receptor subunit expressed in the STN, while the GluN2B subunit also is expressed (Monyer et al., 1994; Standaert et al., 1994; Wenzel et al., 1996). EM data from our collaboration with Dr. Yoland Smith's lab (Pare and Smith, unpublished data; Fig. 6.2) indicate that the GluN2D subunit protein is expressed primarily in dendrites

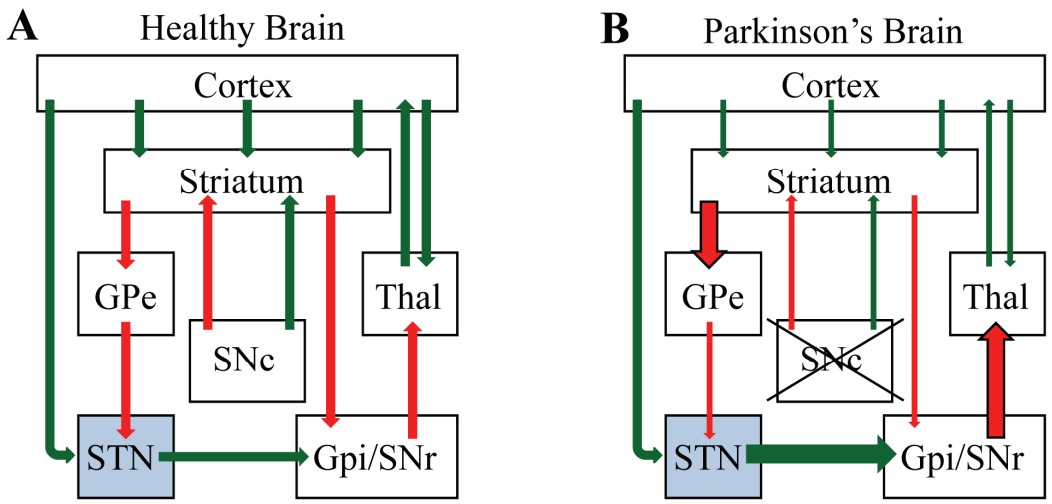


**Figure 6.1.** The basal ganglia circuit. ***A***, The subthalamic nucleus is the lone glutamatergic member of the basal ganglia and receives excitatory input from the thalamus and the cortex and inhibitory input from the globus pallidus external. In a healthy brain, normal activity of the STN leads to glutamatergic input into the inhibitory globus pallidus internal and the substantia nigra pars reticula (Bevan et al., 2002; Wilson and Bevan, 2011). ***B***, In a Parkinson's brain, the death of dopaminergic SNc neurons cause disinhibition of the STN due to decreased activity of the GPe leads to over stimulation of the GPi and SNr. This results in the symptoms of Parkinson's disease, including akinesia, bradykinesia, and tremor (Bergman et al., 1990; DeLong, 1990; Rodriguez et al., 1998; Levy et al., 2000; Obeso et al., 2000). Red arrows indicate a GABAergic inhibitory projection pathway, green arrows indicate a glutamatergic excitatory projection pathway, and the thickness of the arrow indicates the strength of the connection.

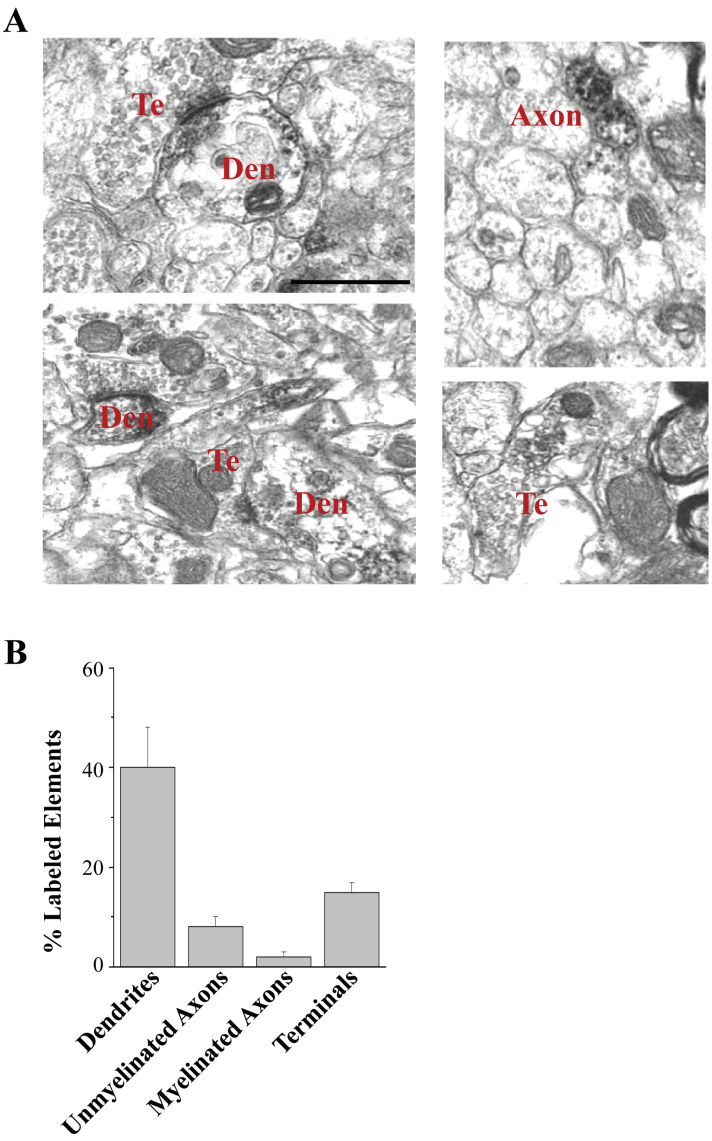


**Figure 6.2**. Features of GluN2D-immunoreactive elements in the rat STN. ***A***, Immunoperoxidase labeled elements were identified in 300 digital micrographs of GluN2D-positive elements taken at 20,000X from the STN of 3 adult rats. A monoclonal GluN2D antibody (Millipore, 1G9.39A5) was used to detect the GluN2D subunit. Staining with a polyclonal antibody for GluN2C/D subunits had similar labeling patterns. Scale bar equals 1 mm. The GluN2D subunit can be found in the postsynaptic density of STN neurons in the dendrites (Den) as well as presynaptically in unmyelinated axons (Ax) and axon terminals (Te). A histogram of the general distribution of GluN2D-immunoreactive neuronal elements with relative percentages of each category of labeled structures is given in ***B***. (Unpublished data by Pare and Smith)

of STN neurons, but also can be found in terminals synapsing upon the STN. Likewise, the GluK2 and GluK5 kainate receptor subunit mRNAs have been shown to be present in rodent STN (Bischoff et al., 1997; Wüllner et al., 1997), while all four AMPA receptor subunits (GluA1-4) have been detected in the STN (Sato et al., 1993; Clarke and Bolam, 1998; Jakowec et al., 1998).

Although NMDA receptors have been identified as having roles in synaptic plasticity, learning, memory, and neuronal development (Lisman, 2003; Cull-Candy and Leszkiewicz, 2004; Pérez-Otaño and Ehlers, 2005; Traynelis et al., 2010), the roles of the individual GluN2 subunits remain unclear due to the lack of GluN2 subunit-specific probes. Ifenprodil and its analogues are subunit-selective noncompetitive antagonists of the GluN2B subunit, allowing for the evaluation of the role of the GluN2B subunit in a range of phenomenon, including synaptic plasticity, neurodegeneration, and neurological diseases (Williams, 1993; Mony et al., 2009; reviewed in Traynelis et al., 2010). Recently, a number of subunit-selective NMDA receptor modulators have been developed for the remaining GluN2 subunits, including the GluN2A antagonist TCN (Bettini et al., 2010; Hansen et al., 2012; McKay et al., 2012), the GluN2C potentiator 1616 (Khatri et al., 2012), and the GluN2C/D antagonists DQP-1105 and 997-33 (Acker et al., 2011; Acker et al., 2012) and potentiator CIQ (Mullasseril et al., 2010).

NMDA receptors previously have been shown to have a role in $Ca^{2+}$-dependent bursting in the STN (Zhu et al., 2005; Shen and Johnson, 2010). The emergence of GluN2 subunit-selective modulators, along with the GluN2B antagonist ifenprodil, provides an excellent opportunity to evaluate the roles of the specific GluN2 subunits in the activity of the STN. First, I evaluated the effectiveness and potencies of GluN2C/D-

specific modulators developed in the Traynelis and Liotta labs on HEK 293 cells to determine if the compounds were good candidates for use in slice recordings. Second, I determined if STN neurons held under voltage-clamp were inhibited or potentiated by GluN2C/D subunit-specific modulators when activated by pressure-applied NMDA and glycine. Finally, I assessed whether GluN2D-containing NMDA receptors contribute to the synaptic activity of the STN by evoking EPSCs in the presence of GluN2C/D-specific inhibitors and potentiators.

## 6.3. Results

### *6.3.a. Positive allosteric modulation of GluN1/GluN2D receptors expressed in HEK 293 cells by CIQ*

CIQ is a subunit-selective positive allosteric modulator of GluN2C/D-containing NMDA receptors that was developed in the Traynelis and Liotta labs (Mullasseril et al., 2010). I evaluated whether CIQ also potentiates recombinant NMDA receptors expressed in mammalian cells using whole cell voltage-clamp recordings of HEK 293 cells activated by 100 μM L-glutamate and 30 μM glycine at pH 7.4. CIQ selectively potentiated current responses of GluN2C- and GluN2D-containing NMDA receptors expressed in transiently transfected HEK 293 cells (Fig. 6.3B; Table 6.1). Maximal potentiation was 180% for both GluN1/GluN2C and GluN1/GluN2D, with $EC_{50}$ values of 1.7 μM for GluN2C (n=5-11) and 4.1 μM for GluN2D (n=4-17; Fig. 6.3C). CIQ had minimal effects on rise time and deactivation time course (Table 6.2; Fig. 6.3D). Current responses for GluN1/GluN2A and GluN1/GluN2B receptors were not potentiated by CIQ

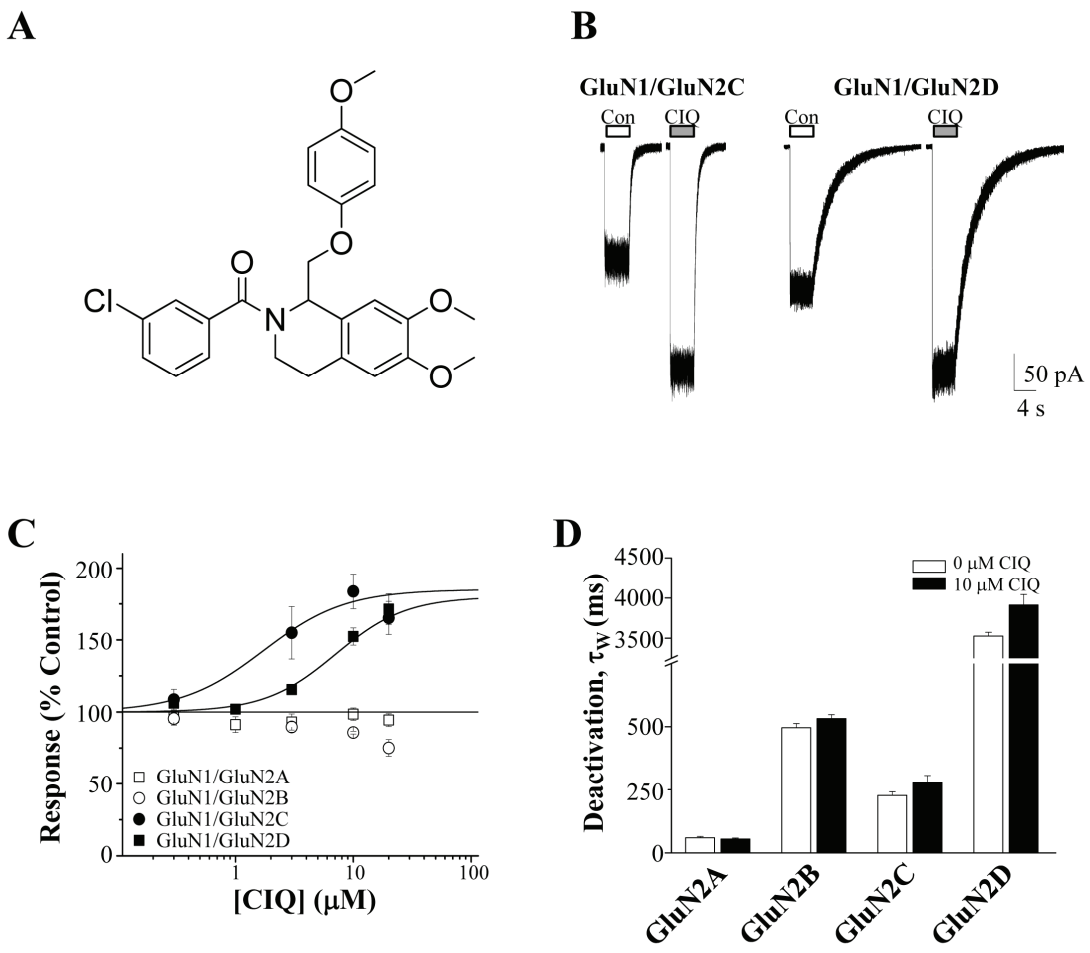


**Figure 6.3**. CIQ potentiates recombinant rat GluN1/GluN2C and GluN1/GluN2D expressed in HEK 293 cells. ***A***, CIQ is an allosteric modulator identified by the Traynelis lab as a potentiator of GluN2C- and GluN2D-containing NMDA receptors (Mullasseril et al., 2010). ***B***, HEK 293 cells expressing rat recombinant GluN1/GluN2C or GluN1/GluN2D were activated by 100 μM L-glutamate and 30 μM glycine at pH 7.4 ($V_{HOLD}$ = -60 mV). GluN1/GluN2C and GluN1/GluN2D were potentiated by application of 100 μM L-glutamate, 30 μM glycine, and 10 μM CIQ. ***C***, CIQ potentiated GluN1/GluN2C with an $EC_{50}$ of 1.7 μM (n=5-11) and GluN1/GluN2D with an $EC_{50}$ of 4.1 μM (n=4-17). CIQ had no effect on GluN1/GluN2A (n=4-15) and inhibited GluN1/GluN2B by 25% at 20 μM (n=5). ***D***, CIQ had no effect on the weighted deactivation time course of GluN2A-, GluN2B, GluN2C-, or GluN2D-containing NMDA receptors when recordings with 0 μM CIQ are compared to recordings with 10 μM CIQ and analyzed using a paired t-test (see Table 6.2).

**Table 6.1.** CIQ potentiates GluN2C/D-containing NMDA receptors expressed in HEK 293 cells.

| | $EC_{50}$ (μM) | Maximal Effect | n |
|---|---|---|---|
| **GluN1/GluN2A** | -- | -- | 4-15 |
| **GluN1/GluN2B** | -- | -25% | 5 |
| **GluN1/GluN2C** | 1.7 | +80% | 5-11 |
| **GluN1/GluN2D** | 4.1 | +80% | 4-17 |

HEK 293 cells expressing recombinant rat GluN2A, GluN2B, GluN2C, or GluN2D co-expressed with GluN1-1a were activated by 100 μM L-glutamate, 30 μM glycine, and 0-100 μM CIQ at pH 7.4. All data are given to two significant figures, and n is the number of cells. Some concentrations did not have equal numbers of cells.

**Table 6.2.** CIQ does not influence GluN1/GluN2D rise time or deactivation kinetics

| | Control | | | + 10 μM CIQ | | | |
|---|---|---|---|---|---|---|---|
| | **Rise Time (ms)** | **$\tau_{FAST}$ (ms)** | **$\tau_{SLOW}$ (ms)** | **Rise Time (ms)** | **$\tau_{FAST}$ (ms)** | **$\tau_{SLOW}$ (ms)** | **n** |
| **GluN2A** | 19 ± 1.7 | 40 ± 4 | 560 ± 140 | 19 ± 2.1 | 45 ± 4.0 | 640 ± 160 | 9 |
| **GluN2B** | 15 ± 1.1 | 310 ± 30 | 1100 ± 190 | 17 ± 1.8 | 320 ± 30 | 1100 ± 120 | 5 |
| **GluN2C** | 6 ± 1.0 | 110 ± 30 | 310 ± 35 | 9 ± 1.0 | 200 ± 30* | 530 ± 60* | 7 |
| **GluN2D** | 13 ± 1.0 | 2100 ± 150 | 5700 ± 510 | 15 ± 2.0 | 2000 ± 270 | 5800 ± 600 | 13 |

HEK 293 cells expressing recombinant rat GluN2A, GluN2B, GluN2C, or GluN2D co-expressed with GluN1-1a were activated by 100 μM L-glutamate and 30 μM glycine or 100 μM L-glutamate, 30 μM glycine, and 10 μM CIQ at pH 7.4. $\tau_{FAST}$, $\tau_{SLOW}$, and rise time are shown as mean ± s.e.m., and n is the number of cells. *$p$<0.05 when compared to the corresponding value in the absence of 10 μM CIQ when analyzed with a paired t-test. All data are given to two significant figures.

(Fig. 6.3B; Table 6.1). These data suggest that CIQ will selectively potentiate GluN2C/D-containing NMDA receptors expressed in the subthalamic nucleus.

### *6.3.b. Negative allosteric NMDA receptor modulation by dihydroquinilone-pyrazolines*

The dihydroquinilone-pyrazoline (DQP) NMDA receptor inhibitory modulator class also was identified in a medium throughput drug screen conducted in the laboratory. DQP-1105, a member of this inhibitory class, was determined to be selective for GluN2C/D-containing NMDA receptors expressed in *Xenopus* oocytes (Acker et al., 2011). I evaluated whether DQP-1105 was selective for recombinant rat GluN2C/D-containing NMDA receptors over GluN2A/B-containing NMDA receptors when transiently expressed in mammalian HEK 293 cells. Cells were activated under voltage-clamp ($V_{HOLD}$= -60 mV) by a 2-3 s pulse of 1 mM glutamate or 1 mM NMDA (0.05 mM of the co-agonist glycine was present in all solutions) at pH 7.4. As observed in *Xenopus* oocytes, DQP-1105 inhibited glutamate-evoked GluN1/GluN2D currents with an $IC_{50}$ of 3.2 μM (n=7) and NMDA-evoked currents with an $IC_{50}$ of 1.9 μM (n=10; Table 6.3; Fig. 6.4A,B). Inhibition by DQP-1105 was use-dependent, as NMDA must be bound before the GluN1/GluN2D receptors could be inhibited. These data show that DPQ-1105 can inhibit GluN2D-containing receptors regardless of the activating agonist. However, DPQ-1105 was not as selective against GluN1/GluN2A receptors in dialyzed HEK 293 cells, as glutamate-evoked currents were inhibited with an $IC_{50}$ of 12 μM (n=8), and NMDA-evoked currents were inhibited with an $IC_{50}$ of 7.3 μM (n=7; Table 6.3; Fig. 6.4A,B). This suggests that dialysis with the patch solution leads to a loss of a factor that influences the activity of DQP-1105 at GluN2A.

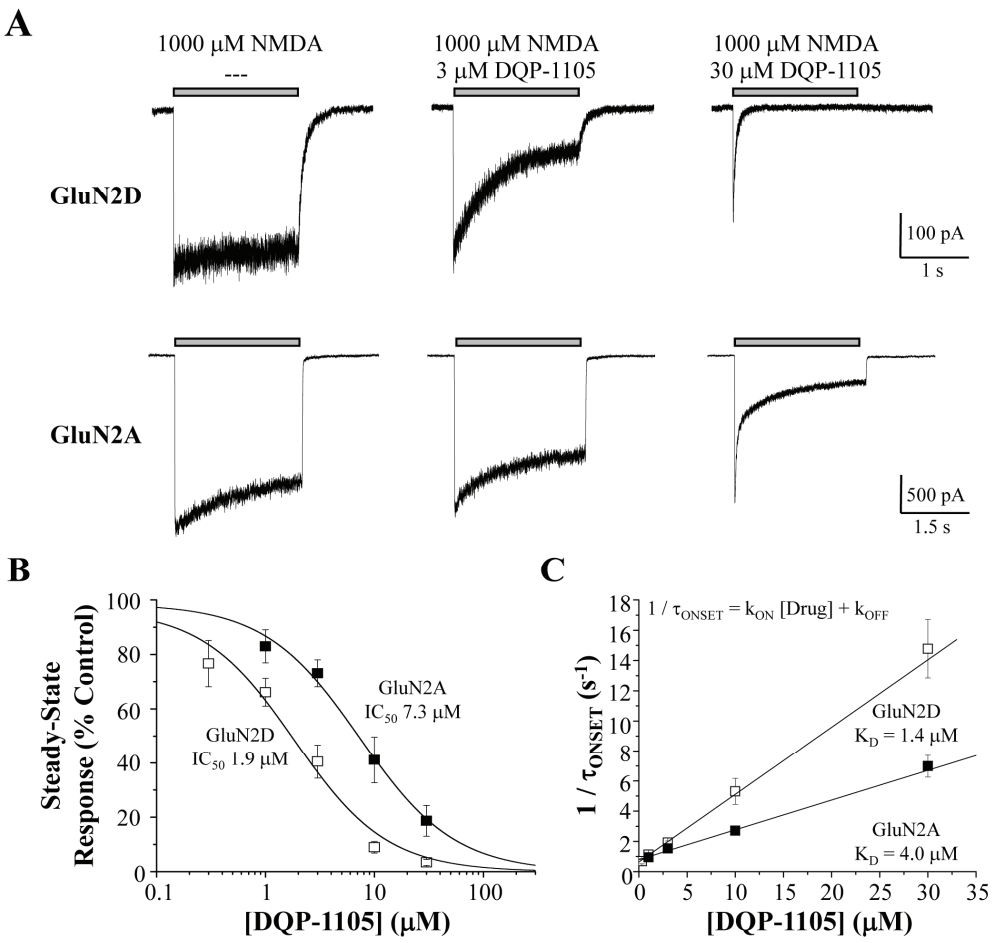


**Figure 6.4.** DQP-1105 inhibits recombinant NMDA receptors expressed in HEK 293 cells. ***A***, (*top*) Whole cell voltage-clamp recordings of currents evoked from recombinant GluN1/GluN2D receptors by 2 s applications of 1000 μM NMDA and 50 μM glycine. DQP-1105 causes a concentration-dependent attenuation of the steady-state current response upon co-application with NMDA and glycine, with a final steady-state response of 3.4 $\pm$ 1.1% (n=8) at 30 μM DQP-1105 compared to the NMDA and glycine only control. (*bottom*) In whole cell voltage-clamp recordings of currents evoked by 3 s applications of 1000 μM NMDA and 50 μM glycine, recombinant GluN1/GluN2A receptors were inhibited modestly by increasing concentrations of DQP-1105. ***B,*** Concentration-response curves of the steady-state current responses indicate that DQP-1105 has an $IC_{50}$ of 1.9 μM for GluN1/GluN2D receptors and 7.3 μM for GluN1/GluN2A receptors. ***C,*** The linear relationship between $1/\tau_{ONSET}$ and DQP-1105 concentration allows the calculation of $K_D$ values of 1.4 μM for GluN1/GluN2D receptors and 4.0 μM for GluN1/GluN2A receptors. All data were from dialyzed HEK 293 cells.

**Table 6.3.** Dihydroquinilone-pyrazolines are moderately selective NMDA receptor antagonists

| | | $IC_{50}$ (μM) | | | |
|---|---|---|---|---|---|
| **Drug** | **Activating Agonist** | **GluN2A** | **GluN2B** | **GluN2C** | **GluN2D** |
| **DQP-1105** | Glutamate | 12 | NA | NA | 3.2 |
| **DQP-1105** | NMDA | 7.3 | NA | NA | 1.9 |
| **997-33** | NMDA | NA | 23 | NA | 0.99 |

HEK 293 cells were activated under voltage-clamp ($V_{HOLD}$= -60 mV) by a 2-3 s pulse of 1 mM glutamate or 1 mM NMDA (0.05 mM of the co-agonist glycine was present in all solutions) at pH 7.4 for the DQP-1105 experiments. HEK 293 cells were activated under voltage-clamp ($V_{HOLD}$ = -60 mV) by 0.2 mM NMDA (0.05 glycine present in all solutions) at pH 7.4 for the 997-33 experiments. $IC_{50}$ values are in μM and are given to two significant figures. NA indicates that the conditions were not analyzed.

The DQP modulator class represents a good scaffold to further develop ligands with increased subunit selectivity and potency, and a number of more potent and more selective compounds have been developed since DQP-1105 was identified as a GluN2C/D-specific modulator (Acker et al., 2011, 2012). One compound, inhibitor 997-33, showed submicromolar potencies for GluN1/GluN2C and GluN1/GluN2D and increased selectivity over GluN1/GluN2A and GluN1/GluN2B in two-electrode voltage-clamp recordings of *Xenopus* oocytes (Acker et al., 2012). I evaluated whether 997-33 was selective for GluN1/GluN2D receptors over GluN1/GluN2B receptors in transiently transfected HEK 293 cells. Cells were activated under voltage-clamp ($V_{HOLD}$ = -60 mV) by 200 μM NMDA and 50 μM glycine at pH 7.4 first, followed by application of 0-30 μM 997-33 in the presence of 200 μM NMDA and 50 μM glycine. Finally, the drug was washed off as the cell was exposed once again to 200 μM NMDA and 50 μM glycine. The modulator 997-33 inhibited GluN1/GluN2D NMDA receptors expressed in HEK 293 cells with an $IC_{50}$ of 0.99 μM (n=4; Table 6.3; Fig. 6.5). Unlike DQP-1105, 997-33 retained modest subunit-selectivity in patch-dialyzed cells, with an $IC_{50}$ of 23 μM (n=3) for GluN1/GluN2B receptors (Table 6.3; Fig. 6.5D).

The onset and offset of inhibition for 997-33 were exceptionally slow for GluN1/GluN2D. At 3 μM 997-33, the $\tau_{ONSET}$ was 3700 $\pm$ 1000 ms, and the $\tau_{OFFSET}$ was 19000 $\pm$ 5800 ms (n=3). I calculated the $k_{ON}$ to be 9.4 x $10^4$ $M^{-1}s^{-1}$ and the $k_{OFF}$ to be 0.046 $s^{-1}$, for a $K_D$ of 0.69 μM, similar to the 997-33 $IC_{50}$ value for GluN1/GluN2D (Table 6.4). Because 997-33 retains more than 20-fold selectivity for GluN1/GluN2D over GluN1/GluN2B in patch-dialyzed cells, this inhibitor may be a useful modulator to determine the role of GluN2D-containing NMDA receptors in neurons.

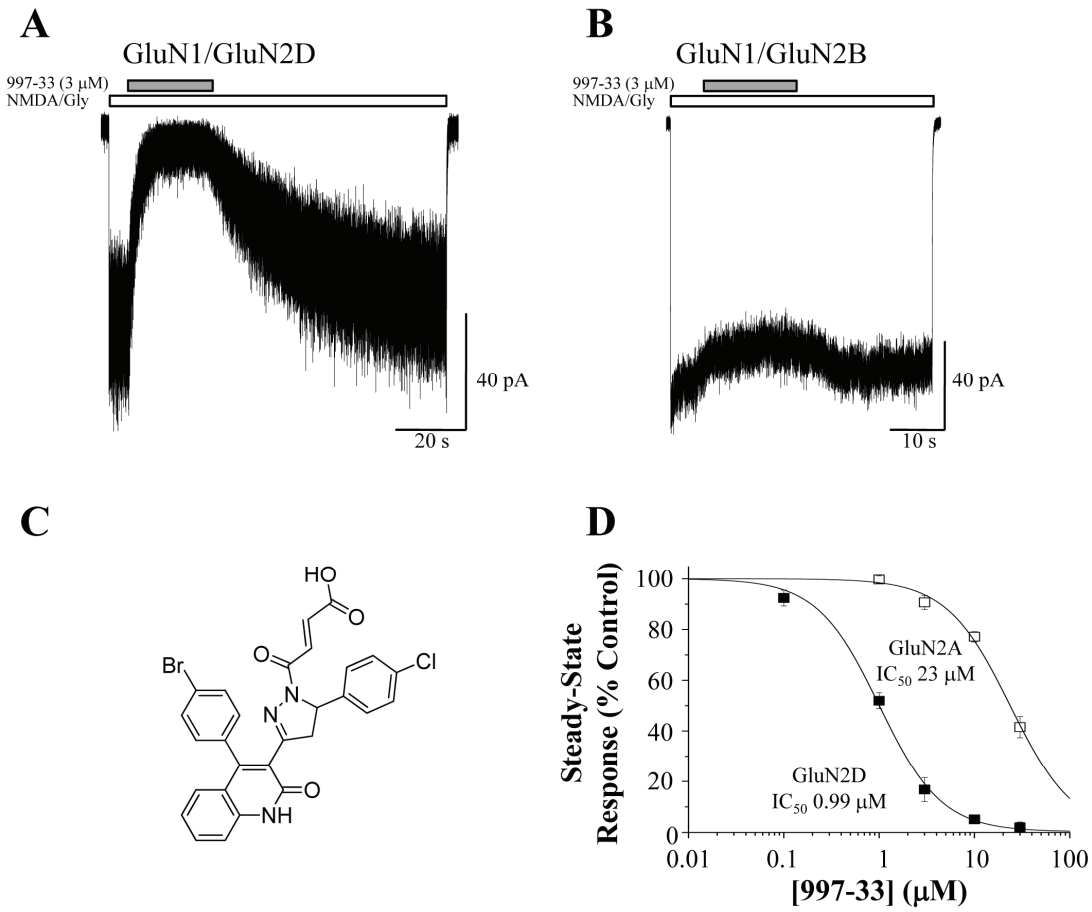


**Figure 6.5.** 997-33 is selective for GluN2D in HEK 293 cells. Whole cell voltage-clamp recordings were conducted on recombinant GluN1/GluN2B and GluN1/GluN2D NMDA receptors expressed in HEK 293 cells. Cells were activated by 200 μM NMDA and 50 μM glycine at pH 7.4, followed by application of 0-30 μM 997-33 in the presence of 200 μM NMDA and 50 μM glycine. 997-33 has slow onset and offset of inhibition for GluN1/GluN2D receptors (***A***), with nearly full inhibition at 3 μM, while GluN1/GluN2B is much less inhibited by 3 μM 997-33 (***B***). The structure of the 997-33 modulator is given in ***C***. ***D***, GluN1/GluN2D is inhibited by 997-33 with an $IC_{50}$ of 0.99 μM, while GluN1/GluN2B is inhibited with an $IC_{50}$ of 23 μM.

**Table 6.4.** Dihydroquinilone-pyrazolines have slow on and off rates

| Drug | Agonist | $\tau_{ONSET}$ (s) | $\tau_{OFFSET}$ (s) | $k_{ON}$ ($M^{-1}s^{-1}$) | $k_{OFF}$ ($s^{-1}$) | $K_D$ (M) | n |
|---|---|---|---|---|---|---|---|
| **DQP-1105** | Glutamate | 3.2 ± 0.14 | -- | 4.4 x $10^5$ | 1.44 | 3.3 x $10^{-6}$ | 7 |
| **DQP-1105** | NMDA | 6.5 ± 0.7 | -- | 4.5 x $10^5$ | 0.65 | 1.4 x $10^{-6}$ | 10 |
| **997-33** | NMDA | 3.7 ± 1.0 | 22 ± 2.9 | 9.4 ± 3.5 x $10^4$ | 0.046 ± 0.0061 | 6.9 ± 3.3 x $10^{-7}$ | 3 |

HEK 293 cells were activated under voltage-clamp ($V_{HOLD}$= -60 mV) by a 2-3 s pulse of 1 mM glutamate or 1 mM NMDA (0.05 mM of the co-agonist glycine was present in all solutions) at pH 7.4 for the DQP-1105 experiments. For the DQP-1105 experiments, $k_{ON}$ and $k_{OFF}$ were determined using regression analysis of the equation $1 / \tau_{ONSET} = k_{ON}$ [Drug] + $k_{OFF}$, where the reciprocal of the $\tau_{ONSET}$ is linearly related to the concentration of DQP-1105, the slope of the line equal to $k_{ON}$, and the intercept equal to $k_{OFF}$. For the 997-33 experiments, HEK 293 cells were activated under voltage-clamp ($V_{HOLD}$ = -60 mV) by 0.2 mM NMDA and 0.05 glycine at pH 7.4. $K_{OFF}$ is equal to $1 / \tau_{OFFSET}$, and $k_{ON}$ was determined by solving the equation $1 / \tau_{ONSET} = k_{ON}$ [Drug] + $k_{OFF}$, when the concentration of 997-33 was 0.000003 M.

### *6.3.c. GluN2B and GluN2D-containing NMDA receptors in the STN are inhibited or potentiated by subunit-selective allosteric modulators*

After confirming that the GluN2C/D allosteric potentiator and inhibitors that our laboratory developed had reasonable selectivity for GluN2D-containing receptors over GluN2A/B-containing receptors when expressed in HEK 293 cells, I subsequently used these modulators to determine if functional GluN2D-containing receptors were expressed in the rat subthalamic nucleus. I also used other available subunit-selective tools for the GluN2A, GluN2B, and GluN2C subunits to determine if these subunits were functionally expressed in the STN. I evaluated the effectiveness of these modulators on current responses to pressure-applied NMDA (1-2 mM) and glycine (0.003-0.5 mM), which were ejected from a micropipette during brief pulses (3-12 psi; 3-100 ms) at 90 second intervals. STN neurons were held under voltage-clamp ($V_{HOLD}$ = -60 mV) in aCSF containing 0.2 mM $Mg^{2+}$, 0.01 mM bicuculline, 0.005 mM nimodipine, 0.0005 mM TTX, and 0.015-0.1% DMSO. Following bath application of aCSF, the slice was perfused with aCSF containing 3-100 μM of the modulators and then washed with aCSF alone. Finally, to confirm that I was measuring responses from NMDA receptors alone, I applied 400 μM D,L-APV to inhibit the NMDAR-dependent current.

I next evaluated whether GluN2D-containing NMDA receptors could be pharmacologically modulated by both the GluN2C/D subunit-selective potentiator CIQ and the inhibitor 997-33 when activated by pressure-applied NMDA and glycine. CIQ (20 μM) potentiated currents 150 $\pm$ 8.6 % compared to the aCSF control (n=6; Fig. 6.6; Table 6.5). Potentiation was reversible (100 $\pm$ 2.3 %) and could be inhibited by application of D,L-APV (3.4 $\pm$ 2.8%). Likewise, GluN2D-containing receptors could be

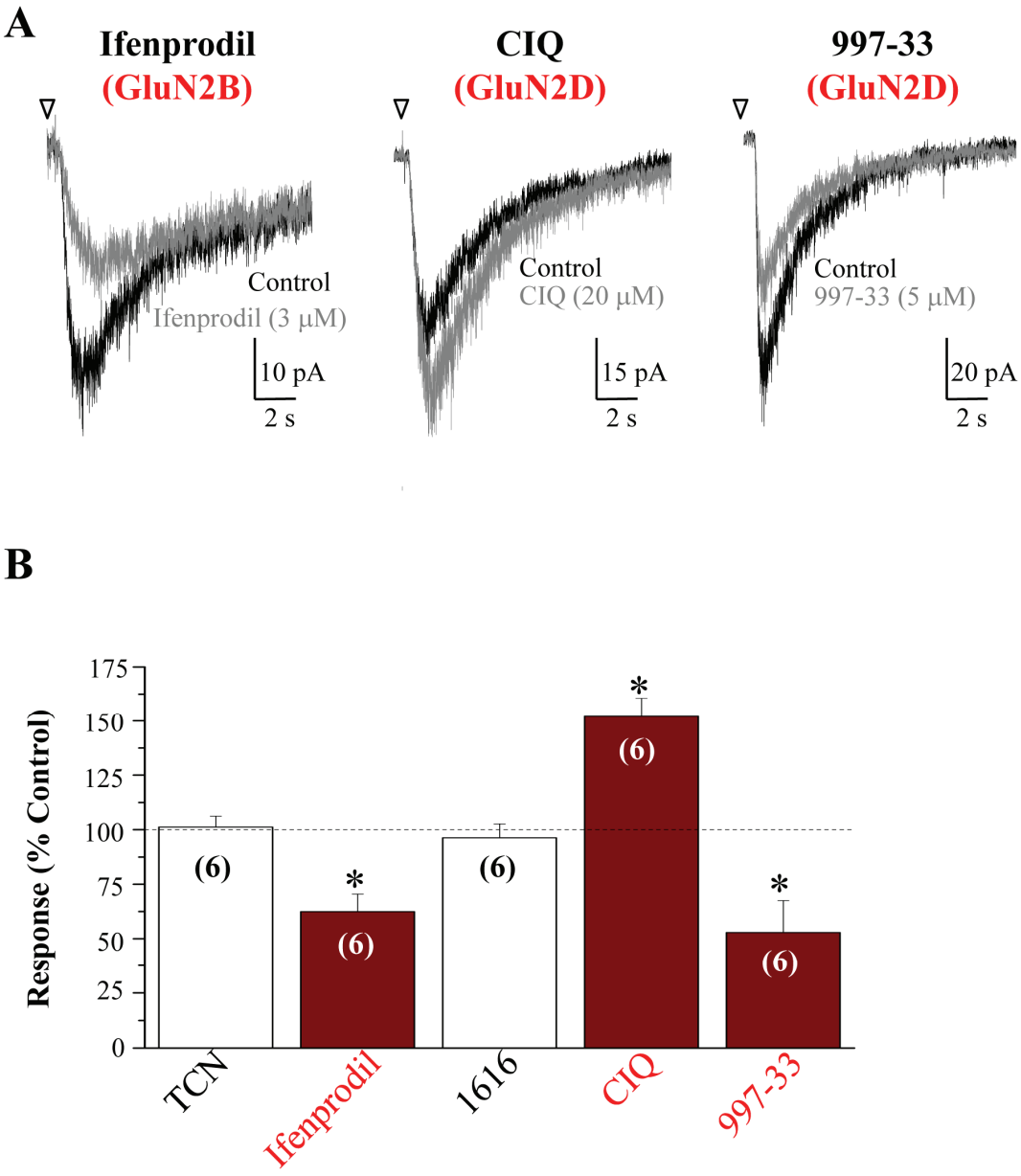


**Figure 6.6.** NMDA and glycine evoked currents are potentiated or inhibited by GluN2D and GluN2B subunit-specific modulators. NMDA (1-2 mM) and glycine (0.003-0.5 mM) were pressure-applied in brief pulses (3-12 psi; 3-100 ms) in 90 second intervals on STN neurons held under voltage clamp ($V_{HOLD}$ = -60 mV) in thin slices. Slices were perfused by aCSF containing 0.2 mM $Mg^{2+}$, 0.01 mM bicuculline, 0.005 mM nimodipine, 0.0005 mM TTX, and 0.015-0.1% DMSO. Modulators (3-100 μM) were bath applied in

aCSF. ***A***, Agonist-evoked currents were inhibited by the GluN2B antagonist ifenprodil (3 μM) to a current response of 62 ± 8.1% compared to the aCSF control (n=6). The GluN2D antagonist 997-33 (5 μM) reduced currents to 53 ± 15% compared to aCSF control (n=6), while the GluN2D potentiator CIQ (20 μM) increased currents to 150 ± 8.6 % compared to the aCSF control (n=6). The GluN2A antagonist TCN (10 μM; 100 ± 5.1%; n=6) and the GluN2C potentiator 1616 (100 μM; 96 ± 6.4%; n=6) did not influence the agonist-evoked currents (***B***). *$p < 0.05$; one-way ANOVA with Tukey's *post-hoc* test when compared to the aCSF control.

**Table 6.5.** Picospritzer-evoked currents from the STN are increased by GluN2D potentiators and inhibited by GluN2D and GluN2B antagonists.

| Modulator | GluN2 Subunit | % Response | n |
|---|---|---|---|
| **TCN** | GluN2A | 100 ± 5.1% | 6 |
| **Ifenprodil** | GluN2B | 62 ± 8.1% | 6 |
| **1616** | GluN2C | 96 ± 6.4% | 6 |
| **CIQ** | GluN2C/D | 150 ± 8.6% | 6 |
| **997-33** | GluN2C/D | 53 ± 15% | 6 |

STN neurons were activated under voltage-clamp ($V_{HOLD}$= -60 mV) in 0.2 mM $Mg^{2+}$ by a 3-100 ms pulse (3-12 psi) of 1-2 mM NMDA and 0.003-0.5 mM glycine. Peak amplitudes of the aCSF control containing 0.2 mM $Mg^{2+}$, 0.01 mM bicuculline, 0.005 mM nimodipine, 0.0005 mM TTX, and 0.015-0.1% DMSO were compared to the peak amplitudes of currents evoked in aCSF containing 3-100 μM of the modulators. Data are given to two significant figures, and n is the number of cells.

inhibited by bath application of 5 μM 997-33 to 53 ± 15% (n=6; Table 6.5; Fig. 6.6) compared to the aCSF control. Inhibition was reversible (100 ± 8.6%) and could be inhibited by bath application of D,L-APV (16 ± 5.5%). I chose to use 5 μM 997-33 because this concentration is 5 times higher than the $IC_{50}$ for GluN1/GluN2D expressed in HEK 293 cells, but is nearly 5 times lower than the $IC_{50}$ for GluN1/GluN2B expressed in HEK 293 cells (see Fig. 6.5; Table 6.3). These data suggest that GluN2D-containing receptors are functional in the rat subthalamic nucleus.

I also evaluated which other NMDA receptor subunits contribute to the agonist-evoked current in rat STN using subunit-selective modulators for GluN2A, GluN2B, and GluN2C. TCN (3 μM), a subunit-selective modulator for GluN2A (Bettini et al., 2010; Hansen et al., 2012; McKay et al., 2012), did not inhibit NMDA and glycine-evoked currents compared to the aCSF control (100 ± 5.1%; n=6; Table 6.5), suggesting that the GluN2A subunit is not a major NMDA receptor subunit expressed in the STN. I used 1 mM NMDA and only 3 μM glycine when evoking currents to evaluate TCN's effectiveness, as TCN has been shown to be less effective at higher concentrations of glycine (Hansen et al., 2012). Because TCN previously had not been evaluated for effectiveness in inhibiting neuronal GluN2A-containing NMDA receptors, I tested TCN's effectiveness on cultured cerebellar granule cells that express GluN2A. TCN inhibited agonist-evoked (50 μM NMDA and 3 μM glycine at pH 7.6) currents to 32 ± 3.4% of control (n=6). These data suggest that had the STN expressed the GluN2A subunit, TCN would have been able to inhibit GluN2A-containing NMDA receptors. Ifenprodil, a subunit-selective inhibitor for GluN2B-containing NMDA receptors, inhibited NMDA and glycine-evoked currents to 62 ± 8.1% of the aCSF control (n=6; Table 6.5; Fig.

6.6B). Inhibition was reversible (100 ± 5.2%), and the NMDA and glycine-evoked currents could be inhibited by 400 μM D,L-APV (0.52 ± 0.52%). Finally, I evaluated whether 1616, a GluN2C-selective potentiator, could increase the current response of NMDA and glycine-evoked currents when bath applied. As with TCN, 1616 (100 μM) had no effect on the agonist-evoked current responses, with responses of 96 ± 6.4% compared to the aCSF control (n=6; Table 6.5; Fig. 6.6B). These data suggest that the GluN2D and GluN2B subunits are the primary GluN2 subunits expressed in the rat subthalamic nucleus, while GluN2A and GluN2C have little to no functional expression in the STN.

### *6.3.d. GluN2D and GluN2B subunits contribute to evoked EPSCs in the STN*

The GluN2D subunit has been suggested to be expressed in several regions of the brain (Monyer et al., 1994; Standaert et al., 1994), but few studies have identified the GluN2D subunit as having a role in excitatory postsynaptic currents (Lozovaya et al., 2004; Logan et al., 2007; Brothwell et al., 2008; Harney et al., 2008). The basic pharmacology of evoked excitatory postsynaptic currents in STN neurons has not been characterized thoroughly. Therefore, before evaluating the role of the GluN2D subunit in the synaptic activity of the STN, I first evaluated the contribution of each ionotropic glutamate receptor, including the AMPA, kainate, and NMDA receptors, to the evoked EPSCs of the STN. I evoked EPSCs by injecting 50-500 μA of current into the slice rostral to the internal capsule using a bipolar tungsten stimulating electrode (Baufreton et al., 2005). EPSCs were evoked at 32°C at a holding potential of +40 mV unless otherwise noted to eliminate any magnesium inhibition of NMDA receptors. First, I

determined the contribution of all NMDA receptors to the synaptic current by evaluating the degree of inhibition of the peak current of the evoked EPSC by bath application of 20 μM DNQX, a competitive antagonist of AMPA and kainate receptors. That is, DNQX should inhibit current from AMPA and kainate receptors, leaving only current from NMDA receptors. DNQX reduced the peak of the EPSC to 45 $\pm$ 5.4% compared to the aCSF control and slowed the fast and slow components of the deactivation time course, consistent with what would be expected when NMDA receptors are mediating the time course of the current (n=14; Fig. 6.7). The relatively large NMDA receptor component of the synaptic current is not without precedent in the basal ganglia, as similar AMPA to NMDA receptor ratios have been observed in the substantia nigra pars compacta, which also exhibits a similar, slow NMDAR-EPSC deactivation time course (Brothwell et al., 2008).

I evaluated the temperature sensitivity of recombinant NMDA receptors expressed in HEK 293 cells in order to compare the NMDAR-EPSC deactivation time course to the deactivation time course of recombinant NMDA receptors. GluN1-1a/GluN2D, GluN1-1b/GluN2D, GluN1-1a/GluN2B, and GluN1-1b/GluN2B NMDA receptors were activated by 2-4 s application of 1 mM L-glutamate (0.05 mM glycine was present in all solutions) at either 23°C or 32°C. The deactivation time course of the NMDA receptor component of the EPSC is intermediate between the deactivation time components of recombinant GluN1-1b/GluN2B and GluN1-1b/GluN2D at 32°C when expressed in HEK 293 cells, a result that is compatible with the idea that these subunits might mediate the time course of synaptic currents in the STN (Fig. 6.8; Table 6.7).

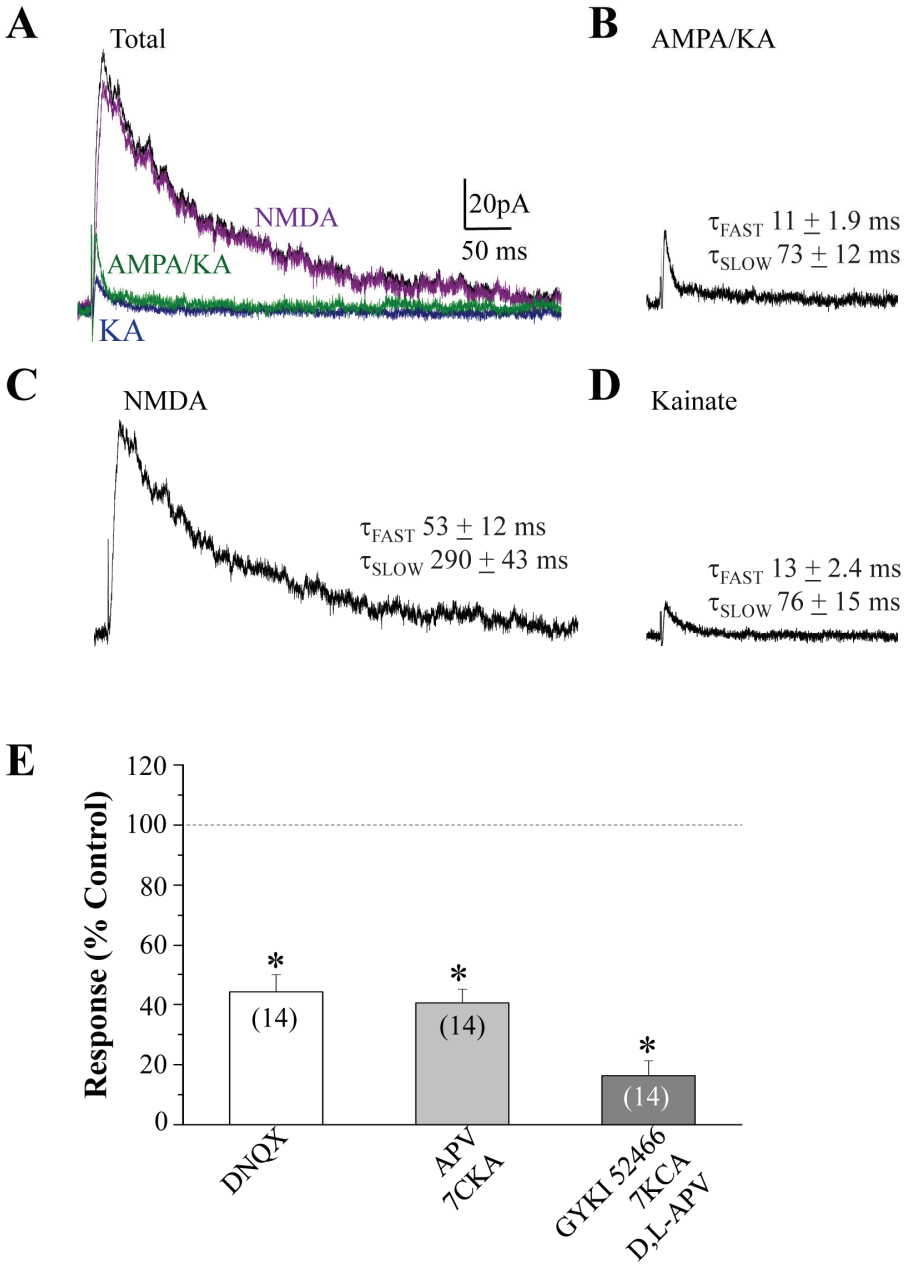


**Figure 6.7.** NMDA, AMPA, and kainate receptors contribute to EPSCs in the STN. EPSCs were evoked by injecting 50-500 μA of current for 0.1 ms into the slice rostral to the internal capsule using a bipolar tungsten stimulating electrode. STN neurons were held at +40 mV. ***A-D***, AMPA and kainate receptors were isolated by bath application of 400 μM D,L-APV and 50 μM 7-CKA (*green*), which reduced the peak current to 41 ± 4.6% compared to the aCSF control (n=14). Kainate receptors (*blue*) were isolated by bath application of 100 μM GYKI-52466, 400 μM D,L-APV, and 50 μM 7-CKA, which reduced the peak

amplitude of the EPSC current to 16 $\pm$ 4.9% (n=14). The NMDA receptor component (*purple*) could be isolated by subtracting the AMPA and kainate receptor EPSC current response recorded in the presence of 400 μM D,L-APV and 50 μM 7-CKA from the evoked EPSC recorded in aCSF alone (*black*). The residual P2X-mediated suramin-sensitive synaptic current recorded in D,L-APV, 7-CKA, and DNQX was subtracted from the aCSF control, AMPA/KA, and kainate traces. The traces presented are an average of 3-5 sweeps. ***E***, A histogram comparing the peak current of the evoked EPSCs in the presence of DNQX, D,L-APV and 7-CKA, or GYKI-52466, D,L-APV, and 7-CKA. *$p < 0.05$ when compared to the aCSF only control; one-way ANOVA with Tukey's *post-hoc* test. The number of cells is given in parenthesis.

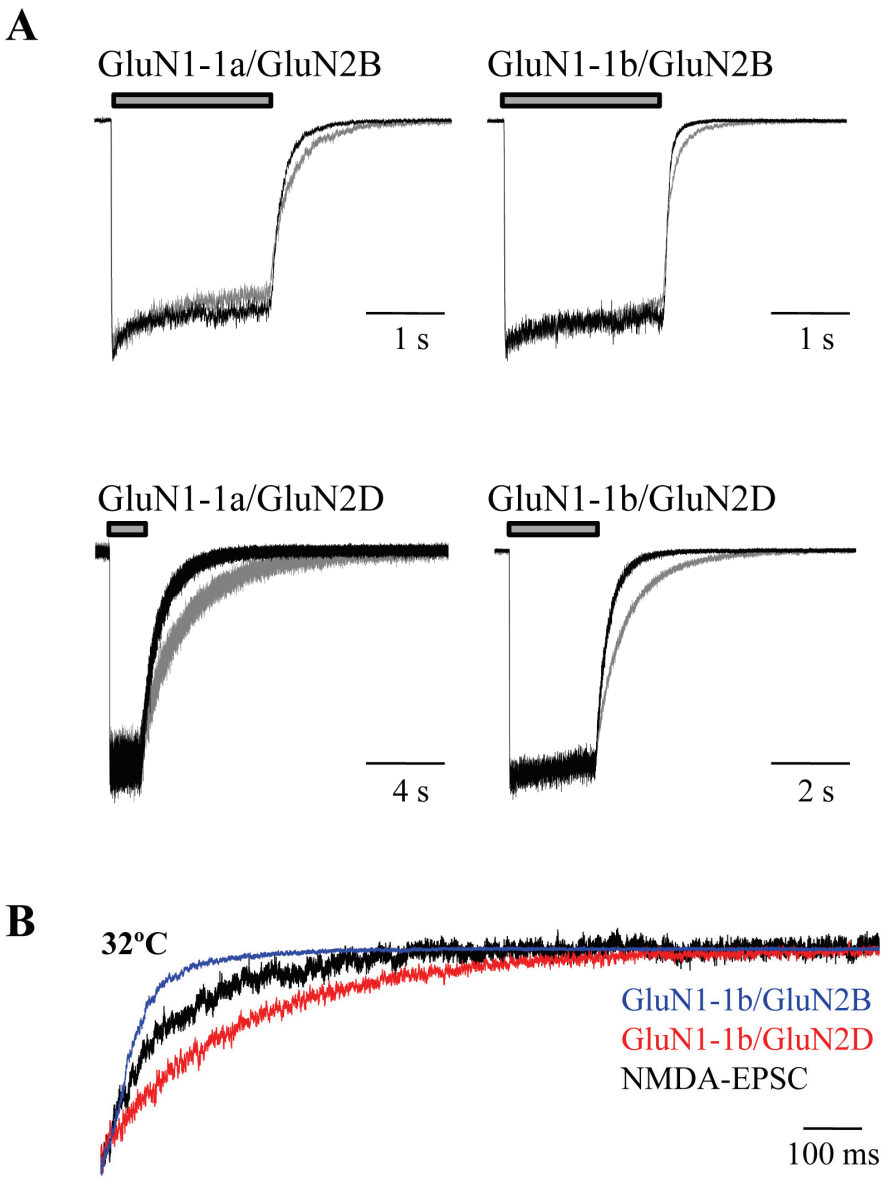


**Figure 6.8.** The deactivation time course of NMDA receptors is temperature sensitive. ***A***, Recombinant GluN1-1a/GluN2D, GluN1-1b/GluN2D, GluN1-1a/GluN2B, and GluN1-1b/GluN2B receptors were expressed in HEK 293 cells and were activated by 2-4 s application of 1 mM L-glutamate and 0.05 mM glycine at pH 8.0 at either 23°C (gray) or 32°C (black) (0.05 mM glycine was present in all solutions). ***B***, The normalized deactivation time courses of GluN1-1b/GluN2B and GluN1-1b/GluN2D are superimposed on the deactivation time course of the NMDA receptor component of an evoked EPSC from an STN neuron (all recordings were performed at 32°C). The deactivation time course of the EPSC lies between the time courses of recombinant GluN1-1b/GluN2B and GluN1-1b/GluN2D.

**Table 6.6.** Deactivation time course is temperature sensitive

| | 23°C | | | | 32°C | | | |
|---|---|---|---|---|---|---|---|---|
| | $\tau_{FAST}$ (ms) | $\tau_{SLOW}$ (ms) | $\tau_W$ (ms) | n | $\tau_{FAST}$ (ms) | $\tau_{SLOW}$ (ms) | $\tau_W$ (ms) | n |
| **1a/2B** | 180 ± 18 | 1100 ± 370 | 360 ± 53 | 5 | 100 ± 6.5* | 380 ± 39 | 150 ± 7.0* | 4 |
| **1b/2B** | 180 ± 74 | 630 ± 120 | 210 ± 68 | 6 | 49 ± 4.4 | 290 ± 97 | 75 ± 4.0 | 5 |
| **1a/2D** | 1500 ± 110 | 4000 ± 590 | 3100 ± 150 | 3 | 450 ± 98* | 1400 ± 94* | 1200 ± 7.8* | 5 |
| **1b/2D** | 270 ± 52 | 860 ± 47 | 650 ± 22 | 5 | 210 ± 23 | 630 ± 110 | 340 ± 25* | 5 |

HEK 293 cells expressing recombinant rat GluN1-1a/GluN2B, GluN1-1b/GluN2D, GluN1-1a/GluN2D, or GluN1-1b/GluN2D were activated at pH 8.0 by 1 mM L-glutamate and 0.05 mM glycine at 23°C or 32°C. $\tau_{FAST}$, $\tau_{SLOW}$, and $\tau_W$ are shown as mean ± s.e.m., and n is the number of cells. *$p < 0.05$ when compared to the corresponding value in at 23°C when analyzed by the Student's t-test. All data are given to two significant figures.

I also evaluated the AMPA and kainate receptor components of the EPSC. Isolation of AMPA and kainate receptors with bath application of 400 μM D,L-APV and 50 μM 7-CKA reduced the peak current to 41 ± 4.6% compared to the aCSF control (n=14). To study the contribution of kainate receptors to the EPSCs of the STN, I pharmacologically isolated kainate receptors by bath application of 400 μM D,L-APV and 50 μM 7-CKA, which inhibit NMDA receptors, plus 100 μM GYKI-52466, an antagonist selective for AMPA receptors (Mott et al., 2008). Inhibiting NMDA and AMPA receptors reduced the peak current to 16 ± 4.9% compared to the peak current of the EPSCs in the presence of aCSF only (n=14; Fig. 6.7), suggesting that kainate receptors comprise approximately half of the AMPA/kainate receptor peak current. However, a residual current remained, as applying 20 μM DNQX, 400 μM D,L-APV, and 50 μM 7-CKA to the same cells could not fully inhibit the EPSC peak amplitude (12 ± 4.8% of the aCSF control). Because expression of purinergic receptors in the STN has been described before (Kanjhan et al., 1999), I evaluated whether these receptors mediate the remaining component of the EPSC, as has been observed in EPSCs of the somatosensory cortex (Pankratov et al., 2003). Bath applying 20 μM DNQX, 400 μM D,L-APV, 50 μM 7-CKA, and the purinergic receptor antagonist suramin (100 μM) nearly fully eliminated the residual current (n=5; 6.0 ± 2.0% of aCSF peak current response). Because the residual does not appear to originate from glutamate receptors, I subtracted the residual current from each EPSC. I repeated the GYKI-52466 experiment in the presence of 100 μM suramin and obtained similar results as before, with peak amplitude reduced to 13 ± 3.9% in the presence of GYKI-52466 compared to the peak current of the EPSCs in the presence of aCSF only (n=3).

I next evaluated how the GluN2D subunit contributes to the synaptic activity of the STN by evoking EPSCs both with and without GluN2D-specific NMDA receptor modulators in the aCSF and 20 μM DNQX to inhibit AMPA and kainate receptors. Evoked EPSCs could be modulated by both the GluN2D allosteric potentiator CIQ and the inhibitor 997-33. The inhibitor 997-33 decreased the peak amplitude of the current to 59 $\pm$ 4.9% compared to the aCSF control peak currents (n=13; Fig. 6.9). The decrease in peak current was accompanied by an apparent acceleration of the slow deactivation component and the weighted deactivation time constant when compared to the aCSF control, although this change was not significant (Table 6.6; $p > 0.05$; one-way ANOVA). This acceleration of the deactivation time course of the synaptic response is consistent with the idea that I am inhibiting the slowly deactivating GluN2D subunit.

Bath application of CIQ (20 μM), the GluN2C/D selective potentiator, increased peak amplitude of the evoked current to 210 $\pm$ 20% (n=10; Fig. 6.10). GluN2D potentiation was accompanied by a slowing of the deactivation time course of the EPSC (Table 6.6; Fig. 6.10), consistent with the increased activity of the slowly deactivating GluN2D subunit. The CIQ experiments were conducted in low (0.2 mM) $Mg^{2+}$ and at $V_{HOLD}$ = -60 mV because EPSCs evoked while holding at +40 mV were inhibited by bath application of CIQ in 8 out of the 9 cells evaluated (peak current 81 $\pm$ 31% compared to aCSF control; n=9). While we currently are not aware of the mechanisms controlling this discrepancy in CIQ activity on STN neurons, EPSCs obtained while holding at -30 mV, a voltage at which magnesium block of GluN2D-containing receptors has been relieved,

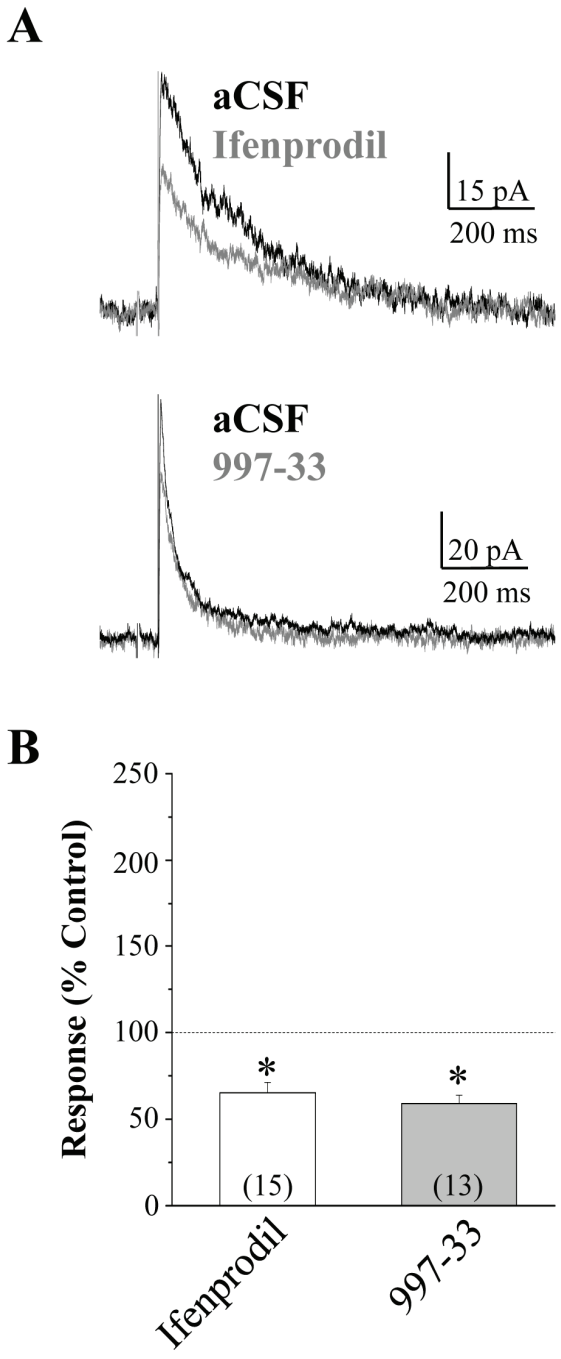


**Figure 6.9.** Subunit-specific inhibitors of GluN2B and GluN2D-containing NMDA receptors decrease the peak amplitudes of evoked EPSCs in the STN. EPSCs were evoked by injecting 50-500 μA of current into the slice rostral to the internal capsule using a bipolar tungsten stimulating electrode. STN neurons were held at +40 mV unless otherwise noted. ***A***, (*top*) Bath application of ifenprodil (3 μM) reduced the peak

current of the evoked EPSC to 41 $\pm$ 4.6% compared to the DNQX control (n=14). (*bottom*) 997-33 (5 μM) decreased the peak amplitude of the current to 59 $\pm$ 4.9% compared to the peak amplitude of the DNQX control EPSCs (n=13). A summary of the effects of ifenprodil and 997-33 on the peak amplitude of the evoked EPSCs is given in ***B***. **p* < 0.05; one-way ANOVA with Tukey's *post-hoc* test when compared to the aCSF control.

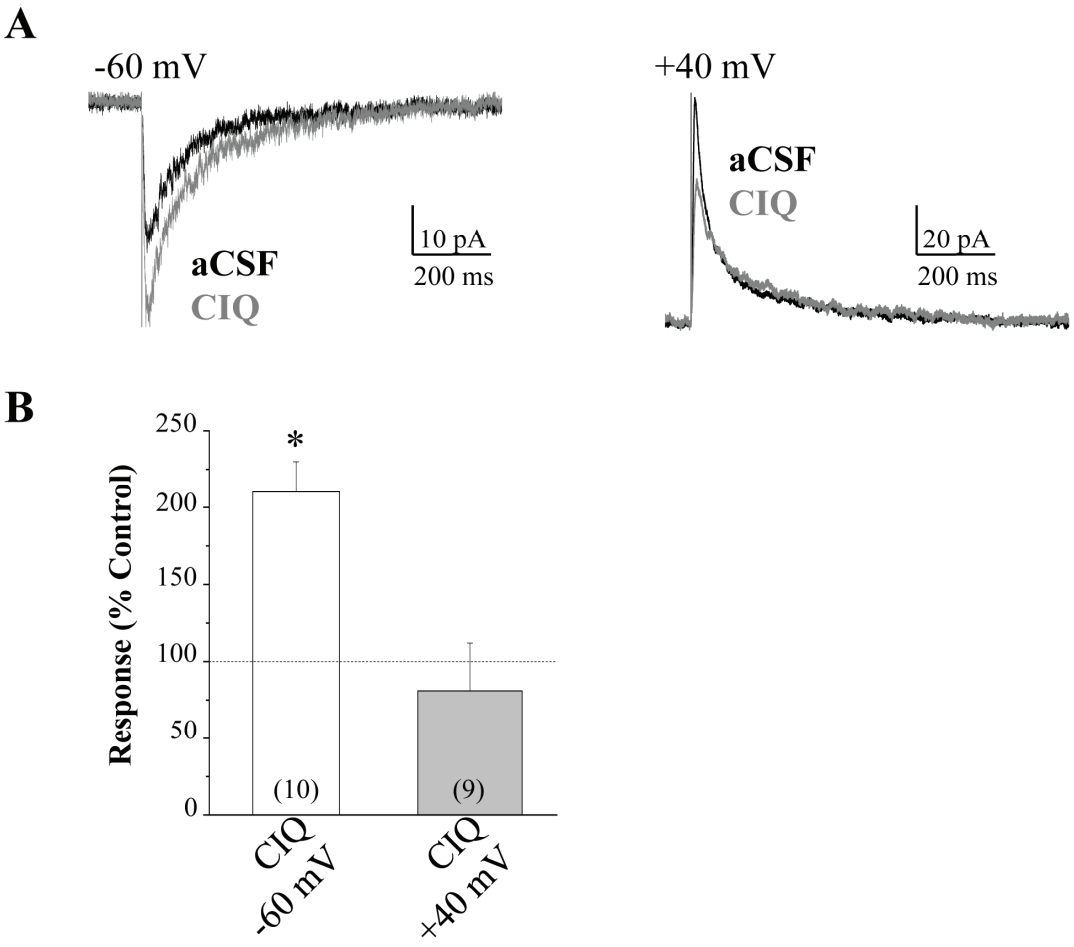


**Figure 6.10.** CIQ potentiates the peak amplitudes of evoked EPSCs in the STN at negative membrane potentials. EPSCs were evoked by injecting 50-500 μA of current into the slice rostral to the internal capsule using a bipolar tungsten stimulating electrode. STN neurons were held at +40 mV or -60 mV. ***A***, CIQ (20 μM) increased the peak amplitude of the evoked EPSCs to 210 $\pm$ 20% (n=10) compared to the DNQX aCSF control. These CIQ experiments were conducted in low (0.2 mM) $Mg^{2+}$ and at $V_{HOLD}$ = -60 mV. ***B***, CIQ (20 μM) decreased the peak amplitude of the evoked EPSCs to 81 $\pm$ 31% (n=9) compared to the DNQX aCSF control. These CIQ experiments were conducted in 1.5 mM $Mg^{2+}$ and at $V_{HOLD}$ = +40 mV. A summary of the effects CIQ on the peak amplitude of the evoked EPSCs at +40 mV or -60 mV is given in ***C***. *$p < 0.05$; one-way ANOVA with Tukey's *post-hoc* test when compared to the aCSF control.

**Table 6.7.** GluN2D and GluN2B modulators influence evoked EPSCs of the STN

| | aCSF bath | | | Modulator in aCSF bath | | | |
|---|---|---|---|---|---|---|---|
| **Modulator** | **$\tau_{FAST}$ (ms)** | **$\tau_{SLOW}$ (ms)** | **$\tau_W$ (ms)** | **$\tau_{FAST}$ (ms)** | **$\tau_{SLOW}$ (ms)** | **$\tau_W$ (ms)** | **n** |
| **Ifenprodil** | 24 ± 8.3 | 220 ± 97 | 100 ± 28 | 26 ± 7.5 | 240 ± 54 | 120 ± 24 | 15 |
| **CIQ** | 25 ± 5.1 | 120 ± 20 | 65 ± 13 | 29 ± 6.3 | 190 ± 33 | 81 ± 14 | 11 |
| **997-33** | 33 ± 6.8 | 340 ± 130 | 120 ± 27 | 30 ± 7.8 | 180 ± 43 | 91 ± 17 | 13 |

EPSCs were evoked at $V_{HOLD}$ = +40 mV for ifenprodil and 997-33 and at $V_{HOLD}$ = -60 mV for CIQ by injecting 50-500 μA of current into the slice rostral to the internal capsule using a tungsten bipolar stimulating electrode. Baseline EPSCs were evoked while in aCSF supplemented with 10 μM glycine, 10 μM bicuculline, and 20 μM DNQX. The deactivation time courses were then compared to evoked EPSCs in the presence of the same aCSF containing 3 μM Ifenprodil, 5 μM 997-33, or 20 μM CIQ. The deactivation time constants were not significantly different when baseline EPSCs were compared to EPSCs in the presence of drug (one-way ANOVA).

also were potentiated by 20 μM CIQ (peak current 190 ± 17% compared to aCSF control; n=3), indicating that CIQ potentiation was not caused by relief of magnesium inhibition. Nevertheless, these data suggest that the GluN2D subunit participates in the excitatory synaptic currents of the subthalamic nucleus. This is only the third time that the GluN2D subunit has been pharmacologically identified as contributing to the current of an EPSC, as previous studies have identified the GluN2D subunit in the EPSCs of the substantia nigra and hippocampal dentate gyrus (Brothwell et al., 2008; Harney et al., 2008).

Finally, I evaluated whether the evoked EPSCs from the STN were modulated by the GluN2B antagonist ifenprodil. Bath application of ifenprodil (3 μM) reduced the peak amplitude of the EPSCs to 65 ± 6.1% of control (n=15; Fig. 6.9). This decrease in peak current was accompanied by a slowing of the deactivation time course of the synaptic current (Table 6.6), which would be expected as the more rapidly deactivating GluN2B subunit was being inhibited over the slowly deactivating GluN2D subunit. These data suggest that the GluN2D and GluN2B subunits mediate the excitatory synaptic current of the rat subthalamic nucleus.

### 6.4. Discussion

There are four main findings in my study of the pharmacology of GluN2D-containing NMDA receptors and their role in the rat subthalamic nucleus. First, CIQ selectively potentiates GluN2D and GluN2C-containing NMDA receptors over GluN2A/B-containing receptors expressed in HEK 293 cells. Second, the DQP class modulators DQP-1105 and 997-33 selectively inhibit GluN2D-containing NMDA receptors in HEK 293 cells. The inhibitor 997-33 has the most selectivity for GluN2D over GluN2B in the

DQP class, so this modulator represents a useful tool for evaluating the role of GluN2D in neurons. Third, the GluN2D and GluN2B subunits are the predominant subunits expressed in rat subthalamic nucleus, as picospritzer-evoked currents could be potentiated or inhibited by GluN2C/D- and GluN2B-selective modulators. Subunit-selective modulators for GluN2A and GluN2C had no effect on agonist-evoked currents in the STN. Finally, the GluN2D and GluN2B subunits control the NMDA receptor component of excitatory postsynaptic currents in the subthalamic nucleus.

Little is known about the role of the GluN2D subunit in the synaptic activity of neurons due to its limited expression and the lack of subunit-selective modulators. My studies of the GluN2D subunit are among the first that have identified the GluN2D subunit as participating in the synaptic current of a neuron. Previous studies have suggested that the GluN2D and GluN2B subunits may be expressed as triheteromeric receptors in the substantia nigra pars compacta (SNc), and it is possible that a similar subunit arrangement is present in the STN (Brothwell et al., 2008). Substantia nigra EPSCs are partially inhibited by ifenprodil and the moderately selective GluN2D antagonist UBP141 (Brothwell et al., 2008). The decrease I observed in the amplitude of the evoked EPSCs by the GluN2D selective antagonist 997-33 and ifenprodil are similar to the decreases in peak amplitudes of SNc NMDAR-EPSCs following application of ifenprodil and UBP141 (Brothwell et al., 2008). Likewise, the deactivation time course of NMDA receptor EPSCs in the STN are similar to the deactivation time course of SNc EPSCs, although STN EPSCs deactivate somewhat slower (Brothwell et al., 2008). The time course of the NMDA receptor component of the STN EPSCs also is intermediate between the time course of recombinant GluN1-1b/GluN2B and GluN1-1b/GluN2D at

32°C (Fig. 6.7B), suggesting again that the NMDA receptors expressed at the STN synapse may be triheteromeric GluN1-1b/GluN2B/GluN2D NMDA receptors.

I observed some variability in the deactivation time courses of the evoked EPSCs I recorded in the STN. The variability was not related to the age of the rats used in my experiments, which could have been explained by a change in NMDA receptor subunit expression (Monyer et al., 1994; Standaert et al., 1994; Brothwell et al., 2008). I hypothesize that the variability in synaptic time course may be due to the different pathways of excitatory input onto the STN. The STN receives excitatory projections largely from the cortex and thalamus (Bevan et al., 2002; Wilson and Bevan, 2011); however, the cortical projections primarily are on smaller, more distal dendrites (Bevan et al., 1995). Postsynaptic NMDA receptor subunit expression might differ according to synaptic input, with one synapse expressing more of the slowly deactivating GluN2D or GluN1-a splice variant subunits, which could cause differences in the deactivation time course of an EPSC. Optogenetics utilizes light-activated channelrhodopsin cation channels to selectively stimulate specific projection pathways in the brain (Ernst et al., 2008; Gradinaru et al., 2009; Zhang et al., 2010). It is possible that using optogenetics to selectively activate the thalamic or cortical pathways projecting into the STN would allow us to evaluate if the characteristics of the excitatory postsynaptic currents evoked by these two pathways differ.

While inhibition by 997-33 was not as pronounced as potentiation by CIQ, it is possible that 997-33 does not inhibit triheteromeric GluN1/GluN2D/GluN2B NMDA receptors as potently or effectively as the antagonist inhibits GluN1/GluN2D receptors. This decrease in effectiveness and potency in 997-33 would be similar to ifenprodil,

which does not act as potently or effectively on triheteromeric GluN1/GluN2A/GluN2B NMDA receptors (Hatton et al., 2005). The use-dependent mechanism of 997-33 requires that the receptors must bind the GluN2 subunit agonist before the receptor can be inhibited by the antagonist, so the relatively rapid time course of the EPSCs may prevent 997-33 from fully binding before the current response has abated. CIQ previously has been shown to potently potentiate triheteromeric NMDA receptors (Mullaseril et al., 2010) and is not use-dependent, suggesting that this drug may be a more effective tool for identifying synapses expressing GluN2D.

Kainate receptors also contribute to the peak current of the EPSCs of the STN. Similar kainate responses have been observed in the pallidum, entorhinal cortex, hippocampal interneurons, and the mossy fiber - CA3 synapse (Castillo et al., 1997; Porter et al., 1998; Frerking and Ohliger-Frerking, 2002; Huettner, 2003; Lerma, 2003; Jin et al., 2006; West et al., 2007; Mott et al., 2008). Interestingly, several of these regions, including the pallidum, CA3 neurons, and hippocampal interneurons, also have been shown to express the GluN2D subunit (Monyer et al., 1994; Standaert et al., 1994; Wenzel et al., 1996). This suggests that neurons that favor the expression of the slowly deactivating GluN2D subunit also may favor the expression of synaptic kainate receptors, which deactivate slower than AMPA receptors (Mott et al., 2003; reviewed in Traynelis et al., 2010). Purinergic receptors also mediate a component of the EPSC, as the residual current not inhibited by a cocktail of D,L-APV, 7-CKA, and DNQZ was inhibited by the purinergic receptor antagonist suramin. While unusual, purinergic EPSC signaling has been observed in EPSCs of the somatosensory cortex (Pankratov et al., 2003), CA1 (Pankratov et al., 1998), and CA3 hippocampal neurons (Kondratskaya et al., 2008).

Previous studies have suggested that P2X(2) purinergic receptors are expressed in the STN (Kanjhan et al., 1999), so it is possible this or other purinergic receptors contribute to the excitatory postsynaptic currents of the STN.

In conclusion, the synaptic activity of the subthalamic nucleus is controlled by a number of different receptors, including NMDA, AMPA, kainate, and purinergic receptors. Synaptic transmission appears to favor slowly deactivating glutamatergic receptors, as both GluN2D- and GluN2B-containing NMDA receptors as well as kainate receptors contribute to the evoked EPSCs in the STN. Because overactivation of the STN contributes to the symptoms of Parkinson's disease (Bergman et al., 1990; DeLong, 1990; Rodriguez et al., 1998; Levy et al., 2000; Obeso et al., 2000), these receptors may be novel therapeutic targets for the treatment of the disease.

# Chapter 7: Discussion and Conclusion

## 7.1. Summary

GluN1/GluN2D receptors are unique from other NMDA receptors in their unusual and, in some cases, conflicting characteristics, including low open probability, rapid rise time of the current response, and slow deactivation time course upon the removal of agonist. I report that these properties are controlled by multiple domains across both the GluN1 and GluN2D subunits (Fig. 7.1). I show that the ligand-binding domain of the GluN2D subunit controls the deactivation time course of a range of NMDA receptor agonists. I also report that the GluN1 amino-terminal domain represents an additional level of control over the behavior of GluN1/GluN2D NMDA receptors, as the GluN1 ATD controls deactivation time course, glutamate $EC_{50}$, and channel open probability (Fig. 7.1). The ability of the GluN1/GluN2D receptor to alter its key characteristics, either through ligand-specific differences in deactivation time course or through the incorporation of specific GluN1 splice variants, may allow neurons expressing the subunit to have more control over the manner by which the GluN2D subunit influences synaptic signaling. I also describe a model of GluN1/GluN2D receptor gating that can predict many of the key characteristics of the receptor as well as identify specific rate constants within the gating scheme that are altered by the GluN1 exon 5 insert.

Finally, I report that the GluN2D subunit contributes to the activity of the subthalamic nucleus. I show that the GluN2D subunit participates in excitatory synaptic transmission and contributes to the slow deactivation time course of evoked EPSCs. I demonstrate that I can either potentiate or inhibit the peak currents of evoked EPSCs

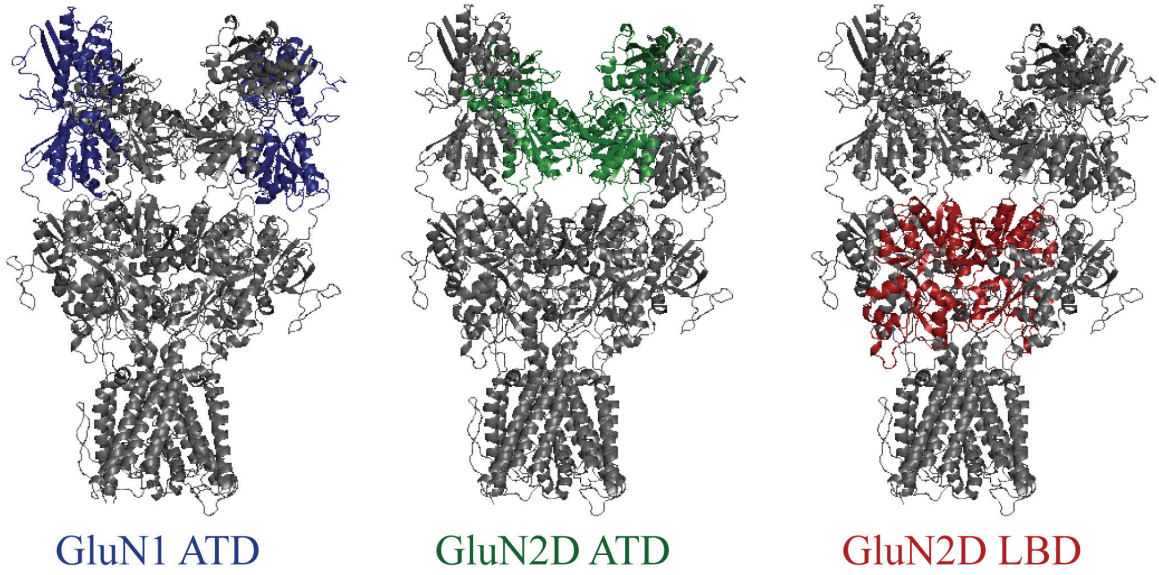


**Figure 7.1.** Multiple domains control the characteristics of GluN1/GluN2D NMDA receptors. (*left*) In Chapter 4, I show that the GluN1 amino-terminal domain (blue) controls the deactivation time course, agonist $EC_{50}$, and channel open probability of GluN2D-containing NMDA receptors. (*middle*) The amino-terminal domain of the GluN2 subunit (green) also controls the deactivation time course, agonist $EC_{50}$, and channel open probability of GluN1/GluN2D receptors. Future studies remain to determine how the amino-terminal domains control these features of the receptor or if they share mechanisms. (*right*) The ligand-binding domain of the GluN1/GluN2D NMDA receptor controls both agonist $EC_{50}$ as well as deactivation time course.

from the STN with our subunit-selective GluN2D modulators. Because STN firing is altered in Parkinson's disease, further studies should evaluate if inhibiting the GluN2D subunit could alter firing patterns and potentially relieve some motor symptoms of the disease.

### 7.2. GluN1/GluN2D deactivation time course is ligand-dependent

The slow deactivation time course of GluN1-1a/GluN2D receptors activated by L-glutamate is considered to be a hallmark of the receptor. I show in Chapter 3 that the deactivation time course of GluN1/GluN2D receptors is highly dependent upon the activating ligand. L-glutamate causes GluN1/GluN2D receptors to deactivate slowly over a period of seconds, while the enantiomer D-glutamate results in deactivation so rapid the receptor is indistinguishable from GluN1/GluN2A receptors. While the deactivation time course of GluN1/GluN2D receptors is influenced by agonist $EC_{50}$ and the dissociation rate, I report here that aspartate analogues with shorter side chains have relaxations that cannot be predicted by agonist potency.

Ligand-specific deactivation time course might have a structural basis and could be due in part to the manner by which the ligand influences the conformation of the GluN2D ligand-binding domain. Our collaborative high resolution structural data with Dr. Hiro Furukawa show that the structure of the NMDA receptor ligand-binding domain is sensitive to activating ligand (Vance et al., 2011). The hinge loop of the GluN2D D2 domain shifts when the slowly deactivating L-glutamate is bound compared to when the rapidly deactivating NMDA, L-aspartate, or D-glutamate are bound. This change in the conformation of the hinge loop alters the intra-protein interactions it can make when the

LBD is bound to L-glutamate, compared when GluN2D is bound to the other agonists (Fig. 1.3; Vance et al., 2011). This difference in hinge loop conformation may alter the gating properties of GluN2D-containing NMDA receptors and thus influence deactivation time course. Indeed, the conformation of the GluN2A hinge region when bound to L-glutamate is similar to the hinge region of GluN2D bound to the rapidly deactivating ligands (Fig. 1.3; Vance et al., 2011). My chimeric receptor data show that inserting the GluN2D LBD into the GluN2A subunit slows the deactivation time course for L-glutamate, while the deactivation time course of D-glutamate is unchanged. These data suggest that the GluN2D LBD uniquely responds to L-glutamate compared to the other ligands I evaluated.

Ligand-specific changes in the structures of AMPA and kainate receptors previously have been related to channel function, as these receptors show significant differences in the degree of ligand-binding domain closure when the receptor is in complex with fully activating agonists compared to partial agonists or inhibitors (Armstrong and Gouaux, 2000; Jin et al., 2003; Mayer, 2005; Kistler and Fleck, 2007; Frydenvang et al., 2009). In previous studies of NMDA receptor ligand-binding domains, partial agonists of the GluN1 subunit did not differ from the structure of glycine-bound GluN1 (Furukawa and Gouaux, 2003; Inanobe et al., 2005). Therefore, our work is novel for the NMDA receptor field as no previously published work has shown agonist-specific conformational changes in the LBDs of NMDA receptors that can be related to receptor gating (Vance et al., 2011).

The properties of a ligand, including structure and agonist $EC_{50}$, have long been known to alter the characteristics of ligand-gated ion channels. For example, the

deactivation time course of nicotinic acetylcholine receptors is accelerated by acetylmonoethylcholine and other less potent acetylcholine analogues, which also have brief channel open times compared to acetylcholine (Colquhoun et al., 1977; Colquhoun and Sakmann; 1985; Papke et al., 1988; Lape et al., 2008). $GABA_A$ receptor deactivation time course is slower for more potent ligands in cultured rat hippocampal neurons (Jones et al., 1998; Bianchi et al., 2007). Similar experiments with cultured hippocampal neurons loaded with D-glutamate illustrate that the deactivation rate of a synapse with NMDA receptors is dependent on the activating ligand (Pan et al, 1993). Furthermore, multiple studies on native and recombinant NMDA receptors have described an agonist-dependence of deactivation rate and single channel properties, including mean open time and shut time durations (Shinozaki et al., 1989; Lester et al., 1990; Lester and Jahr, 1992; Banke and Traynelis, 2003; Erreger et al., 2005b; Kussius and Popescu, 2009).

L-aspartate, an agonist that evokes a more rapid deactivation time course in GluN1/GluN2D NMDA receptors than L-glutamate, may act as an endogenous neurotransmitter for native NMDA receptors. The ligand has been shown to be stored in synaptic vesicles in the Schaffer collateral-commissural pathways of the hippocampal CA1 and CA3 and the associational-commissural pathway of the dentate gyrus (Gundersen et al., 1991; Gundersen et al., 1998; Gundersen et al., 2001; Gundersen et al., 2004) and is released from neurons in a calcium-dependent manner (Wang and Nadler, 2007; Cavallero et al., 2009). L-aspartate is cleared from synapses by the excitatory amino acid transporter (EAAT; Kanai and Hediger, 1992; Storck et al., 1992). While L-aspartate has not been identified as the primary neurotransmitter in a synapse, it has been observed to be a co-transmitter with L-glutamate (Nadler et al., 1976; Gundersen et al.,

1998) or GABA (Gundersen et al., 2004), although L-aspartate and L-glutamate may not be released using the same mechanisms (Peterson et al., 1995; Zhou et al., 1995; Fleck et al., 2001; Cavallero et al., 2009). Recently, synaptically released endogenous L-aspartate has been shown to alter the time course of excitatory postsynaptic currents. Zhang and Nadler observed a more rapid NMDAR-EPSC deactivation time course in whole cell voltage-clamp recordings of hippocampal CA1 neurons after glutamate release was prevented by botulinum neurotoxin C (Zhang and Nadler, 2009). These data suggest that the time course of postsynaptic excitatory currents is dependent upon the neurotransmitter released at the synapse.

Agonist-specific differences in deactivation time course could have profound effects on neuronal signaling. The firing of cat spinal cord neurons is ligand-dependent when excitatory amino acids are ionophoretically applied to the neurons (Curtis et al., 1960; Stone and Burton, 1988). Interestingly, the duration of increased rate of firing when the ligands were applied was longer for L-glutamate and L-aspartate than N-methyl-D,L-aspartate (Curtis and Watkins, 1960). Ionophoretically applying NMDA to the rat hippocampus induces depolarization in CA1 neurons; however, depolarization becomes more prolonged when the more potent L-aspartate or L-glutamate are applied (Collingridge et al., 1983). In lamprey spinal cord, firing rate is higher when NMDA is applied when compared to when the less potent D-glutamate is applied (Grillner et al., 1981). In all of the above examples, firing or the duration of depolarization is higher when a ligand that evokes a slower NMDA receptor deactivation time course is applied.

More work remains to be conducted on the identification of synapses at which glutamate is not the sole or primary neurotransmitter. In addition to L-aspartate, putative

endogenous agonists include D-aspartate (Benveniste, 1989; Nicholls, 1989; Fleck et al., 1993; Schell et al., 1997; Errico et al., 2008), homocysteate, and cysteinesulfinate (Do et al., 1986; Olney et al., 1987; Do et al., 1988; Provini et al., 1991; Yuzaki and Connor, 1999). Inhibiting L-homocysteate reuptake at the Schaffer collateral-CA1 synapse increases the amplitude of excitatory postsynaptic potentials, although the contribution of L-homocysteate to the deactivation time course of EPSCs or EPSPs in this synapse has not been evaluated (Ito et al., 1991). However, my data suggest that synapses that release other neurotransmitters in addition to or in the place of L-glutamate would have profoundly different time courses of synaptic activity, particularly in GluN2D-containing synapses.

While my work has demonstrated a clear dependence upon the ligand for GluN1/GluN2D deactivation time course, the data was obtained from recombinant receptors expressed transiently in non-neuronal HEK 293 cells. It is possible that potential NMDA receptor auxiliary subunits that have yet to be identified and could be expressed in the brain might alter the deactivation kinetics of GluN1/GluN2D NMDA receptors, as has been observed in AMPA and kainate receptors (Tomita et al., 2003; Priel et al., 2005; Turetsky et al., 2005; Nicoll et al., 2006; Cho et al., 2007; Kato et al., 2007; Menuz et al., 2007; Milstein and Nicoll, 2008; Zhang et al., 2009; Gill et al., 2012). Furthermore, future studies also need to be conducted to evaluate how ligands other than L-glutamate alter the single channel kinetics of GluN1/GluN2D receptors, as GluN1 and GluN2 site partial agonists have previously been found to influence gating rates of GluN1/GluN2A and GluN1/GluN2B single channel recordings (Banke and Traynelis, 2003; Erreger et al., 2005b; Kussius and Popescu, 2009).

### 7.3. Splice variant control over GluN1/GluN2D NMDA receptor function

Eight GluN1 splice variants and four GluN2 subunits have been identified and combine to form functional NMDA receptors. In Chapter 4, I show that the GluN1 splice variant controls agonist $EC_{50}$, deactivation time course, and open probability of GluN2D-containing NMDA receptors. GluN2D-containing NMDA receptors that contain GluN1 splice variants that include exon 5 in the amino-terminal domain have less potent L-glutamate $EC_{50}$ values and deactivate more rapidly than GluN2D receptors containing GluN1 splice variants that lack exon 5. A single residue within exon 5, Lys211, mediates GluN1 control over deactivation time course and L-glutamate $EC_{50}$. GluN1 exon 5 also increases the open probability of GluN1/GluN2D NMDA receptors in single channel recordings in excised outside-out patch and cell-attached recordings. These data, along with a number of previously published papers (Durand et al., 1993; Hollmann et al., 1993; Williams, 1994; Zhang et al., 1994; Traynelis et al., 1998; Rumbaugh et al., 2000), suggest that the GluN1 amino-terminal domain is a key determinant of many of the properties of NMDA receptors.

Multiple domains across both the GluN1 and the GluN2 subunits appear to control the properties of the NMDA receptors (Fig. 7.1). While the GluN1 amino-terminal domain controls several of the characteristics of NMDA receptors, the amino-terminal domain of the GluN2 subunit also has been shown to control agonist $EC_{50}$, deactivation time course, and channel open probability (Gielen et al., 2009; Yuan et al., 2009). Removal or exchange of the GluN2 ATD can either increase or decrease deactivation time course depending on the identity of the GluN2 subunit (Yuan et al., 2009; Gielen et al., 2009). For example, the deactivation time course of the GluN1/GluN2A receptor,

which has the most rapid deactivation time course of all NMDA receptors (Monyer et al., 1994; Vicini et al., 1998; Wyllie et al., 1998; Zhang et al., 2008; Vance et al., 2011), can be slowed when the GluN2A ATD is removed or replaced with the GluN2D ATD, while the L-glutamate and glycine potencies increase (Yuan et al., 2009; Gielen et al., 2009). In turn, the deactivation time course of GluN1/GluN2D, which has the most prolonged deactivation time course of all NMDA receptors, becomes more rapid when the GluN2D ATD is removed or replaced with the GluN2A ATD, and the potencies of L-glutamate and glycine decrease (Yuan et al., 2009; Gielen et al., 2009). The slowing of the deactivation time course in GluN2A-containing receptors when the ATD is removed or replaced with the GluN2D ATD is paralleled by a decrease in channel open probability from 0.5 for wild type GluN2A to 0.006 for GluN2A-ΔATD and 0.035 for GluN2A-(GluN2D ATD) (Yuan et al., 2009). Conversely, while the deactivation time course of GluN2D becomes more rapid when the GluN2D ATD is removed or exchanged for the GluN2A ATD, the open probability increases (Gielen et al., 2009; Yuan et al., 2009).

While the structural determinants of the GluN2 amino-terminal domain's control over agonist potency, deactivation time course, and channel open probability remain unclear, the linker region connecting the GluN2 ATD to the ligand-binding domain appears to mediate about half of the effects of the GluN2 ATD on the properties of the receptor (Yuan et al., 2009). In addition, Geilen et al. (2009) suggested that the GluN2A ATD favors an open-cleft conformation that allows for higher open probability (Gielen et al., 2009), unlike the potential mechanism for the allosteric inhibitor zinc, which promotes closure of the ATD cleft (Paoletti et al., 2000; Rachline et al., 2005; Gielen et al., 2008). NMDA receptor ATD cleft closure leads to a rearrangement in the conformation of the

ligand-binding domain dimer interface, resulting in channel closure in a mechanism similar to what is observed in AMPA and kainate receptors (Sun et al., 2002; Mayer, 2006; Gielen et al., 2008; Chaudhry et al., 2009). It remains to be determined if the GluN2D ATD favors a closed conformation that leads to lower open probability or if this mechanism applies to the GluN1 subunit ATD. It is possible that exon 5 increases the time the GluN1 ATD spends in an open cleft conformation, leading to higher open probability.

Modal gating, in which a channel slowly shuttles between two modes, each of which has a distinct set of properties, has been observed in a number of ion channels and appears to be a common feature that regulates channel function. In L-type and P/Q-type calcium channels, modal gating has been attributed to both phosphorylation and voltage dependence (Hess and Tsien, 1984; Ochi and Kawashima, 1990; Yue et al., 1990; Dzhura et al., 2000; Alt et al., 2004; Fellin et al., 2004; Luvisetto et al., 2004; Hashambhoy et al., 2009). In addition, phosphorylation has been implicated in modal gating in $K^+$ channels (Marrion, 1996; Smith and Ashford, 1998; Singer-Lahat et al., 1999; Mullner et al., 2003). Auxiliary subunits, G-protein subunits, and other intracellular signaling molecules lead to models of modal gating in a number of other receptors, including $Na^+$, acetylcholine, and calcium channels (Delcour et al., 1993; Naranjo and Brehm, 1993; Imredy and Yue, 1994; Chang et al., 1996; Peterson et al., 1999; Singer-Lahat et al., 1999; Wakamori et al., 1999; Meir et al., 2000).

Glutamate receptors also undergo a form of modal gating, which has been identified in GluN1/GluN2A (Popescu and Auerbach, 2003; Zhang et al., 2008; Popescu, 2012) and GluN1/GluN2B (Amico-Ruvio and Popescu, 2010) NMDA receptors as well as AMPA

receptors (Poon et al., 2010; Prieto and Wollmuth, 2010; Poon et al., 2011). My data presented in Chapter 4 suggest that GluN1/GluN2D NMDA receptors may undergo a form of modal gating, as I observed brief periods of exceptionally high open probability, which I have called "superclusters." Although the mechanisms controlling modal gating of glutamate receptors are unknown, it is possible that modal gating of NMDA and AMPA receptors is controlled by similar mechanisms as other ion channels. My study and other studies evaluating glutamate receptor gating have been conducted in HEK 293 cells on recombinant receptors, so it is possible that modal gating of these receptors is more prevalent in native tissues due to the presence of potential auxiliary subunits, intracellular modulators, or phosphorylation. While the superclusters in GluN1/GluN2D receptors are brief and rare, my experiments were performed at room temperature, and it is possible that recording at 32$^{\circ}$C would increase the amount of time the GluN1/GluN2D receptor spends in the supercluster bursts.

While I have shown that GluN1 Lys211 controls agonist $EC_{50}$ and deactivation time course, it remains to be determined if the same residue mediates GluN1 splice variant control of channel open probability. In addition, I focused my study on the GluN1-1a and GluN1-1b splice variants to evaluate how the GluN1 amino-terminal domain regulates GluN2D receptor function, but it is unknown how the GluN1 carboxyl-terminal domain influences the single channel function of NMDA receptors. GluN1-3 and GluN1-4 splice variants contain an alternate C22' cassette, which enables interactions with a number of intracellular proteins, including PSD-95 (Kornau et al., 1995; Rutter et al., 2002; Lin et al., 2004) and calmodulin (Ehlers et al., 1996). Alpha-actinin and calmodulin have been shown to alter the gating properties of native hippocampal NMDA

receptors, so it is possible that the GluN1-3 or GluN1-4 CTDs or the intracellular proteins that associate with them also might influence the gating properties of GluN2D-containing channels (Rycroft and Gibb, 2004). Data presented here show that the GluN1 subunit has a role in agonist potency, deactivation time course, and channel open probability; however, future studies will need to be conducted to determine in greater detail the mechanism of splice variant control over NMDA receptor function.

### 7.4. A two-arm linear model best predicts GluN1/GluN2D activation

Although a number of models have been developed to describe NMDA receptor gating, none could predict the single channel and macroscopic properties of GluN1/GluN2D NMDA receptors. Therefore, in Chapter 5, I described *Scheme 5*, a two-arm linear model that can approximate many of the characteristics of GluN1/GluN2D NMDA receptors, including the low open probability, multiple shut components, rapid response rise time, slow deactivation time course, and little desensitization. The upper arm activates rapidly, which allows for rapid rise time of the macroscopic current response. Preferential occupancy of the lower arm that opens rarely allows the gating scheme to predict a low channel open probability. In addition to being able to describe the gating of GluN1-1a/GluN2D NMDA receptors, *Scheme 5* also is capable of identifying specific rate constants altered by exon 5 of the GluN1-1b subunit.

The state connectivity proposed in the dual-armed *Scheme 5* is similar to that used to represent the effects of proton inhibition of NMDA receptors (Banke et al., 2005) and activation properties of voltage-gated sodium channels (Kuo and Bean, 1994; Taddese and Bean, 2002) and potassium channels (Koren et al., 1990; Zagotta and Aldrich, 1990).

These models are similar in that they describe allosteric modulation of the receptor, by either a molecule applied exogenously, as in the case of protons on NMDA channels (Banke et al., 2005), or by actual channel block by a portion of the receptor itself in the case of sodium and potassium channels (Koren et al., 1990; Zagotta and Aldrich, 1990; Kuo and Bean, 1994; Taddese and Bean, 2002). While these models were designed for very different receptors, the presence of a second "arm" within each gating scheme allows each receptor to transition into a low open probability or inactive state while maintaining the ability of the receptor to transition back into the more active "arm" at each gating step (Koren et al., 1990; Zagotta and Aldrich, 1990; Kuo and Bean, 1994; Taddese and Bean, 2002; Banke et al., 2005). This suggests that the receptors are able to transition through the steps necessary for channel opening through both arms independently and in spite of the inhibitory modulation.

The two parallel arms of *Scheme 5* could be due to two GluN1/GluN2D receptor conformations, each capable of activation but at different speeds and with dramatically different open probabilities. Structurally, this could be due to two potential arrangements of the GluN1/GluN2D receptor's intra- or inter-subunit interfaces. *Scheme 5* also resembles models of AMPA receptor activation, which incorporate connected states corresponding to receptor desensitization (Jonas and Sakmann, 1992; Heckmann et al., 1996; Banke et al., 2000). Desensitization of AMPA and kainate receptors occurs by disruption of the ligand-binding domain dimer following closure of the ATD cleft (Sun et al., 2002; Mayer, 2006; Gielen et al., 2008; Chaudhry et al., 2009). It is possible that the second arm in *Scheme 5* reflects a similar structural rearrangement, although this alternative conformation in GluN1/GluN2D receptors can occur before agonist binding

and can still lead to channel opening, albeit rarely.

While *Scheme 5* was developed for GluN1/GluN2D receptors, it remains to be seen if the model would be able to adequately predict the gating of GluN2A-, GluN2B-, or GluN2C-containing NMDA receptors. Recently, Zhang et al. (2008) developed a gating scheme to describe the modal gating of GluN1/GluN2A NMDA receptors (Zhang et al., 2008). The model was similar to *Scheme 5*, as it had two linear and connected arms and allowed the receptor to transition from high to medium or low gating modes; however, the connectivity between the two linear schemes describing the modes was not determined or described (Zhang et al., 2008). *Scheme 5* may be able to better predict the modal gating clearly observed in GluN1/GluN2A and GluN1/GluN2B cell-attached patch single channel recordings. Additionally, a model of GluN1/GluN2C activation has been described that could not fully predict the rapid rise time of the current response of the receptor (Dravid et al., 2008). Because GluN1/GluN2C and GluN1/GluN2D receptors share the characteristics of low open channel open probability and rapid rise time of the macroscopic current response (Monyer et al., 1992; Stern et al., 1992; Vicini et al., 1998; Wyllie et al., 1998; Dravid et al., 2008; Yuan et al., 2009; Vance et al., 2011; Vance et al., 2012), it is possible that *Scheme 5* would be able to better predict GluN1/GluN2C gating.

### 7.5. GluN2D receptors contribute to the synaptic activity of the subthalamic nucleus

Little is known about how GluN2D-containing NMDA receptors contribute to synaptic activity due to a lack of available subunit-selective NMDA receptor modulators. Therefore, in Chapter 6, I describe two classes of modulators specific for the GluN2D

subunit. One class, typified by modulators DQP-1105 and 997-33, inhibits agonist-evoked currents in a use-dependent manner, and, in the case of 997-33, is more than 20-fold selective for GluN2D- over GluN2B-containing NMDA receptors. CIQ represents the second modulator class and potentiates GluN2C/D NMDA receptors with complete selectivity over GluN2A/B NMDA receptors. I used these novel pharmacological tools to evaluate the role of the GluN2D subunit in the subthalamic nucleus. Inhibitor 997-33 decreased both agonist-evoked currents as well as evoked excitatory postsynaptic currents. The potentiator CIQ increased agonist-evoked currents as well as EPSC peak currents. These data are among the first to identify the GluN2D subunit as participating in the synaptic activity of a brain region (Lozovava et al., 2004; Brothwell et al., 2008; Harney et al., 2008).

The subthalamic nucleus is an unusual member of the forebrain basal ganglia, as it is the lone excitatory nucleus. The STN receives substantial inhibitory input from the motor, associative, and limbic sections of the globus pallidus external (Smith and Grace, 1992; Shink et al., 1996; Karachi et al., 2005). The GPe exerts powerful control over the activity of the STN, regulating both firing rates and firing patterns, primarily through activation of $GABA_A$ receptors (Bevan et al., 2002; Baufreton et al., 2005; Baufreton et al., 2009). The STN also receives monosynaptic excitatory input from the ipsilateral cerebral cortex, the parafascicular nucleus of the thalamus, as well as some innervation by the pedunculopontine nucleus (Afsharpour, 1985; Canteras et al., 1988; Feger et al., 1994; Nambu et al., 1996; Feger, 1997). However, the STN also is a fast-spiking autonomous pacemaker, which is independent of external excitatory input and is dependent upon voltage-dependent sodium channels (Beurrier et al., 2000; Do and Bean,

2003; Surmeier et al., 2005; Atherton et al., 2008; Wilson and Bevan, 2011).

Two pathways have been identified in the transmission of cortical information through the basal ganglia: a direct pathway in which the output nuclei receive corticostriatal information directly, and an indirect pathway in which the GP and STN relay corticostriatal information to the output nuclei (See Figs. 6.1; 7.2; Albin et al., 1989; DeLong, 1990; Shink et al., 1996). Under normal resting conditions, the total output signal from the basal ganglia is believed to be inhibition driven by the tonic activity of the STN, while movement leads to a loss of inhibition (Nakanishi et al., 1987; Albin et al., 1989; DeLong, 1990; Bevan and Wilson, 1999; Kolomiets et al., 2001). Activation of the direct pathway leads to the disinhibition of the basal ganglia targets, including the cortex, thalamus, and other brain stem structures, leading to movement (DeLong, 1990; Bolam et al., 2000). The indirect pathway is thought to terminate a signal associated with movement or repress unwanted movement through the increased activity of the STN, which causes increased firing of the inhibitory SNr and GPi (Mink, 1996; Bolam et al., 2000).

In Parkinson's disease, loss of the dopaminergic SNc neurons that project to the striatum leads to an imbalance in cortical signaling, in which the indirect pathway is favored over the direct pathway (Fig. 7.2A; Albin et al., 1989; DeLong, 1990; Bolam et al., 2000). STN output increases by about 40% and leads to the symptoms associated with Parkinson's disease, such as akinesia, bradykinesia, and tremor (Fig. 7.2A; Bergman et al., 1990; DeLong, 1990; Rodriguez et al., 1998; Levy et al., 2000; Obeso et al., 2000;

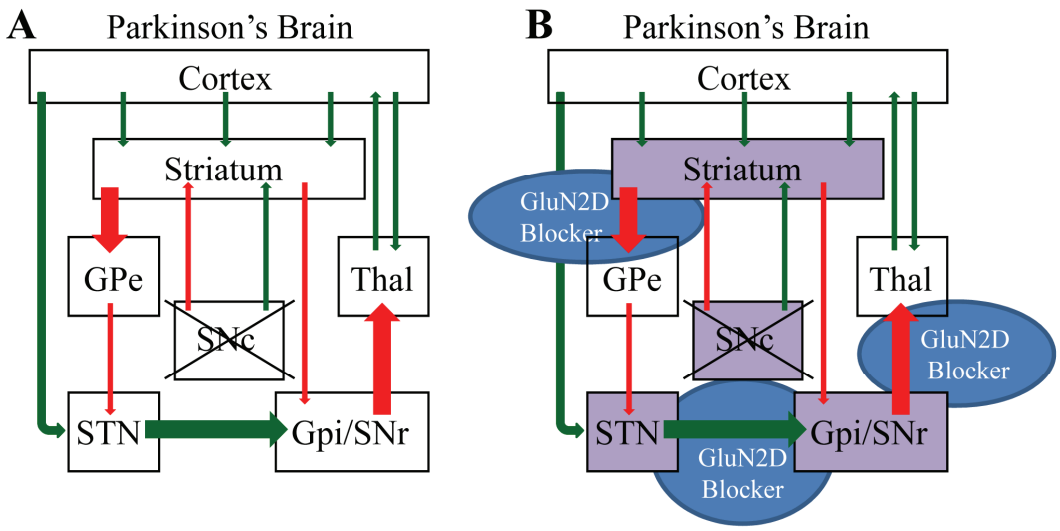


**Figure 7.2**. The GluN2D subunit is expressed in several areas of the basal ganglia and may represent a unique target for the treatment of Parkinson's disease. The basal ganglia circuit of a Parkinson's disease brain is given in ***A***. ***B***, The GluN2D subunit is expressed in the striatum, SNc, STN, GPi, and SNr (purple). Inhibiting the GluN2D subunit may improve parkinsonian symptoms by decreasing inhibition of the thalamocortical loop (Hallett and Standaert, 2004). Red arrows indicate a GABAergic inhibitory pathway, green arrows indicate a glutamatergic excitatory pathway, and the thickness of the arrow indicates the strength of the connection.

Galvan and Wichmann, 2008). In Parkinson's disease, STN burst firing increases, and synchronous firing occurs within the neurons of the STN as well as between the STN, GPe, and GPi (Hammond et al., 2007; Galvan and Wichmann, 2008). This may be due to increased sensitivity of the STN, GPe, and GPi to the rhythmic cortical input (Magill et al., 2004; Baufreton et al., 2005; Bevan et al., 2006; Mallet et al., 2006; Brown, 2007; Galvan and Wichmann, 2008; Mallet et al., 2008). Deep brain stimulation (DBS) of the STN, in which stimulation electrodes are implanted into the brain and deliver electrical high-frequency stimulation, relieves the motor symptoms of Parkinson's disease (Kumar et al., 1998; Obeso et al., 2001; Benabid, 2003; Rodriguez-Oroz et al., 2005; Deuschl et al., 2006; Wichmann and DeLong, 2006). Although the exact mechanism of DBS currently is unknown, stimulation may alter the temporal firing patterns of the STN (Hashimoto et al., 2003; Brown et al., 2004; McIntyre et al., 2004).

The GluN2D subunit is expressed in a number of basal ganglia nuclei, including the STN, GPi, SNc, and striatum (Fig. 7.2B; Standaert et al., 1993; Laurie and Seeburg, 1994; Monyer et al., 1994; Standaert et al., 1994). NMDA receptors containing the GluN2D subunit have many unique characteristics, including a slow deactivation time course following the removal of agonist, high affinities for glutamate and glycine, and less sensitivity to magnesium inhibition (Monyer et al., 1994; Vicini et al., 1998; Erreger et al., 2007; Chen et al., 2008; Traynelis et al., 2010; Vance et al., 2011; Retchless et al., 2012; Vance et al., 2012). The deactivation time course of GluN2D-containing NMDA receptors leads to prolonged excitatory postsynaptic currents, as I observed in the STN and others have observed elsewhere (Lozovaya et al., 2004; Brothwell et al., 2008; Harney et al., 2008). This prolonged deactivation time course, along with the weaker

magnesium block of synaptic GluN2D-containing NMDA receptors, would improve the temporal summation of excitatory synaptic inputs into the STN and increase STN neuronal excitability (Forsythe and Westbrook, 1988; Bourne and Nicoll, 1993; Edmonds et al., 1995), which may be important for a neuron with relatively low excitatory input and a high NMDA receptor to AMPA receptor ratio (see Chapter 6; Wolf et al., 2005). Indeed, longer EPSC deactivation time courses have been linked to stronger synaptic plasticity (Mayer and Miller, 1990; Fox et al., 1991; Carmignoto and Vicini, 1992; Edmonds et al., 1995).

The relatively slow deactivation time course the GluN2D subunit confers upon the synapse compared to the other GluN2 subunits would cause higher and longer charge transfer compared to the more rapidly deactivating GluN2A subunit, allowing for increased calcium entry into the STN neuron and activation of a number of different calcium-activated signals and genes (DeMaria et al., 2001; Deisseroth et al., 2003; Erreger et al., 2005a; Wolf et al., 2005). Extrasynaptic GluN2D-containing NMDA receptors might also be essential for the behavior of STN neurons, as the slow deactivation time course, weak magnesium block, and higher glutamate and glycine affinities also could lead to higher tonic NMDA receptor activity in the subthalamic nucleus, causing depolarization and increased burst firing (Zhu et al., 2004; Zhu et al., 2005).

The inclusion of the GluN1-b splice variant in the STN (Standaert et al., 1993; Laurie and Seeburg, 1994; Monyer et al., 1994; Standaert et al., 1994) might provide an additional mechanism for controlling the time course of synaptic activity. As I presented in Chapter 4, GluN1-b/GluN2D receptors have more rapid deactivation time courses and

decreased agonist affinities (Vance et al., 2012). GluN2D-containing NMDA receptors with shorter deactivation time courses but with relatively poor magnesium block may allow the neuron to activate in spite of weak depolarization while retaining more control over the temporal coupling of synaptic activity.

As discussed above, firing in the STN increases and becomes more synchronous in Parkinson's disease (Hammond et al., 2007; Galvan and Wichmann, 2008). GluN2D-containing receptors could in turn further increase excitability in the STN due to their ability to control high charge transfer and calcium influx into the neuron (Carmignoto and Vicini, 1992; Erreger et al., 2005a). Therefore, the GluN2D subunit may represent a unique target for the treatment of Parkinson's disease. Our collaborators at Lundbeck in Copenhagen, Denmark, evaluated the potentiator CIQ and the inhibitor DQP-1105 to determine if modulating the GluN2D subunit could increase or decrease spike firing of the STN. Potentiating the GluN2D subunit with CIQ doubled the firing rate of the STN (Fig. 7.3) in a manner that could be inhibited by the NMDA receptor channel blocker MK-801. Inhibiting the GluN2D subunit by direct application of DQP-1105 decreased the firing rate of the STN by about 40% (Fig. 7.4). These data suggest that the GluN2D subunit indeed has an important role in the firing of the STN. Future studies remain to be conducted to determine if the decrease in firing rate by 997-33 can impact the symptoms of Parkinson's disease. However, these data and my studies on the role of the GluN2D subunit in the excitatory postsynaptic currents of the STN suggest that the GluN2D subunit could be a useful pharmacological target in the treatment of disease.

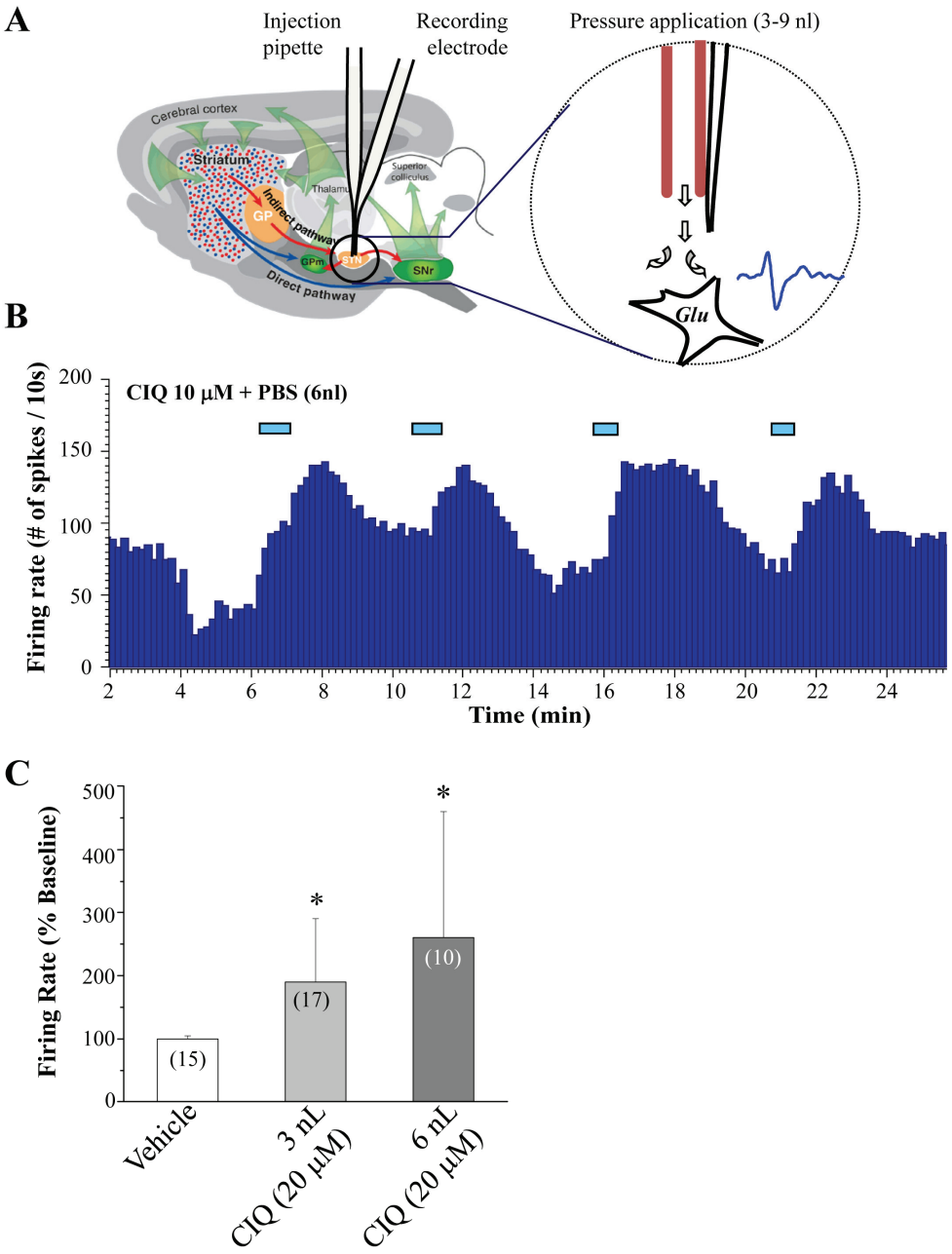


**Figure 7.3**. Potentiating GluN2D with CIQ increases the firing rate of STN neurons *in vivo*. ***A***, Extracellular single-cell recordings were performed on anaesthetized adult male rats (intraperitoneal injection of urethane (1.2-1.5 g/kg)) using a recording glass electrode and an ejection pipette for local drug delivery lowered to the following coordinates: AP 4.2-3.6 mm posterior to bregma; L 2.2-2.8 mm lateral to the midline. **B**, The drug or vehicle control was applied after 5 minutes of stable baseline recordings

through repeated pressure pulses (10-40 ms duration; 10-20 psi) in small volumes (3-6nl). The change in firing rate induced by drug application was compared to the baseline firing rate by measuring the maximal firing rate during the last 10-20 s of drug application, and expressed in percent of baseline firing rate measured 3-5 minutes before drug application. ***C***, CIQ (20 μM) increased the firing rate to 200% of the vehicle control when applied at 3 nL (n=17), and firing rate was increased to 250% of control when applied at 6 nL (n=10). *$p < 0.05$; one-way ANOVA with Tukey's *post-hoc* test. (Unpublished data, Sotty, Fog, and Traynelis)

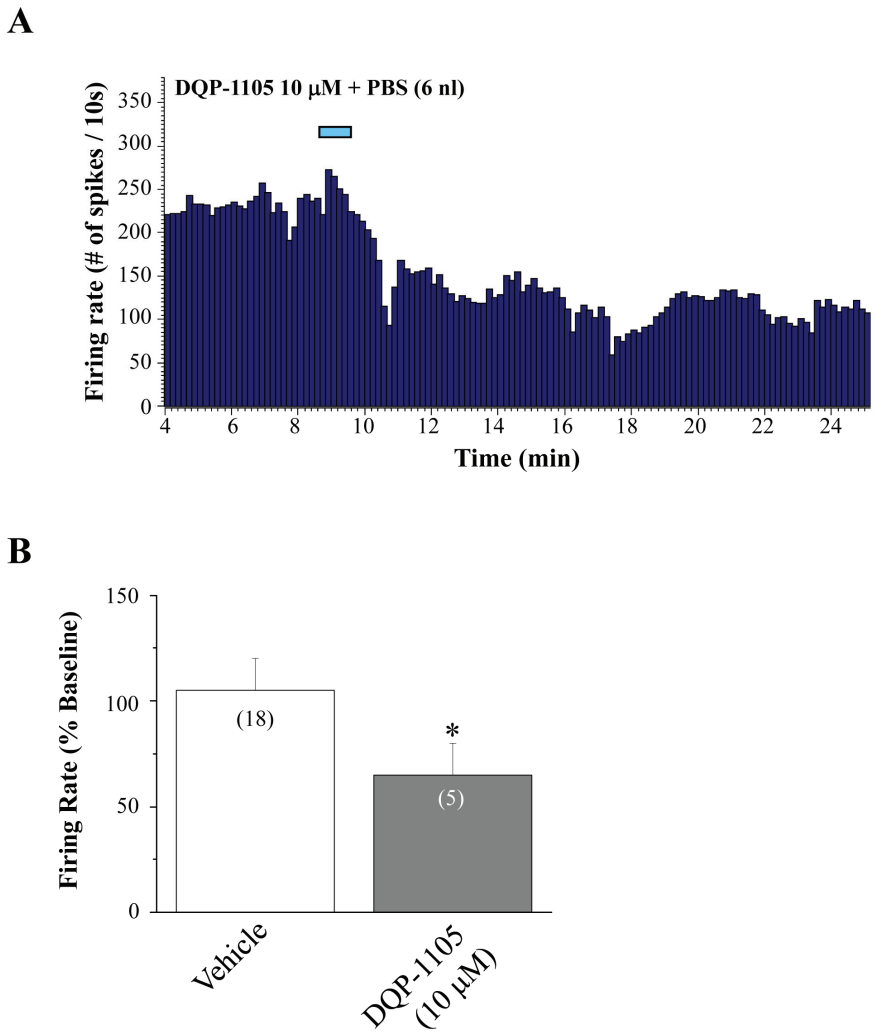


**Figure 7.4**. Inhibiting GluN2D with DQP-1105 decreases the firing rate of STN neurons *in vivo*. ***A***, DQP-1105 (10 μM) was applied in 6 nL pulses to the STN caused a long-lasting decrease in firing rate. ***B***, DQP-1105 decreased STN firing rate significantly by approximately 40% compared to the DMSO and PBS vehicle control. *$p < 0.05$; unpaired t-test. (Unpublished data, Sotty, Fog, and Traynelis)

## 7.6. Conclusion

GluN2D-containing NMDA receptors have long been known to have unusual properties, including a slow deactivation time course, high agonist affinity, and low channel open probability, that distinguish it from other NMDA receptors (Monyer et al., 1994; Vicini et al., 1998; Wyllie et al., 1998; Vance et al., 2011; Vance et al., 2012). However, little was known about the mechanisms controlling the behavior of GluN1/GluN2D NMDA receptors. Because the GluN2D subunit is expressed in regions of the brain of interest to a number of diseases, including Parkinson's disease (Monyer et al., 1994; Standaert et al., 1994; Standaert et al., 1996; Dunah and Standaert, 2003), understanding the basic mechanisms controlling GluN2D-containing NMDA receptors is essential before we can thoroughly evaluate their roles in the brain. This thesis contributes to our understanding of how the GluN2D receptor is regulated by multiple domains across the receptor, including the GluN2D ligand-binding domain and the GluN1 amino-terminal domain, as well as how the GluN2D receptor can be controlled by novel allosteric modulators. Finally, I conclude this thesis with a study of how the GluN2D subunit contributes to the synaptic activity of the STN. This study suggests that the unique properties of the GluN2D subunit, as well as its role in the synaptic activity of the STN, make it an interesting target for the treatment of neurological diseases.

## Appendix A


**Appendix A**. The linear amino acid sequences of the S2 domains of the GluN2A, GluN2B, GluN2C, and GluN2D ligand-binding domains are given. The hinge loop is in purple, Helix D/Loop D are in orange, Helix E is in red, Helix F is in green, and Helix H is in blue.

## Appendix B

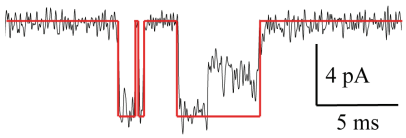


**Appendix B**. Conversion of SCAN data to a QUB-compatible format eliminates the differences in conductance levels. An example of a GluN1-1a/GluN2D single channel in an excised outside-out patch activated by 1 mM L-glutamate and 0.05 mM glycine is given. In red is the QUB-compatible idealization of the open and shut states. Because the QUB-compatible format does not distinguish between amplitude levels, all openings are considered to be of the same amplitude.

## Appendix C

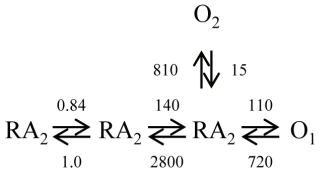


**LL 65720**

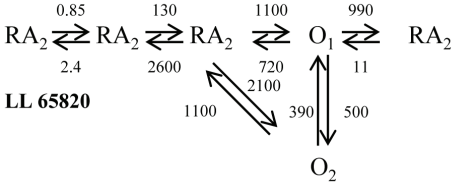


**LL 65820**

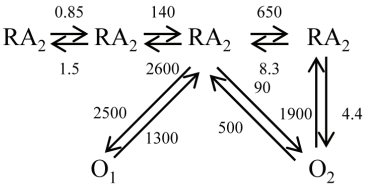


**LL 65820**

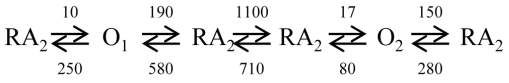


**LL 57440**

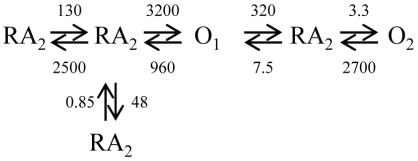


**LL 65810**

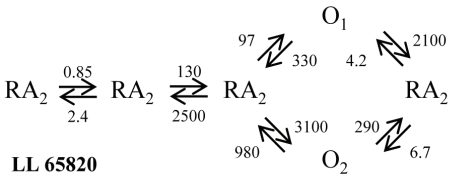


**LL 65820**

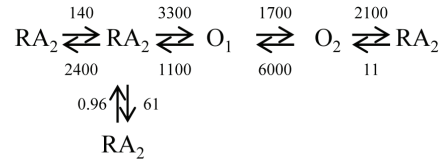


**LL 65790**

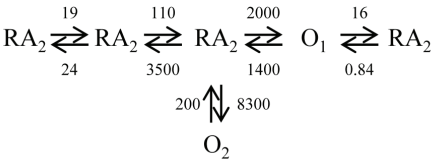


**LL 65720**

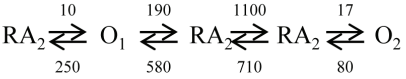


**LL 57440**

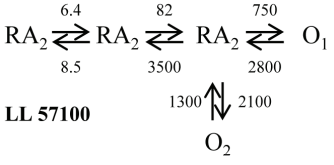


**LL 57100**

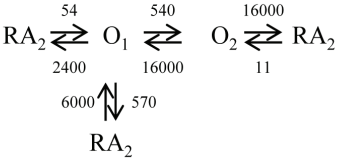


**LL 57190**

**LL 57110**

**Appendix C**. Additional models from the QUB model search. The random model generating software in QUB was used to evaluate potential gating schemes with unique connectivity between the open and shut states using idealized data from one of my GluN1-1a/GluN2D single channels activated by 1 mM L-glutamate and 0.05 mM glycine. None of the included models could adequately describe GluN1-1a/GluN2D gating.

## Chapter 8: References

Acker TM, Yuan HJ, Hansen KB, Vance KM, Ogden KK, Jensen HS, Burger PB, Mullasseril P, Snyder JP, Liotta DC and Traynelis SF (2011) Mechanism for Noncompetitive Inhibition by Novel GluN2C/D N-Methyl-D-aspartate Receptor Subunit-Selective Modulators. *Mol Pharmacol* **80**(5): 782-795.

Acker TM, Snyder JP, Liotta DC and Traynelis SF (2012) Noncompetitve inhibition of GluN2C/D NMDA receptors. *In preparation*.

Afsharpour S (1985) Topographical projections of the cerebral cortex to the subthalamic nucleus. *Journal of Comparative Neurology* **236**(1): 14-28.

Albin RL, Young AB and Penney JB (1989) The functional anatomy of basal ganglia disorders. *Trends in Neurosciences* **12**(10): 366-375.

Alt A, Weiss B, Ogden AM, Knauss JL, Oler J, Ho K, Large TH and Bleakman D (2004) Pharmacological characterization of glutamatergic agonists and antagonists at recombinant human homomeric and heteromeric kainate receptors in vitro. *Neuropharmacology* **46**(6): 793-806.

Amico-Ruvio SA and Popescu GK (2010) Stationary Gating of GluN1/GluN2B Receptors in Intact Membrane Patches. *Biophys J* **98**(7): 1160-1169.

Armstrong N and Gouaux E (2000) Mechanisms for activation and antagonism of an AMPA-sensitive glutamate receptor: crystal structures of the GluR2 ligand binding core. *Neuron* **28**(1): 165-181.

Armstrong N, Jasti J, Beich-Frandsen M and Gouaux E (2006) Measurement of conformational changes accompanying desensitization in an ionotropic glutamate receptor. *Cell* **127**(1): 85-97.

Atherton JF, Wokosin DL, Ramanathan S and Bevan MD (2008) Autonomous initiation and propagation of action potentials in neurons of the subthalamic nucleus. *J Physiol* **586**(23): 5679-5700.

Auerbach A and Zhou Y (2005) Gating Reaction Mechanisms for NMDA Receptor Channels. *J Neurosci* **25**(35): 7914-7923.

Banke TG, Bowie D, Lee HK, Huganir RL, Schousboe A and Traynelis SF (2000) Control of GluR1 AMPA Receptor Function by cAMP-Dependent Protein Kinase. *J Neurosci* **20**(1): 89-102.

Banke TG, Dravid SM and Traynelis SF (2005) Protons Trap NR1/NR2B NMDA Receptors in a Nonconducting State. *J Neurosci* **25**(1): 42-51.

Banke TG and Traynelis SF (2003) Activation of NR1/NR2B NMDA receptors. *Nat Neurosci* **6**(2): 144-152.

Bardoni R, Magherini PC and MacDermott AB (1998) NMDA EPSCs at Glutamatergic Synapses in the Spinal Cord Dorsal Horn of the Postnatal Rat. *J Neurosci* **18**(16): 6558-6567.

Barton ME and White HS (2004) The effect of CGX-1007 and CI-1041, novel NMDA receptor antagonists, on kindling acquisition and expression. *Epilepsy Res* **59**(1): 1-12.

Bassand P, Bernard A, Rafiki A, Gayet D and Khrestchatisky M (1999) Differential interaction of the tSXV motifs of the NR1 and NR2A NMDA receptor subunits with PSD-95 and SAP97. *European Journal of Neuroscience* **11**(6): 2031-2043.

Basu AC, Tsai GE, Ma CL, Ehmsen JT, Mustafa AK, Han L, Jiang ZI, Benneyworth MA, Froimowitz MP, Lange N, Snyder SH, Bergeron R and Coyle JT (2009) Targeted disruption of serine racemase affects glutamatergic neurotransmission and behavior. *Molecular Psychiatry* **14**(7): 719-727.

Baufreton J, Atherton JF, Surmeier DJ and Bevan MD (2005) Enhancement of excitatory synaptic integration by GABAergic inhibition in the subthalamic nucleus. *J Neurosci* **25**(37): 8505-8517.

Baufreton J, Kirkham E, Atherton JF, Menard A, Magill PJ, Bolam JP and Bevan MD (2009) Sparse but Selective and Potent Synaptic Transmission From the Globus Pallidus to the Subthalamic Nucleus. *J Neurophysiol* **102**(1): 532-545.

Benabid AL (2003) Deep brain stimulation for Parkinson's disease. *Current Opinion in Neurobiology* **13**(6): 696-706.

Benveniste H (1989) Brain Microdialysis. *J Neurochem* **52**(6): 1667-1679.

Benveniste M, Mienville JM, Sernagor E and Mayer ML (1990) Concentration-jump experiments with NMDA antagonists in mouse cultured hippocampal neurons. *J Neurophysiol* **63**(6): 1373-1384.

Berger AJ, Dieudonna S and Ascher P (1998) Glycine Uptake Governs Glycine Site Occupancy at NMDA Receptors of Excitatory Synapses. *J Neurophysiol* **80**(6): 3336-3340.

Bergeron R, Meyer TM, Coyle JT and Greene RW (1998) Modulation of N-methyl-D-aspartate receptor function by glycine transport. *Proc Natl Acad Sci U S A* **95**(26): 15730-15734.

Bergman H, Wichmann T and DeLong M (1990) Reversal of experimental parkinsonism by lesions of subthalamic nucleus. *Science* **249**(4975): 1436-1438.

Bettini E, Sava A, Griffante C, Carignani C, Buson A, Capelli AM, Negri M, Andreetta F, Senar-Sancho SA, Guiral L and Cardullo F (2010) Identification and Characterization of Novel NMDA Receptor Antagonists Selective for NR2A- over NR2B-Containing Receptors. *J Pharmacol Exp Ther* **335**(3): 636-644.

Beurrier C, Bioulac B and Hammond C (2000) Slowly inactivating sodium current (I-NaP) underlies single-spike activity in rat subthalamic neurons. *J Neurophysiol* **83**(4): 1951-1957.

Bevan MD, Atherton JF and Baufreton J (2006) Cellular principles underlying normal and pathological activity in the subthalamic nucleus. *Current Opinion in Neurobiology* **16**(6): 621-628.

Bevan MD, Francis CM and Bolam JP (1995) The glutamate-enriched cortical and thalamic input to neurons in the subthalamic nucleus of the rat - convergence with GABA-positive terminals. *Journal of Comparative Neurology* **361**(3): 491-511.

Bevan MD, Magill PJ, Terman D, Bolam JP and Wilson CJ (2002) Move to the rhythm: oscillations in the subthalamic nucleus-external globus pallidus network. *Trends in Neurosciences* **25**(10): 525-531.

Bevan MD and Wilson CJ (1999) Mechanisms underlying spontaneous oscillation and rhythmic firing in rat subthalamic neurons. *J Neurosci* **19**(17): 7617-7628.

Bianchi MT, Botzolakis EJ, Haas KF, Fisher JL and Macdonald RL (2007) Microscopic kinetic determinants of macroscopic currents: insights from coupling and uncoupling of GABAA receptor desensitization and deactivation. *The Journal of Physiology* **584**(3): 769-787.

Billups D and Attwell D (2003) Active release of glycine or D-serine saturates the glycine site of NMDA receptors at the cerebellar mossy fibre to granule cell synapse. *European Journal of Neuroscience* **18**(11): 2975-2980.

Bischoff S, Barhanin J, Bettler B, Mulle C and Heinemann S (1997) Spatial distribution of kainate receptor subunit mRNA in the mouse basal ganglia and ventral mesencephalon. *The Journal of Comparative Neurology* **379**(4): 541-562.

Blanke ML and VanDongen AMJ (2008) Constitutive activation of the N-methyl-D-aspartate receptor via cleft-spanning disulfide bonds. *Journal of Biological Chemistry* **283**(31): 21519-21529.

Bolam JP, Hanley JJ, Booth PAC and Bevan MD (2000) Synaptic organisation of the basal ganglia. *Journal of Anatomy* **196**: 527-542.

Bourne HR and Nicoll R (1993) Molecular machines integrate coincident synaptic signals. *Cell* **72**: 65-75.

Brickley SG, Misra C, Mok MHS, Mishina M and Cull-Candy SG (2003) NR2B and NR2D Subunits Coassemble in Cerebellar Golgi Cells to Form a Distinct NMDA Receptor Subtype Restricted to Extrasynaptic Sites. *J Neurosci* **23**(12): 4958-4966.

Brothwell SLC, Barber JL, Monaghan DT, Jane DE, Gibb AJ and Jones S (2008) NR2B- and NR2D-containing synaptic NMDA receptors in developing rat substantia nigra pars compacta dopaminergic neurones. *J Physiol* **586**(3): 739-750.

Brown P (2007) Abnormal oscillatory synchronisation in the motor system leads to impaired movement. *Current Opinion in Neurobiology* **17**(6): 656-664.

Brown P, Mazzone P, Oliviero A, Altibrandi MG, Pilato F, Tonali PA and Di Lazzaro V (2004) Effects of stimulation of the subthalamic area on oscillatory pallidal activity in Parkinson's disease. *Exp Neurol* **188**(2): 480-490.

Canteras NS, Shammahlagnado SJ, Silva BA and Ricardo JA (1988) Somatosensory inputs to the subthalamic nucleus - a combined retrograde and anterograde horseradish-peroxidase study in the rat. *Brain Research* **458**(1): 53-64.

Carmignoto G and Vicini S (1992) Activity-dependent decrease in NMDA receptor response during development of the visual cortex. *Science* **258**(5084): 1007-1011.

Castillo PE, Malenka RC and Nicoll RA (1997) Kainate receptors mediate a slow postsynaptic current in hippocampal CA3 neurons. *Nature* **388**(6638): 182-186.

Cavallero A, Marte A and Fedele E (2009) l-Aspartate as an amino acid neurotransmitter: mechanisms of the depolarization-induced release from cerebrocortical synaptosomes. *J Neurochem* **110**(3): 924-934.

Chang SY, Satin J and Fozzard HA (1996) Modal behavior of the mu 1 Na+ channel and effects of coexpression of the beta(1)-subunit. *Biophys J* **70**(6): 2581-2592.

Chao J, Seiler N, Renault J, Kashiwagi K, Masuko T, Igarashi K and Williams K (1997) N-1-dansyl-spermine and N-1-(n-octanesulfonyl)-spermine, novel glutamate receptor antagonists: Block and permeation of N-methyl-D-aspartate receptors. *Mol Pharmacol* **51**(5): 861-871.

Chatterton JE, Awobuluyi M, Premkumar LS, Takahashi H, Talantova M, Shin Y, Cui J, Tu S, Sevarino K, Nakanishi N, Tong G, Lipton SA and Zhang D (2002)

Excitatory glycine receptors containing the NR3 family of NMDA receptor subunits. *Nature* **415**: 793-798.

Chaudhry C, Weston MC, Schuck P, Rosenmund C and Mayer ML (2009) Stability of ligand-binding domain dimer assembly controls kainate receptor desensitization. *Embo J* **28**(10): 1518-1530.

Chazot PL and Stephenson FA (1997) Molecular dissection of native mammalian forebrain NMDA receptors containing the NR1 C2 exon: Direct demonstration of NMDA receptors comprising NR1, NR2A, and NR2B subunits within the same complex. *J Neurochem* **69**(5): 2138-2144.

Cheffings CM and Colquhoun D (2000) Single channel analysis of a novel NMDA channel from Xenopus oocytes expressing recombinant NR1a, NR2A and NR2D subunits. *J Physiol* **526**(3): 481-491.

Chen H and Lipton SA (2006) The chemical biology of clinically tolerated NMDA receptor antagonists. *J Neurochem* **97**(6): 1611-1626.

Chen L, Muhlhauser M and Yang CR (2003) Glycine tranporter-1 blockade potentiates NMDA-mediated responses in rat prefrontal cortical neurons in vitro and in vivo. *J Neurophysiol* **89**(2): 691-703.

Chen PE, Geballe MT, Katz E, Erreger K, Livesey MR, O'Toole KK, Le P, Lee CJ, Snyder JP, Traynelis SF and Wyllie DJA (2008) Modulation of glycine potency in rat recombinant NMDA receptors containing chimeric NR2A/2D subunits expressed in Xenopus laevis oocytes. *J Physiol* **586**(1): 227-245.

Chen PE, Johnston AR, Mok MHS, Schoepfer R and Wyllie DJA (2004) Influence of a threonine residue in the S2 ligand binding domain in determining agonist potency and deactivation rate of recombinant NR1a/NR2D NMDA receptors. *J Physiol* **558**(1): 45-58.

Chenard BL, Bordner J, Butler TW, Chambers LK, Collins MA, Decosta DL, Ducat MF, Dumont ML, Fox CB, Mena EE, Menniti FS, Nielsen J, Pagnozzi MJ, Richter KEG, Ronau RT, Shalaby IA, Stemple JZ and White WF (1995) (1S,2S)-1-(4-hydroxyphenyl)-2-(4-hydroxy-4-phenylpiperidino)-1-propanol - a potent new neuroprotectant which blocks N-methyl-D-aspartate responses. *J Med Chem* **38**(16): 3138-3145.

Cho CH, St-Gelais F, Zhang W, Tomita S and Howe JR (2007) Two families of TARP isoforms that have distinct effects on the kinetic properties of AMPA receptors and synaptic currents. *Neuron* **55**(6): 890-904.

Christopoulos A (1998) Assessing the distribution of parameters in models of ligand-receptor interaction: to log or not to log. *Trends Pharmacol Sci* **19**: 351-357.

Clarke NP and Bolam JP (1998) Distribution of glutamate receptor subunits at neurochemically characterized synapses in the entopeduncular nucleus and subthalamic nucleus of the rat. *Journal of Comparative Neurology* **397**(3): 403-420.

Clayton A, Siebold C, Gilbert RJC, Sutton GC, Harlos K, McIlhinney RAJ, Jones EY and Aricescu AR (2009) Crystal Structure of the GluR2 Amino-Terminal Domain Provides Insights into the Architecture and Assembly of Ionotropic Glutamate Receptors. *J Mol Biol* **392**(5): 1125-1132.

Clements JD, Lester RAJ, Tong G, Jahr CE and Westbrook GL (1992) The time course of glutamate in the synaptic cleft. *Science* **258**(5087): 1498-1501.

Collingridge GL, Kehl SJ and McLennan H (1983) Excitatory amino-acids in synaptic transmission in the Schaffer collateral commissural pathway of the rat hippocampus. *Journal of Physiology-London* **334**(JAN): 33-46.

Colquhoun D and Hawkes A (1990) Stochastic properties of ion channel openings and bursts in a membrane patch that contains two channels: evidence concerning the number of channels present when a record containing only single openings is observed. *Proc R Soc Lond B Biol Sci* **240**(1299): 453-457.

Colquhoun D and Hawkes AG (1987) A note on correlations in single channel ion records. *Proc R Soc Lond Ser B-Biol Sci* **230**(1258): 15-52.

Colquhoun D, Large WA and Rang HP (1977) An analysis of the action of a false transmitter at the neuromuscular junction. *The Journal of Physiology* **266**(2): 361-395.

Colquhoun D and Sakmann B (1985) Fast events in single-channel currents activated by acetylcholine and its analogues at the frog muscle end-plate. *The Journal of Physiology* **369**(1): 501-557.

Costa BM, Irvine MW, Fang GY, Eaves RJ, Mayo-Martin MB, Skifter DA, Jane DE and Monaghan DT (2010) A Novel Family of Negative and Positive Allosteric Modulators of NMDA Receptors. *J Pharmacol Exp Ther* **335**(3): 614-621.

Cull-Candy SG and Leszkiewicz DN (2004) Role of Distinct NMDA Receptor Subtypes at Central Synapses. *Sci STKE* **2004**(255): 1-9.

Curras MC and Dingledine R (1992) Selectivity of amino acid transmitters acting at N-methyl-D-aspartate and amino-3-hydroxy-5-methyl-4-isoxazolepropionate receptors. *Mol Pharmacol* **41**(3): 520-526.

Curtis DR and Watkins JC (1960) The excitation and depression of spinal neurons by structurally related amino acids. *J Neurochem* **6**(2): 117-141.

Curtis DR, Phillis JW and Watkins JC (1960) The chemical excitation of spinal neurons by certain acidic amino acids. *Journal of Physiology-London* **150**(3): 656-682.

Das S, Sasaki YF, Rothe T, Premkumar LS, Takasu M, Crandall JE, Dikkes P, Conner DA, Rayudu PV and Cheung W (1998) Increased NMDA current and spine density in mice lacking the NMDA receptor subunit NR3A. *Nature* **393**(6683): 377 - 381.

Davies J, Evans RH, Francis A, Jones AW and Watkins J (1981) Antagonism of excitatory amino acid-induced and synaptic excitation of spinal neurones by cis-2,3-piperidine dicarboxylate. *J Neurochem* **36**(3): 1305-1307.

Deisseroth K, Mermelstein PG, Xia HH and Tsien RW (2003) Signaling from synapse to nucleus: the logic behind the mechanisms. *Current Opinion in Neurobiology* **13**(3): 354-365.

Delcour AH, Lipscombe D and Tsien RW (1993) Multiple modes of N-type calcium channel activity distinguished by differences in gating. *J Neurosci* **13**(1): 181-194.

DeLong MR (1990) Primate models of movement disorders of basal ganglia origin. *Trends in Neurosciences* **13**(7): 281-285.

DeMaria CD, Soong TW, Alseikhan BA, Alvania RS and Yue DT (2001) Calmodulin bifurcates the local Ca2+ signal that modulates P/Q-type Ca2+ channels. *Nature* **411**(6836): 484-489.

Deuschl G, Schade-Brittinger C, Krack P, Volkmann J, Schaefer H, Boetzel K, Daniels C, Deutschlaender A, Dillmann U, Eisner W, Gruber D, Hamel W, Herzog J, Hilker R, Klebe S, Kloss M, Koy J, Krause M, Kupsch A, Lorenz D, Lorenzl S, Mehdorn HM, Moringlane JR, Oertel W, Pinsker MO, Reichmann H, Reuss A, Schneider G-H, Schnitzler A, Steude U, Sturm V, Timmermann L, Tronnier V, Trottenberg T, Wojtecki L, Wolf E, Poewe W, Voges J and German Parkinson Study G (2006) A randomized trial of deep-brain stimulation for Parkinson's disease. *New England Journal of Medicine* **355**(9): 896-908.

Do K, Herrling PL, Streit P and Cuenod M (1988) Release of neuroactive substances: homocysteic acid as an endogenous agonist of the NMDA receptor. *J Neural Transm* **72**(3): 185-190.

Do KQ, Herrling PL, Streit P, Turski WA and Cuenod M (1986) In vitro release and electrophysiological effects in situ of homocysteic acid, an endogenous N-methyl-(D)-aspartic acid agonist, in the mammalian striatum. *J Neurosci* **6**(8): 2226-2234.

Do MTH and Bean BP (2003) Subthreshold Sodium Currents and Pacemaking of Subthalamic Neurons: Modulation by Slow Inactivation. *Neuron* **39**(1): 109-120.

Dogan A, Rao A, Baskaya M, Rao V, Rastl J, Donaldson D and Dempsey R (1997) Effects of ifenprodil, a polyamine site NMDA receptor antagonist, on reperfusion injury after transient focal cerebral ischemia. *J Neurosurg* **87**(6): 921-926.

Dravid SM, Burger PB, Prakash A, Geballe MT, Yadav R, Le P, Vellano K, Snyder JP and Traynelis SF (2010) Structural Determinants of D-Cycloserine Efficacy at the NR1/NR2C NMDA Receptors. *J Neurosci* **30**(7): 2741-2754.

Dravid SM, Prakash A and Traynelis SF (2008) Activation of recombinant NR1/NR2C NMDA receptors. *J Physiol* **586**(18): 4425-4439.

Dunah AW, Yasuda RP, Wang Y-h, Luo J, Dávila-García MI, Gbadegesin M, Vicini S and Wolfe BB (1996) Regional and Ontogenic Expression of the NMDA Receptor Subunit NR2D Protein in Rat Brain Using a Subunit-Specific Antibody. *J Neurochem* **67**(6): 2335-2345.

Dunah A and Standaert D (2003) Subcellular segregation of distinct heteromeric NMDA glutamate receptors in the striatum. *J Neurochem* **85**(4): 935-943.

Durand GM, Gregor P, Zheng X, Bennett MV, Uhl GR and Zukin RS (1992) Cloning of an apparent splice variant of the rat N-methyl-D-aspartate receptor NMDAR1 with altered sensitivity to polyamines and activators of protein kinase C. *Proc Natl Acad Sci USA* **89**(19): 9359 - 9363.

Dzhura I, Wu YJ, Colbran RJ, Balser JR and Anderson ME (2000) Calmodulin kinase determines calcium-dependent facilitation of L-type calcium channels. *Nature Cell Biology* **2**(3): 173-177.

Edmonds B, Gibb AJ and Colquhoun D (1995) Mechanisms of activation of glutamate receptors and the time-course of excitatory synaptic currents. *Annu Rev Physiol* **57**: 495-519.

Ehlers MD, Fung ET, O'Brien RJ and Huganir RL (1998) Splice Variant-Specific Interaction of the NMDA Receptor Subunit NR1 with Neuronal Intermediate Filaments. *J Neurosci* **18**(2): 720-730.

Ehlers MD, Tingley WG and Huganir RL (1995) Regulated subcellular distribution of the NR1 subunit of the NMDA receptor. *Science* **269**(5231): 1734-1737.

Ehlers MD, Zhang S, Bernhardt JP and Huganir RL (1996) Inactivation of NMDA receptors by direct interaction of calmodulin with the NR1 subunit. *Cell* **84**(5): 745-755.

Ernst OP, Murcia PAS, Daldrop P, Tsunoda SP, Kateriya S and Hegemann P (2008) Photoactivation of channelrhodopsin. *Journal of Biological Chemistry* **283**(3): 1637-1643.

Erreger K, Chen P, Wyllie D and Traynelis S (2004) Glutamate receptor gating. *Crit Rev Neurobiol* **16**(3): 187-224.

Erreger K, Dravid SM, Banke TG, Wyllie DJA and Traynelis SF (2005a) Subunit-specific gating controls rat NR1/NR2A and NR1/NR2B NMDA channel kinetics and synaptic signalling profiles. *J Physiol* **563**(2): 345-358.

Erreger K, Geballe MT, Dravid SM, Snyder JP, Wyllie DJA and Traynelis SF (2005b) Mechanism of Partial Agonism at NMDA Receptors for a Conformationally Restricted Glutamate Analog. *J Neurosci* **25**(34): 7858-7866.

Erreger K, Geballe MT, Kristensen A, Chen PE, Hansen KB, Lee CJ, Yuan H, Le P, Lyuboslavsky PN, Micale N, Jorgensen L, Clausen RP, Wyllie DJA, Snyder JP and Traynelis SF (2007) Subunit-Specific Agonist Activity at NR2A-, NR2B-, NR2C-, and NR2D-Containing N-Methyl-D-aspartate Glutamate Receptors. *Mol Pharmacol* **72**(4): 907-920.

Errico F, Rossi S, Napolitano F, Catuogno V, Topo E, Fisone G, D'Aniello A, Centonze D and Usiello A (2008) D-Aspartate Prevents Corticostriatal Long-Term Depression and Attenuates Schizophrenia-Like Symptoms Induced by Amphetamine and MK-801. *J Neurosci* **28**(41): 10404-10414.

Evans RH, Francis A, Jones AW, Smith DAS and Watkins JC (1981) The effects of a series of ö-phosphonic R-carboxylic amino acids on electrically evoked and amino acid induced responses in isolated spinal cord preparations. *British Journal of Pharmacology* **75**: 65-75.

Feger J (1997) Updating the functional model of the basal ganglia. *Trends in Neurosciences* **20**(4): 152-153.

Feger J, Bevan M and Crossman AR (1994) The projections from the parafascicular thalmic nucleus to the subthalamic nucleus and the striatum arise from separate neuronal populations - a comparison with the corticostriatal and corticosubthalamic efferents in a retrograde fluorescent double-labeling study. *Neuroscience* **60**(1): 125-132.

Fellin T, Luvisetto S, Spagnolo M and Pietrobon D (2004) Modal gating of human Ca(v)2.1 (P/Q-type) calcium channels: II. The b mode and reversible uncoupling of inactivation. *J Gen Physiol* **124**(5): 463-474.

Feng B, Morley RM, Jane DE and Monaghan DT (2005) The effect of competitive antagonist chain length on NMDA receptor subunit selectivity. *Neuropharmacology* **48**(3): 354-359.

Feng B, Tse HW, Skifter DA, Morley R, Jane DE and Monaghan DT (2004) Structure-activity analysis of a novel NR2C//NR2D-preferring NMDA receptor antagonist: 1-(phenanthrene-2-carbonyl) piperazine-2,3-dicarboxylic acid. *Br J Pharmacol* **141**(3): 508-516.

Fischer G, Mutel V, Trube G, Malherbe P, Kew J, Mohacsi E, Heitz M-P and Kemp J (1997) Ro 25-6981, a highly potent and selective blocker of N-methyl-D-aspartate receptors containing the NR2B subunit. *J Pharmacol Exp Ther* **283**(1285-1292).

Fleck MW, Barrionuevo G and Palmer AM (2001) Release of D,L-threo-beta-hydroxyaspartate as a false transmitter from excitatory amino acid-releasing nerve terminals. *Neurochem Int* **39**(1): 75-81.

Fleck MW, Henze DA, Barrionuevo G and Palmer AM (1993) Aspartate and glutamate mediate excitatory synaptic transmission in area CA1 of the hippocampus. *J Neurosci* **13**(9): 3944-3955.

Forsythe ID and Westbrook GL (1988) Slow excitatory postsynaptic currents mediated by N-methyl-D-aspartate receptors on cultured mouse central neurones. *The Journal of Physiology* **396**(1): 515-533.

Fox K, Daw N, Sato H and Czepita D (1991) Dark-rearing delays the loss of NMDA receptor function in kitten visual cortex. *Nature* **350**(6316): 342-344.

Frerking M and Ohliger-Frerking P (2002) AMPA Receptors and Kainate Receptors Encode Different Features of Afferent Activity. *The Journal of Neuroscience* **22**(17): 7434-7443.

Frydenvang K, Lash LL, Naur P, Postila PA, Pickering DS, Smith CM, Gajhede M, Sasaki M, Sakai R, Pentikainen OT, Swanson GT and Kastrup JS (2009) Full Domain Closure of the Ligand-binding Core of the Ionotropic Glutamate Receptor iGluR5 Induced by the High Affinity Agonist Dysiherbaine and the Functional Antagonist 8,9-Dideoxyneodysiherbaine. *Journal of Biological Chemistry* **284**(21): 14219-14229.

Fu Z, Logan SM and Vicini S (2005) Deletion of the NR2A subunit prevents developmental changes of NMDA-mEPSCs in cultured mouse cerebellar granule neurones. *J Physiol* **563**(3): 867-881.

Furukawa H (2012) Structure and function of glutamate receptor amino terminal domains. *Journal of Physiology-London* **590**(1): 63-72.

Furukawa H and Gouaux E (2003) Mechanisms of activation, inhibition and specificity: crystal structures of the NMDA receptor NR1 ligand-binding core. *EMBO J* **22**(12): 2873-2885.

Furukawa H, Singh SK, Mancusso R and Gouaux E (2005) Subunit arrangement and function in NMDA receptors. *Nature* **438**(7065): 185-192.

Galvan A and Wichmann T (2008) Pathophysiology of parkinsonism. *Clinical Neurophysiology* **119**(7): 1459-1474.

Gielen M, Le Goff A, Stroebel D, Johnson JW, Neyton J and Paoletti P (2008) Structural Rearrangements of NR1/NR2A NMDA receptors during allosteric inhibition. *Neuron* **57**(1): 80-93.

Gielen M, Retchless BS, Mony L, Johnson JW and Paoletti P (2009) Mechanism of differential control of NMDA receptor activity by NR2 subunits. *Nature* **459**(7247): 703-707.

Gill A, Birdsey-Benson A, Jones BL, Henderson LP and Madden DR (2008) Correlating AMPA Receptor Activation and Cleft Closure across Subunits: Crystal Structures of the GluR4 Ligand-Binding Domain in Complex with Full and Partial Agonists *Biochemistry* **47**(52): 13831-13841.

Gill MB, Kato AS, Wang H and Bredt DS (2012) AMPA receptor modulation by cornichon-2 dictated by transmembrane AMPA receptor regulatory protein isoform. *European Journal of Neuroscience* **35**(2): 182-194.

Gill R, Alanine A, Bourson A, Buttelmann B, Fischer G, Heitz MP, Kew JNC, Levet-Trafit B, Lorez HP, Malherbe P, Miss MT, Mutel V, Pinard E, Roever S, Schmitt M, Trube G, Wybrecht R, Wyler R and Kemp JA (2002) Pharmacological characterization of Ro 63-1908 (1- 2-(4-hydroxy-phenoxy)-ethyl -4-(4-methyl-benzyl)-piperidin-4-ol), a novel subtype-selective N-methyl-D-aspartate antagonist. *J Pharmacol Exp Ther* **302**(3): 940-948.

Goebel DJ and Poosch MS (1999) NMDA receptor subunit gene expression in the rat brain: a quantitative analysis of endogenous mRNA levels of NR1Com, NR2A, NR2B, NR2C, NR2D and NR3A. *Molecular Brain Research* **69**(2): 164-170.

Gotti B, Duverger D, Bertin J, Carter C, Dupont R, Frost J, Gaudilliere B, MacKenzie ET, Rousseau J and Scatton B (1988) Ifenprodil and SL 82.0715 as cerebral anti-ischemic agents. I. Evidence for efficacy in models of focal cerebral ischemia. *J Pharmacol Exp Ther* **247**(3): 1211-1221.

Gradinaru V, Mogri M, Thompson KR, Henderson JM and Deisseroth K (2009) Optical Deconstruction of Parkinsonian Neural Circuitry. *Science* **324**(5925): 354-359.

Grillner S, McClellan A, Sigvardt K, WallÉN P and WilÉN M (1981) Activation of NMDA-receptors elicits "Fictive locomotion" in lamprey spinal cord in vitro. *Acta Physiologica Scandinavica* **113**(4): 549-551.

Gundersen V, Chaudhry FA, Bjaalie JG, Fonnum F, Ottersen OP and Storm-Mathisen J (1998) Synaptic vesicular localization and exocytosis of L-aspartate in excitatory nerve terminals: A quantitative immunogold analysis in rat hippocampus. *J Neurosci* **18**(16): 6059-6070.

Gundersen V, Fonnum F, Ottersen OP and Storm-Mathisen J (2001) Redistribution of neuroactive amino acids in hippocampus and striatum during hypoglycemia: A quantitative immunogold study. *J Cereb Blood Flow Metab* **21**(1): 41-51.

Gundersen V, Holten AT and Storm-Mathisen J (2004) GABAergic synapses in hippocampus exocytose aspartate on to NMDA receptors: quantitative immunogold evidence for co-transmission. *Mol Cell Neurosci* **26**(1): 156-165.

Gundersen V, Ottersen OP and Stormmathisen J (1991) Aspartate-like and glutamate-like immunoreactivities in rat hippocampal slices - depolarization-induced redistribution and effects of precursors. *European Journal of Neuroscience* **3**(12): 1281-1299.

Guzman JN, Sanchez-Padilla J, Chan CS and Surmeier DJ (2009) Robust Pacemaking in Substantia Nigra Dopaminergic Neurons. *J Neurosci* **29**(35): 11011-11019.

Hammond C, Bergman H and Brown P (2007) Pathological synchronization in Parkinson's disease: networks, models and treatments. *Trends in Neurosciences* **30**(7): 357-364.

Hansen KB, Furukawa H and Traynelis SF (2010) Control of assembly and function of glutamate receptors by the amino-terminal domain. *Mol Pharmacol 78(4): 535-549.*

Hansen KB, Ogden KK and Traynelis SF (2012) Subunit-Selective Allosteric Inhibition of Glycine Binding to NMDA Receptors. *The Journal of Neuroscience* **32**(18): 6197-6208.

Hansen KB and Traynelis SF (2011) Structural and Mechanistic Determinants of a Novel Site for Noncompetitive Inhibition of GluN2D-Containing NMDA Receptors. *J Neurosci* **31**(10): 3650-3661.

Harney SC, Jane DE and Anwyl R (2008) Extrasynaptic NR2D-Containing NMDARs Are Recruited to the Synapse during LTP of NMDAR-EPSCs. *J Neurosci* **28**(45): 11685-11694.

Hashambhoy YL, Winslow RL and Greenstein JL (2009) CaMKII-induced Shift in Modal Gating Explains L-Type Ca2+ Current Facilitation: A Modeling Study. *Biophys J* **96**(5): 1770-1785.

Hashimoto T, Elder CM, Okun MS, Patrick SK and Vitek JL (2003) Stimulation of the subthalamic nucleus changes the firing pattern of pallidal neurons. *J Neurosci* **23**(5): 1916-1923.

Hatton CJ and Paoletti P (2005) Modulation of Triheteromeric NMDA Receptors by N-Terminal Domain Ligands. *Neuron* **46**(2): 261-274.

Heckmann M, Bufler J, Franke C and Dudel J (1996) Kinetics of homomeric GluR6 glutamate receptor channels. *Biophys J* **71**(4): 1743-1750.

Hess P and Tsien RW (1984) Mechanism of ion permeation through calcium channels. *Nature* **309**(5967): 453-456.

Hess SD, Lorrie PD, Charles D, Chin-Chun L, Edwin CJ and Gönül V (1998) Functional Characterization of Human N-Methyl-d-Aspartate Subtype 1A/2D Receptors. *J Neurochem* **70**(3): 1269-1279.

Hoffmann H, Gremme T, Hatt H and Gottmann K (2000) Synaptic activity-dependent developmental regulation of NMDA receptor subunit expression in cultured neocortical neurons. *J Neurochem* **75**(4): 1590-1599.

Hollmann M, Boulter J, Maron C, Beasley L, Sullivan J, Pecht G and Heinemann S (1993) Zinc potentiates agonist-lnduced currents at certain splice variants of the NMDA receptor. *Neuron* **10**(5): 943-954.

Hood WF, Compton RP and Monahan JB (1989) d-Cycloserine: A ligand for the N-methyl-d-aspartate coupled glycine receptor has partial agonist characteristics. *Neurosci Lett* **98**(1): 91-95.

Horak M and Wenthold RJ (2009) Different Roles of C-terminal Cassettes in the Trafficking of Full-length NR1 Subunits to the Cell Surface. *J Biol Chem* **284**(15): 9683-9691.

Hu B and Zheng F (2005) Molecular Determinants of Glycine-Independent Desensitization of NR1/NR2A Receptors. *J Pharmacol Exp Ther* **313**(2): 563-569.

Huettner JE (2003) Kainate receptors and synaptic transmission. *Prog Neurobiol* **70**(5): 387-407.

Igarashi K, Shirahata A, Pahk AJ, Kashiwagi K and Williams K (1997) Benzyl-polyamines: Novel, potent N-methyl-d-aspartate receptor antagonists. *J Pharmacol Exp Ther* **283**(2): 533-540.

Ikeda K, Nagasawa M, Mori H, Araki K, Sakimura K, Watanabe M, Inoue Y and Mishina M (1992) Cloning and expression of the [var epsilon]4 subunit of the NMDA receptor channel. *FEBS Letters* **313**(1): 34-38.

Ikeda K, Araki K, Takayama C, Inoue Y, Yagi T, Aizawa S, Mishina M (1995) Reduced spontaneous activity of mice defective in the ε4 subunit of the NMDA receptor channel. *Mol. Brain Res*. **33**: 61-71.

Imredy JP and Yue DT (1994) Mechanism of Ca2+-sensitive inactivation of L-type Ca2+ channels. *Neuron* **12**(6): 1301-1318.

Inanobe A, Furukawa H and Gouaux E (2005) Mechanism of Partial Agonist Action at the NR1 Subunit of NMDA Receptors. *Neuron* **47**(1): 71-84.

Jackson MB, Wong BS, Morris CE, Lecar H and Christian CN (1983) Successive openings of the same acetylcholine receptor channel are correlated in open time. *Biophys J* **42**(1): 109-114.

Jakowec MW, Jackson-Lewis V, Chen XQ, Langston JW and Przedborski S (1998) The postnatal development of AMPA receptor subunits in the basal ganglia of the rat. *Dev Neurosci* **20**(1): 19-33.

Jin LH, Sugiyama H, Takigawa M, Katagiri D, Tomitori H, Nishimura K, Kaur N, Phanstiel O, Kitajima M, Takayama H, Okawara T, Williams K, Kashiwagi K and Igarashi K (2007) Comparative studies of anthraquinone- and anthracene-tetraamines as blockers of N-methyl-D-aspartate receptors. *J Pharmacol Exp Ther* **320**(1): 47-55.

Jin R, Banke TG, Mayer ML, Traynelis SF and Gouaux E (2003) Structural basis for partial agonist action at ionotropic glutamate receptors. *Nat Neurosci* **6**(8): 803-810.

Jin R, Clark S, Weeks AM, Dudman JT, Gouaux E and Partin KM (2005) Mechanism of Positive Allosteric Modulators Acting on AMPA Receptors. *J Neurosci* **25**(39): 9027-9036.

Jin RS, Singh SK, Gu SY, Furukawa H, Sobolevsky AI, Zhou J, Jin Y and Gouaux E (2009) Crystal structure and association behaviour of the GluR2 amino-terminal domain. *Embo J* **28**(12): 1812-1823.

Jin XT, Pare JF, Raju DV and Smith Y (2006) Localization and function of pre- and postsynaptic kainate receptors in the rat globus pallidus. *European Journal of Neuroscience* **23**(2): 374-386.

Johnson JW and Ascher P (1987) Glycine potentiates the NMDA response in cultured mouse brain neurons. *Nature* **325**(5): 529-531.

Johnson RR, Jiang XP and Burkhalter A (1996) Regional and laminar differences in synaptic localization of NMDA receptor subunit NR1 splice variants in rat visual cortex and hippocampus. *Journal of Comparative Neurology* **368**(3): 335-355.

Jonas P and Sakmann B (1992) Glutamate receptor channels in isolated patches from CA1 and CA3 pyramidal cells of rat hippocampal slices. *Journal of Physiology-London* **455**: 143-171.

Jones MV, Sahara Y, Dzubay JA and Westbrook GL (1998) Defining affinity with the GABA(A) receptor. *J Neurosci* **18**(21): 8590-8604.

Jones S and Gibb AJ (2005) Functional NR2B- and NR2D-containing NMDA receptor channels in rat substantia nigra dopaminergic neurones. *J Physiol* **569**(1): 209-221.

Kanai Y & Hediger MA. (1992) Primary structure and functional characterization of a high-affinity glutamate transporter. *Nature* **360,** 467-471.

Kanjhan R, Housley GD, Burton LD, Christie DL, Kippenberger A, Thorne PR, Luo L and Ryan AF (1999) Distribution of the P2X(2) receptor subunit of the ATP-gated ion channels in the rat central nervous system. *Journal of Comparative Neurology* **407**(1): 11-32.

Karachi C, Yelnik M, Tande D, Tremblay L, Hirsch EC and Francois C (2005) The pallidosubthalamic projection: An anatomical substrate for nonmotor functions of the subthalamic nucleus in primates. *Movement Disorders* **20**(2): 172-180.

Karakas E, Simorowski N and Furukawa H (2009) Structure of the zinc-bound amino-terminal domain of the NMDA receptor NR2B subunit. *Embo J* **28**(24): 3910-3920.

Karakas E, Simorowski N and Furukawa H (2011) Subunit arrangement and phenylethanolamine binding in GluN1/GluN2B NMDA receptors. *Nature* **475**(7355): 249-U170.

Kashiwagi K, Masuko T, Nguyen CD, Kuno T, Tanaka I, Igarashi K and Williams K (2002) Channel blockers acting at N-methyl-D-aspartate receptors: Differential effects of mutations in the vestibule and ion channel pore. *Mol Pharmacol* **61**(3): 533-545.

Kato AS, Zhou W, Milstein AD, Knierman MD, Siuda ER, Dotzlaf JE, Yu H, Hale JE, Nisenbaum ES, Nicoll RA and Bredt DS (2007) New transmembrane AMPA receptor regulatory protein isoform, gamma-7, differentially regulates AMPA receptors. *J Neurosci* **27**(18): 4969-4977.

Kew JN, Trube G and Kemp JA (1996) A novel mechanism of activity-dependent NMDA receptor antagonism describes the effect of ifenprodil in rat cultured cortical neurones. *The Journal of Physiology* **497**(Pt 3): 761-772.

Kinarsky L, Feng B, Skifter DA, Morley RM, Sherman S, Jane DE and Monaghan DT (2005) Identification of Subunit- and Antagonist-Specific Amino Acid Residues in the N-Methyl-D-aspartate Receptor Glutamate-Binding Pocket. *J Pharmacol Exp Ther* **313**(3): 1066-1074.

Kistler T and Fleck MW (2007) Functional consequences of natural substitutions in the GluR6 kainate receptor subunit ligand-binding site. *Channels* **1**(6): 417-428.

Kleckner NW and Dingledine R (1988) Requirement for Glycine in Activation of NMDA-Receptors Expressed in Xenopus Oocytes. *Science* **241**(4867): 835-837.

Kolomiets BP, Deniau JM, Mailly P, Menetrey A, Glowinski J and Thierry AM (2001) Segregation and convergence of information flow through the cortico-subthalamic pathways. *J Neurosci* **21**(15): 5764-5772.

Kondratskaya E, Nonaka K and Akaike N (2008) Influence of Purinergic Modulators on eEPSCs in Rat CA3 Hippocampal Neurons: Contribution of Ionotropic ATP Receptors. *Neurophysiology* **40**(1): 17-25.

Koren G, Liman ER, Logothetis DE, Nadalginard B and Hess P (1990) Gating mechanism of a cloned potassium channel expressed in frog oocytes and mammalian cells. *Neuron* **4**(1): 39-51.

Kornau HC, Schenker LT, Kennedy MB and Seeburg PH (1995) Domain interaction between NMDA receptor subunits and the postsynaptic density protein PSD-95. *Science* **269**(5231): 1737-1740.

Kotermanski SE and Johnson JW (2009) Mg2+ Imparts NMDA Receptor Subtype Selectivity to the Alzheimer's Drug Memantine. *J Neurosci* **29**(9): 2774-2779.

Kotermanski SE, Wood JT and Johnson JW (2009) Memantine binding to a superficial site on NMDA receptors contributes to partial trapping. *The Journal of Physiology* **587**(19): 4589-4604.

Krupp JJ, Vissel B, Thomas CG, Heinemann SF and Westbrook GL (2002) Calcineurin acts via the C-terminus of NR2A to modulate desensitization of NMDA receptors. *Neuropharmacology* **42**(5): 593-602.

Kumar J, Schuck P, Jin R and Mayer ML (2009) The N-terminal domain of GluR6-subtype glutamate receptor ion channels. *Nat Struct Mol Biol* **16**(6): 631-638.

Kumar R, Lozano AM, Kim YJ, Hutchison WD, Sime E, Halket E and Lang AE (1998) Double-blind evaluation of subthalamic nucleus deep brain stimulation in advanced Parkinson's disease. *Neurology* **51**(3): 850-855.

Kuner T and Schoepfer R (1996) Multiple Structural Elements Determine Subunit Specificity of Mg2+ Block in NMDA Receptor Channels. *J Neurosci* **16**(11): 3549-3558.

Kuner T, Seeburg PH and Guy HR (2003) A common architecture for K+ channels and ionotropic glutamate receptors? *Trends in Neurosciences* **26**(1): 27-32.

Kuo CC and Bean BP (1994) Na+ channels must deactivate to recover from inactivation. *Neuron* **12**(4): 819-829.

Kussius CL and Popescu GK (2009) Kinetic basis of partial agonism at NMDA receptors. *Nat Neurosci* **12**(9): 1114-1120.

Kutsuwada T, Kashiwabuchi N, Mori H, Sakimura K, Kushiya E, Araki K, Meguro H, Masaki H, Kumanishi T, Arakawa M and Mishina M (1992) Molecular diversity of the NMDA receptor channel. *Nature* **358**: 36-41.

Lape R, Colquhoun D and Sivilotti LG (2008) On the nature of partial agonism in the nicotinic receptor superfamily. *Nature* **454**(7205): 722-U756.

Laurie DJ and Seeburg PH (1994) Regional and developmental heterogeneity in splicing of the rat brain NMDAR1 mRNA. *J Neurosci* **14**(5): 3180-3194.

Lee CJ, Mannaioni G, Yuan H, Woo DH, Gingrich MB and Traynelis SF (2007) Astrocytic control of synaptic NMDA receptors. *J Physiol* **581**(3): 1057-1081.

Legendre P, Rosenmund C and Westbrook G (1993) Inactivation of NMDA channels in cultured hippocampal neurons by intracellular calcium. *The Journal of Neuroscience* **13**(2): 674-684.

LePage KT, Ishmael JE, Low CM, Traynelis SF and Murray TF (2005) Differential binding properties of [3H]dextrorphan and [3H]MK-801 in heterologously expressed NMDA receptors. *Neuropharmacology* **49**(1): 1-16.

Lerma J (2003) Roles and rules of kainate receptors in synaptic transmission. *Nat Rev Neurosci* **4**(6): 481-495.

Lester RA and Jahr CE (1992) NMDA channel behavior depends on agonist affinity. *J Neurosci* **12**(2): 635-643.

Lester RA, Tong G and Jahr CE (1993) Interactions between the glycine and glutamate binding sites of the NMDA receptor. *J Neurosci* **13**(3): 1088-1096.

Lester RAJ, Clements JD, Westbrook GL and Jahr CE (1990) Channel kinetics determine the time course of NMDA receptor-mediated synaptic currents. *Nature* **346**(6284): 565-567.

Levy R, Hutchison WD, Lozano AM and Dostrovsky JO (2000) High-frequency Synchronization of Neuronal Activity in the Subthalamic Nucleus of Parkinsonian Patients with Limb Tremor. *The Journal of Neuroscience* **20**(20): 7766-7775.

Lin Y, Skeberdis VA, Francesconi A, Bennett MVL and Zukin RS (2004) Postsynaptic density protein-95 regulates NMDA channel gating and surface expression. *J Neurosci* **24**(45): 10138-10148.

Lisman J (2003) Long-term potentiation: outstanding questions and attempted synthesis. *Philosophical Transactions of the Royal Society B: Biological Sciences* **358**(1432): 829-842.

Logan SM, Partridge JG, Matta JA, Buonanno A and Vicini S (2007) Long-Lasting NMDA Receptor-Mediated EPSCs in Mouse Striatal Medium Spiny Neurons. *J Neurophysiol* **98**(5): 2693-2704.

Logan SM, Rivera FE and Leonard JP (1999) Protein kinase C modulation of recombinant NMDA receptor currents: Roles for the C-terminal C1 exon and calcium ions. *J Neurosci* **19**(3): 974-986.

Lozovaya NA, Grebenyuk SE, Tsintsadze TS, Feng B, Monaghan DT and Krishtal OA (2004) Extrasynaptic NR2B and NR2D subunits of NMDA receptors shape 'superslow' afterburst EPSC in rat hippocampus. *J Physiol* **558**(2): 451-463.

Luo JH, Wang YH, Yasuda RP, Dunah AW and Wolfe BB (1997) The majority of N-methyl-D-aspartate receptor complexes in adult rat cerebral cortex contain at least three different subunits (NR1/NR2A/NR2B). *Mol Pharmacol* **51**(1): 79-86.

Luvisetto S, Fellin T, Spagnolo M, Hivert B, Brust PF, Harpold MM, Stauderman KA, Williams ME and Pietrobon D (2004) Modal gating of human Ca(v)2.1 (P/Q-type) calcium channels: I. The slow and the fast gating modes and their modulation by beta subunits. *J Gen Physiol* **124**(5): 445-461.

Magill PJ, Sharott A, Bevan MD, Brown P and Bolam JP (2004) Synchronous unit activity and local field potentials evoked in the subthalamic nucleus by cortical stimulation. *J Neurophysiol* **92**(2): 700-714.

Mainen ZF, Malinow R and Svoboda K (1999) Synaptic calcium transients in single spines indicate that NMDA receptors are not saturated. *Nature* **399**(6732): 151-155.

Mallet N, Ballion B, Le Moine C and Gonon F (2006) Cortical inputs and GABA interneurons imbalance projection neurons in the striatum of parkinsonian rats. *J Neurosci* **26**(14): 3875-3884.

Mallet N, Pogosyan A, Sharott A, Csicsvari J, Bolam JP, Brown P and Magill PJ (2008) Disrupted dopamine transmission and the emergence of exaggerated beta oscillations in subthalamic nucleus and cerebral cortex. *J Neurosci* **28**(18): 4795-4806.

Marrion NV (1996) Calcineurin regulates M channel modal gating in sympathetic neurons. *Neuron* **16**(1): 163-173.

Martina M, Gorfinkel Y, Halman S, Lowe JA, Periyalwar P, Schmidt CJ and Bergeron R (2004) Glycine transporter type 1 blockade changes NMDA receptor-mediated responses and LTP in hippocampal CA1 pyramidal cells by altering extracellular glycine levels. *The Journal of Physiology* **557**(2): 489-500.

Masuko T, Kashiwagi K, Kuno T, Nguyen ND, Pahk AJ, Fukuchi J, Igarashi K and Williams K (1999) A regulatory domain (R1-R2) in the amino terminus of the N-methyl-D-aspartate receptor: Effects of spermine, protons, and ifenprodil, and structural similarity to bacterial leucine/isoleucine/valine binding protein. *Mol Pharmacol* **55**(6): 957-969.

Matsui T-a, Sekiguchi M, Hashimoto A, Tomita U, Nishikawa T and Wada K (1995) Functional Comparison of d-Serine and Glycine in Rodents: The Effect on Cloned NMDA Receptors and the Extracellular Concentration, pp 454-458, Blackwell Science Ltd.

Mayer ML (2005) Glutamate receptor ion channels. *Current Opinion in Neurobiology* **15**(3): 282-288.

Mayer ML (2006) Glutamate receptors at atomic resolution. *Nature* **440**(7083): 456-462.

Mayer ML, Ghosal A, Dolman NP and Jane DE (2006) Crystal Structures of the Kainate Receptor GluR5 Ligand Binding Core Dimer with Novel GluR5-Selective Antagonists. *J Neurosci* **26**(11): 2852-2861.

Mayer ML and Miller RJ (1990) Excitatory amino acid receptors, 2nd messengers and regulation of intracellular Ca2+ in mammalian neurons. *Trends Pharmacol Sci* **11**(6): 254-260.

Mayer ML, Vyklicky L and Clements J (1989) Regulation of NMDA receptor desensitization in mouse hippocampal neurons by glycine. *Nature* **338**(6214): 425-427.

McBain CJ, Kleckner NW, Wyrick S and Dingledine R (1989) Structural requirements for activation of the glycine coagonist site of N-methyl-D-aspartate receptors expressed in Xenopus oocytes. *Mol Pharmacol* **36**(4): 556-565.

McIntyre CC, Grill WM, Sherman DL and Thakor NV (2004) Cellular effects of deep brain stimulation: Model-based analysis of activation and inhibition. *J Neurophysiol* **91**(4): 1457-1469.

McKay S, Griffiths NH, Butters PA, Thubron EB, Hardingham GE and Wyllie DJA (2012) Direct pharmacological monitoring of the developmental switch in NMDA receptor subunit composition using TCN 213, a GluN2A-selective, glycine-dependent antagonist. *British Journal of Pharmacology* **166**(3): 924-937.

Meir A, Bell DC, Stephens GJ, Page KM and Dolphin AC (2000) Calcium channel beta subunit promotes voltage-dependent modulation of alpha 1B by G beta gamma. *Biophys J* **79**(2): 731-746.

Menuz K, Stroud RM, Nicoll RA and Hays FA (2007) TARP auxiliary subunits switch AMPA receptor antagonists into partial agonists. *Science* **318**(5851): 815-817.

Milstein AD and Nicoll RA (2008) Regulation of AMPA receptor gating and pharmacology by TARP auxiliary subunits. *Trends Pharmacol Sci* **29**(7): 333-339.

Mink JW (1996) The basal ganglia: Focused selection and inhibition of competing motor programs. *Prog Neurobiol* **50**(4): 381-425.

Misra C, Brickley SG, Farrant M and Cull-Candy SG (2000a) Identification of subunits contributing to synaptic and extrasynaptic NMDA receptors in Golgi cells of the rat cerebellum. *J Physiol* **524**(1): 147-162.

Misra C, Brickley SG, Wyllie DJA and Cull-Candy SG (2000b) Slow deactivation kinetics of NMDA receptors containing NR1 and NR2D subunits in rat cerebellar Purkinje cells. *J Physiol* **525**(2): 299-305.

Momiyama A (2000) Distinct synaptic and extrasynaptic NMDA receptors identified in dorsal horn neurones of the adult rat spinal cord. *J Physiol* **523**(3): 621-628.

Momiyama A, Feldmeyer D and Cull-Candy SG (1996) Identification of a native low-conductance NMDA channel with reduced sensitivity to Mg2+ in rat central neurones. *J Physiol* **494**(Pt_2): 479-492.

Mony L, Kew JNC, Gunthorpe MJ and Paoletti P (2009) Allosteric modulators of NR2B-containing NMDA receptors: molecular mechanisms and therapeutic potential. *British Journal of Pharmacology* **157**(8): 1301-1317.

Mony L, Zhu S, Carvalho S and Paoletti P (2011) Molecular basis of positive allosteric modulation of GluN2B NMDA receptors by polyamines. *Embo J* **30**(15): 3134-3146.

Monyer H, Burnashev N, Laurie DJ, Sakmann B and Seeburg PH (1994) Developmental and regional expression in the rat brain and functional properties of four NMDA receptors. *Neuron* **12**(3): 529-540.

Monyer H, Sprengel R, Schoepfer R, Herb A, Higuchi M, Lomeli H, Burnashev N, Sakmann B and Seeburg PH (1992) Heteromeric NMDA receptors: molecular and functional distinction of subtypes. *Science* **256**(5060): 1217-1221.

Morley RM, Tse H-W, Feng B, Miller JC, Monaghan DT and Jane DE (2005) Synthesis and Pharmacology of N1-Substituted Piperazine-2,3-dicarboxylic Acid Derivatives Acting as NMDA Receptor Antagonists. *J Med Chem* **48**(7): 2627-2637.

Mosbacher J, Schoepfer R, Monyer H, Burnashev N, Seeburg PH and Ruppersberg JP (1994) A molecular determinant for submillisecond desensitization in glutamate receptors. *Science* **266**(5187): 1059-1062.

Mosley CA, Myers SJ, Murray EE, Santangelo R, Tahirovic YA, Kurtkaya N, Mullasseril P, Yuan H, Lyuboslavsky P, Le P, Wilson LJ, Yepes M, Dingledine R, Traynelis SF and Liotta DC (2009) Synthesis, structural activity-relationships, and biological evaluation of novel amide-based allosteric binding site antagonists in NR1A/NR2B N-methyl-d-aspartate receptors. *Bioorganic & Medicinal Chemistry* **17**(17): 6463-6480.

Mott DD, Benveniste M and Dingledine RJ (2008) pH-Dependent inhibition of kainate receptors by zinc. *J Neurosci* **28**(7): 1659-1671.

Mott DD, Washburn MS, Zhang SN and Dingledine RJ (2003) Subunit-dependent modulation of kainate receptors by extracellular protons and polyamines. *J Neurosci* **23**(4): 1179-1188.

Mullasseril P, Hansen KB, Vance KM, Ogden KK, Yuan H, Kurtkaya NL, Santangelo R, Orr AG, Le P, Vellano KM, Liotta DC and Traynelis SF (2010) A subunit-

selective potentiator of NR2C- and NR2D-containing NMDA receptors. *Nat Commun* **1**(7): 90.

Mullner C, Yakubovich D, Dessauer CW, Platzer D and Schreibmayer W (2003) Single channel analysis of the regulation of GIRK1/GIRK4 channels by protein phosphorylation. *Biophys J* **84**(2): 1399-1409.

Nadler JV, Vaca KW, White WF, Lynch GS and Cotman CW (1976) Aspartate and glutamate as possible transmitters of excitatory hippocampal afferents. *Nature* **260**(5551): 538-540.

Nakanishi H, Kita H and Kitai ST (1987) Electrical membrane properties of rat subthalamic neurons in an in vitro slice preparation. *Brain Research* **437**(1): 35-44.

Nahum-Levy R, Lipinski D, Shavit S and Benveniste M (2001) Desensitization of NMDA Receptor Channels Is Modulated by Glutamate Agonists. *Biophys J* **80**(5): 2152-2166.

Nambu A, Takada M, Inase M and Tokuno H (1996) Dual somatotopical representations in the primate subthalamic nucleus: Evidence for ordered but reversed body-map transformations from the primary motor cortex and the supplementary motor area. *J Neurosci* **16**(8): 2671-2683.

Naranjo D and Brehm P (1993) Modal shifts in acetylcholine receptor channel gating confer subunit-dependent desensitization. *Science* **260**(5115): 1811-1814.

Neyton J and Paoletti P (2006) Relating NMDA Receptor Function to Receptor Subunit Composition: Limitations of the Pharmacological Approach. *J Neurosci* **26**(5): 1331-1333.

Nicholls D (1989) Release of glutamate, aspartate, and gamma-aminobutyric acid from isolated nerve terminals. *J Neurochem* **52**(2): 331-341.

Nicoll RA, Tomita S and Bredt DS (2006) Auxiliary subunits assist AMPA-type glutamate receptors. *Science* **311**(5765): 1253-1256.

Nikam SS and Meltzer LT (2002) NR2B Selective NMDA Receptor Antagonists. *Current Pharmaceutical Design* **8**(10): 845.

Obeso J, Rodriguez-Oroz M, Rodriguez M, Macias R, Alvarez L, Guridi O, Vitek J and DeLong M (2000) Pathophysiologic basis of surgery for Parkinson's disease. *Neurology* **55**(12 Suppl 6): S7-S12.

Obeso JA, Guridi J, Rodriguez-Oroz MC, Agid Y, Bejjani P, Bonnet AM, Lang AE, Lozano AM, Kumar R, Benabid A, Pollack P, Krack P, Rehncrona S, Ekberg R,

Grabowski M, Albanese A, Scerrati M, Moro E, Koller W, Wilkinson SB, Pahwa R, Volkmann J, Allert N, Freund HJ, Kulisevsky J, Gironell A, Molet J, Tronnier V, Fogel W, Krause M, Funk T, Kern C, Kestenbach U, Iansek R, Rosenfeld J, Churchyard A, O'Sullivan D, Pell M, Markus R, Bayes A, Blesa R, Oliver B, Olanow CW, Germano IM, Brin M, Jankovic J, Grossman RG, Ondo WG, Vitek JL, Bakay RAE, DeLong MR, Tolosa E, Rumia J, Valldeoriola F, Lang AM, Lozano A, Koller WC, Vitek J, Wilkinson S and Deep-Brain Stimulation P (2001) Deep-brain stimulation of the subthalamic nucleus or the pars interna of the globus pallidus in Parkinson's disease. *New England Journal of Medicine* **345**(13): 956-963.

Ochi R and Kawashima Y (1990) Modulation of slow gating process of calcium channels by isoprenaline in guinea pig ventricular cells. *Journal of Physiology-London* **424**: 187-204.

Olney JW, Price MT, Salles KS, Labruyere J, Ryerson R, Mahan K, Frierdich G and Samson L (1987) L-Homocysteic acid: An endogenous excitotoxic ligand of the NMDA receptor. *Brain Research Bulletin* **19**(5): 597-602.

Pan Z, Tong G and Jahr CE (1993) A false transmitter at excitatory synapses. *Neuron* **11**(1): 85-91.

Panatier A, Theodosis DT, Mothet JP, Touquet B, Pollegioni L, Poulain DA and Oliet SHR (2006) Glia-derived D-serine controls NMDA receptor activity and synaptic memory. *Cell* **125**(4): 775-784.

Pankratov Y, Castro E, Miras-Portugal MT and Krishtal O (1998) A purinergic component of the excitatory postsynaptic current mediated by P2X receptors in the CA1 neurons of the rat hippocampus. *European Journal of Neuroscience* **10**(12): 3898-3902.

Pankratov Y, Lalo U, Krishtal O and Verkhratsky A (2003) P2X receptor-mediated excitatory synaptic currents in somatosensory cortex. *Mol Cell Neurosci* **24**(3): 842-849.

Paoletti P (2011) Molecular basis of NMDA receptor functional diversity. *European Journal of Neuroscience* **33**(8): 1351-1365.

Paoletti P and Neyton J (2007) NMDA receptor subunits: function and pharmacology. *Current Opinion in Pharmacology* **7**(1): 39-47.

Paoletti P, Perin-Dureau F, Fayyazuddin A, Le Goff A, Callebaut I and Neyton J (2000) Molecular organization of a zinc binding n-terminal modulatory domain in a NMDA receptor subunit. *Neuron* **28**(3): 991-925.

Papke RL, Millhauser G, Lieberman Z and Oswald RE (1988) Relationships of agonist properties to the single channel kinetics of nicotinic acetylcholine receptors. *Biophys J* **53**(1): 1-10.

Parsons CG, Danysz W and Quack G (1999) Memantine is a clinically well tolerated N-methyl--aspartate (NMDA) receptor antagonist--a review of preclinical data. *Neuropharmacology* **38**(6): 735-767.

Paxinos and Watson (1998) *The Rat Brain in Stereotaxic Coordinates*, 4th ed., Academic Press, New York.

Pérez-Otaño I and Ehlers MD (2005) Homeostatic plasticity and NMDA receptor trafficking. *Trends in Neurosciences* **28**(5): 229-238.

Perez-Otano I, Schulteis CT, Contractor A, Lipton SA, Trimmer JS, Sucher NJ and Heinemann SF (2001) Assembly with the NR1 subunit is required for surface expression of NR3A-containing NMDA receptors. *J Neurosci* **21**(4): 1228 - 1237.

Perin-Dureau F, Rachline J, Neyton J and Paoletti P (2002) Mapping the Binding Site of the Neuroprotectant Ifenprodil on NMDA Receptors. *J Neurosci* **22**(14): 5955-5965.

Peterson BZ, DeMaria CD and Yue DT (1999) Calmodulin is the Ca2+ sensor for Ca2+-dependent inactivation of l-type calcium channels. *Neuron* **22**(3): 549-558.

Peterson CL, Thompson MA, Martin D and Nadler JV (1995) Modulation of glutamate and aspartate release from slices of hippocampal area CA1 by inhibitors of arachidonic acid metabolism. *J Neurochem* **64**(3): 1152-1160.

Pina-Crespo JC and Gibb AJ (2002) Subtypes of NMDA receptors in new-born rat hippocampal granule cells. *J Physiol* **541**(1): 41-64.

Plenz D and Kital ST (1999) A basal ganglia pacemaker formed by the subthalamic nucleus and external globus pallidus. *Nature* **400**(6745): 677-682.

Plested AJR and Mayer ML (2007) Structure and mechanism of kainate receptor modulation by anions. *Neuron* **53**(6): 829-841.

Poon K, Ahmed AH, Nowak LM and Oswald RE (2011) Mechanisms of Modal Activation of GluA3 Receptors. *Mol Pharmacol* **80**(1): 49-59.

Poon K, Nowak LM and Oswald RE (2010) Characterizing Single-Channel Behavior of GluA3 Receptors. *Biophys J* **99**(5): 1437-1446.

Popescu G and Auerbach A (2003) Modal gating of NMDA receptors and the shape of their synaptic response. *Nature Neuroscience* **6**(5): 476-483.

Popescu GK (2012) Modes of glutamate receptor gating. *Journal of Physiology-London* **590**(1): 73-91.

Porter J, Cauli B, Staiger J, Lambolez B, Rossier J and Audinat E (1998) Properties of bipolar VIPergic interneurons and their excitation by pyramidal neurons in the rat neocortex. *European Journal of Neuroscience* **10**(12): 3617-3628.

Pullan L, Olney JW, Price M, Compton R, Hood W, Michel J and Monahan J (1987) Excitatory amino acid receptor potency and subclass specificity of sulfur-containing amino acids. *J Neurochem* **49**(4): 1301-1307.

Priel A, Kolleker A, Ayalon G, Gillor M, Osten P and Stern-Bach Y (2005) Stargazin reduces desensitization and slows deactivation of the AMPA-type glutamate receptors. *J Neurosci* **25**(10): 2682-2686.

Priestley T and Kemp JA (1994) Kinetic study of the interactions between the glutamate and glycine recognition sites on the N-methyl-D-aspartic acid receptor complex. *Mol Pharmacol* **46**(6): 1191-1196.

Prieto ML and Wollmuth LP (2010) Gating Modes in AMPA Receptors. *J Neurosci* **30**(12): 4449-4459.

Qian A, Buller AL and Johnson JW (2005) NR2 subunit-depenclence of NMDA receptor channel block by external Mg2+. *Journal of Physiology-London* **562**(2): 319-331.

Qin F, Auerbach A and Sachs F (1997) Maximum likelihood estimation of aggregated Markov processes. *Proceedings of the Royal Society B: Biological Sciences* **264**(1380): 375-383.

Rachline J, Perin-Dureau F, Le Goff A, Neyton J and Paoletti P (2005) The Micromolar Zinc-Binding Domain on the NMDA Receptor Subunit NR2B. *J Neurosci* **25**(2): 308-317.

Reisberg B, Doody R, Stoffler A, Schmitt F, Ferris S and Mobius HJ (2003) Memantine in moderate-to-severe Alzheimer's disease. *New England Journal of Medicine* **348**(14): 1333-1341.

Renzi M, Farrant M and Cull-Candy SG (2007) Climbing-fibre activation of NMDA receptors in Purkinje cells of adult mice. *J Physiol* **585**(1): 91-101.

Retchless BS, Gao W and Johnson JW (2012) A single GluN2 subunit residue controls NMDA receptor channel properties via intersubunit interaction *Nature Neuroscience* **15**(3): 406-413.

Rodriguez-Oroz MC, Obeso JA, Lang AE, Houeto JL, Pollak P, Rehncrona S, Kulisevsky J, Albanese A, Volkmann J, Hariz MI, Quinn NP, Speelman JD, Guridi J, Zamarbide I, Gironell A, Molet J, Pascual-Sedano B, Pidoux B, Bonnet AM, Agid Y, Xie J, Benabid AL, Lozano AM, Saint-Cyr J, Romito L, Contarino MF, Scerrati M, Fraix V and Van Blercom N (2005) Bilateral deep brain stimulation in Parkinson's disease: a multicentre study with 4 years follow-up. *Brain* **128**: 2240-2249.

Rodriguez M, Guridi O, Lavarez L, Mewes K, Macias R, Vitek J, DeLong M and Obeso J (1998) The subthalamic nucleus and tremor in Parkinson's disease. *Movement Disorders* **13**(Suppl 3): 111-118.

Rumbaugh G, Prybylowski K, Wang JF and Vicini S (2000) Exon 5 and Spermine Regulate Deactivation of NMDA Receptor Subtypes. *J Neurophysiol* **83**(3): 1300-1306.

Rusakov DA and Kullmann DM (1998) Extrasynaptic glutamate diffusion in the hippocampus: Ultrastructural constraints, uptake, and receptor activation. *J Neurosci* **18**(9): 3158-3170.

Rutter A, Freeman F and Stephenson F (2002) Further characterization of the molecular interaction between PSD-95 and NMDA receptors: the effect of the NR1 splice variant and evidence for modulation of channel gating. *J Neurochem* **81**(6): 1298-1307.

Rycroft BK and Gibb AJ (2004) Regulation of single NMDA receptor channel activity by alpha-actinin and calmodulin in rat hippocampal granule cells. *Journal of Physiology-London* **557**(3): 795-808.

Salt TE (1989) Modulation of NMDA receptor-mediated responses by glycien and D-serine in the rat thalamus in vivo. *Brain Research* **481**(2): 403-406.

Salussolia CL, Prodromou ML, Borker P and Wollmuth LP (2011) Arrangement of Subunits in Functional NMDA Receptors. *J Neurosci* **31**(31): 11295-11304.

Sasaki YF, Rothe T, Premkumar LS, Das S, Cui JK, Talantova MV, Wong HK, Gong XD, Chan SF, Zhang DX, Nakanishi N, Sucher NJ and Lipton SA (2002) Characterization and comparison of the NR3A subunit of the NMDA receptor in recombinant systems and primary cortical neurons. *J Neurophysiol* **87**(4): 2052-2063.

Sato K, Kiyama H and Tohyama M (1993) The differential expression patterns of messenger RNAs encoding non-N-methyl-d-aspartate glutamate receptor subunits (GluR1–4) in the rat brain. *Neuroscience* **52**(3): 515-539.

Schell M, Cooper O and Snyder S (1997) D-aspartate localizations imply neuronal and neuroendocrine roles. *Proc Natl Acad Sci* **94**: 2013-2018.

Schoepp DD, Smith CL, Lodge D, Millar JD, Leander JD, Sacaan AI and Lunn WHW (1991) D,L-(Tetrazol-5-yl) glycine: a novel and highly potent NMDA receptor agonist. *European Journal of Pharmacology* **203**(2): 237-243.

Schorge S and Colquhoun D (2003) Studies of NMDA receptor function and stoichiometry with truncated and tandem subunits. *J Neurosci* **23**(4): 1151-1158.

Schorge S, Elenes S and Colquhoun D (2005) Maximum likelihood fitting of single channel NMDA activity with a mechanism composed of independent dimers of subunits. *J Physiol* **569**(2): 395-418.

Sessoms-Sikes S, Honse Y, Lovinger DM and Colbran RJ (2005) CaMKII alpha enhances the desensitization of NR2B-containing NMDA receptors by an autophosphorylation-dependent mechanism. *Mol Cell Neurosci* **29**(1): 139-147.

Sheinin A, Shavit S and Benveniste M (2001) Subunit specificity and mechanism of action of NMDA partial agonist -cycloserine. *Neuropharmacology* **41**(2): 151-158.

Shen KZ and Johnson SW (2010) Ca(2+) Influx through NMDA-Gated Channels Activates ATP-Sensitive K(+) Currents through a Nitric Oxide-cGMP Pathway in Subthalamic Neurons. *J Neurosci* **30**(5): 1882-1893.

Shink E, Bevan MD, Bolam JP and Smith Y (1996) The subthalamic nucleus and the external pallidum: Two tightly interconnected structures that control the output of the basal ganglia in the monkey. *Neuroscience* **73**(2): 335-357.

Shinozaki H, Ishida M, Shimamoto K and Ohfune Y (1989) A conformationally restricted analogue of -glutamate, the (2S,3R,4S) isomer of -[alpha](carboxycyclopropyl)glycine, activates the NMDA-type receptor more markedly than NMDA in the isolated rat spinal cord. *Brain Research* **480**(1-2): 355-359.

Singer-Lahat D, Dascal N and Lotan I (1999) Modal behavior of the Kv1.1 channel conferred by the Kv beta 1.1 subunit and its regulation by dephosphorylation of Kv1.1. *Pflugers Archiv-European Journal of Physiology* **439**(1-2): 18-26.

Smith ID and Grace AA (1992) Role of the subthalamic nucleus in the regulation of nigral dopamine neuron activity. *Synapse* **12**(4): 287-303.

Smith MA and Ashford MLJ (1998) Mode switching characterizes the activity of large conductance potassium channels recorded from rat cortical fused nerve terminals. *Journal of Physiology-London* **513**(3): 733-747.

Smothers CT and Woodward JJ (2007) Pharmacological Characterization of Glycine-Activated Currents in HEK 293 Cells Expressing N-Methyl-D-aspartate NR1 and NR3 Subunits. *J Pharmacol Exp Ther* **322**(2): 739-748.

Sobolevsky AI, Rosconi MP and Gouaux E (2009) X-ray structure, symmetry and mechanism of an AMPA-subtype glutamate receptor. *Nature* **462**(7274): 745-756.

Standaert DG, Bernhard Landwehrmeyer G, Kerner JA, Penney JB and Young AB (1996) Expression of NMDAR2D glutamate receptor subunit mRNA in neurochemically identified interneurons in the rat neostriatum, neocortex and hippocampus. *Molecular Brain Research* **42**(1): 89-102.

Standaert DG, Friberg IK, Landwehrmeyer GB, Young AB and Penney JB (1999) Expression of NMDA glutamate receptor subunit mRNAs in neurochemically identified projection and interneurons in the striatum of the rat. *Molecular Brain Research* **64**(1): 11-23.

Standaert DG, Testa CM, Penney Jr JB and Young AB (1993) Alternatively spliced isoforms of the NMDAR1 glutamate receptor subunit: Differential expression in the basal ganglia of the rat. *Neurosci Lett* **152**(1-2): 161-164.

Standaert DG, Testa CM, Young A and Penney Jr JB (1994) Organization of N-methyl-D-aspartate glutamate receptor gene expression in the basal ganglia of the rat. *J Comp Neurol* **343**: 1-16.

Stern P, Behe P, Schoepfer R and Colquhoun D (1992) Single-Channel Conductances of NMDA Receptors Expressed from Cloned cDNAs: Comparison with Native Receptors. *Proceedings of the Royal Society B: Biological Sciences* **250**(1329): 271-277.

Stroebel D, Carvalho S and Paoletti P (2011) Functional evidence for a twisted conformation of the NMDA receptor GluN2A subunit N-terminal domain. *Neuropharmacology* **60**(1): 151-158.

Stone TW and Burton NR (1988) NMDA receptors and ligands in the vertebrate CNS. *Prog Neurobiol* **30**(4): 333-368.

Storck T, Schulte S, Hofmann K & Stoffel W. (1992). Structure, expression, and functional analysis of a Na+-dependent glutamate aspartate transporter from rat brain. *Proc Natl Acad Sci U S A* **89,** 10955-10959.

Sun Y, Olson R, Horning M, Armstrong N, Mayer M and Gouaux E (2002) Mechanism of glutamate receptor desensitization. *Nature* **417**(6886): 245-253.

Surmeier DJ, Mercer JN and Chan CS (2005) Autonomous pacemakers in the basal ganglia: who needs excitatory synapses anyway? *Current Opinion in Neurobiology* **15**(3): 312-318.

Taddese A and Bean BP (2002) Subthreshold sodium current from rapidly inactivating sodium channels drives spontaneous firing of tuberomammillary neurons. *Neuron* **33**(4): 587-600.

Talukder I, Borker P and Wollmuth LP (2010) Specific Sites within the Ligand-Binding Domain and Ion Channel Linkers Modulate NMDA Receptor Gating. *J Neurosci* **30**(35): 11792-11804.

Tariot PN, Farlow MR, Grossberg GT, Graham SM, McDonald S and Gergel I (2004) Memantine treatment in patients with moderate to severe Alzheimer disease already receiving donepezil - A randomized controlled trial. *Jama-Journal of the American Medical Association* **291**(3): 317-324.

Thompson C, Drewery D, Atkins H, Stephenson F and Chazot P (2002) Immunohistochemical localization of N-methyl-D-aspartate receptor subunits in teh adult murine hippocampal formation: evidence for a unique role of the NR2D subunit. *Mol Brain Res* **102**: 55-61.

Timmerman W and Westerink BHC (1997) Brain microdialysis of GABA and glutamate: What does it signify? *Synapse* **27**(3): 242-261.

Tomita S, Chen L, Kawasaki Y, Petralia RS, Wenthold RJ, Nicoll RA and Bredt DS (2003) Functional studies and distribution define a family of transmembrane AMPA receptor regulatory proteins. *J Cell Biol* **161**(4): 805-816.

Traynelis SF, Burgess MF, Zheng F, Lyuboslavsky P and Powers JL (1998) Control of voltage-independent zinc inhibition of NMDA receptors by the NR1 subunit. *J Neurosci* **18**(16): 6163-6175.

Traynelis SF and Cull-Candy SG (1991) Pharmacological properties and H+ sensitivity of excitatory amino acid receptor channels in rat cerebellar granule neurons. *Journal of Physiology-London* **433**: 727-763.

Traynelis SF, Hartley M and Heinemann S (1995) Control of proton sensitivity of the NMDA receptor by RNA splicing and polyamines. *Science* **18**: 6163-6175.

Traynelis SF, Wollmuth LP, McBain CJ, Menniti FS, Vance KM, Ogden KK, Hansen KB, Yuan H, Myers SJ and Dingledine R (2010) Glutamate Receptor Ion Channels: Structure, Regulation, and Function. *Pharmacological Reviews* **62**(3): 405-496.

Turetsky D, Garringer E and Patneau DK (2005) Stargazin modulates native AMPA receptor functional properties by two distinct mechanisms. *J Neurosci* **25**(32): 7438-7448.

Ulbrich MH and Isacoff EY (2008) Rules of engagement for NMDA receptor subunits. *Proc Natl Acad Sci U S A* **105**(37): 14163-14168.

Vance KM, Hansen KB and Traynelis SF (2012) GluN1 splice variant control of GluN1/GluN2D NMDA receptors. *Journal of Physiology-London*., in press.

Vance KM, Simorowski N, Traynelis SF and Furukawa H (2011) Ligand-specific deactivation time course of GluN1/GluN2D NMDA receptors. *Nat Commun* **2**: 11.

Vicini S, Wang JF, Li JH, Zhu WJ, Wang YH, Luo JH, Wolfe BB and Grayson DR (1998) Functional and Pharmacological Differences Between Recombinant N-Methyl-D-Aspartate Receptors. *J Neurophysiol* **79**(2): 555-566.

Vyklický L (1993) Calcium-mediated modulation of N-methyl-D-aspartate (NMDA) responses in cultured rat hippocampal neurones. *The Journal of Physiology* **470**(1): 575-600.

Wakamori M, Mikala G and Mori Y (1999) Auxiliary subunits operate as a molecular switch in determining gating behaviour of the unitary N-type Ca2+ channel current in Xenopus oocytes. *Journal of Physiology-London* **517**(3): 659-672.

Wang L and Nadler JV (2007) Reduced aspartate release from rat hippocampal synaptosomes loaded with Clostridial toxin light chain by electroporation: Evidence for an exocytotic mechanism. *Neurosci Lett* **412**(3): 239-242.

Wenzel A, Villa M and Mohler H (1996) Developmental and Regional Expression of NMDA Receptor Subtypes Containing the NR2D Subunit in Rat Brain. *J Neurochem* **66**(3): 1240-1248.

West PJ, Dalpe-Charron A and Wilcox KS (2007) Differential contribution of kainate receptors to excitatory postsynaptic currents in superficial layer neurons of the rat medial entorhinal cortex. *Neuroscience* **146**(3): 1000-1012.

Weston MC, Gertler C, Mayer ML and Rosenmund C (2006) Interdomain Interactions in AMPA and Kainate Receptors Regulate Affinity for Glutamate. *J Neurosci* **26**(29): 7650-7658.

Wichmann T and DeLong MR (2006) Deep brain stimulation for neurologic and neuropsychiatric disorders. *Neuron* **52**(1): 197-204.

Williams K (1993) Ifenprodil discriminates subtypes of the N-methyl-D-aspartate receptor: selectivity and mechanisms at recombinant heteromeric receptors. *Mol Pharmacol* **44**: 851-859.

Williams K (1994) Subunit-specific potentiation of recombinant N-methyl-D-aspartate receptors by histamine. *Mol Pharmacol* **46**(3): 531-541.

Wilson CJ and Bevan MD (2011) Intrinsic dynamics and synaptic inputs control the activity patterns of subthalamic nucleus neurons in health and in Parkinson's disease. *Neuroscience* **198**(0): 54-68.

Wo ZG and Oswald RE (1995) Unraveling the modular designe of glutamate-gated ion channels. *Trends in Neurosciences* **18**(4): 161-168.

Wolf JA, Moyer JT, Lazarewicz MT, Contreras D, Benoit-Marand M, O'Donnell P and Finkel LH (2005) NMDA/AMPA ratio impacts state transitions and entrainment to oscillations in a computational model of the nucleus Accumbens medium spiny projection neuron. *J Neurosci* **25**(40): 9080-9095.

Wood MW, Vandongen HMA and Vandongen AMJ (1995) Structural conservation of ion conduction pathways in K-channels and glutamate receptors. *Proc Natl Acad Sci U S A* **92**(11): 4882-4886.

Wüllner U, Standaert DG, Testa CM, Penney JB and Young AB (1997) Differential expression of kainate receptors in the basal ganglia of the developing and adult rat brain. *Brain Research* **768**(1–2): 215-223.

Wyllie DJA, Behe P and Colquhoun D (1998) Single-channel activations and concentration jumps: comparison of recombinant NR1a/NR2A and NR1a/NR2D NMDA receptors. *J Physiol* **510**(1): 1-18.

Wyllie DJA, Behe P, Nassar M, Schoepfer R and Colquhoun D (1996) Single-Channel Currents from Recombinant NMDA NR1a/NR2D Receptors Expressed in Xenopus Oocytes. *Proceedings of the Royal Society B: Biological Sciences* **263**(1373): 1079-1086.

Yamakura T, Mori H, Masaki H, Shimoji K and Mishina M (1993) Different sensitivities of NMDA receptor channel subtypes to noncompetitive antagonists. *Neuroreport* **4**(6): 687-690.

Yamakura T and Shimoji K (1999) Subunit- and site-specific pharmacology of the NMDA receptor channel. *Prog Neurobiol* **59**(3): 279-298.

Yuan H, Hansen KB, Vance KM, Ogden KK and Traynelis SF (2009) Control of NMDA Receptor Function by the NR2 Subunit Amino-Terminal Domain. *J Neurosci* **29**(39): 12045-12058.

Yue DT, Backx PH and Imredy JP (1990) Calcium-sensitive inactivation in the gating of single calcium channels. *Science* **250**(4988): 1735-1738.

Yuzaki M and Connor JA (1999) Characterization of L-Homocysteate-Induced Currents in Purkinje Cells From Wild-Type and NMDA Receptor Knockout Mice. *J Neurophysiol* **82**(5): 2820-2826.

Zagotta WN and Aldrich RW (1990) Voltage-dependent gating of Shaker A-type potassium channels in Drosophila muscle. *J Gen Physiol* **95**(1): 29-60.

Zhang F, Gradinaru V, Adamantidis AR, Durand R, Airan RD, de Lecea L and Deisseroth K (2010) Optogenetic interrogation of neural circuits: technology for probing mammalian brain structures. *Nat Protoc* **5**(3): 439-456.

Zhang L, Zheng X, Paupard MC, Wang AP, Santchi L, Friedman LK, Zukin RS and Bennett MVL (1994) Spermine potentiation of recombinant N-methyl-D-asparate receptors is affected by subunit composition. *Proc Natl Acad Sci U S A* **91**(23): 10883-10887.

Zhang W, Howe JR and Popescu GK (2008) Distinct gating modes determine the biphasic relaxation of NMDA receptor currents. *Nat Neurosci* **11**(12): 1373-1375.

Zhang W, Robert A, Vogensen S and Howe J (2006) The relationship between agonist potency and AMPA receptor kinetics. *Biophys J* **91**(4): 1336-1346.

Zhang W, St-Gelais F, Grabner CP, Trinidad JC, Sumioka A, Morimoto-Tomita M, Kim KS, Straub C, Burlingame AL, Howe JR and Tomita S (2009) A Transmembrane Accessory Subunit that Modulates Kainate-Type Glutamate Receptors. **61**(3): 385-396.

Zhang XY and Nadler JV (2009) Postsynaptic response to stimulation of the Schaffer collaterals with properties similar to those of synaptosomal aspartate release. *Brain Research* **1295**: 13-20.

Zhou M and Baudry M (2006) Developmental Changes in NMDA Neurotoxicity Reflect Developmental Changes in Subunit Composition of NMDA Receptors. *J Neurosci* **26**(11): 2956-2963.

Zhou M, Peterson CL, Lu YB and Nadler JV (1995) Release of glutamate and aspartate from CA1 synaptosomes - selective modulation of aspartate release by ionotropic glutamate receptor ligands. *J Neurochem* **64**(4): 1556-1566.

Zhu Z-T, Munhall A, Shen K-Z and Johnson SW (2005) NMDA enhances a depolarization-activated inward current in subthalamic neurons. *Neuropharmacology* **49**(3): 317-327.

Zhu ZT, Munhall A, Shen KZ and Johnson SW (2004) Calcium-dependent subthreshold oscillations determine bursting activity induced by N-methyl-D-aspartate in rat subthalamic neurons in vitro. *European Journal of Neuroscience* **19**(5): 1296-1304.

Zukin RS and Bennett MVL (1995) Alternatively spliced isoforms of the NMDARI receptor subunit. *Trends in Neurosciences* **18**(7): 306-313.